

FIXED FREQUENCY DISSOCIATION OF METAL OXIDE CATIONS AND
INFRARED PHOTODISSOCIATION STUDIES OF METAL CARBONYL CATION
SYSTEMS

by

ZACHARY DAVID REED

(Under the Direction of Michael A. Duncan)

ABSTRACT

Metal oxide clusters of the form $M_nO_m^+$ ($M=Y,La,In$), transition metal carbonyl complexes of the form $TM-(CO)_n^+$ ($TM=Mn,Cu,Au$), and mixed vanadium benzene carbonyl complexes of the form $V-bz-(CO)_n^+$ are produced in the gas phase by laser vaporization in a pulsed nozzle and detected with time-of-flight mass spectrometry. The metal oxide clusters are studied using fixed frequency photodissociation. A limited number of stoichiometries are found for each value of n . Clusters are mass selected and photodissociated using the third harmonic (355 nm) of an Nd:YAG laser. Larger clusters undergo fission to produce certain stable cation clusters. Yttrium and lanthanum oxide clusters of the form $MO(M_2O_3)_n^+$ are found to be particularly stable, along with $Y_6O_8^+$. Density functional theory (DFT) calculations were performed to investigate the structures and bonding of these clusters. The stability of some indium oxide clusters, including $In_5O_4^+$, $In_5O_4^+$, and $In_3O_2^+$ can be understood in terms of Wade's Rules of electron counting. Other indium oxide clusters with enhanced stability do not follow Wade's Rules, including $In_3O_1^+$, and In_2O^+ .

The carbonyl and mixed benzene-carbonyl complexes are studied using infrared photodissociation spectroscopy and density functional theory. $\text{Mn}(\text{CO})_6^+$ has a completed coordination sphere, consistent with its expected 18 electron stability. All manganese carbonyl complexes feature red-shifted ν_{CO} . The argon tagged analogues of the small ($n=1-6$) complexes are studied by IRPD. The spin state of small clusters is observed to gradually decrease as additional ligands are added, from a quintet MnCO^+ to a singlet $\text{Mn}(\text{CO})_5^+$. Copper carbonyl cations are observed to have blue-shifted ν_{CO} , demonstrating that they are non-classical carbonyls. $\text{Cu}(\text{CO})_4^+$ has a completed coordination sphere, in line with the 18 electron rule. All small complexes are observed exclusively as singlets, but some triplet population is observed for $n=7,8$. This is explained in terms of the increased oscillator strengths of the triplets. $\text{Au}(\text{CO})_n^+$ is demonstrated to have a completed coordination sphere at $n=4$, despite having significant reduced binding energy for $n=3,4$. It is also a non-classical carbonyl. $\text{V-bz}-(\text{CO})_n^+$ is demonstrated to have two different coordination numbers, with $n=3$ and $n=4$. Both feature redshifted ν_{CO} . The symmetric CO stretch is strongly activated in these complexes.

INDEX WORDS: Gas phase, laser vaporization, IR photodissociation, carbonyl, metal oxide, clusters, molecular beams, carbon monoxide, metal carbonyl

FIXED FREQUENCY DISSOCIATION OF METAL OXIDE CATIONS AND
INFRARED PHOTODISSOCIATION STUDIES OF METAL CARBONYL CATION
SYSTEMS

by

ZACHARY DAVID REED

B.S., College of William and Mary, 2005

A Dissertation Submitted to the Graduate Faculty of The University of Georgia in Partial
Fulfillment of the Requirements for the Degree

DOCTOR OF PHILOSOPHY

ATHENS, GEORGIA

2009

© 2009

Zachary David Reed

All Rights Reserved

FIXED FREQUENCY DISSOCIATION OF METAL OXIDE CATIONS AND
INFRARED PHOTODISSOCIATION STUDIES OF METAL CARBONYL CATION
SYSTEMS

by

ZACHARY DAVID REED

Major Professor: Michael A. Duncan

Committee: Charles Kotal
Nigel Adams

Electronic Version Approved:

Maureen Grasso
Dean of the Graduate School
The University of Georgia
December 2009

DEDICATION

I first dedicate this work to my wife, Sara. Chemistry can be a harsh mistress, but we've endured through the long nights at the lab, the days spend writing in front of the computer, and the constant stress of research. You've helped keep me motivated, and more importantly, kept me sane. I've often noted that the spouses of physical scientists tend to be either from other highly driven professions, or are saints. I'm lucky enough to have found someone that's both. Our life together has been the best part of the last few years together

My parents have contributed so much to my life. My father demonstrated to me from a young age just what hard work is, and even after expanding my capacity dramatically during the last few years of graduate work, I know I still can't match his dedication or passion for his work. It's always been an inspiration. My mother has always been one of the rocks of my life, always available to talk or to listen. I've had many an early (or late) evening talk with her while leaving the lab or waiting for an experiment. She has been a connection to a family life that I sorely miss and has helped me through many of the hard times of the last several years and has always been there to celebrate the best times.

This time away from Virginia, which I still consider "home," has not been without costs. I've seen several beloved members of my family pass away, while I was hundreds of miles away. Most of all, I regret not being able to see my grandmother more during these years. She was the spirit of family embodied. I deeply regret that she can

not attend the two life changing events in my life this year, my wedding and my PhD graduation.

TABLE OF CONTENTS

	Page
CHAPTER	
1 INTRODUCTION.....	1
1.1 Chemistry and Bonding of Metal Oxides	2
1.2 Chemistry and Bonding in Metal Carbonyls	3
1.3 Generation and Ionization of Gas Phase Clusters	6
1.4 Studies of Metal Clusters and complexes in the gas phase.....	7
1.5 References	16
2 EXPERIMENTAL	51
2.1 References	70
3 PHOTODISSOCIATION OF YTTRIUM AND LANTHANUM OXIDE	
CLUSTER CATIONS	73
3.1 Abstract	74
3.2 Introduction	74
3.3 Experimental	78
3.4 Results and Discussion	79
3.5 Conclusions	95
3.6 Acknowledgements.....	96
3.7 References	97

4	MASS SPECTRA AND PHOTODISSOCIATION OF INDIUM OXIDE	
	(In _n O _m ⁺) CLUSTER CATIONS	120
	4.1 Abstract	121
	4.2 Introduction	121
	4.3 Experimental	124
	4.4 Results and Discussion	125
	4.5 Conclusion.....	131
	4.6 Acknowledgements.....	131
	4.7 References	132
5	INFRARED SPECTROSCOPY AND STRUCTURES OF MANGANESE	
	CARBONYL CATIONS, Mn(CO) _n ⁺ (n=1-9)	145
	5.1 Abstract	146
	5.2 Introduction	149
	5.3 Experimental	149
	5.4 Results and Discussion	151
	5.5 Conclusion.....	162
	5.6 Acknowledgements.....	163
	5.7 References	164
6	INFRARED SPECTROSCOPY OF COPPER AND GOLD CARBONYL	
	CATIONS: NONCLASSICAL CARBONYLS.....	183
	6.1 Abstract	184
	6.2 Introduction	184
	6.3 Experimental	187

6.4 Results and Discussion	189
6.5 Conclusion.....	200
6.6 Acknowledgements.....	201
6.7 References	202
7 INFRARED PHOTODISSOCIATION SPECTROSCOPY OF BENZENE	
VANADIUM CARBONYL CATIONS, bz-V ⁺ -(CO) _n	225
6.1 Abstract	226
6.2 Introduction	226
6.3 Experimental	228
6.4 Results and Discussion	230
6.5 Conclusion.....	237
6.6 Acknowledgements.....	238
6.7 References	239
8 CONCLUSIONS.....	254
APPENDICES	
A PHOTODISSOCIATION OF YTTRIUM AND LANTHANUM OXIDE	
CLUSTER CATIONS STRUCTURES, ENERGIES, AND	
FREQUENCIES.....	259
B INFRARED SPECTROSCOPY AND STRUCTURES OF MANGANESE	
CARBONYL CATIONS, Mn(CO) _n ⁺ (n=1-9) CALCULATED	
STRUCTURES, ENERGETICS, AND VIBRATIONS	276

C	INFRARED SPECTROSCOPY AND STRUCTURES OF COPPER CARBONYL CATIONS, $\text{Cu}(\text{CO})_{n+}$ ($n=1-8$) CALCULATED STRUCTURES, ENERGETICS, AND VIBRATIONS	319
D	INFRARED PHOTODISSOCIATION SPECTROSCOPY AND STRUCTURES OF BENZENE VANADIUM CARBONYL CATIONS, $\text{bz-V}^+(\text{CO})_n$ CALCULATED STRUCTURES, ENERGETICS, AND VIBRATIONS	337

CHAPTER 1

INTRODUCTION

Metals have always played fundamental roles in chemistry. The first known pure elements were metals, as the noble metals are found in their elemental form in nature. Metals are commonly found as ions due to their low ionization potentials and thus readily donate their valence electrons to form bonds [1-3]. Metal ions play fundamental roles in catalysis, organometallic chemistry, biological systems, atmospheric chemistry and astrophysical chemistry. Transition metals are integral to industrial catalysis, with the metals serving as heterogeneous catalysts, homogeneous catalysts, and as supports in both the pure and oxide form [4-8]. The Fischer-Tropsch catalyst, for example, is composed of small crystals of transition metals supported on an inert surface, such as silica [9]. Even gold, nearly unreactive in the bulk, serves as a highly active catalyst for the oxidation of carbon monoxide when gold nanoparticles are supported on an oxide surface [10]. Many enzymes and proteins feature transition metals in their active sites, which govern their function and chemistry [11-13]. Many diseases are thought to be related to dysfunction in the body's transition metal chemistry [14].

All metals, like all other elements, have a stellar origin and the bombardment of the Earth by meteors introduces metal ions into the atmosphere, which drives some atmospheric reactions [15-17]. Other metals still in space, such as metal-carbides and metal-polyaromatic hydrocarbon complexes (PAHs), may act as seed materials for condensation reactions in the stellar and interstellar medium [18-21]. With metal ions

playing such a rich and varied role in the chemical processes of the universe, their study is of great interest. Gas phase studies allow for the fundamental interactions of these systems to be probed without interference from the various interactions that occur in the condensed phase. Additionally, gas phase experiments enable the study of complexes that are not stable at room temperature. These gas phase complexes serve as excellent model systems to expand our understanding of metal-ligand and metal-cluster bonding. Experimental measurements can be compared to theoretical calculations, many of which have difficulty accurately predicting the properties of transition metal complexes, due to the high number of electrons and the multiple possible configurations. The work in this dissertation focuses on fixed frequency ultraviolet-visible (UV/Vis) dissociation studies of metal oxide clusters and infrared spectroscopy studies of transition metal carbonyl complexes, including mixed carbonyl and benzene systems. All these systems are catalytically relevant, and their study in the gas phase provides insight into their fundamental properties. UV/Vis studies aid in the determination of the stoichiometries of stable clusters, and infrared spectroscopic studies help elucidate the structures, coordination numbers, and electronic configuration of the carbonyl complexes studied. These experimental data are compared to density functional theory (DFT) calculations to provide insights into the structure and bonding properties of these systems.

1.1 Chemistry and Bonding of Metal Oxides

Nearly all metals are found in nature in their oxide form. Metal oxides are widely used in catalysis, electronics, ceramics, and magnetic materials [22-29]. Transition metal oxides often have multiple stable oxidation states, which makes them valuable in catalytic oxidation applications and electronics [25]. Metal oxides also exhibit

fascinating properties on the nanoscale. Very small metal oxide particles often demonstrate properties quite different from those of the bulk. There has been tremendous interest in application of metal oxide clusters in magnetism, catalysis, and biotechnology [30-36]. Increased relative surface area of small particle and differences in bonding on the nanoscale play a crucial role in the difference in properties [37]. There is great interest in the bonding, reactivity, and stabilities of small metal oxide clusters. Transition metal oxide bonding is usually understood in terms of localized ionic bonding, but main group metal oxide bonding is often understood by electron counting rules such as Wade's Rules [41]. Transition metal oxide clusters usually have sufficient electrons to allow for metal-oxygen bonding networks and conventional oxidation states. Main group oxides, however, are often electron deficient and must share electrons across a polyhedral framework to maximize electron density on the interior of the cluster. Gas phase studies of metal oxide nanoparticles can provide information on the bonding and identify particularly stable clusters, which may be interesting for future isolation.

1.2 Chemistry and Bonding in Metal Carbonyls

Transition metal carbonyls are significant in organometallic and inorganic chemistry and provide classic examples of bonding [1,42,43]. They are valuable in many synthetic schemes and catalysis [6]. Among other reactions, transition metals and carbon monoxide are involved hydroformylation, the Fischer-Tropsch synthesis, the synthesis of acetic acid, and the water-gas shift reaction [6]. Mixed "piano stool" complexes, with an aromatic molecule such as benzene as the top and carbonyl "legs" are involved in many industrial catalysis processes as well [1,6].

The strong binding of carbon monoxide in transition metal carbonyls can be viewed on a basic level in terms of the 18 electron rule [1,42]. Most stable carbonyl complexes adhere to this rule, where the carbonyl contributes two electrons and lead to a filled valence shell of 18 electrons. Many metal carbonyl complexes are multinuclear, having more than one metal atom, which share electrons via metal-metal bonding. One example is manganese carbonyl, stable at room temperature as $\text{Mn}_2(\text{CO})_{10}$. There are stable metal carbonyl complexes that do not obey the 18 electron rule, such as $\text{V}(\text{CO})_6$, which has 17 electrons.

The 18 electron rule is only a starting point in understanding metal carbonyl bonding. As noted, some complexes do not follow the 18 electron rule. It also does not address the spectral shifts of the carbonyl vibration observed in the infrared and the variable bond lengths measured in different solid metal carbonyl complexes. The bonding in metal carbonyls can be further understood through the Dewar Chatt Duncanson model of bonding [1,44-47]. Carbonyls generally bond to metals through the carbon terminus, and binding occurs through two simultaneous contributions. There is an on-axis σ -type interaction, where electron density is donated from the HOMO of the carbonyl into the empty metal orbitals. The 5σ HOMO of CO has partially antibonding character, and removing electron density from this orbital strengthens the C-O bond. At the same time, π -type bonding occurs when electrons are donated from the partially filled d-orbitals on the metal into the antibonding π^* LUMO of the CO. This results in a weakened C-O bond. In frequency terms, σ -bonding causes a blue shift (higher energy bonds) and π -type bonding causes a red-shift (lower energy bonds). In most carbonyl

complexes, dubbed “classical” carbonyls, π -type bonding dominates and the carbonyl stretching frequency (ν_{CO}) is lowered from the gas phase value for free CO of 2143 cm^{-1} .

There are a growing number of metal carbonyls that are “non-classical”, that is, featuring shortened C-O bonds and blue-shifted carbonyl stretches [48-52]. The very first carbonyl complex synthesized, $\text{Pt}(\text{CO})_2\text{Cl}_2$ is actually non-classical [43]. These non-classical complexes usually feature filled d-shells which cannot donate or accept charge effectively, leading to the domination of σ donation over π backbonding. The binding in these complexes has been studied theoretically by several groups [53-57]. A study by Lupinetti and coworkers on the effect of a charge on C-O indicates that the positive charge polarizes the carbonyl on the carbon end, resulting in a more homogeneous electron distribution than free CO [58]. This results in a blue-shift of the carbonyl stretch. This effect is actually present in *all* metal carbonyl systems, but is typically overwhelmed by the red-shift caused by π backbonding.

The charge on the metal has been observed to play a significant role in the bonding of these systems. Greater electron density on the metal center is understood to cause weakened C-O bonding through increased π backbonding. Various isoelectronic series have been studied in the condensed phase, which illustrate this behavior. The isoelectronic series $\text{Ni}(\text{CO})_4$, $\text{Co}(\text{CO})_4^-$, and $\text{Fe}(\text{CO})_4^{2-}$, which have CO stretching frequencies of 2094, 1946, and 1799 cm^{-1} respectively, is an excellent example [59-61]. Cationic species have more tightly bound d electrons, which inhibits backbonding. We have observed this in studies of gas phase $\text{Co}(\text{CO})_5^+$, whose bands are blue-shifted nearly 100 cm^{-1} from those of its isoelectronic analogue $\text{Fe}(\text{CO})_5^+$ [62,63]. Recent ab initio calculations suggest that metal charge may play an important role in the polarization and

electron density distribution of the CO orbitals, but relatively few isolated gas phase metal carbonyl cations have been studied to investigate this idea [64].

1.3 Generation and Ionization of Gas Phase clusters

There are several issues that must be addressed to study gas phase ions. Complexes must first be introduced into the gas phase, and they must also be ionized. Producing cold ions is also highly desirable for spectroscopic studies. A few transition metal compounds have a high vapor pressure, which can be entrained in a molecular beam. Most transition metals are not so simple to vaporize. One approach is to simply heat them to their boiling point in a Knudsen diffusion oven, and some groups have taken this approach for transition metals [65]. This method is limited to relatively low boiling point metals and by modest cooling potential. High energy particle bombardment has been used in some studies [66]. Laser vaporization is now the most widely employed method to generate transition metal clusters in the gas phase [66-68], due to the high sample density created, high cooling potential, the wide availability of pulsed lasers, and the ability to create ions directly in the source.

While laser vaporization can produce ions directly, some other techniques do not, and some laser vaporization studies also employ other ionization techniques. Electron impact (EI) tend to cause fragmentation, making study of weakly bound systems difficult [69-70]. They are also limited to high vapor pressure or low melting point materials, eliminating most transition metals. Electrical discharge sources can produce a continuous beam of ions, but this results in low instantaneous ion densities [69,71]. Their internal energies are usually high, even when cooled by supersonic expansions[72-74]. They are also limited to highly conductive materials, which is not an issue for pure metals but

potentially a problem for metal oxide systems. Ion-molecule reactions can be used to ionize and grow transition metal complexes, but this technique is not ubiquitous and requires considerable caution when analyzing unknown metal complexes [75].

Complexes can also be photoionized, but this tends to produce hotter complexes than those produced directly in a laser vaporization source, which leads to broader spectra [67].

Laser vaporization coupled with pulsed nozzles allows for the creation of high densities of cold neutrals and ions. Laser vaporization was initially used to generate neutral metal clusters, which were subsequently ionized by photoionized, but it is also possible to sample ions from the laser plasma. The ions produced directly in the laser plasma are initially hot, but are cooled much more efficiently in pulsed nozzle expansions than with EI. Our group and others have shown that it is possible to produce metal ion complexes with very low internal temperatures using this technique [76-80]. It is also convenient to introduce ligands in this setup, simply by seeding them into the expansion gas. Laser vaporization produces fairly high densities of ions, increasing signal levels [81,82]. These factors make vaporization in pulsed nozzles sources an excellent technique for the spectroscopic study of transition metal complexes.

1.4 Studies of Metal clusters and complexes in the gas phase

Metal complexes have been studied in the gas phase for more than 50 years. Many experiments have used mass spectrometric techniques. The reactivities and thermodynamics of metal cluster ions and metal ion ligand have been studied extensively [83-91]. Early molecular beam experiments studied small transition metal clusters and larger clusters of alkali metals [92,93]. Collision induced dissociation (CID) [94,95],

radiative association techniques [96,97], and equilibrium mass spectrometry [98,99] can measure the dissociation energies and coordination numbers of metal and metal-ligand complexes. High energy atom bombardment has been used to study the metastable decay of metal oxide and other systems [100]. Fixed frequency dissociation studies can reveal fragmentation pathways, stable fragment ions, and occasionally photochemistry and charge transfer processes [87,101,102]. Our group has used fixed frequency techniques to study pure metal clusters like Te_n^+ and Sn_n^+ , metal alloys such as Pb_nSb_m^+ and Bi_nCr_m^+ , various metal oxide systems, metal carbides, and metal-ligand complexes including M^+ -(benzene) $_n$ and M^+ -(coronene) $_n$ [101,102]. Castleman and coworkers have studied the mass spectrometry and collisional dissociation patterns of oxide clusters and various alloy clusters [103,104]. Bernstein and coworkers have used ultraviolet photoionization to study the mass spectra of metal oxide systems [105]. These techniques are valuable for obtaining stoichiometric information, but they cannot fully reveal structural information, electronic states, or coordination numbers. This information can be revealed by spectroscopic measurements.

Obtaining spectroscopic information on gas phase metal complexes can be challenging. Ion densities are typically low, making traditional absorption techniques infeasible. Some alternatives, like cavity ring down spectroscopy [106,107], have been created to increase the effective path length and thus the signal levels. Ion traps have been used to increase ion densities [108,109]. Matrix isolation spectroscopy allows for the accumulation of complexes of interest in a frozen rare gas matrix. Small metal oxides and various metal carbonyl systems have been studied in the infrared using this technique [110,111]. However, matrix isolation does not allow for size selection and matrix shifts

perturb the spectra [111]. One excellent family of techniques is “action” spectroscopy, where some secondary signal carrier is observed to generate spectra [112]. Action spectroscopy often works on a zero background, leading to greatly enhanced signal to noise. Many studies have used electronic resonance enhanced photodissociation (REPD) spectroscopy in the ultraviolet and visible regions (UV-Vis) [113-119]. There are practical benefits to working in this frequency regime, as these regions are accessible with good power using tunable dye lasers and visible Optical Parametric Oscillator (OPO) laser systems. Many have focused on the spectroscopy of a single metal ion bound to one molecule or a noble gas atom. These systems are accessible with the previously mentioned light sources, and tend to have their transitions relatively near the known metal atomic transitions. Several groups have studied the electronic spectroscopy of metal ions systems for structural and electronic information. Our group has studied main group metal interactions with ligands such as CO₂, N₂, H₂O, and noble gases [119]. Fuke and co-workers [120], along with Kleiber and coworkers [116], have studied main group metals bound to other ligands. Other groups, including Brucat and co-workers [115], have studied transition metal interactions with small molecules.

Transition metal-ligand complexes are particularly interesting due to the low lying excited states available for bonding. The electronic spectra of metal-ion complexes with a single ligand often contain vibrational bands. Analysis of the vibrational structure can be used to determine the binding energy of the complexes. Rotational structure is present in some spectra, and can be analyzed to give accurate structural parameters. Optical spectroscopy is an effective tool to examine the interplay between ionic and covalent bonding forces, which are often prevalent in metal-molecule complexes.

While electronic REPD spectroscopy is attractive for many systems, it does have disadvantages. The most fundamental issue is that complexes with more than one ligand are prone to predissociation, which leads to broad, featureless spectra. Additionally, UV-Vis light has enough energy to cause photochemical reactions in some systems.

Although photochemical reactions are an interesting topic in chemistry, they are difficult to study with electronic spectroscopy. The low lying excited states that make transition metal chemistry so interesting can also add complexity to the spectrum. Two alternative techniques are mass analyzed threshold ionization spectroscopy (MATI) [121], and zero electron kinetic energy photoelectron spectroscopy (ZEKE) [121].

ZEKE and MATI spectroscopy are attractive alternative techniques for probing the ground state of metal-ligand complexes. Several groups have studied such complexes [122-126]. ZEKE spectroscopy has also been used for some ions [127-129]. ZEKE can provide rotationally resolved spectra for some systems, in which case the geometric structures and electronic states can be determined. Our group has studied Al^+Ar and $\text{Al}^+\text{H}_2\text{O}$ using ZEKE [124]. Yang and coworkers have studied many pure metal, metal oxide, and metal ligand systems [122]. ZEKE and MATI have limitations as well. They usually require Franck-Condon factor calculations, since many ions have significantly different structures from their corresponding neutrals. The biggest limitation is that size selection is not possible.

Infrared spectroscopy overcomes many of these limitations. Infrared photodissociation (IRPD) spectroscopy elucidates structure, coordination numbers, and electronic states. The photons are generally of low enough energy that photochemistry is avoided. It can be employed on systems with multiple ligands, and even multiple types

of ligands. It can be applied to metallic and non-metallic systems, both ions and neutrals. This field developed somewhat slower than UV/Vis spectroscopy due to the lack of intense, tunable light sources. Early experiments demonstrated IRPD using line tunable CO₂ lasers, proving that vibrational spectra of metal-ligand systems could be obtained with this technique [130-136]. However, the narrow tuning range (line tunable from 9-11 μm) significantly limited these studies and the spectra had very poor resolution. Infrared free electron lasers (FELs), developed in the 1970s, and infrared optical parametric oscillator/amplifier (OPO/OPA) systems brought infrared spectroscopy into the forefront by offering good power, resolution, and tunability. IR free electron lasers generate tunable light from roughly 200-1800 cm^{-1} . Our group has collaborated with Meijer and co-workers to study metal-oxides, metal-carbides, and metal-benzene systems using a free electron source [137,138]. Maitre and co-workers and Meijer and co-workers have studied metal oxide and metal-ligand systems using this source as well [139,140]. FELs are a considerable expense to build and operate, and the spectral resolution is rather poor, usually $>20 \text{ cm}^{-1}$.

Benchtop OPO/OPA systems offer an alternative. OPO/OPA systems, depending on the crystals used, can cover from 800 cm^{-1} to 4500 cm^{-1} , with linewidths around 1 cm^{-1} . Lisy first used these systems to study alkali and alkali earth metal systems [141], and Inokuchi and co-workers have studied similar complexes [142]. Johnson and coworkers have studied various systems using OPO/OPA systems, including water clusters [143]. Our group has studied main group and transition metal cation-ligand complexes, with ligands including benzene [144], water [145], nitrogen [146], acetylene

[147], carbon dioxide [148], and carbon monoxide [149]. We have been able to learn a great deal about the bonding and structure of these systems.

However, infrared photodissociation does have certain limitations [150]. The complex must be able to fragment under infrared excitation for a signal to be observed. Complexes absorb energy in the ligand vibrational coordinate, which is transferred through intramolecular vibrational redistribution (IVR) into other vibrational coordinates. If energy is transferred into a coordinate with a ligand binding energy less than that of the photon energy, fragmentation will occur. However, even if a complex is weakly bound enough to fragment, the fragmentation must occur within the timescale of the experiment to be detected. Large complexes have many possible coordinates for energy transfer, which increases their lifetime. In some cases they do not dissociate within the experimental timescale and the spectra cannot be measured. Small complexes are troublesome to probe with IRPD for different reasons. The per-ligand binding energies can be quite high, often greater than the energy of one (or even several) infrared photons. These complexes could conceivably dissociate through multi-photon excitation, but this is inefficient due to low laser power in our OPO system and anharmonicity at higher vibrational levels in small complexes, which can make resonant absorption of the second photon impossible [131]. As additional ligands are added, the per-ligand binding energy generally decreases, but quite a few ligands can be added in some cases before the binding energy is less than the photon energy. Once the first solvation shell is filled, the binding energy of external ligands is generally much lower, on the order of the ligand-ligand dimer bonding energy. In this case, the complex dissociates readily. Much of the

particularly interesting information in metal-ligand systems comes from studying the first solvation shell interactions, and alternate techniques must be employed to do so.

The method of “rare-gas tagging” allows for the study of small, strongly bound complexes by attaching a weakly bound “messenger” atom [151.152]. The Y.T. Lee group was one of the early practitioners of this technique, utilizing H₂ and N₂ as tagging molecules, along with neon [153]. Many groups now utilize rare gas atoms as tags [154-156], since these generally cause less perturbation on the system. Our group has studied various strongly bound ion-molecules complexes with this technique [157-162]. The rare gas atom binds electrostatically, through a charge-induced dipole interaction. This leads to binding energies that are usually quite low, on the order of a few thousand cm⁻¹ for argon. This is usually enough to allow for dissociation through IVR excitation of the rare gas coordinate. The addition of the rare gas also increases the state density and makes it more likely that IVR will transfer energy to this coordinate. However, the argon does not strongly couple to the complex in some systems and fragmentation is not observed even when photon energies are in excess of the binding energy. These “tagged” complexes usually give an excellent approximation of the spectrum of the neat complex, but we have observed significant perturbations in some systems.

Theoretical calculations are an excellent complement to spectroscopy. Spectroscopic measurements alone cannot fully elucidate bonding and structure, without comparison to theory. The number of bands gives some clue to the symmetry and structure. The band positions can give hints about the bond length in some systems. The C-O stretch of metal carbonyls red-shift from the gas phase CO stretch value when the C-O bond length increases, and blue-shifts when the C-O bond length increases [163]. But

without theoretical calculations, we cannot really identify the electronic configurations or the exact structures in most cases. Density functional theory (DFT) calculations are an excellent tool for elucidating the structure, electronic configuration, and bonding details of transition metal-ligand systems. High end *ab initio* methods like Couple Cluster Singles and Doubles (CCSD) and MultiConfiguration Interaction modified pair coupled function (MCI), or Moller-Plesset perturbation theory (MP2) are attractive for high accuracy calculations, but they are difficult to apply to transition metal systems due to the large number of electrons, the large number of spin states available, and the resulting enormous computational cost. Several groups have performed such calculations [164-166]. DFT can produce reasonably accurate calculations, even for large metal-ligand complexes, at fairly reasonable computational cost [167]. Both metal oxide clusters and metal carbonyl complexes have been extensively studied by theory [168-181].

Density functional theory does have drawbacks [182]. Transition metals frequently have low-lying excited states, which are difficult to determine experimentally. DFT often miscalculates the energy differences between electronic states, often favoring low spin complexes [182]. It also has difficulty at accurately calculating properties of van der Waals molecules and complexes with purely electrostatic bonding [182]. DFT is simply not designed to treat the dispersion forces which govern bonding in such systems. The argon tagged complexes studied in this work are a difficult problem with DFT, and the results must be analyzed with caution. Even with these limitations, DFT has proven to be an excellent tool for investigating the structures of metal-oxide clusters, and helping to determine the structure and electronic configuration of the metal carbonyl complexes studied in this work. Comparisons of IRPD spectroscopy to theoretical calculations have

yielded a great deal of information which has enhanced our understanding of the bonding of these systems.

This work uses fixed frequency photodissociation and DFT calculations to study the bonding of several metal oxide systems. Fragmentation patterns are used to determine the stoichiometries of particularly stable clusters. Additional studies use IRPD techniques to study the carbonyl systems of manganese, copper, and gold cations, along with mixed vanadium carbonyl benzene systems. These systems are excellent models for catalytically relevant systems and give insight into the fundamental bonding in these systems. The rare gas tagging technique is used to acquire spectra for the smaller complexes in the homoleptic systems. Vibrational excitation occurs in the fundamental carbonyl stretching region ($2000\text{-}2300\text{ cm}^{-1}$) for all four systems. The coordination numbers are determined for each system, and comparison to DFT calculations helps elucidate the structures and electronic configurations.

1.5 References

- (1) Cotton, F. A.; Wilkinson, G.; Murillo, C. A.; Bochmann, M. *Advanced Inorganic Chemistry*, 6th ed. John Wiley, New York, **1999**.
- (2) Huheey, J. E.; Keiter, E. A.; Keiter, R. L. *Inorganic Chemistry*, 4th ed., HarperCollins, New York **1993**.
- (3) Shriver, D.; Atkins, P. *Inorganic Chemistry*, 3rd ed., W. H. Freeman and Company, New York **1999**.
- (4) Heck, R. F. *Organotransition Metal Chemistry*; Academic Press: New York, 1974.
- (5) Jolly, P. W.; Wilke, G. *The Organic Chemistry of Nickel*; John Wiley: New York, 1974.
- (6) Somorjai, G. A. *Introduction to Surface Chemistry and Catalysis*; John Wiley: New York, 1994.
- (7) Henrich, V.E.; Cox, P.A. *The Surface Science of Metal Oxides*, Royal Society of Chemistry, Cambridge, 1994.
- (8) *The Surface Science of Metal Oxides*, Faraday Discussions of the Royal Society of Chemistry, Cambridge, 1999.
- (9) Mills, G.A., Steffgen, F.W. *Catal. Rev.* **1973**, 8, 159
- (10) Haruta, M. *Chem. Rec.* **2003**, 3, 75
- (11) *Iron-Sulfur Proteins*; Academic Press: San Diego, 1999.
- (12) a) Walters, E. M.; Johnson, M. K. *Photosynthesis Research* **2004**, 79, 249.
b) Jameson, G. N. L.; Walters, E. M.; Manieri, W.; Schuermann, P.; Johnson, M. K.; Huynh, B. H. *J. Am. Chem. Soc.* **2003**, 125, 1146.

- (13) a) Ma, J.C.; Dougherty, D.A. *Chem. Rev.* **1997**, *97*, 1303. b) Dougherty, D.A. *Science* **1996**, *271*, 163.
- (14) *Metal Ions and Neurodegenerative Disorders*; World Scientific Publishing: New York, 2004
- (15) Plane, J.M.C.; *Int. Rev. Phys. Chem.* **1991**, *10*, 55.
- (16) a) Gardner, J.A.; Viereck, R.A.; Murad, E.; Knecht, D.J., Pike, C.P.; Broadfoot, A.L.; Anderson, E.R. *Geophys. Res. Lett.* **1995**, *22*, 2119. b) McNeil, W.J.; Lai, S.T., Murad, E. *J. Geophys. Res.* **1996**, *101*, 5251. c) Viereck, R.A.; Murad, E.; Lai, S.T.; Knecht, D.J.; Pike, C.P.; Gardner, J.A.; Broadfoot, A.L.; Anderson, E.R.; McNeil, W.J. *Adv. Space Res.* **1996**, *18*, 61. d) McNeil, W.J.; Lai, S.T.; Murad, E. *J. Geophys. Res.* **1998**, *103*, 10899.
- (17) Lyons, J.R. *Science.* **1995**, *267*, 648.
- (18) Millar, T.J.; Williams, D.A., eds. *Dust and Chemistry in Astronomy*, Institute of Physics, London, 1993.
- (19) Henning, T.; *Chem. Soc. Rev.* **1998**, *27*, 315.
- (20) a) Chaudret, B.; Le Beuze, A.; Rabaa, H.; Saillard, J.Y.; Serra, G. *New J. Chem.* **1991**, *15*, 791. b) Serra, G.; Chaudret, B.; Saillard, J.Y.; Le Beuze, A.; Rabaa, H.; Ristorcelli, I.; Klotz A. *Astron. Astrophys.*, **1992**, *260*, 489. c) Marty, P.; Serra, G.; Chaudret, B.; Ristorcelli, I. *Astron. Astrophys.* **1994**, *282*, 916. d) Klotz, A; Marty, P.; Boissel, P.; Serra, G.; Chaudret, B.; Daudey, J.P. *Astron. Astrophys.* **1995**, *304*, 520. e) Klotz, A; Marty, P.; Boissel, P.; De Caro, D.; Serra, G.; Mascetti, J.; De Parseval, P.; Derouault, J.; Duadey, J.P.; Chaudret, B. *Planet. Space Sci.* **1996**, *44*, 957

- (21) Patrie, S.; Becker, H.; Baranov, V.; Bohme, D.K. *Astrophys. J.* **1997**, *476*, 191.
- (22) Cox, P. A., *Transition Metal Oxides*, Clarendon Press, Oxford, 1992.
- (23) Rao, C. N.; Raveau, B. *Transition Metal Oxides*, John Wiley, New York, 1998.
- (24) Hayashi, C.; Uyeda, R.; Tasaki, A., *Ultra-Fine Particles*; Noyes, Westwood, 1997.
- (25) Henrich, V. E.; Cox, P. A., *The Surface Science of Metal Oxides*; Cambridge University Press, Cambridge, 1994.
- (26) Somorjai, G. A., *Introduction to Surface Chemistry and Catalysis*; Wiley-Interscience, New York, 1994.
- (27) Gates, B. C. *Chem. Rev.* **1995**, *95*, 511.
- (28) a) Rainer, D. R.; Goodman, D. W. *J. Mol. Catal. A: Chem.* **1998**, *131*, 259. b) St. Clair, T. P.; Goodman, D. W. *Top. Catal.* **2000**, *13*, 5. c) Wallace, W. T.; Min, B. K.; Goodman, D. W. *Top. Catal.* **2005**, *34*, 17. d) Chen, M. S.; Goodman, D. W. *Acc. Chem. Res.* **2006**, *39*, 739.
- (29) a) Wachs, I. E.; Briand, L. E.; Jehng, J. M.; Burcham, L.; Gao, X. T. *Catal. Today* **2000**, *57*, 323. b) Chen, Y. S.; Wachs, I. E. *J. Catal.* **2003**, *217*, 468. c) Wachs, I. E. *Catal. Today* **2005**, *100*, 79. d) Wachs, I. E.; Jehng, J. M.; Ueda, W. *J. Phys. Chem. B* **2005**, *109*, 2275. e) Tian, H. J.; Ross, E. I.; Wachs, I. E., *J. Phys. Chem. B* **2006**, *110*, 9593.
- (30) Pope, M.T; Müller, A. *Poloyoxometalate Chemistry From Topology via Self-Assembly to Applications*; Kluwer: Boston, 2001.

- (31) Crans, D.C.; Smee, J.J.; Gaidamauskas, E.; Yang, L.Q. *Chem. Rev.* **2004**, *104*, 849.
- (32) a) Rockenberger, J.; Scher, E.C.; Alivisatos, A.P. *J. Am. Chem. Soc.* **1999**, *121*, 11595 b) Puentes, V.F.; Krishnan, K.M.; Alivisatos, A.P. *Science* **2001**, *291*, 2115. c) Nolting, F.; Luning, J.; Rockenberger, J.; Hu, J.; Alivisatos, A.P. *Surf. Rev. Lett.* **2002**, *9*, 437. d) Jun, Y.W.; Casula, M.F.; Sim, J.H.; Kim, S.Y.; Cheon, J.; Alivisatos, A.P. *J. Am. Chem. Soc.* **2003**, *125*, 15981. e) Casula, M.F.; Jun, Y.W.; Zaziski, D.J.; Chan, E.M.; Corrias, A.; Alivisatos, A.P. *J. Am. Chem. Soc.* **2006**, *128*, 1675.
- (33) Ayers, T.M.; Fye, J.L.; Li, Q.; Duncan, M.A. *J. Cluster Sci.* **2003**, *14*, 97.
- (34) Cushings, B.L.; Kolesnichenko, V.L.; O'Connor, C.J. *Chem. Rev.* **2004**, *104*, 3893.
- (35) Fernandez-Garcia, M.; Martinez-Arias, A.; Hanson, J.C.; Rodriguez, J.A. *Chem. Rev.* **2004**, *104*, 4063.
- (36) Stepanov, A.L.; Boura, G.; Gartzza, M.; Osinb, Yu.N.; Reinholdta, A.; Kreibig, U. *Vacuum* **2004**, *64*, 9.
- (37) Nanoparticles; Schmid, G., Ed.; WILEY-VCH: Weinheim, 2004.
- (38) K.S. Molek, T.D. Jaeger, M.A. Duncan, J. *Chem. Phys.* *123* (2005) 144313
- (39) K.S. Molek, Z.D. Reed, A.M. Ricks, M.A. Duncan *J. Phys. Chem. A* *111* (2007) 8080
- (40) Z.D. Reed, M.A. Duncan *J. Phys. Chem. A* *112* (2008) 5354
- (41) K. Wade, K. *Adv. Inorg. Chem. Radiochem.* *18* (1976) 1

- (42) Huheey, J. E.; Keiter, E. A.; Keiter, R. L. *Inorganic Chemistry Principles of Structure and Reactivity*, Harper Collins, New York, 1993.
- (43) Wrighton, M. "The Photochemistry of Metal Carbonyls," *Chem. Rev.* **1974**, *74*, 401.
- (44) Frenking, G.; Fröhlich, N. "The Nature of the Bonding in Transition-Metal Compounds," *Chem. Rev.* **2000**, *100*, 717.
- (45) Zhou, M.; Andrews, L.; Bauschlicher, C. W. "Spectroscopic and Theoretical Investigations of Vibrational Frequencies in Binary Unsaturated Transition-Metal Carbonyl Cations, Neutrals, and Anions," *Chem. Rev.* **2001**, *101*, 1931.
- (46) Chatt, J.; Duncanson, L.A. *J. Chem. Soc.* **1953**, 2939.
- (47) Dewar, M.J.S. *Bull. Soc. Chim. Fr.* **1951**, *18*, C79
- (48) Schroeder, D.; Hrusak, J.; Hertwig, R. H.; Koch, W.; Schwerdtfeger, P.; Schwarz, H. *Organometallics* **1995**, *14*, 312.
- (49) Schroeder, D.; Schwarz, H.; Hrusak, J.; Pyykko, P. *Inorg. Chem.* **1998**, *37*, 624.
- (50) Willner, H.; Aubke, F. *Inorg. Chem.* **1990**, *29*, 2195.
- (51) a) Willner, H.; Aubke, F. *Inorg. Chem.* **1990**, *29*, 2195. b) Aubke, F. *J. Fluorine Chem.* **1995**, *72*, 195.
- (52) Strauss, S.H. *J. Chem. Soc. Dalton Trans.* **2000**, 1-6
- (53) Huo, C.-H.; Li, Y.-W.; Wu, G.-S.; Beller, M.; Jiao, H. "Structures and energies of $[\text{Co}(\text{CO})_n]^m$ ($m=0, 1+, 1-$) and $\text{HCo}(\text{CO})_n$: Density functional studies," *J. Phys. Chem. A* **2002**, *106*, 12161.
- (54) Barnes, L. A.; Rosi, M.; Bauschlicher, C. W., Jr. *J. Chem. Phys.* **1990**, *93*, 609.

- (55) Veldkamp, A.; Frenking, G. *Organometallics* **1993**, *12*, 4613.
- (56) Dargel, T. K.; Hertwig, R. H.; Koch, W.; Horn, H. *J. Chem. Phys.* **1998**, *108*, 3876.
- (57) Jonas, V.; Thiel, W. *J. Phys. Chem. A* **1999**, *103*, 1381.
- (58) a) Lupinetti, A. J.; Frenking, G.; Strauss, S. H. "Nonclassical Metal Carbonyls," *Angew. Chem. Int. Ed.* **1998**, *37*, 2113. b) Lupinetti, A. J.; Jonas, V.; Thiel, W.; Strauss, S. H.; Frenking, G. "Trends in Molecular Geometries and Bond Strengths of the Homoleptic d10 Metal Carbonyl Cations: A Theoretical Study," *Chem. Eur. J.* **1999**, *5*, 2573. c) Lupinetti, A. J.; Fau, S.; Frenking, G.; Strauss, S. H. "Theoretical Analysis of the Bonding between CO and Positively Charged Atoms," *J. Phys. Chem.* **1997**, *101*, 9551.
- (59) Jones, L. H.; McDowell, R. S.; Goldblatt, M. "Infrared spectra of Cr(CO)₆, Mo(CO)₆ and W(CO)₆ Gas phase," *Inorg. Chem.* **1969**, *28*, 2349.
- (60) Stammerich, H.; Kawai, K.; Tavares, Y.; Krumholz, P.; Behmoiras, J.; Bril, S. "Infrared spectra of Fe(CO)₄²⁻ in aqueous solution," *J. Chem. Phys.* **1960**, *32*, 1482.
- (61) Edgell, W. F.; Lyford, J. I. "Infrared spectra of Co(CO)₄⁻ in DMF solution," *J. Chem. Phys.* **1970**, *52*, 4329.
- (62) Ricks, A.M.; Bakker, J.M.; Douberly, G.E.; Duncan, M.A. *J. Phys. Chem. A.* **2009**, *113*, 4701
- (63) Jang, J. H.; Lee, G. J.; Lee, H.; Xie, Y.; Schaefer, F. H. "Molecular Structures and Vibrational Frequencies of Iron Carbonyls: Fe(CO)₅, Fe₂(CO)₉, and Fe₃(CO)₁₂," *J. Phys. Chem. A.* **1998**, *102*, 5298.

- (64) Goldman, A. S.; Krogh-Jespersen, K. "Why do cationic carbon monoxide complexes have high CO stretching force constants and short CO bonds? Electrostatic effects, not σ bonding," *J. Am. Chem. Soc.* **1996**, *118*, 12159.
- (65) Rockenberger, J.; Scher, E. C.; Alivisatos, A. P. "A new nonhydrolytic single-precursor approach to surfactant-capped nanocrystals of transition metal oxides," *J. Am. Chem. Soc.* 1999, *121*, 11595. Puentes, V. F.; Krishnan, K. M.; Alivisatos, A. P. "Colloidal nanocrystal shape and size control: The case of cobalt," *Science* 2001, *291*, 2115. Nolting, F.; Luning, J.; Rockenberger, J.; Hu, J.; Alivisatos, A. P. "A PEEM study of small agglomerates of colloidal iron oxide nanocrystals," *Surf. Rev. Lett.* 2002, *9*, 437. Jun, Y. W.; Casula, M. F.; Sim, J. H.; Kim, S. Y.; Cheon, J.; Alivisatos, A. P. "Surfactant-assisted elimination of a high energy facet as a means of controlling the shapes of TiO₂ nanocrystals," *J. Am. Chem. Soc.* 2003, *125*, 15981. Casula, M. F.; Jun, Y. W.; Zaziski, D. J.; Chan, E. M.; Corrias, A.; Alivisatos, A. P. "The concept of delayed nucleation in nanocrystal growth demonstrated for the case of iron oxide nanodisks," *J. Am. Chem. Soc.* 2006, *128*, 1675. Farrell, D.; Majetich, S. A.; Wilcoxon, J. P. "Preparation and characterization of monodisperse Fe nanoparticles," *J. Phys. Chem. B* 2003, *107*, 11022.
- (66) a) I. Katakuse, T. Ichihara, Y. Fujita, T. Matsuo, T. Sakurai, and H. Matsuda (1985). *Int. J. M.S. and ion Proc.* 67,229; (b) R. B. Freas and J. E. Campana (1985). *J. Am. Chem. Soc.* 107, 6202; (c) P. Sharpe and C. J. Cassady (1992). *Chem. Phys. Lett.* 191, 111.
- (67) O'Hair, R.A.J.; Khairallah, G.N. *J. Cluster. Sci.* **2004**, *15*, 331)

- (68) S. Keki, L. S. Szilagyi, J. Torok, G. Deak, and M. Zsuga *J. Phys. Chem. B.* 2003, 107, 4818. U. Hild, G. Dietrich, S. Kruckeberg, M. Lindinger, K. Lutzenkirchen, L. Schweikhard, C. Walther, and J. Ziegler (1998). *Phys rev A*, 57, 2786; (b) S. K. Loh, D. A. Hales, and P.B. Armentrout (1986). *Chem. Phys. Lett.* 129, 527; (c) I. G. Dance, K. J. Fisher, and G. D. Willett (1997). *J. Chem. Soc., Dalton Trans.* 15, 2557; (d) K. Koszinowski, D. Schroder, and H. Schwarz (2003). *J. Am. Chem. Soc.* 125, 3676; (e) P. Milani and W.A. Deheer (1990). *Rev. Sci. Instrum.*, 61, 1835; (f) A. Dinca, T. P. Davis, K. J. Fisher, D. R. Smith, and G. D. Willett (1999). *Int. J. Mass Spectrom.* 182/183, 73; (g) J. El Nakat, K. J. Fisher, I. G. Dance, and G. D. Willett (1993). *Inorg Chem.* 32, 1931; 360 O’Hair and Khairallah (h) J. L. Gole, R. Woodward, J. S. Hayden, and D. A. Dixon (1985). *J. Phys. Chem.* 89,4905; (i) T. G. Dietz, M. A. Duncan, D. E. Powers, and R. E. Smalley (1981). *J. Chem. Phys.* 74, 6511; (j) H. Rashidzadeh and B. Guo (1999). *Chem. Phys. Lett.* 310, 466; (k) C. Berg, T. Schindler, M. Kantlehner, G. Niedner-Schatteburg, and V. E. Bondybey (2000). *Chem. Phys.* 262,143.
- (69) Massey, H.S.W. *Electron Collisions with Molecules and Photoionization*, Oxford University Press, Oxford, 1969.
- (70) Johnstone, R.A.W.; Rose, M. E. *Mass Spectrometry for Chemists and Biochemists*, Cambridge University Press, 1996.
- (71) Blausen, B.D., ed. “Chemical Reactions in Electrical Discharges” *Advances in Chemistry Series No. 80*, Am. Chem. Soc., 1969.

- (72) a) Corderman, R.R.; Lineberger, W.C. *Annu. Rev. Phys. Chem.* **1979**, *30*, 347.
 b) Neumark, D.M.; Lykke, K.R.; Anderson, T.; Lineberger, W.C. *J. Chem. Phys.* **1985**, *83*, 4364. c) Leopold, D.; Ho, J.; Lineberger, W.C. *J. Chem. Phys.* **1987**, *86*, 1715. d) Ervin, K.M.; Ho, J.; Lineberger, W.C. *ibid.* **1989**, *91*, 5974. e) Ho, J.; Ervin, K.M.; Lineberger, W.C. *ibid.* **1990**, *93*, 6987.
- (73) a) a) Woods, R. Claude; Dixon, Thomas A.; Saykally, Richard J.; Szanto, Peter G. *Phys. Rev. Lett.* **1975**, *35*, 1269. b) Rosenbaum, Neil H.; Owrutsky, Jeffrey C.; Tack, Leslie M.; Saykally, Richard J. *J. Chem. Phys.* **1986**, *84*, 5308. c) Hovde, David C.; Saykally, Richard J. *J. Chem. Phys.* **1987**, *87*, 4332. d) Coe, J.V.; Saykally, R.J. in *Ion and Cluster Ion Spectroscopy and Structure*, Maier, J.P., ed., Elsevier, Amsterdam, **1989**, 131. e) Petek, H.; Nesbitt, D. J.; Owrutsky, J. C.; Gudeman, C. S.; Yang, X.; Harris, D. O.; Moore, C. B.; Saykally, R. J. *J. Chem. Phys.* **1990**, *92*, 3257. f) Michael, E. A.; Keoshian, C. J.; Anderson, S. K.; Saykally, R. J. *J.Mol. Spec.* **2001**, *208*, 219.
- (74) a) Linnartz, H.; Motylewski, T.; Vaizert, O.; Maier, J. P.; Apponi, A. J.; McCarthy, M. C.; Gottlieb, C. A.; Thaddeus, P. *J. Mol. Spec.* **1999**, *197*, 1.
 b) Tulej, M.; Guethe, F.; Schnaiter, M.; Pachkov, M. V.; Kirkwood, D. A.; Maier, J. P.; Fischer, G. *J. Phys. Chem. A* **1999**, *103*, 9712. c) Pfluger, D.; Motylewski, T.; Linnartz, H.; Sinclair, W. E.; Maier, J. P. *Chem. Phys. Lett.* **2000**, *329*, 29. d) Birza, P.; Motylewski, T.; Khoroshev, D.; Chirokolava, A.; Linnartz, H.; Maier, J. P. *Chem. Phys.* **2002**, *283*, 119. e) Schmidt, T. W.; Ding, H.; Boguslavskiy, A. E.; Pino, T.; Maier, J. P. *J. Phys. Chem. A* **2003**,

- 107, 6550. f) Khoroshev, Dmitriy; Araki, Mitsunori; Kolek, Przemyslaw; Birza, Petre; Chirokolava, Andrei; Maier, John P. *J. Mol. Spec.* **2004**, 227, 81.
- (75) D. L. Vollmer, M.L. Gross, R.J. Waugh, M.I. Bruce, and J.H. Bowie (1994). *Organometallics*, 13, 3564; (b) D. H. Russell, D. Anderson Fredeen, and R. E. Tecklenburg, in D. H. Russell (ed.), *Gas Phase Inorganic Chemistry* (Plenum Press, New York, 1989), pp. 115–135.
- (76) a) Niles, S.; Prinslow, D.A.; Wight, C.A.; Armentrout, P.B. *J. Chem. Phys.* **1990**, 93, 6186. b) Niles, S.; Armentrout, P.B.; Wight, C.A. *Chem. Phys.* **1992**, 165, 143. c) Niles, S.; Prinslow, D.A.; Wight, C.A.; Armentrout, P.B. *J. Chem. Phys.* **1992**, 97, 3115. d) Russon, L.M.; Heidecke, S.A.; Birke, M.K.; Conceicao, J.; Morse, M.D.; Armentrout, P.B. *J. Chem. Phys.* **1994**, 100, 4747.
- (77) a) Willey, K. F.; Cheng, P. Y.; Yeh, C. S.; Robbins, D. L.; Duncan, M. A. *J. Chem. Phys.* **1991**, 95, 6249. b) Yeh, C. S.; Robbins, D. L.; Pilgrim, J. S.; Duncan, M. A. *Chem. Phys. Lett.* **1993**, 206, 509. c) Brock, L. R.; Pilgrim, J. S.; Duncan, M. A. *Chem. Phys. Lett.* **1994**, 230, 93. d) Pilgrim, J. S.; Duncan, M. A. *Chem. Phys. Lett.* **1995**, 232, 335. e) Brock, L. R.; Knight, A. M.; Reddic, J. E.; Pilgrim, J. S.; Duncan, M. A. *J. Chem. Phys.* **1997**, 106, 6268. f) Berry, K. R.; Duncan, M. A. *Chem. Phys. Lett.* **1997**, 279, 44. g) Stangassinger, A.; Knight, A. M.; Duncan, M. A. *J. Phys. Chem. A* **1999**, 103, 1547.

- (78) a) Kirkwood, D.A.; Winkel, J.F.; Stace, A.J. *Chem. Phys. Lett.* **1995**, *247*, 332. b) Woodward, C.A.; Dobson, M.P.; Stace, A.J. *J. Phys. Chem.* **1996**, *100*, 5605. c) Dobson, M.P.; Stace, A.J. *Chem. Comm.* **1996**, *13*, 1533. d) Walker, N.R.; Firth, S.; Stace, A.J. *Chem. Phys. Lett.* **1998**, *292*, 125. e) Kirkwood, D.A.; Stace, A.J. *J. Am. Chem. Soc.* **1998**, *120*, 12316. f) Walker, N.R.; Wright, R.R.; Stace, A.J. *J. Am. Chem. Soc.* **1999**, *121*, 4837. g) Walker, N.R.; Wright, R.R.; Barran, P.E.; Stace, A.J. *Organometallics* **1999**, *18*, 3569. h) Walker, N.R.; Dobson, M.P.; Wright, R.R.; Barran, P.E.; Murrell, J.N.; Stace, A.J. *J. Am. Chem. Soc.* **2000**, *122*, 11138. i) Wright, R.R.; Walker, N.R.; Firth, S.; Stace, A.J. *J. Phys. Chem. A* **2001**, *105*, 54. j) Walker, N.R.; Wright, R.R.; Barran, P.E.; Murrell, J.N.; Stace, A.J. *J. Am. Chem. Soc.* **2001**, *123*, 4223. k) Stace, A. J. *J. Phys. Chem. A* **2002**, *106*, 7993. l) Puskar, L.; Barran, P.E.; Duncombe, B.J.; Chapman, D.; Stace, A.J. *J. Phys. Chem. A* **2005**, *109*, 273. m) Stace, A.J. *Adv. Met. Semicond. Clusters* **2001**, *5*, 121.
- (79) a) Willey, K.F.; Yeh, C.S; Robbins, D.L.; Pilgrim, J.S.; Duncan, M.A. *J. Chem. Phys.* **1992**, *97*, 8886. b) Yeh, C. S.; Willey, K. F.; Robbins, D. L.; Pilgrim, J. S.; Duncan, M. A. *Chem. Phys. Lett.* **1992**, *196*, 233. c) Pilgrim, J. S.; Yeh, C. S.; Duncan, M. A. *Chem. Phys. Lett.* **1993**, *210*, 322. d) Pilgrim, J. S.; Yeh, C. S.; Berry, K. R.; Duncan, M. A. *J. Chem. Phys.* **1994**, *100*, 7945. e) Scurlock, C. T.; Pilgrim, J. S.; Duncan, M. A. *J. Chem. Phys.* **1995**, *103*, 3293. f) Yeh, C. S.; Pilgrim, J. S.; Willey, K. F.; Robbins, D. L.; Duncan, M. A. *Int. Rev. Phys. Chem.* **1994**, *13*, 231. g) Yeh, C. S.; Willey,

- K. F.; Robbins, D. L.; Duncan, M. A. *J. Phys. Chem.* **1992**, *96*, 7833. h) Willey, K. F.; Yeh, C. S.; Robbins, D. L.; Duncan, M. A. *Chem. Phys. Lett.* **1992**, *192*, 179. i) Yeh, C.S.; Willey, K.F.; Robbins, D.L.; Duncan, M.A. *J. Chem. Phys.* **1993**, *98*, 1867. j) Robbins, D.L.; Brock, L.R.; Pilgrim, J.S.; Duncan, M.A. *J. Chem. Phys.* **1995**, *102*, 1481. k) France, M.R.; Pullins, S.H.; Duncan, M.A. *Chem. Phys.* **1998**, *239*, 447. l) Reddic, J.E.; Duncan, M.A. *Chem. Phys. Lett.* **1999**, *312*, 96. m) Reddic, J.E.; Duncan, M.A. *J. Chem. Phys.* **1999**, *110*, 9948.
- (80) a) Scurlock, C.T.; Pullins, S.H.; Reddic, J.E.; Duncan, M.A. *J. Chem. Phys.* **1996**, *104*, 4591. b) Pullins, S.H.; Scurlock, C.T.; Reddic, J.E.; Duncan, M.A. *J. Chem. Phys.* **1996**, *104*, 7518. c) Velasquez, J.; Kirschner, K.N.; Reddic, J.E.; Duncan, M.A. *Chem. Phys. Lett.* **2001**, *343*, 613. d) Reddic, J.E.; Duncan, M.A. *J. Chem. Phys.* **2000**, *112*, 4974. e) Scurlock, C.T.; Pullins, S.H.; Duncan, M.A. *J. Chem. Phys.* **1996**, *105*, 3579. f) Kirschner, K.N.; Ma, B.; Bowen, J.P.; Duncan, M.A. *Chem. Phys. Lett.* **1998**, *295*, 204. g) Pullins, S.H.; Reddic, J.E.; France, M.R.; Duncan, M.A. *J. Chem. Phys.* **1998**, *108*, 2725. h) Weslowski, S. S.; King, R. A.; Schaefer, H. F.; Duncan, M. A. *J. Chem. Phys.* **2000**, *113*, 701. i) France, M. R.; Pullins, S. H.; Duncan, M. A. *J. Chem. Phys.* **1998**, *108*, 7049. j) France, M. R.; Pullins, S. H.; Duncan, M. A. *J. Chem. Phys.* **1998**, *109*, 8842.
- (81) Dietz, T.G.; Duncan, M.A.; Powers, D.E.; Smalley, R.E. *J. Chem. Phys.* **1981**, *74*, 6511

- (82) Brucat, P.J.; Zheng, L.S.; Pattiette, C.L.; Yang, S.; Smalley, R.E. *J. Chem. Phys.* **1986**, *84*, 3078.
- (83) a) Tanaka, K., et al. *Rapid Commun. Mass Sp.* **1988**, *2*, 151. b) Tanka, K. *Angew. Chem. Int. Edit.* **2003**, *42*, 3861.
- (84) a) Dietz, T.G.; Duncan, M.A.; Powers, D.E.; Smalley, R.E. *J. Chem. Phys.* **1981**, *74*, 6511. b) Zheng, L.S.; Brucat, P.J.; Pettiette, C.L.; Yang, S.; Smalley, R.E. *J. Chem. Phys.* **1985**, *83*, 4273. c) Brucat, P.J.; Zheng, L.S.; Pattiette, C.L.; Yang, S.; Smalley, R.E. *J. Chem. Phys.* **1986**, *84*, 3078. d) Zheng, L.S.; Carner, C.M.; Brucat, P.J.; Yang, S.H.; Pettiette, C.L.; Craycraft, M.J.; Smalley, R.E. *J. Chem. Phys.* **1986**, *85*, 1681. e) Chesnovsky, O.; Yang, S.H.; Pettiette, C.L.; Craycraft, M.J.; Liu, Y.; Smalley, R.E. *Chem. Phys. Lett.* **1987**, *138*, 119. f) Yang, S.; Taylor, K.J.; Craycraft, M.J.; Conceicao, J.; Pettiette, C.L.; Chesnovsky, O.; Smalley, R.E. *Chem. Phys. Lett.* **1988**, *144*, 431. g) Chesnovsky, O.; Taylor, K.J.; Conceicao, J.; Smalley, R.E. *Phys. Rev. Lett.* **1990**, *64*, 1785. h) Jin, C.; Taylor, K.J.; Conceicao, J.; Smalley, R.E. *Chem. Phys. Lett.* **1990**, *175*, 17.
- (85) a) Heath J. R.; Cooksy A. L.; Gruebele M. H.; Schmuttenmaer C. A.; Saykally R. J. *Science* **1989**, *244*, 564. b) Heath, J. R.; Sheeks, R. A.; Cooksy, A. L.; Saykally, R. J. *Science* **1990**, *249*, 895. c) Van Orden, A.; Giesen, T. F.; Provencal, R. A.; Hwang, H. J.; Saykally, R. J. *J. Chem. Phys.* **1994**, *101*, 10237. d) Van Orden, Alan; Saykally, Richard J. *Chem. Rev.* **1998**, *98*, 2313. e) Casaes, Raphael; Provencal, Robert; Paul, Joshua; Saykally, Richard J. *J. Chem. Phys.* **2002**, *116*, 6640.

- (86) a) Rohlfing, E. A.; Cox, D. M.; Kaldor, A. *Chem. Phys. Lett.* **1983**, *99*, 161.
b) Rohlfing, E. A.; Cox, D. M.; Kaldor, A. *J. Phys. Chem.* **1984**, *88*, 4497.
c) Rohlfing, E. A.; Cox, D. M.; Kaldor, A. *J. Chem. Phys.* **1984**, *81*, 3322. d)
Trevor, D. J.; Whetten, R. L.; Cox, D. M.; Kaldor, A. *J. Am. Chem. Soc.*
1985, *107*, 518. e) Cox, D. M.; Trevor, D. J.; Reichmann, K. C.; Kaldor, A.
J. Am. Chem. Soc. **1986**, *108*, 2457. f) Trevor, D. J.; Cox, D. M.; Reichmann,
K. C.; Brickman, R. O.; Kaldor, A. *J. Phys. Chem.* **1987**, *91*, 2598. g) Cox,
D. M.; Reichmann, K. C.; Trevor, D. J.; Kaldor, A. *J. Chem. Phys.* **1988**, *88*,
111. h) Eberhardt, W.; Fayet, P.; Cox, D. M.; Fu, Z.; Kaldor, A.; Sherwood,
R.; Sondericker, D. *Phys. Rev. Lett.* **1990**, *64*, 780. i) Heiz, U.; Sherwood,
R.; Cox, D. M.; Kaldor, A.; Yates, J. T., Jr. *J. Phys. Chem.* **1995**, *99*, 8730.
- (87) a) Jacobson, D.B.; Freiser, B.S. *J. Am. Chem. Soc.* **1984**, *106*, 3900. b)
Jacobson, D.B.; Freiser, B.S. *J. Am. Chem. Soc.* **1984**, *106*, 4623. c) Phelps,
D.K.; Gord, J.R.; Freiser, B.S.; Weaver, M.J. *J. Phys. Chem.* **1991**, *95*, 4338.
d) Huang, Y.; Freiser, B.S. *J. Am. Chem. Soc.* **1991**, *113*, 9418. e) Yeh, C.S.;
Byun, Y.G.; Afzaal, S.; Kan, S.Z.; Lee, S.; Freiser, B.S.; Hay, P.J. *J. Am.*
Chem. Soc. **1995**, *117*, 4042. f) Rufus, D.; Ranatunga, A.; Freiser, B.S.
Chem. Phys. Lett. **1995**, *233*, 319. g) Jiao, C.Q.; Freiser, B.S. *J. Phys. Chem.*
1995, *99*, 10723. h) Freiser, B.S. *Organometallic Ion Chemistry*. Kluwer,
Dordrecht, 1996.
- (88) a) Tonkyn, R.; Weisshaar, J.C. *J. Phys. Chem.* **1986**, *90*, 2305. b) Tonkyn,
R.; Weisshaar, J.C. *J. Am. Chem. Soc.* **1986**, *108*, 71280. c) Sappey, A.D.;
Harrington, J.E.; Weisshaar, J.C. *J. Chem. Phys.* **1988**, *88*, 5243. d) Ritter,

- D.; Weisshaar, J.C. *J. Phys. Chem.* **1989**, *93*, 1576. e) Sanders, L.; Hanton, S.D.; Weisshaar, J.C. *J. Chem. Phys.* **1990**, *92*, 3485. f) Weisshaar, J.C. *Acc. Chem. Res.* **1993**, *26*, 213. g) Blomberg, M.; Yi, S.S.; Noll, R.J.; Weisshaar, J.C. *J. Phys. Chem. A* **1999**, *103*, 7254. h) Reichert, E.L.; Weisshaar, J.C. *J. Phys. Chem. A* **2002**, *106*, 5563.
- (89) a) Leuchtner, R. E.; Harms, A. C.; Castleman, A. W., Jr. *J. Chem. Phys.* **1990**, *92*, 6527. b) Guo, B. C.; Kerns, K. P.; Castleman, A. W., Jr. *Science* **1992**, *255*, 1411. c) Guo, B. C.; Castleman, A. W., Jr. *J. Am. Chem. Soc.* **1992**, *114*, 6152. d) Cartier, S. F.; May, B. D.; Castleman, A.W., Jr. *J. Am. Chem. Soc.* **1994**, *116*, 5295. e) Kerns, K. P.; Guo, B. C.; Deng, H. T.; Castleman, A. W., Jr. *J. Am. Chem. Soc.* **1995**, *117*, 4026. f) Kerns, K. P.; Guo, B. C.; Deng, H. T.; Castleman, A. W. Jr. *J. Phys. Chem.* **1996**, *100*, 16817. g) Vann, W. D.; Wagner, R. L.; Castleman, A. W. Jr. *J. Phys. Chem. A* **1998**, *102*, 1708. h) Zemski, K. A.; Justes, D. R.; Castleman, A. W., Jr. *J. Phys. Chem. B* **2002**, *106*, 6136.
- (90) a) Beyer, M.; Berg, C.; Görlitzer, H.W.; Schindler, T.; Achatz, U.; Albert, G.; Niedner-Schatteburg, G.; Bondybey, V.E. *J. Am. Chem. Soc.* **1996**, *118*, 7386. b) Beyer, M.; Achatz, U.; Berg, C.; Joos, S.; Niedner-Schatteburg, G.; Bondybey, V.E. *J. Phys. Chem. A* **1999**, *103*, 671. c) Bondybey, V.E.; Beyer, M.K. *Int. Rev. Phys. Chem.* **2002**, *21*, 277. d) Fox, B.S.; Balteanu, I.; Balaj, O.P.; Liu, H.; Beyer, M.K; Bondybey, V.E. *Phys. Chem. Chem. Phys.* **2002**, *4*, 2224. e) Berg C.; Achatz, U.; Beyer, M.; Joos, S.; Albert, G.; Schindler, T.; Niedner-Schattburg, G.; Bondybey, V.E. *Int. J. Mass Spectrom.* **1997**, *167*,

723. f) Berg, C.; Beyer, M.; Achatz, U.; Joos, S.; Niedner-Schattburg, G.; Bondybey, V.E. *Chem. Phys.* **1998**, *239*, 379.
- (91) a) Schalley, C.; Schroeder, D.; Schwarz, H. *Organometallics* **1995**, *14*, 316.
 b) Schwarz, J.; Heinemann, C.; Schwarz, H. *J. Phys. Chem.* **1995**, *99*, 11405.
 c) Schalley, C.A.; Wesendrup, R.; Schroeder, D.; Schwarz, H. *Organometallics* **1996**, *15*, 678. d) Schroeter, K.; Schalley, C.A.; Wesendrup, R.; Schroeder, D.; Schwarz, H. *Organometallics* **1997**, *16*, 986.
 e) Schroeder, D.; Kretzschmar, I.; Schwarz, H.; Rue, C.; Armentrout, P.B. *Inorg. Chem.* **1999**, *38*, 3474. f) Jackson, P.; Harvey, J.N.; Schroeder, D.; Schwarz, H. *Int. J. Mass Spectrom.* **2001**, *204*, 233. g) Schwarz, H. *Ang. Chem., Int. Ed.* **2003**, *42*, 4442.
- (92) Preuss, D.R.; Pace, S.A.; Gole, J.L. *J. Chem. Phys.* **1979**, *71*, 3553
- (93) (a) Leutwyler, S.; Herman, A.; Woste, L.; Schumacher, E. *Chem. Phys.* **1980**, *48*, 253 (b) Herman, A.; Woste, L.; Schumacher, E. *J. Chem. Phys.* **1978**, *68m* 2327
- (94) a) Aristov, N.; Armentrout, P. B. *J. Am. Chem. Soc.* **1986**, *108*, 1806. b) Fisher, E. R.; Armentrout, P. B. *J. Phys. Chem.* **1990**, *94*, 1674. c) Fisher, E. R.; Armentrout, P. B. *J. Phys. Chem.* **1990**, *94*, 1674. d) Tjelta, B. L.; Walter, D.; Armentrout, P. B. *Intl. J. Mass. Spec.* **2001**, *204*, 7. e) Dalleska, N. F.; Honma, K.; Sunderlin, L. S.; Armentrout, P. B. *J. Am. Chem. Soc.* **1994**, *116*, 3519. f) Armentrout, P.B.; Beauchamp, J. L. *Acc. Chem. Res.* **1989**, *22*, 315. g) Tan, L.; Liu, F.; Armentrout, P.B. *J. Chem. Phys.* **2006**, *124*, 1.

- (95) Rodriguez-Cruz, S.; Jockusch, R. A.; Williams, E. R. *J. Am. Chem. Soc.* **1999**, *121*, 1986.
- (96) Ho, Y.P.; Yang, Y.C.; Klippenstein, S.J.; Dunbar, R.C., *J. Phys. Chem. A* **1997**, *101*, 3338. Petrie, S.; Dunbar, R.C. *J. Phys. Chem. A* **2000**, *104*, 4480. Petrie, S. *J. Phys. Chem.* **2002**, *106*, 7034.
- (97) Schroeder, D.; Hrušák, J.; Hertwig, R.; Koch, W.; Schwerdtfeger, P.; Schwarz, H. *Organometallics* **1995**, *14*, 312. b) Stoeckigt, D.; Hrušák, J.; Schwarz, H. *Int. J. Mass Spectrom. Ion Proc.* **1995**, *149*, 1. c) Schroeder, D.; Schwarz, H.; Hrušák, J.; Pyykkoe, P. *Inorg. Chem.* **1998**, *37*, 624.
- (98) a) Kabarle, P. *Ann. Rev. Phys. Chem.* **1977**, *28*, 445. b) Jayaweera, P.; Blades, A.T.; Ikonomou, M.G.; Kebarle, P. *J. Am. Chem. Soc.* **1990**, *112*, 2452. c) Nielsen, S.B.; Masella, M.; Kebarle, P. *J. Phys. Chem. A* **1999**, *103*, 9891. d) Peschke, M.; Blades, AT.; Kebarle, P. *Adv. Met. Semicond. Clusters.* **2001**, *5*, 77.
- (99) a) Bushnell, J.E.; Kemper, P.R.; Bowers, M.T. *J. Phys. Chem.* **1995**, *99*, 15602. b) Weis, P.; Kemper, P.R.; Bowers, M.T., *J. Phys. Chem. A* **1997**, *101*, 8207. c) Kemper, P.R.; Bushnell, J.; Bowers, M.T.; Gellene, G.I. *J. Phys. Chem. A.* **1998**, *102*, 8590. d) Manard, M.J.; Kemper, P.R.; Bowers, M.T. *Int. J. Mass Spectrom.* **2005**, *241*, 109.
- (100) a) Van Stipdonk, M.J.; Schweikert, E.A. *Nuclear Instruments and Methods in Physics Research B* **1995**, *96*, 530 b) Van Stipdonk, M.J.; Justes, D. R.; English, R. D.; Schweikert, E.A. *J. Mass Spectrom.* **1999**, *34*, 677

- (101) a) LaiHing, K.; Cheng, P. Y.; Taylor, T. G.; Willey, K. F.; Peschke, M.; Duncan, M. A. *Anal. Chem.* **1989**, *61*, 1458. b) Willey, K. F.; Cheng, P. Y.; Taylor, T. G.; Bishop, M. B.; Duncan, M. A. *J. Phys. Chem.* **1990**, *94*, 1544. c) Cornett, D. S.; Peschke, M.; LaiHing, K.; Cheng, P. Y.; Willey, K. F.; Duncan, M. A. *Rev. Sci. Instr.* **1992**, *63*, 2177. d) Pilgrim, J. S.; Duncan, M. A. *J. Am. Chem. Soc.* **1993**, *115*, 4395. e) Pilgrim, J. S.; Duncan, M. A. *J. Am. Chem. Soc.* **1993**, *115*, 6958. f) Pilgrim, J. S.; Duncan, M. A. *J. Am. Chem. Soc.* **1993**, *115*, 9724. g) Pilgrim, J. S.; Brock, L. R.; Duncan, M. A. *J. Phys. Chem.* **1995**, *99*, 544. h) France, M. R.; Buchanan, J. W.; Robinson, J. C.; Pullins, S. H.; Tucker, J. L.; King, R. B.; Duncan, M. A. *J. Phys. Chem. A* **1997**, *101*, 6214. i) Buchanan, J. W.; Reddic, J. E.; Grieves, G. A.; Duncan, M. A. *J. Phys. Chem. A* **1998**, *102*, 6390. j) Foster, N. R.; Grieves, G. A.; Buchanan, J. W.; Flynn, N. D.; Duncan, M. A. *J. Phys. Chem. A* **2000**, *104*, 11055. k) Grieves, G. A.; Buchanan, J. W.; Reddic, J. E.; Duncan, M. A. *Int. J. Mass Spectrom.* **2001**, *204*, 223. l) Walker, N. R.; Grieves, G. A.; Jaeger, J. B.; Walters, R. S.; Duncan, M. A. *Int. J. Mass Spectrom.* **2003**, *228*, 285. m) Jaeger, T. D.; Duncan, M. A. *J. Phys. Chem. A* **2004**, *108*, 11296. n) Pillai, E. D.; Molek, K. S.; Duncan, M. A. *Chem. Phys. Lett.* **2005**, *405*, 247. o) Ticknor, B. W.; Duncan, M. A. *Chem. Phys. Lett.* **2005**, *405*, 214.
- (102) a) Molek, K. S.; Jaeger, T. D.; Duncan, M. A., *J. Chem. Phys.* **2005**, *123*. b) Molek, K.S., Reed, Z.D., Ricks, A.M., Duncan, M.A. *J. Phys. Chem. A* **2007**, *111*, 8080

- (103) a) Deng, H. T.; Kerns, K. P.; Castleman, A. W. *J. Phys. Chem.* **1996**, *100*, 13386. b) Bell, R. C.; Zemski, K. A.; Kerns, K. P.; Deng, H. T.; Castleman, A. W. *J. Phys. Chem. A* **1998**, *102*, 1733. c) Bell, R. C.; Zemski, K. A.; Castleman, A. W. *J. Cluster Sci.* **1999**, *10*, 509. d) Zemski, K. A.; Justes, D. R.; Castleman, A. W. *J. Phys. Chem. B* **2002**, *106*, 6136. e) Justes, D. R.; Mitric, R.; Moore, N. A.; Bonacic-Koutecky, V.; Castleman, A. W. *J. Am. Chem. Soc.* **2003**, *125*, 6289. f) Justes, D. R.; Moore, N. A.; Castleman, A. W. *J. Phys. Chem. B* **2004**, *108*, 3855. g) Bergeron, D. E.; Castleman, A. W.; Jones, N. O.; Khanna, S. N. *Nano. Lett.* **2004**, *4*, 261. h) p) Moore, N. A.; Mitric, R.; Justes, D. R.; Bonacic-Koutecky, V.; Castleman, A. W. *J. Phys. Chem. B* **2006**, *110*, 3015. i) Reilly, N. M., Reveles, J. U., Johnson, G. E., Khanna, S. N., Castleman, A. W. *Chem. Phys. Lett.* **2007**, *435*, 295.
- (104) a) Yamada, Y.; Castleman, A. W., Jr. *J. Chem. Phys.* **1992**, *97*, 4543-8. b) Wagner, R. L.; Vann, W. D.; Castleman, A. W., Jr. *Rev. Sci. Instrum.* **1997**, *68*, 8 c) Jones, Charles E., Jr.; Clayborne, Penee A.; Reveles, J. Ulises; Melko, Joshua J.; Gupta, Ujjwal; Khanna, Shiv N.; Castleman, A. W., Jr. *J. Phys. Chem. A* **2008**, *112*, 13316-13325
- (105) a) Foltin, M.; Stueber, G. J.; Bernstein, E. R. *J. Chem. Phys.* **1999**, *111*, 9577. b) Shin, D. N.; Matsuda, Y.; Bernstein, E. R. *J. Chem. Phys.* **2004**, *120*, 4150. c) Shin, D. N.; Matsuda, Y.; Bernstein, E. R. *J. Chem. Phys.* **2004**, *120*, 4157. d) Matsuda, Y.; Bernstein, E. R. *J. Phys. Chem. A* **2005**, *109*, 314. e) Matsuda, Y.; Bernstein, E. R. *J. Phys. Chem. A* **2005**, *109*, 3803. f) Kang, Y.; Bernstein, E. R. *Bull. Korean Chem. Soc.* **2005**, *26*, 345. g) Dong, F.;

- Heinbuch, S.; He, S. G.; Xie, Y.; Rocca, J. J.; Bernstein, E. R. *J. Chem. Phys.* **2006**, *125*, 164318.
- (106) O'Keefe, A.; D.; Deacon, A.G. *Rev. Sci. Instrum.* **1988**, *59*, 254
- (107) Giel Berden, B.; Rudy Peeters, R.; Gerard Meijer, G. *Int. Rev. Phys. Chem.* **2000**, *19*, 565–607
- (108) Rizzo, TR; Stearns, JA; Boyarkin, OV *Int. Rev. Phys. Chem.* **2009**, *28*, 481
- (109) Eyler, JR *Mass Spec. Rev.* **2009**, *28*, 448
- (110) a) Chertihin, G. V.; Bare, W. D.; Andrews, L. *J. Chem. Phys.* **1997**, *107*, 2798. b) Zhou, M. F.; Andrews, L. *J. Chem. Phys.* **1999**, *111*, 4230. c) Andrews, L.; Rohrbacher, A.; Laperle, C. M.; Continetti, R. E. *J. Phys. Chem. A* **2000**, *104*, 8173.
- (111) a) Zhou, M.; Andrews, L. “Infrared Spectra of RhCO^+ , RhCO , and RhCO^- in solid neon: a scale for charge support in catalyst systems,” *J. Am. Chem. Soc.* **1999**, *121*, 9171. b) Zhou, M.; Andrews, L. “Infrared Spectra and density functional calculations of CuCO_n^+ ($n=1-4$), CuCO_n ($n=1-3$), and CuCO_n^- ($n=1-3$), in solid neon,” *J. Chem. Phys.* **1999**, *111*, 4548. c) Zhou, M.; Andrews, L. “Infrared spectra and density functional calculations of RuCO^+ , OsCO^+ , $\text{Ru}(\text{CO})_x$, $\text{Os}(\text{CO})_x$, $\text{Ru}(\text{CO})_x^-$, and $\text{Os}(\text{CO})_x^-$ ($x=1-4$) in solid neon,” *J. Phys. Chem. A* **1999**, *103*, 6956. d) Zhou, M.; Andrews, L. “Reactions of laser-ablated iron atoms and cations with carbon monoxide: Infrared spectra of FeCO^+ , $\text{Fe}(\text{CO})_2^+$, $\text{Fe}(\text{CO})_x$ and $\text{Fe}(\text{CO})_x^-$ ($x=1-4$) in solid neon,” *J. Chem. Phys.* **1999**, *110*, 10370. e) Zhou, M.; Andrews, L. “Matrix infrared spectra and density functional calculations of ScCO , ScCO^- , and ScCO^+ ,” *J. Phys.*

Chem. A. **1999**, *103*, 2964. f) Zhou, M.; Andrews, L. “Infrared spectra and density functional calculations for OMCO, and OM-(η^2 -CO⁻), OMCO⁺ and OMOC⁺ (M=V, Ti) in solid argon,” *J. Phys. Chem. A.* **1999**, *103*, 5259. g) Zhou, M.; Andrews, L. “Reactions of laser ablated Co, Rh, and Ir with CO: Infrared spectra and density functional calculations of the metal carbonyl molecules, cations and anions in solid neon,” *J. Phys. Chem. A.* **1999**, *103*, 7773. h) Liang, B.; Andrews, L. “Reactions of Laser-Ablated Ag and Au atoms with carbon monoxide: Matrix Infrared Spectra and Density Functional Calculations on Au(CO)_n (n=2,3), Au(CO)_n⁻ (n=1,2), and M(CO)_n (n=1-4), (M=Ag, Au),” *J. Phys. Chem. A.* **2000**, *104*, 9156. i) Liang, B.; Zhou, M.; Andrews, L. “Reactions of Laser-Ablated Ni, Pd, and Pt atoms with carbon monoxide: Matrix Infrared Spectra and Density Functional Calculations on M(CO)_n (n=1-4), M(CO)_n⁻ (n=1-3), and M(CO)_n⁺ (n=1-2), (M=Ni, Pd, Pt),” *J. Phys. Chem. A.* **2000**, *104*, 3905. j) Andrews, L.; Zhou, M.; Wang, X.; Bauschlicher, C.W. “Matrix Infrared Spectra and DFT Calculations of Manganese and Rhenium Carbonyl Neutral and Anion Complexes” *J. Phys. Chem. A* **2000**, *104*, 8887

(112) Berkowitz, J. *Photoabsorption, Photoionization and Photoelectron Spectroscopy*, Academic, New York, 1979.

(113) a) Watanabe, H.; Iwata, S.; Hashimoto, K.; Misaizu, F.; Fuke, K. *J. Am. Chem. Soc.* **1995**, *117*, 755. b) Fuke, K.; Hashimoto, K.; Takasu, R. *Adv. Met. Semicond. Clusters* **2001**, *5*, 1.

- (114) a) Liu, H.; Guo, W.; Yang, S. *J. Chem. Phys.* **2002**, *116*, 9690. b) Yang, X.; Hu, Y.; Yang, S. *J. Phys. Chem. A* **2000**, *104*, 8496.
- (115) Asher, R.L.; Bellert, D.; Buthelezi, T.; Lessen, D.; Brucat, P.J. *Chem. Phys. Lett.* **1995**, *234*, 119. b) Buthelezi, T.; Bellert, D.; Lewis, V.; Brucat, P.J. *Chem. Phys. Lett.* **1995**, *246*, 145. c) Buthelezi, T.; Bellert, D.; Lewis, V.; Brucat, P.J. *Chem. Phys. Lett.* **1995**, *242*, 627. d) Bellert, D.; Buthelezi, Dezfulian, K.; T.; Hayes, T.; Brucat, P.J. *Chem. Phys. Lett.* **1996**, *260*, 458. e) Hayes, T.; Bellert, D.; Buthelezi, T.; Brucat, P.J. *Chem. Phys. Lett.* **1998**, *287*, 22. f) Bellert, D.; Buthelezi, T.; Brucat, P.J. *Chem. Phys. Lett.* **1998**, *290*, 316.
- (116) a) Kleiber, P.D.; Chen, J. *Int. Rev. Phys. Chem.* **1998**, *17*, 1. b) Chen, J.; Wong, T.H.; Cheng, Y.C.; Montgomery, K.; Kleiber, P.D. *J. Chem. Phys.* **1998**, *108*, 2285. c) Chen, J.; Wong, T.H.; Kleiber, P.D.; Wang, K.H. *J. Chem. Phys.* **1999**, *110*, 11798. d) Cheng, Y.C.; Chen, J.; Ding, L.N.; Wong, T.H.; Kleiber, P.D.; Liu, D. K. *J. Chem. Phys.* **1996**, *104*, 6452.
- (117) Shen, M.H.; Farrar, J.M. *J. Chem. Phys.* **1991**, *94*, 3322. b) Donnelly, S.G.; Farrar, J.M. *J. Chem. Phys.* **1993**, *98*, 5450. c) Qian, J.; Midey, A.J.; Donnelly, S.G.; Lee, J.I.; Farrar, J.M. *Chem. Phys. Lett.* **1995**, *244*, 414.
- (118) a) Husband, J.; Aguirre, F.; Thompson, C.J.; Laperle, C.M.; Metz, R.B. *J. Phys. Chem. A* **2000**, *104*, 2020. b) Thompson, C.J.; Husband, J.; Aguirre, F.; Metz, R.B. *J. Phys. Chem. A* **2000**, *104*, 8155. c) Thompson, C.J.; Aguirre, F.; Husband, J.; Metz, R.B. *J. Phys. Chem. A* **2000**, *104*, 9901. d) Faherty,

- K.P.; Thompson, C.J.; Aguirre, F.; Michen, J.; Metz, R.B. *J. Phys. Chem. A* **2001**, *105*, 10054.
- (119) a) Scurlock, C.T.; Pullins, S.H.; Reddic, J.E.; Duncan, M.A. *J. Chem. Phys.* **1996**, *104*, 4591. b) Pullins, S.H.; Scurlock, C.T.; Reddic, J.E.; Duncan, M.A. *J. Chem. Phys.* **1996**, *104*, 7518. c) Velasquez, J.; Kirschner, K.N.; Reddic, J.E.; Duncan, M.A. *Chem. Phys. Lett.* **2001**, *343*, 613. d) Reddic, J.E.; Duncan, M.A. *J. Chem. Phys.* **2000**, *112*, 4974. e) Pullins, S.H.; Reddic, J.E.; France, M.R.; Duncan, M.A. *J. Chem. Phys.* **1998**, *108*, 2725. f) France, M. R.; Pullins, S. H.; Duncan, M. A. *J. Chem. Phys.* **1998**, *109*, 8842. g) France, M. R.; Pullins, S. H.; Duncan, M. A. *J. Chem. Phys.* **1998**, *108*, 7049. h) Kirschner, K.N.; Ma, B.; Bowen, J.P.; Duncan, M.A. *Chem. Phys. Lett.* **1998**, *295*, 204. i) Yeh, C. S.; Willey, K. F.; Robbins, D. L.; Pilgrim, J. S.; Duncan, M. A. *Chem. Phys. Lett.* **1992**, *196*, 233. j) Yeh, C. S.; Pilgrim, J. S.; Willey, K. F.; Robbins, D. L.; Duncan, M. A. *Int. Rev. Phys. Chem.* **1994**, *13*, 231. k) Pilgrim, J. S.; Yeh, C. S.; Berry, K. R.; Duncan, M. A. *J. Chem. Phys.* **1994**, *100*, 7945. l) Scurlock, C. T.; Pilgrim, J. S.; Duncan, M. A. *J. Chem. Phys.* **1995**, *103*, 3293. m) Yeh, C.S.; Willey, K.F.; Robbins, D.L.; Duncan, M.A. *J. Chem. Phys.* **1993**, *98*, 1867. n) France, M.R.; Pullins, S. H.; Duncan, M.A. *Chem. Phys.* **1998**, *239*, 447. o) Reddic, J.E.; Duncan, M.A. *Chem. Phys. Lett.* **1999**, *312*, 96.
- (120) a) Misaizu, F.; Sanekata, M.; Tsukamoto, K.; Fuke, K.; Iwata, S. *J. Phys. Chem.* **1992**, *96*, 8259. b) Sanekata, M.; Misaizu, F.; Fuke, K.; Iwata, S.; Hashimoto, K.; *J. Am. Chem. Soc.* **1995**, *117*, 747. c) Watanabe, H.; Iwata, S.

- J. Phys. Chem.* **1996**, *100*, 3377. d) Sanekata, M.; Misaizu, F.; Fuke, K. *J. Chem. Phys.* **1996**, *104*, 9768. e) Fuke, K.; Hashimoto, K.; Takasu, R. *Adv. Met. Semicond. Clusters* **2001**, *5*, 1. f) Yoshida, S.; Okai, N.; Fuke, K. *Chem. Phys. Lett.* **2001**, *347*, 93.
- (121) Merkt, F. *Ann. Rev. Phys. Chem.* "Molecules in high Rydberg states" **1997**, *48*, 675
- (122) a) Rothschoopf, G.K.; Perkins, J.S.; Li, S.; Yang, D.S. *J. Phys. Chem. A* **2000**, *104*, 8178. b) Li, S.; Rothschoopf, G.K.; Pillai, E.D.; Sohnlein, B.R.; Wilson, B.M.; Yang, D.S. *J. Chem. Phys.* **2001**, *115*, 7968. c) Yang, D. S. *Adv. Met. Semicond. Clusters.* **2001**, *5*, 187. d) Rothschoopf, G.K.; Li, S.; Yang, D.S. *J. Chem. Phys.* **2002**, *117*, 8800. e) Li, S.; Sohnlein, B.R.; Rothschoopf, G.K.; Fuller, J.F.; Yang, D.S. *J. Chem. Phys.* **2003**, *119*, 5406. f) Sohnlein, B. R.; Fuller, J. F.; Yang, D. S. *J. Am. Chem. Soc.* **2006**, *128*, 10692. g) Yang, D. S. *Coord. Chem. Rev.* **2001**, *214*, 187.
- (123) a) Wang, K.; Rodham, D.A.; McKoy, V.; Blake, G.A. *J. Chem. Phys.* **1998**, *108*, 4817. b) Rodham, D.A.; Blake, G.A. *Chem. Phys. Lett.* **1997**, *264*, 522.
- (124) a) Wiley, K. F.; Yeh, C. S.; Duncan, M. A. *Chem. Phys. Lett.* **1993**, *211*, 156. b) Agreiter, J. K.; Knight, A. M.; Duncan, M. A. *Chem. Phys. Lett.* **1999**, *313*, 162.
- (125) a) Robles, E.S.J.; Ellis, A.M.; Miller, T.A. *J. Phys. Chem.* **1992**, *96*, 3247. b) Robles, E.S.J.; Ellis, A.M.; Miller, T.A. *J. Phys. Chem.* **1992**, *96*, 8791. c) Panov, S.I.; Williamson, J.M.; Miller, T.A. *J. Chem. Phys.* **1995**, *102*, 7359.
- (126) Cockett, M. C. R. *Chem. Soc. Rev.* **2005**, *34*, 935.

- (127) Willey, K. F.; Yeh, C. S.; Duncan, M. A. *Chem. Phys. Lett.* **1993**, *211*, 156.
- (128) a) Gantefor, G. F.; Cox, D. M.; Kaldor, A. *J. Chem. Phys.* **1990**, *93*, 8395. b) Gantefor, G. F.; Cox, D. M.; Kaldor, A. *J. Chem. Phys.* **1992**, *96*, 4102.
- (129) a) Wang, K.; Rodham, D.A.; McKoy, V.; Blake, G.A. *J. Chem. Phys.* **1998**, *108*, 4817. b) Rodham, D.A.; Blake, G.A. *Chem. Phys. Lett.* **1997**, *264*, 522.
- (130) a) Bloembergen, N.; Cantrell, C.D.; Larssen, D.M. *Springer Ser. Opt. Sci.* **1976**, *3*, 162. b) McDowell, R.S.; Galbraith, H.W.; Krohn, B.J.; Cantrell, C.D.; Hinkley, E. D. *Opt. Comm.* **1976**, *17*, 178.
- (131) Letokhov, V.S.; *Multiphoton Processes*, Proceedings of International Conference, **1978**, 331.
- (132) Marcus, R.A.; Noid, D.W.; Koszykowski, M.L. *Springer Ser. Chem. Phys.* **1978**, *3*, 298.
- (133) Kung, A.H.; Dai, H.L.; Berman, M.R.; Moore, C.B. *Springer Ser. Opt. Sci.* **1979**, *21*, 309.
- (134) King, D.S. *Adv. Chem. Phys.* **1982**, *50*, 105.
- (135) Thorne, L.R.; Beauchamp, J.L. *Gas Phase Ion Chemistry*, **1984**, *3*, 41.
- (136) a) Knickelbein, M.B.; Menezes, W.J.C. *Phys. Rev. Lett.* **1992**, *69*, 1046. b) Menezes, W.J.C.; Knickelbein, M.B. *J. Chem. Phys.* **1993**, *98*, 1856. c) Knickelbein, M.B. *J. Chem. Phys.* **1993**, *99*, 2377. Knickelbein, M.B. *Chem. Phys. Lett.* **1995**, *239*, 11. Knickelbein, M.B. *J. Chem. Phys.* **1996**, *104*, 3217. Koretsky, G.M.; Knickelbein, M.B. *Chem. Phys. Lett.* **1997**, *267*, 485.
- (137) a) van Heijnsbergen, D.; Jaeger, T.D.; von Helden, G.; Meijer, G.; Duncan, M.A. *Chem. Phys. Lett.* **2002**, *364*, 345. b) van Heijnsbergen, D.; von Helden,

- G.; Meijer, G.; Maitre, P.; Duncan, M.A. *J. Am. Chem. Soc.* **2002**, *124*, 1562.
- c) Jaeger, T.D.; Fielicke, A.; von Helden, G.; Meijer, G.; Duncan, M.A. *Chem. Phys. Lett.* **2004**, *392*, 409. d) Jaeger, T.D.; van Heijnsbergen, D.; Klippenstein, S.J.; von Helden, G.; Meijer, G.; Duncan, M.A. *J. Am. Chem. Soc.* **2004**, *126*, 10981.
- (138) a) van Heijnsbergen, D.; von Helden, G.; Duncan, M.A.; van Roij, A. J. A.; Meijer, G. *Phys. Rev. Lett.* **1999**, *83*, 4983. b) von Helden, G.; van Heijnsbergen, D.; Duncan, M.A.; Meijer, G. *Chem. Phys. Lett.* **2001**, *333*, 350. c) von Helden, G.; Kirilyuk, A.; van Heijnsbergen, D.; Sartakov, B.; Duncan, M.A.; Meijer, G. *Chem. Phys.* **2000**, *262*, 31. d) van Heijnsbergen, D.; Duncan, M.A.; Meijer, G.; von Helden, G. *Chem. Phys. Lett.* **2001**, *349*, 220. e) van Heijnsbergen, D.; Demyk, K.; Duncan, M.A.; Meijer, G.; von Helden, G. *Phys. Chem. Chem. Phys.* **2003**, *5*, 2515.
- (139) a) Fielicke, A.; Meijer, G.; von Helden, G. *Eur. Phys. J. D.* **2003**, *24*, 69. b) Fielicke, A.; Meijer, G.; von Helden, G.; Simard, B.; Denomme, S.; Rayner, D. *J. Am. Chem. Soc.* **2003**, *125*, 11184. c) Fielicke, A.; Mitric, R.; Meijer, G.; Bonacic-Koutecky, V.; von Helden, G. *J. Am. Chem. Soc.* **2003**, *125*, 15716. d) Fielicke, A.; von Helden, G.; Meijer, G. *J. Phys. Chem. B.* **2004**, *108*, 14591. e) Fielicke, A.; Kirilyuk, A.; Ratsch, C.; Behler, J.; Scheffler, M.; von Helden, G.; Meijer, G. *Phys. Rev. Lett.* **2004**, *93*, 023401. f) Oomens, J.; Moore, D.T.; von Helden, G.; Meijer, G.; Dunbar, R.C. *J. Am. Chem. Soc.* **2004**, *126*, 724.

- (140) a) Lemaire, J.; Boissel, P.; Heninger, M.; Mestdagh, H.; Mauclaire, G.; Le Caer, S.; Ortega, J.M.; Maitre, P. *Spectra Anal.* **2003**, *32*, 28. b) Le Caer, S.; Heninger, M.; Lemaire, J.; Boissel, P.; Maitre, P.; Mestdagh, H. *Chem. Phys. Lett.* **2004**, *385*, 273. c) Simon, A.; Jones, W.; Ortega, J.M.; Boissel, P.; Lemaire, J.; Maitre, P. *J. Am. Chem. Soc.* **2004**, *126*, 11666
- (141) a) Lisy, J.M. *Cluster Ions*, Ng. C; Baer, T.; Powis, I. (Eds.) Wiley, Chichester, **1993**. b) Weinheimer, C.J.; Lisy, J.M. *Int. J. Mass Spectrom Ion Process* **1996**, *159*, 197. c) Weinheimer, C.J.; Lisy, J.M. *J. Phys. Chem.* **1996**, *100*, 15303. d) Weinheimer, C.J.; Lisy, J.M. *J. Chem. Phys.* **1996**, *105*, 2938. e) Lisy, J.M. *Int. Rev. Phys. Chem.* **1997**, *16*, 267. f) Cabarcos, O.M.; Weinheimer, C.J.; Lisy, J.M. *J. Chem. Phys.* **1998**, *108*, 5151. g) Cabarcos, O.M.; Weinheimer, C.J.; Lisy, J.M.; Xantheas, S.S. *J. Chem. Phys.* **1999**, *110*, 5. h) Cabarcos, O.M.; Weinheimer, C.J.; Lisy, J.M.; Xantheas, S.S. *J. Chem. Phys.* **1999**, *110*, 9516. i) Cabarcos; O.M.; Weinheimer, C.J.; Lisy, J.M., *J. Chem. Phys.* **1999**, *110*, 8429. j) Vaden, T.D.; Forinash, B.; Lisy, J.M. *J. Chem. Phys.* **2002** *117*, 4628. k) Kim, D.; Hu, S.; Tarakeshwar, P.; Kim, K. S.; Lisy, J. M. *J. Phys. Chem. A.* **2003**, *107*, 1228. l) Vaden, T. D.; Lisy, J. M. *J. Chem. Phys.* **2004**, *120*, 721. m) Vaden, T. D.; Weinheimer, C. J.; Lisy, J. M. *J. Chem. Phys.* **2004**, *121*, 3102. n) Vaden, T. D.; Lisy, J. M. *J. Chem. Phys.* **2005**, *123*, 743021. o) Vaden, T. D.; Lisy, J. M. *J. Chem. Phys.* **2006**, *124*, 21431. p)) Vaden, T. D.; Lisy, J. M. *J. Chem. Phys.* **2006**, *124*, 14315.

- (142) a) Inokuchi, Y.; Ohshimo, K.; Misaizu, F.; Nishi, N. *Chem. Phys. Lett.* **2004**, *390*, 140. b) Inokuchi, Y.; Ohshimo, K.; Misaizu, F.; Nishi, N. *J. Phys. Chem. A*, **2004**, *108*, 5034.
- (143) a) Shin, J-W.; Hammer, N.I.; Johnson, M.A.; Schneider, H.; Glob, A. Weber, J.M. *J. Phys. Chem. A*, **109**, 3146-3152, 2005. b) Headrick, J.M.; Diken, E.G.; Walters, R.S.; Hammer, N.I.; Christie, R.A.; Cui, J.; Myshakin, E.M.; Duncan, M.A.; Johnson, M.A.; Jordan, K.D. *Science*, **308**, 1765-1769, 2005. c) Hammer, N.I.; Roscioli, J.R.; Bopp, J.C.; Headrick, J.M.; Johnson, M.A. *J. Chem. Phys.*, **123**, 244311, 2005.
- (144) a) Jaeger, T. D.; Pillai, E. D.; Duncan, M. A. *J. Phys. Chem. A* **2004**, *108*, 6605. b) Jaeger, T. D.; Duncan, M. A. *J. Phys. Chem. A* **2005**, *109*, 3311. c) Jaeger, J. B.; Pillai, E. D.; Jaeger, T. D.; Duncan, M. A. *J. Phys. Chem. A* **2005**, *109*, 2801.
- (145) a) Walker, N.R.; Walters, R.S.; Pillai, E.D.; Duncan, M.A. *J. Chem. Phys.* **2003**, *119*, 10471. b) Walters, R.S.; Duncan, M.A. *Austr. J. Chem.* **2004**, *57*, 1145.
- (146) Pillai, E. D.; Jaeger, T. D.; Duncan, M. A. *J. Phys. Chem. A* **2005**, *109*, 3521.
- (147) a) Walters, R. S.; Jaeger, T. D.; Duncan, M. A. *J. Phys. Chem. A* **2002**, *106*, 10482. b) Walters, Richard S.; Schleyer, Paul v. R.; Corminboeuf, Clemence; Duncan, Michael A. *J. Am. Chem. Soc.* **2005**, *127*, 1100.
- (148) a) Gregoire, G.; Velasquez, J.; Duncan, M. A. *Chem. Phys. Lett.* **2001**, *349*, 451. b) Gregoire, G.; Duncan, M. A. *J. Chem. Phys.* **2002**, *117*, 2120. c) Gregoire, G.; Brinkmann, N. R.; van Heijnsbergen, D.; Schaefer, H. F.;

- Duncan, M. A. *J. Phys. Chem. A* **2003**, *107*, 218. d) Walters, R. S.; Brinkmann, N. R.; Schaefer, H. F.; Duncan, M. A. *J. Phys. Chem. A* **2003**, *107*, 7396. e) Walker, N. R.; Grieves, G. A.; Walters, R. S.; Duncan, M. A. *Chem. Phys. Lett.* **2003**, *380*, 230. f) Walker, N. R.; Walters, R. S.; Grieves, G. A.; Duncan, M. A. *J. Chem. Phys.* **2004**, *121*, 10498. g) Walker, N. R.; Walters, R. S.; Duncan, M. A. *J. Chem. Phys.* **2004**, *120*, 10037. h) Jaeger, J. B.; Jaeger, T. D.; Brinkmann, N. R.; Schaefer, H. F.; Duncan, M. A. *Can. J. Chem.* **2004**, *82*, 934.
- (149) a) Ricks, A.M.; Bakker, J.M.; Douberly, G.E.; Duncan, M.A. *J. Phys. Chem. A* **2009**, *113*, 4701 b) Ricks, A.M.; Reed, Z.D.; Duncan, M.A. *J. Am. Chem. Soc.*, 2009, *131*, 9176–9177
- (150) Duncan, Michael A. *Int. Rev. Phys. Chem.* **2003**, *22*, 407.
- (151) Duncan, M. A. “Infrared spectroscopy to probe structure and dynamics in metal ion-molecule complexes,” *Intl. Rev. Phys. Chem.* **2003**, *22*, 407.
- (152) Walker, N. R.; Walters, R. S.; Duncan, M. A. “Frontiers in the infrared spectroscopy of gas phase metal ion complexes,” *New J. Chem.* **2005**, *29*, 1495.
- (153) a) Okumura, M.; Yeh, L.I.; Lee, Y.T. *J. Chem. Phys.* **1985**, *83*, 3705. b) Okumura, M.; Yeh, L.I.; Lee, Y.T. *J. Chem. Phys.* **1988**, *88*, 79. c) Yeh, L.I.; Okumura, M.; Meyers, J.D.; Price, J.M.; Lee, Y.T. *J. Chem. Phys.* **1989**, *91*, 7319. d) Yeh, L.I.; Lee, Y.T.; Hougen, J.T. *J. Mol. Spectrosc.* **1994**, *164*, 473. e) Crofteon, M.W.; Price, J.M.; Lee, Y.T. *Springer Ser. Chem. Phys.* **1994**, *56*, 44. f) Boo, D.W.; Liu, Z.F.; Suits, A.G.; Tse, J.S.; Lee, Y.T.

- Science* **1995**, 269, 57. g) Wu, C.C.; Jiang, J.C.; Boo, D.W.; Lin, S.H.; Lee, Y.T. Chang, H.C.; *J. Chem. Phys.* **2000**, 112, 176. h) Wu, C.C.; Jian, J.C.; Hahndorf, I.; Choudhuri, C.; Lee, Y.T.; Chang, H.C. *J. Phys. Chem. A* **2000**, 104, 9556.
- (154) a) Ayotte, P.; Bailey, C.G.; Kim, J.; Johnson, M.A. *J. Chem. Phys.* **1998**, 108, 444. b) Ayotte, P.; Weddle, G.H.; Kim, J.; Johnson, M.A. *J. Am. Chem. Soc.* **1998**, 120, 12361. c) Ayotte, P.; Weddle, G.H.; Bailey, C.G.; Johnson, M.A.; Vila, F.; Jordan, K.D. *J. Chem. Phys.* **1999**, 110, 6268. d) Ayotte, P.; Weddle, G.H.; Johnson, M.A. *J. Chem. Phys.* **1999**, 110, 7129 e) Ayotte, P.; Kim, J.; Kelley, J.A.; Nielson, S.B.; Johnson, M.A. *J. Am. Chem. Soc.* **1999**, 121, 6950. f) Ayotte, P.; Nielson, S.B.; Weddle, G.H.; Johnson, M.A.; Xantheas, S.S. *J. Phys. Chem. A* **1999**, 103, 10665. g) Nielson, S.B.; Ayotte, P.; Kelley, J.A.; Weddle, G.H.; Johnson, M.A. *J. Chem. Phys.* **1999**, 111, 10464.
- (155) a) Lisy, J.M. *Cluster Ions*, Ng, C; Baer, T.; Powis, I. (Eds.) Wiley, Chichester, 1993. b) Weinheimer, C.J.; Lisy, J.M. *Int. J. Mass Spectrom Ion Process* **1996**, 159, 197. c) Weinheimer, C.J.; Lisy, J.M. *J. Phys. Chem.* **1996**, 100, 15303. d) Weinheimer, C.J.; Lisy, J.M. *J. Chem. Phys.* **1996**, 105, 2938. e) Lisy, J.M. *Int. Rev. Phys. Chem.* **1997**, 16, 267. f) Cabarcos, O.M.; Weinheimer, C.J.; Lisy, J.M. *J. Chem. Phys.* **1998**, 108, 5151. g) Cabarcos, O.M.; Weinheimer, C.J.; Lisy, J.M.; Xantheas, S.S. *J. Chem. Phys.* **1999**, 110, 5. h) Cabarcos, O.M.; Weinheimer, C.J.; Lisy, J.M.; Xantheas, S.S. *J. Chem. Phys.* **1999**, 110, 9516. i) Vaden, T.D.; Forinash, B.; Lisy, J.M. *J. Chem. Phys.* **2002** 117, 4628.

- (156) a) Inokuchi, Y.; Ohshimo, K.; Misaizu, F.; Nishi, N. *Chem. Phys. Lett.* **2004**, 390, 140. b) Inokuchi, Y.; Ohshimo, K.; Misaizu, F.; Nishi, N. *J. Phys. Chem. A*, **2004**, 108, 5034.
- (157) a) Gregoire, G.; Velasquez, J.; Duncan, M. A. *Chem. Phys. Lett.* **2001**, 349, 451. b) Gregoire, G.; Duncan, M. A. *J. Chem. Phys.* **2002**, 117, 2120. c) Gregoire, G.; Brinkmann, N. R.; van Heijnsbergen, D.; Schaefer, H. F.; Duncan, M. A. *J. Phys. Chem. A* **2003**, 107, 218. d) Walters, R. S.; Brinkmann, N. R.; Schaefer, H. F.; Duncan, M. A. *J. Phys. Chem. A* **2003**, 107, 7396. e) Walker, N. R.; Grieves, G. A.; Walters, R. S.; Duncan, M. A. *Chem. Phys. Lett.* **2003**, 380, 230. f) Walker, N. R.; Walters, R. S.; Grieves, G. A.; Duncan, M. A. *J. Chem. Phys.* **2004**, 121, 10498. g) Walker, N. R.; Walters, R. S.; Duncan, M. A. *J. Chem. Phys.* **2004**, 120, 10037. h) Jaeger, J. B.; Jaeger, T. D.; Brinkmann, N. R.; Schaefer, H. F.; Duncan, M. A. *Can. J. Chem.* **2004**, 82, 934.
- (158) Pillai, E. D.; Jaeger, T. D.; Duncan, M. A. *J. Phys. Chem. A* **2005**, 109, 3521.
- (159) a) Walker, N.R.; Walters, R.S.; Pillai, E.D.; Duncan, M.A. *J. Chem. Phys.* **2003**, 119, 10471. b) Walters, R.S.; Duncan, M.A. *Austr. J. Chem.* **2004**, 57, 1145.
- (160) a) Walters, R. S.; Jaeger, T. D.; Duncan, M. A. *J. Phys. Chem. A* **2002**, 106, 10482. b) Walters, Richard S.; Schleyer, Paul v. R.; Corminboeuf, Clemence; Duncan, Michael A. *J. Am. Chem. Soc.* **2005**, 127, 1100. c) Walters, R. S.; Pillai, E. D.; Schleyer, P. v. R.; Duncan, M. A. *J. Am. Chem. Soc.*, to be

- submitted. d) Walters, R. S.; Pillai, E. D.; Schleyer, P. v. R.; Duncan, M. A. *J. Am. Chem. Soc.*, to be submitted.
- (161) a) Jaeger, T. D.; Pillai, E. D.; Duncan, M. A. *J. Phys. Chem. A* **2004**, *108*, 6605. b) Jaeger, T. D.; Duncan, M. A. *J. Phys. Chem. A* **2005**, *109*, 3311. c) Jaeger, J. B.; Pillai, E. D.; Jaeger, T. D.; Duncan, M. A. *J. Phys. Chem. A* **2005**, *109*, 2801.
- (162) Duncan, Michael A. *Int. Rev. Phys. Chem.* **2003**, *22*, 407.
- (163) Strauss, S.H. *J. Chem. Soc., Dalton Trans.* **2000**, 1-6
- (164) a) Bauschlicher, C.W., Jr.; Partridge, H.; Langhoff, S.R. *J. Phys. Chem.* **1992**, *96*, 3273. b) Sodupe, M.; Bauschlicher, C.W., Jr.; Langhoff, S.R. *J. Phys. Chem.* **1992**, *96*, 5350. c) Sodupe, M.; Bauschlicher, C.W.; Langhoff, S.R.; Partridge, H., *J. Phys. Chem.* **1992**, *96*, 2118. d) Partridge, H.; Bauschlicher, C.W., Jr.; Langhoff, S.R. *J. Phys. Chem.* **1992**, *96*, 5350. e) Bauschlicher, C.W., Jr.; Sodupe, M.; Partridge, H. *J. Chem. Phys.* **1992**, *96*, 4453. f) Partridge, H.; Bauschlicher, C.W., Jr. *Chem. Phys. Lett.* **1992**, *195*, 494. g) Sodupe, M.; Bauschlicher, C.W., Jr.; Partridge, H. *Chem. Phys. Lett.* **1992**, *192*, 185.
- (165) a) Lupinetti, A.J.; Fau, S.; Frenking, G.; Strauss, S.H. *J. Phys. Chem.* **1997**, *101*, 9951. b) Frenking, G.; Pidun, U. *J. Chem. Soc., Dalton Trans.* **1997**, 1653. c) Frenking, G.; Frohlich, N. *Chem. Rev.* **2000**, *100*, 717.
- (166) a) Pandey, R.; Rao, B. K.; Jena, P.; Miguel, A. B. *J. Am. Chem. Soc.* **2001**, *123*, 7744. b) Gutsev, G. L.; Mochena, M. D.; Jena, P.; Bauschlicher, C. W. Jr. Partridge, H. *J. Chem. Phys.* **2004**, *121*, 6785.

- (167) Kock, W.; Holthausen, M. C. *A Chemist's Guide to Density Functional Theory*, 2nd ed. Wiley-Vch, Amsterdam, **2002**.
- (168) a) Sambrano, J. R.; Andres, J.; Beltran, A.; Sensato, F.; Longo, E. *Chem. Phys. Lett.* **1998**, 287, 620. b) Calatayud, M.; Silvi, B.; Andres, J.; Beltran, A. *Chem. Phys. Lett.* **2001**, 333, 493. c) Calatayud, M.; Andres, J.; Beltran, A. *J. Phys. Chem. A* **2001**, 105, 9760. d) Sambrano, J. R.; Gracia, L.; Andres, J.; Berski, S.; Beltran, A. *J. Phys. Chem. A* **2004**, 108, 10850. e) Sambrano, J. R.; Andres, J.; Gracia, L.; Safont, V. S.; Beltran, A. *Chem. Phys. Lett.* **2004**, 384, 56. f) Gracia, L.; Andres, J.; Safont, V. S.; Beltran, A. *Organometallics* **2004**, 23, 730.
- (169) a) Veliah, S.; Xiang, K. H.; Pandey, R.; Recio, J. M.; Newsam, J. M. *J. Phys. Chem. B* **1998**, 102, 1126. b) Xiang, K. H.; Pandey, R.; Recio, J. M.; Francisco, E.; Newsam, J. M. *J. Phys. Chem. A* **2000**, 104, 990.
- (170) a) Reddy, B. V.; Khanna, S. N. *Phys. Rev. Lett.* **1999**, 83, 3170. b) Morisato, T.; Jones, N. O.; Khanna, S. N.; Kawazoe, Y. *Comp. Mater. Sci.* **2006**, 35, 366.
- (171) Chakrabarti, A.; Hermann, K.; Druzinic, R.; Witko, M.; Wagner, F.; Petersen, M. *Phys. Rev. B* **1999**, 59, 10583.
- (172) Zimmermann, R.; Steiner, P.; Claessen, R.; Reinert, F.; Hufner, S.; Blaha, P.; Dufek, P. *J. Phys.: Condens. Matter* **1999**, 11, 1657.
- (173) a) Vyboishchikov, S. F.; Sauer, J. *J. Phys. Chem. A* **2000**, 104, 10913. b) Vyboishchikov, S. F.; Sauer, J. *J. Phys. Chem. A* **2001**, 105, 8588. c) Vyboishchikov, S. F. *J. Mol. Struct. Theochem.* **2005**, 723, 53.

- (174) Albaret, T.; Finocchi, F.; Noguera, C. *J. Chem. Phys.* **2000**, *113*, 2238.
- (175) Gutsev, G. L.; Andrews, L.; Bauschlicher, C. W. *Theo. Chem. Accts.* **2003**, *109*, 298.
- (176) Ayuela, A.; March, N.H.; Klein, D.J. *J. Phys. Chem. A* **2007**, *111*, 10162
- (177) Goldman, A. S.; Krogh-Jespersen, K. "Why do cationic carbon monoxide complexes have high CO stretching force constants and short CO bonds? Electrostatic effects, not σ bonding," *J. Am. Chem. Soc.* **1996**, *118*, 12159.
- (178) a) Lupinetti, A. J.; Frenking, G.; Strauss, S. H. "Nonclassical Metal Carbonyls," *Angew. Chem. Int. Ed.* **1998**, *37*, 2113. b) Lupinetti, A. J.; Jonas, V.; Thiel, W.; Strauss, S. H.; Frenking, G. "Trends in Molecular Geometries and Bond Strengths of the Homoleptic d10 Metal Carbonyl Cations: A Theoretical Study," *Chem. Eur. J.* **1999**, *5*, 2573. c) Lupinetti, A. J.; Fau, S.; Frenking, G.; Strauss, S. H. "Theoretical Analysis of the Bonding between CO and Positively Charged Atoms," *J. Phys. Chem.* **1997**, *101*, 9551.
- (179) Barnes, L.A.; Rosi, M.; Bauschlicher, C.W. "Theoretical studies of the first- and second-row mono- and di-carbonyl positive ions," *J. Chem. Phys.* **1990**, *93*, 609.
- (180) Huo, C.-H.; Li, Y.-W.; Wu, G.-S.; Beller, M.; Jiao, H. "Structures and energies of $[\text{Co}(\text{CO})_n]^m$ ($m=0, 1+, 1-$) and $\text{HCo}(\text{CO})_n$: Density functional studies," *J. Phys. Chem. A* **2002**, *106*, 12161.
- (181) Wu, G.; Li, Y.-W.; Xiang, H.-W.; Xu, Y.-Y.; Sun, Y.-H.; Jiao, H. *Journal of Molecular Structure (Theochem)* **2003**, *637*, 101–107
- (182) Yang, Y.; Weaver, M.N.; Merz, K.M. *J. Phys. Chem. A* **2009**, *113*, 9843–9851

- (183) Perdew, J.P.; Schmidt, K. *AIP Conference Proceedings*; AIP: Melville, NY, 2001; Vol. 577 pg 1-20
- (184) Becke, A. D. "3 term correlation functional," *J. Chem. Phys.* **1993**, 98, 5648.
- (185) Lee, C.; Yang, W.; Parr, R. G. Lee Yang Parr, "Correlation functional," *Phys. Rev B.* **1998**, 98, 5648.

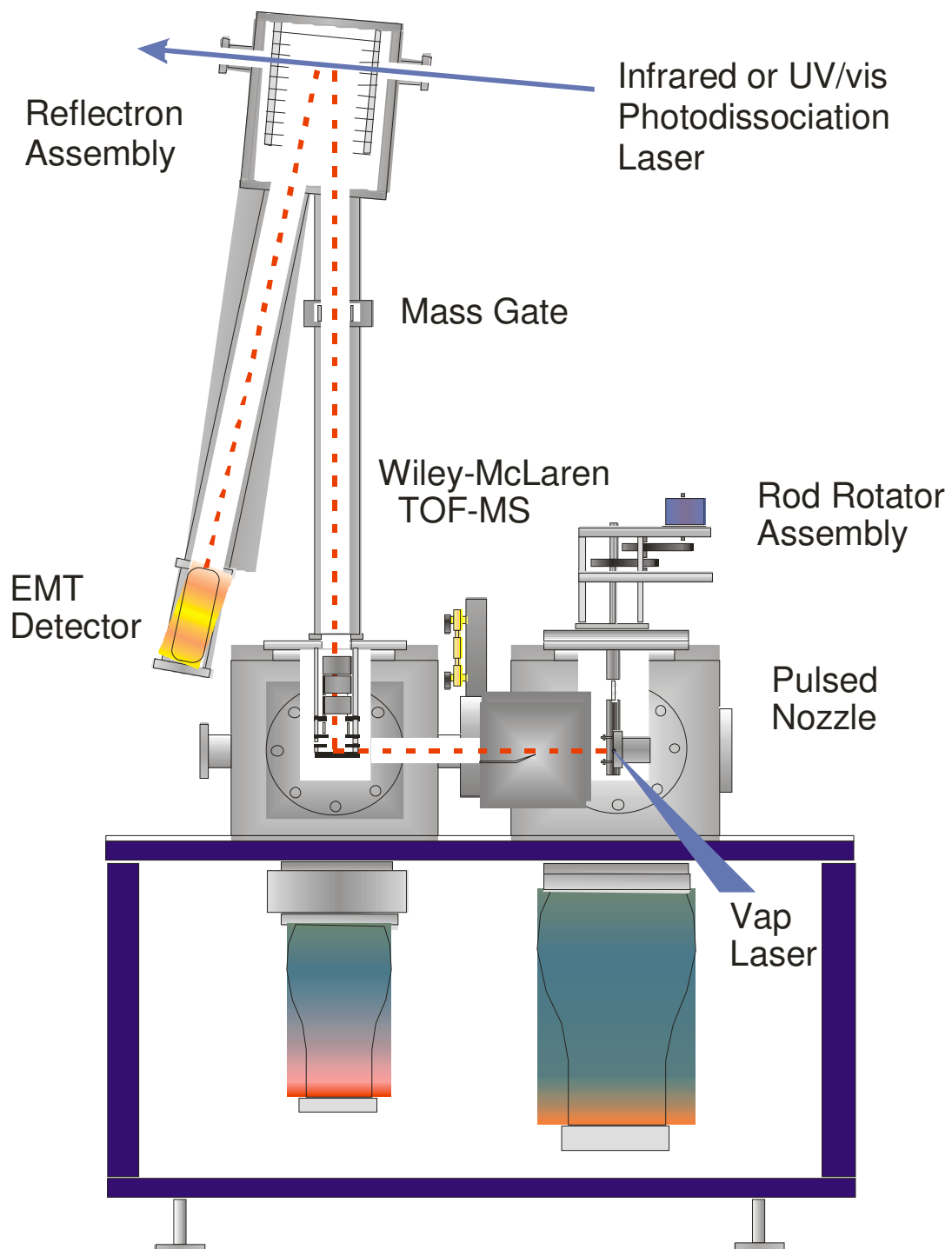
CHAPTER 2

EXPERIMENTAL

Generating and studying cationic complexes presents a difficult experimental problem. Many interesting complexes are highly reactive or weakly bound, and would not survive at room temperature. Solution or solid phase studies introduce solvent, counterion, or matrix effects, which can perturb the structure of the complexes. Our approach to generating and studying cationic complexes is to study the complexes in the gas phase, where they can be studied with minimal perturbation [1]. We use laser vaporization to generate our complexes, mass analyze and select individual complexes using mass spectroscopy, and study the complexes using either fixed frequency UV/Vis photodissociation or infrared photodissociation spectroscopy (IRPD).

Metal ion complexes are generated in the gas phase by laser vaporization in a pulsed nozzle source. The resulting expansion is skimmed into a differentially pumped second chamber and then sampled by pulsed electrical grids into a Wiley-McLaren type time of flight mass spectrometer, the details of which have been published elsewhere [2-6]. A schematic of this apparatus is presented in Figure 2.1. The first chamber is colloquially known as the “source” chamber, and is pumped by a Varian VHS-10 diffusion pump and maintains pressure of roughly 10^{-6} torr when gas is not being pulsed. The mass spectrometer section maintains a vacuum of nearly 10^{-8} torr.

Figure 2.1 Molecular Beam Apparatus with Reflectron Time-of-Flight Mass Spectrometer



In the source chamber, the second (532 nm) or third (355 nm) harmonic of a Nd:YAG laser is focused onto a metal rod, which rotates and translates to provide a fresh surface for each shot. The full details of this apparatus have been discussed in previous work [4]. The color of laser light used for each experiment is determined empirically and varies with the metal used. Similarly, the laser energy typically varies from 1-20 mJ/pulse and is varied to maximize production of the ions of interest.

Behind the metal rod, a General Valve Series 9 pulsed valve produces a supersonic expansion and cools the complexes, and also entrains them in the molecular beam. The nozzle is typically operated with pulse widths between 200-400 μ s, with pressures varying from 40-400 psi. The expansion gas can be solely the complex of interest, such as carbon monoxide, or the gas of interest seeded in noble gases, usually helium, neon, or argon. It is also possible to pass the gas flow over a reservoir of liquid, such as benzene, to entrain some of the partial pressure into the gas flow and introduce them as ligands. This technique can be used to produce mixed clusters, such as metal-carbonyl-benzene complexes when used with seeded gas mixtures.

The placement of the rod and the apparatus used to hold it significantly influences the growth conditions of the clusters, and thus we have developed several different types of rod-holders depending on the details of the system to be studied. A “full-block” configuration is used when larger clusters with multiple metal atoms are desired. Additional growth regions can be added to the block to encourage even larger cluster growth. These configurations encourage higher metal concentration in the growth region, but limits cooling [1]. Complexes like metal-oxides and metal-carbides, which are strongly bound, are efficiently produced in this setup. A “cut-away” or “offset”

configuration is used for single metal ion complexes with multiple weakly bound ligands. The “cut-away” places the rod, and the subsequent laser plasma, directly in the throat of the expansion and has no subsequent growth channel. This setup allows additional cooling over the full-block and enables the production of more weakly bound electrostatic and van der Waals complexes. However, we have found that this configuration is not tremendously efficient at producing noble gas tagged complexes and can produce pure ligand clusters, such as $(\text{CO})_n^+$, due to the proximity of the plasma to the expansion. To remedy this, we use an “offset” configuration, where the rod is translated laterally by $\frac{3}{4}$ of an inch. The expansion now occurs into free space, and the metal ions are ablated into the expansion where metal-ligand complexes are then formed. We have found that this configuration greatly increases the efficiency of argon tagging and largely eliminates the production of pure ligand clusters. Schematics and sample mass spectra from each configuration can be found in Figure 2.2. Here, a full-block configuration was used for all metal-oxide experiments and an offset configuration for the metal-carbonyl and mixed metal-carbonyl-benzene systems.

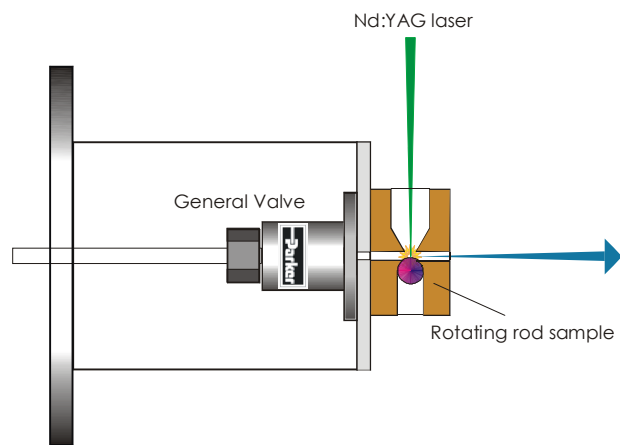
In both configurations, ions are produced directly out of the jet. They are skimmed with a 3 mm aperture (Beam Dynamics, Inc.) into the mass spectrometer region of the apparatus. The ions are pulse extracted into a two-stage Wiley-McLaren reflectron time of flight mass spectrometer (RTOF) [2]. A schematic of the RTOF is shown in Figure 2.3. Both the repeller plate and draw out grid (DOG) are kept at ground until the ion packet enters the extraction region, when the two plates are pulsed to voltage using fast rise time high voltage pulse switches (Behlke Corporation HTS-50, 50 nsec rise time). Voltages of 1100V and 1000V are used on the repeller and DOG,

respectively. These fields accelerate the ions down the first drift tube leg of the mass spectrometer. A deflection plate and an Einzel lens are used to correct for differing trajectories of low and high mass ions and focus the ion beam on the detector. The deflection plates are operated around 30V and the Einzel lens at around 500V. Midway through the first drift tube, the ions pass a pulsed deflection plate, the mass gate. This is typically held at a constant DC voltage around 500V, and briefly pulsed to ground when the ions of interest are passing. The mass gate is held at ground when an entire mass spectrum is being collected. From here the ions enter the reflectron region [7], where a voltage gradient slows the ions and turns them down the second leg of the flight tube. The front end of the reflectron is held at ground and the back end is held at a constant DC voltage of 1210V. The ions can be conveniently crossed with an infrared or UV/vis laser at this point as well.

After being reaccelerated by the reflectron, the ions enter the second flight tube and strike an electron multiplier tube (EMT, Hamamatsu R595) detector at its end. A floating second tube is present inside this second leg, which can be pulsed to high voltage for additional acceleration of the ions. This “post acceleration stage” is driven by another Behlke switch, and is typically run around 2700V. It can be used to enhance the signal in a mass spectrum, or reject inconvenient ions in the second flight tube before they are detected. The ions are detected as a voltage signal after being amplified by a pre-amplifier, and are recorded with a digital oscilloscope (LeCroy Waverunner). The data is transferred to a PC through an IEEE-488 interface.

Figure 2.2 shows the rod holder configurations and representative mass spectrums collected in each setup.

Laser Vaporization Cluster Source



Full block assembly

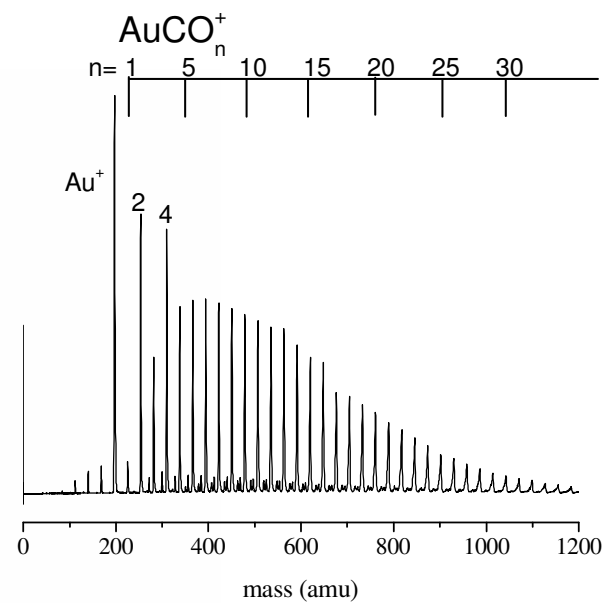
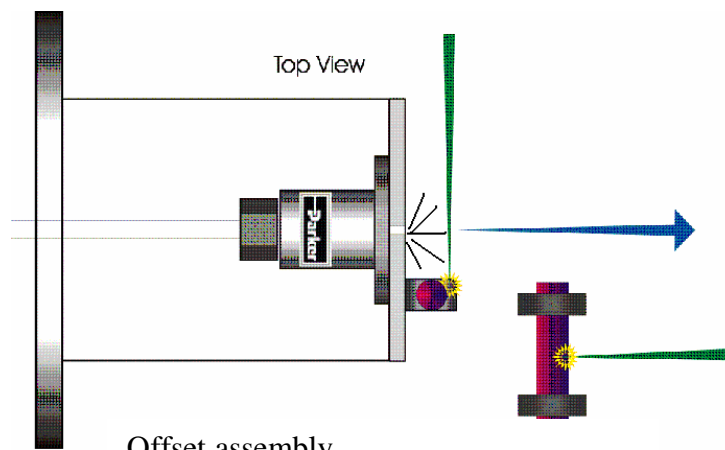
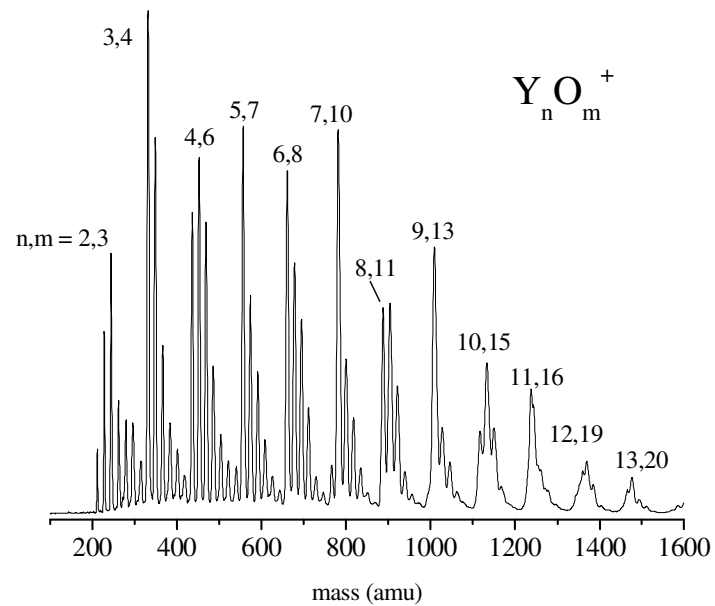
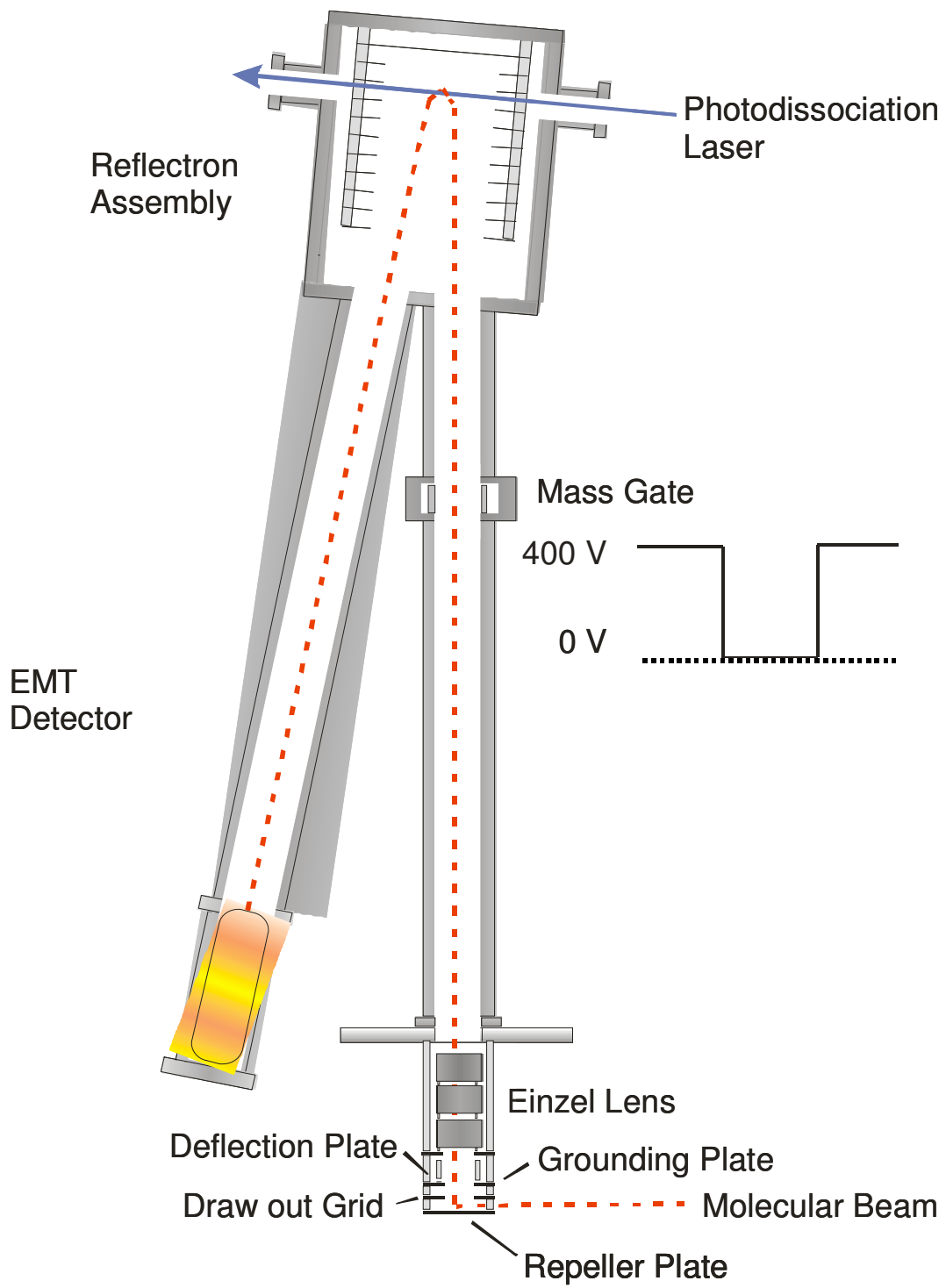


Figure 2.3 The reflectron time-of-flight mass spectrometer



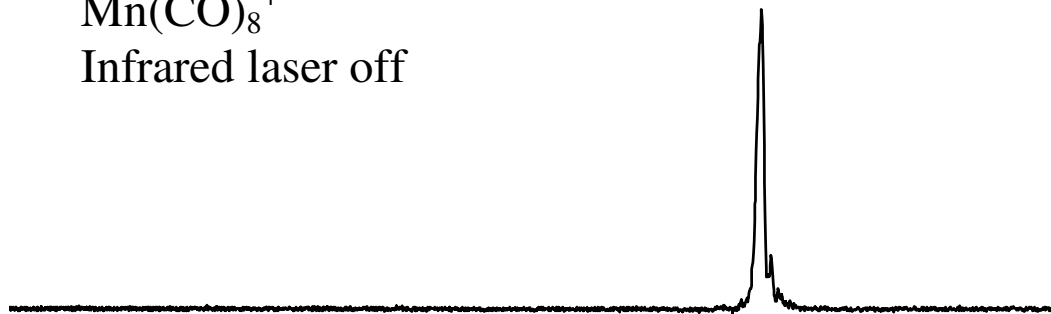
The electrical field that samples the ions accelerates them perpendicularly to their translational velocities in the molecular beam. This leads them to separate in space and arrive at the detector at different times according to their mass, as defined by the following equation:

$$\text{Kinetic Energy} = \frac{1}{2} * \text{Mass} * \text{Velocity}^2$$

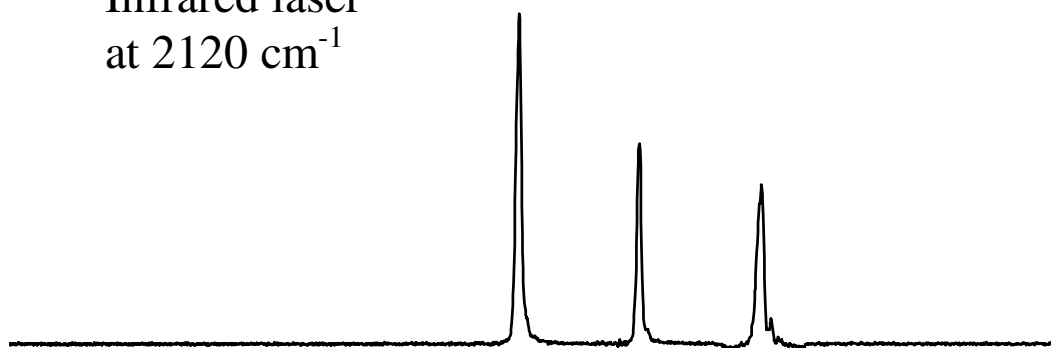
The time when the acceleration field is pulsed is known and defines time zero. The arrival time of the ions is measured by the oscilloscope. Since all ions pass through the same electric field, they acquire the same amount of kinetic energy, and it is thus possible to determine the mass of any ion by its arrival time if the mass corresponding to any other time is known. In practice, the metal atomic ion usually serves as the initial calibration point. The mass selection and photodissociation process is illustrated in Figure 2.4. The process varies only slightly when using tunable infrared light or fixed frequency UV/vis light. Ions of interest are selected by the mass gate, and then overlapped in the turning region of the reflection. If the ions absorb the laser radiation and fragment, the fragment ions will appear earlier in time at the detector after being accelerated. A difference mass spectrum is then created by subtracting the mass spectrum with the fragmentation laser on from that with the laser off. This results in a negative going parent ion and positive going fragment ions. The masses of the fragments can be assigned by altering time zero to the time the fragmentation laser is fired, then using the known mass of the parent as the reference. In fixed frequency experiments, the excitation laser is either the second or third harmonic (532 nm or 355 nm) of an Nd:YAG laser, and pulse energies from 15-60 mJ/pulse are used.

Figure 2.4 Mass selection and photodissociation mass spectra. The upper trace shows the mass selected parent ion with no excitation laser present. The middle trace show the mass spectrum obtained when the excitation laser causes fragmentation. The lower trace is a difference of the first two.

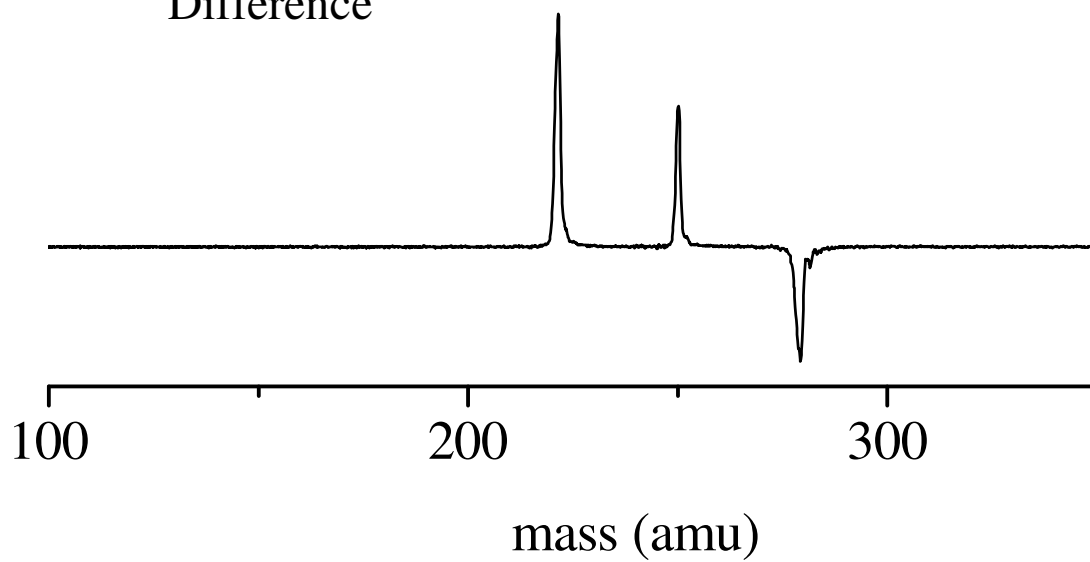
$\text{Mn}(\text{CO})_8^+$
Infrared laser off



Infrared laser
at 2120 cm^{-1}



Difference



By comparing prominent peaks in the mass spectrum to peaks repeatedly produced by fragmentation, we can identify which stoichiometries are particularly stable. We cannot directly detect neutral losses, which are inferred by mass conservation. In tunable infrared experiments, the determination of fragmentation patterns is merely the first step. Once a suitable frequency for fragmentation has been identified, the intensity of the observed fragments is measured as a function of the infrared wavelength. The fragment signal is then plotted to yield a spectrum. Fragmentation is much more efficient on resonance, and this technique allows us to determine the vibrational bands of the parent molecule. This “action” technique allows us to measure extremely low concentrations of parent ion, as we are operating on a zero background and are thus have high sensitivity.

The infrared light is generated in a benchtop OPO/OPA system (LaserVision), a schematic of which is shown in Figure 2.5. The OPO/OPA system is pumped with roughly 500 mJ/pulse of the fundamental (1064 nm) of an Nd:YAG laser (Continuum 8010), which is horizontally polarized. The beam is split by a 70:30 beamsplitter in the OPO/OPA, with the smaller fraction of the light passing through a KTP doubling crystal and the larger fraction passing through a delay line into the amplifier. The doubled light (532 nm) passes through an angled tuned KTP crystal, which splits the light into two beams, a signal and an idler according to the following relationships:

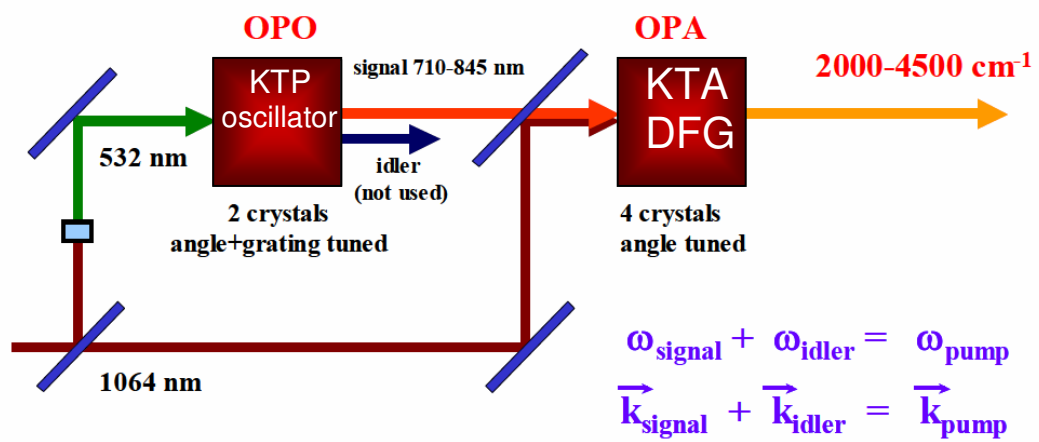
$$\omega_{\text{pump}} = \omega_{\text{signal}} + \omega_{\text{idler}}$$

$$\omega_{\text{signal}} \neq \omega_{\text{idler}} \text{ and } \omega_{\text{signal}} > \omega_{\text{idler}}$$

where ω is the frequency in cm^{-1} of the photons [8]. The signal output ranges from 14,000 - 11,300 cm^{-1} and the idler ranges from 7,400 - 4,700 cm^{-1} . The signal is rejected and the idler passes through to the OPA, which consists of four angled tuned KTA crystals, where it is combined with the remaining 1064 nm light from the delay line. Difference frequency generation between these two beams produces mid-infrared light between 2000 cm^{-1} and 4500 cm^{-1} , with pulse energies varying from <1 mJ/pulse around 2000 cm^{-1} to 30 mJ/pulse in the high wavelength regions. In the $\sim 2140 \text{ cm}^{-1}$ carbonyl stretching region [9] where most of the spectroscopy in this work was performed, 2-3 mJ/pulse was produced. The linewidth is roughly 1 cm^{-1} . The laser scans continuously, and the scanning rate is set to approximate step sizes around 0.5 cm^{-1} for most scans. Typically, 30-50 oscilloscope traces are recorded at each point.

While the experimental process is quite similar for fixed frequency and tunable infrared experiments, the fragmentation dynamics vary significantly. Fixed frequency experiments rely on coincidental absorption cross-section overlap with the chosen excitation wavelength. UV/Vis photons have a tremendous amount of energy compared to infrared photon (28,000 cm^{-1} for a 355 nm photon, compared to 2100 cm^{-1} for a typical infrared photon in these experiments), so much stronger bonds can be broken, even when the laser is not tuned directly to a resonance. The much higher laser fluences also allows for multiple photon absorption, which can break even stronger bonds. In tunable infrared experiments, we are able to match the vibrational absorptions of many metal-ligand complexes, but we must have enough energy to actually break a bond to detect this absorption.

Figure 2.5 *LaserVision* Optical Parametric Oscillator / Amplifier System



Many ligands bind too strongly to metal ions to be eliminated with an infrared photon. As more ligands are attached, the per-ligand binding energy decreases and eventually we can dissociate them.

To study smaller complexes, we must employ the technique of “rare-gas tagging”, adding an additional more weakly bound messenger atom. The weakly bound messenger atom is then lost when the complex absorbs light and we obtain the IRPD spectrum from this fragmentation. The rare gas tagging technique was required to study small transition metal carbonyl complexes in this work. Ideally, we would apply this technique to more strongly bound clusters like metal-oxides to study their spectroscopy, but have so far been largely unsuccessful due to their high internal energy and are thus limited to fixed frequency techniques. Our group has previously studied metal oxides [10,11], metal carbides [12], and metal silicon clusters [13] using the fixed frequency technique. We have studied various metal ligand complexes, with the ligands including benzene [14], carbon dioxide [15], acetylene [16], water [17], and nitrogen [18]. The work presented here is an extension of those studies, focusing on fixed frequency studies of metal oxide cations and infrared spectroscopic studies of transition metal carbonyl cation systems.

Along with experimental techniques, theoretical calculations provide a powerful tool to further investigate these systems. In the fixed frequency experiments, we performed density functional calculations (DFT) to help predict the structures of stoichiometries that were predicted to be stable, and to gain insight on the bonding motifs. For the spectroscopy experiments, DFT calculations were performed to identify

the electronic structure and geometries of measured complexes by comparing the spectra predicted by theory with those measured. We used the B3LYP functional for each system [19,20]. Various basis sets were used depending on the details of system being investigated.

2.1 References

- (1) a) Dietz, T.G.; Duncan, M.A.; Powers, D.E.; Smalley, R.E. *J. Chem. Phys.* **1981**, *74*, 6511. b) Zheng, L.S.; Brucat, P.J.; Pettiette, C.L.; Yang, S.; Smalley, R.E. *J. Chem. Phys.* **1985**, *83*, 4273. c) Brucat, P.J.; Zheng, L.S.; Pettiette, C.L.; Yang, S.; Smalley, R.E. *J. Chem. Phys.* **1986**, *84*, 3078.
- (2) Wiley, W.C.; McLaren, I.H. *Rev. Sci. Instrum.* **1955**, *26*, 1150.
- (3) LaiHing, K.; Cheng, P. Y.; Taylor, T. G.; Willey, K. F.; Peschke, M.; Duncan, M. A. *Anal. Chem.* **1989**, *61*, 1458.
- (4) Cornett, D. S.; Peschke, M.; LaiHing, K.; Cheng, P. Y.; Willey, K. F.; Duncan, M. A. *Rev. Sci. Instr.* **1992**, *63*, 2177.
- (5) Yeh, C. S.; Pilgrim, J. S.; Willey, K. F.; Robbins, D. L.; Duncan, M. A. *Int. Rev. Phys. Chem.* **1994**, *13*, 231.
- (6) Duncan, Michael A. *Int. Rev. Phys. Chem.* **2003**, *22*, 407.
- (7) a) Mamyrin, B.A.; Karataeu, V.I.; Shmikk, D.V.; Zagulin, V.A. *Zh. Eksp. Teor. Fiz.* **1973**, *64*, 82. b) Boesl, U.; Neusser, H.J.; Weinkauff, R.; Schlag, E.W. *J. Phys. Chem.* **1982**, *86*, 4857.
- (8) Demtroder, W. *Laser Spectroscopy* Springer-Verlag: Berlin, 1996.
- (9) Shimanouchi, T. *Molecular Vibrational Frequencies*; 69th ed.; Chemistry WebBook, NIST Standard Reference Database (<http://webbook.nist.gov>), 2001
- (10) Molek, K.S.; Jaeger, T.D.; Duncan, M.A. *J. Chem. Phys. A* **2005**, *123*, 144313
- (11) Molek, K.S.; Reed, Z.D.; Ricks, A.M.; Duncan, M.A. *J. Phys. Chem. A* **2007**, *111*, 8080

- (12) a) Ticknor, B.W.; Duncan, M.A. *Chem. Phys. Lett.* **2005**, *214*, 214.
a. b) Jaeger, J.B.; Jaeger, T.D.; Duncan, M.A. *J. Chem. Phys. A* **2006**, *110*,
9310
- (13) a) Pilgrim, J.S.; Duncan, M.A. *J. Am. Chem. Soc.* **1993**, *115*, 9724 b) Pilgrim,
J.S.; Duncan, M.A. *J. Am. Chem. Soc.* **1993**, *115*, 6958 c) Duncan, M.A.; *J.*
Cluster Sci. **1997**, *8*, 239.
- (14) a) Jaeger, T. D.; Pillai, E. D.; Duncan, M. A. *J. Phys. Chem. A* **2004**, *108*, 6605.
b) Jaeger, T. D.; Duncan, M. A. *J. Phys. Chem. A* **2005**, *109*, 3311. c) Jaeger, J.
B.; Pillai, E. D.; Jaeger, T. D.; Duncan, M. A. *J. Phys. Chem. A* **2005**, *109*, 2801.
- (15) a) Gregoire, G.; Velasquez, J.; Duncan, M. A. *Chem. Phys. Lett.* **2001**, *349*, 451.
b) Gregoire, G.; Duncan, M. A. *J. Chem. Phys.* **2002**, *117*, 2120. c) Gregoire,
G.; Brinkmann, N. R.; van Heijnsbergen, D.; Schaefer, H. F.; Duncan, M. A. *J.*
Phys. Chem. A **2003**, *107*, 218. d) Walters, R. S.; Brinkmann, N. R.; Schaefer, H.
F.; Duncan, M. A. *J. Phys. Chem. A* **2003**, *107*, 7396. e) Walker, N. R.; Grieves,
G. A.; Walters, R. S.; Duncan, M. A. *Chem. Phys. Lett.* **2003**, *380*, 230. f)
Walker, N. R.; Walters, R. S.; Grieves, G. A.; Duncan, M. A. *J. Chem. Phys.*
2004, *121*, 10498. g) Walker, N. R.; Walters, R. S.; Duncan, M. A. *J. Chem.*
Phys. **2004**, *120*, 10037. h) Jaeger, J. B.; Jaeger, T. D.; Brinkmann, N. R.;
Schaefer, H. F.; Duncan, M. A. *Can. J. Chem.* **2004**, *82*, 934.
- (16) a) Walters, R. S.; Jaeger, T. D.; Duncan, M. A. *J. Phys. Chem. A* **2002**, *106*,
10482. b) Walters, Richard S.; Schleyer, Paul v. R.; Corminboeuf, Clemence;
Duncan, Michael A. *J. Am. Chem. Soc.* **2005**, *127*, 1100.

- (17) a) Walker, N. R.; Walters, R. S.; Pillai, E. D.; Duncan, M. A. *J. Chem. Phys.* **2003**, *119*, 10471. b) Walters, Richard S.; Duncan, Michael A. *Austr. J. Chem.* **2004**, *57*, 1145. c) Tsai, Brad M.; Jordan, Kenneth D.; Walters, Richard S.; Duncan, Michael A. *J. Phys. Chem. A*, **2005**, *109*, 7057–7067
- (18) Pillai, E. D.; Jaeger, T. D.; Duncan, M. A. *J. Phys. Chem. A* **2005**, *109*, 3521.
- (19) Becke, A. D. “3 term correlation functional,” *J. Chem. Phys.* 1993, *98*, 5648.
- (20) Lee, C.; Yang, W.; Parr, R. G. Lee Yang Parr, “Correlation functional,” *Phys. Rev B*. 1998, *98*, 5648.

CHAPTER 3

PHOTODISSOCIATION OF YTTRIUM AND LANTHANUM OXIDE CLUSTER CATIONS¹

¹Reed, Z.D. and Duncan, M.A. To be submitted to *Int. J. Mass Spec.*

3.1 Abstract

Transition metal oxide cations of the form $M_nO_m^+$ ($M=Y, La$) are produced by laser vaporization in a pulsed nozzle source and detected with time-of-flight mass spectrometry. Cluster oxides for each value of n form only a limited number of stoichiometries; $MO(M_2O_3)_x^+$ species are particularly intense. Cluster cations are mass selected and photodissociated using the third harmonic (355 nm) of a Nd:YAG laser. Multiphoton excitation is required to dissociate these clusters due to their strong bonding. Yttrium and lanthanum oxides exhibit different dissociation channels, but some common trends can be identified. Larger clusters for both metals undergo fission to make certain stable cation clusters, especially $MO(M_2O_3)_x^+$ species. Specific cations are identified to be especially stable due to their repeated production in the decomposition of larger clusters. These include $M_3O_4^+$, $M_5O_7^+$, $M_7O_{10}^+$, and $M_9O_{13}^+$, along with $Y_6O_8^+$. Density functional theory calculations were performed to investigate the relative stabilities and structures of these systems.

3.2 Introduction

Transition metal oxides have applications in electronics, ceramics, magnetic materials, and catalysis [1-9]. Their corresponding metal oxide nanoparticles expand the range of applications in magnetics, catalysis, and medicine [10-16]. Gas phase experiments on metal oxide clusters composed of fewer atoms (up to 50-60) have been investigated to model the stability, reactivity and structure of solids and particles [17-45]. Many experiments have used mass spectrometry to probe these systems [17-34], and

some optical spectroscopy has been performed [35-45]. Theoretical calculations have examined the cage and network structures of oxide clusters, as well as their stabilities and spectra [46-54]. In the present work, we use time-of-flight mass spectrometry and mass-selected photodissociation measurements, along with density functional theory (DFT) calculations, to investigate the stability and structures of yttrium and lanthanum oxide cluster cations.

Mass spectrometry has been the standard method with which to investigate gas phase transition metal oxide clusters [17-34]. These experiments have most often used the relative intensities in the mass spectrum or patterns of reactivity to gauge relative cluster stability. Unlike the dramatic “magic numbers” seen for metal carbides [55-61], a variety of stoichiometries are seen for transition metal oxide clusters. Castleman and coworkers have studied the mass spectrometry and collisional dissociation patterns of oxide clusters as well as their reactions with small hydrocarbons [26]. Bernstein and coworkers have used ultraviolet photoionization to study the mass spectra of these systems [28], including yttrium oxide [28i]. Our research group has employed mass spectrometry and mass selected photodissociation to a number of transition metal systems [27]. Matrix isolation [35] infrared and anion photoelectron techniques [36-42] have been used to examine the spectroscopy of certain small metal oxide molecules. Infrared resonance enhanced photodissociation (IR-REPD) in the far IR has been demonstrated to probe the vibrational spectroscopy of larger, more strongly bound clusters. Our group, along with Meijer and coworkers, has investigated metal oxide [43] and metal carbide [58] clusters using this technique. Other work on mass selected cations and anions has been performed by Fielicke, von Helden, Meijer, and Asmis [44,45]. Theoretical

calculations have been performed to gain information on the structures, stabilities, and spectra of various smaller metal oxide clusters to complement these experiments [46-54].

The previous studies of metal oxide clusters [63,64] have revealed limitations and problems in the determination of relative cluster stabilities. The distribution of clusters produced in any experiment may be strongly influenced by the kind of source and the growth conditions, introducing possible biases toward larger or smaller clusters. Furthermore, some form of ionization is always necessary to detect clusters in mass spectrometers. Electron impact ionization and photoionization are both influenced by the unknown ionization potentials, size-dependent cross sections, and fragmentation processes. Variable energy collision induced dissociation (CID) has been used to fragment clusters to measure their dissociation energies [33], but significant kinetic shifts, especially for strongly bound clusters, limit the accuracy of this technique. Variable energy photoabsorption experiments have been attempted for the same purpose, but absorption may not be efficient in the threshold region. Equilibrium mass spectrometry measurements have been performed for small vanadium oxide clusters [17], and photofragmentation has been performed on bismuth and antimony oxides [27a], the vanadium group oxides [27b], as well as the oxide clusters of chromium [27c] and iron [27d]. High energy atom bombardment has been used to study the metastable decay of lanthanum oxide [24]. In spite of these various studies, much uncertainty remains about which specific oxide clusters are stable, what causes the stability, and how the stoichiometries in stable clusters relate to those in known bulk oxide phases.

Our group has previously demonstrated that mass-selected photodissociation of metal compound cluster ions can be used to identify the stoichiometries that are the most

stable [27,56,65]. These studies show that the stable cation clusters may or may not be prominent in the mass spectra of clusters produced initially by growth processes. However, stable cluster cations are resistant to decomposition, and they are likely to be produced more often on average than others in the fragmentation of larger clusters. Stable neutral clusters cannot be detected directly, but they can be inferred by mass conservation as the common leaving group in the fragmentation of larger clusters. This photodissociation methodology has been used to study various metal carbides [56], metal-silicon clusters [65], and several metal-oxide cluster systems [27]. These studies have found trends in the dissociation behavior of these clusters, and have identified a number of specific clusters of each type with special stability. In the case of oxides, we have found that stable species exhibit stoichiometries quite different from those that would be predicted on the basis of common metal oxidation states. Metal-oxygen ratios corresponding to less common bulk phases (e.g., FeO) are often formed in small clusters. Unlike the previously studied transition metals (V, Nb, Ta, Cr, Fe), which have several common oxidation states, yttrium and lanthanum, with valence configurations of $4d^15s^2$ and $5d^16s^2$ respectively, usually have only the +3 oxidation state in solid materials [3]. The mass spectrum of yttrium oxide has been studied by Bernstein [28i] and that of lanthanum oxide has been studied by Gibson [23] and Van Stipdonk [24], but photodissociation studies have not been applied to these systems. In the present work, we investigate the stabilities of yttrium oxide and lanthanum oxide clusters using photodissociation measurements along with density functional theory calculations.

3.3 Experimental

Metal oxide cluster ions are produced by laser vaporization in a pulsed nozzle source and mass analyzed in a reflectron time-of-flight spectrometer. This setup has been described previously [27,56,65]. The third harmonic (355 nm) of a Nd:YAG laser (Spectra Physics INDI-40) is employed to vaporize metal from the surface of a rotating and translating metal rod. Helium gas seeded with 1-10% oxygen is pulsed with a General Valve (60 psi backing pressure) through the sample rod holder, which has a 5 mm diameter bore and a 1 inch long growth channel. The metal oxide cluster cations grow directly in the laser-generated plasma, and expand to form a molecular beam which is skimmed before it passes into a differentially-pumped mass spectrometer chamber. A reflectron time-of-flight mass spectrometer with pulsed acceleration fields is used to sample the mass spectra of cation clusters produced under different conditions. To mass select specific clusters for photodissociation measurements, pulsed deflection plates are employed in the first flight tube section of the reflectron. Photoexcitation occurs in the turning region of the reflectron, where another Nd:YAG laser (Continuum Surelite) is timed to intersect the mass selected cation clusters. The parent ion and any fragment ions are mass analyzed in the second flight tube and are subsequently detected using an electron multiplier tube. The data are collected with a digital oscilloscope (Lecroy Waverunner 342) and transferred to a PC computer using an IEEE-488 interface. Studies were performed at different fragmentation laser wavelengths (532 and 355 nm) and pulse energies (20-60 mJ/pulse over a roughly 1 cm² spot) to investigate the photodissociation mechanism.

To investigate the possible structures and energetics of these metal oxides, geometry optimizations were performed using density functional theory (DFT) computations with the Gaussian 03W program [66]. The Beck-3 Lee-Yang-Parr (B3LYP) [67,68] functional was used with the LANL2DZ basis set [69-71]. Atomization energies and energies per bond are reported for the minimum energy structures. No symmetry restrictions were placed on the clusters. Theoretical investigations focused on the yttrium oxide clusters, with some selected lanthanum oxide cluster calculations performed to investigate the possible differences between the two systems. Calculations were performed for YO, YO₂, YO₃, Y₂O₃, Y₂O₃⁺, Y₃O₄, Y₃O₄⁺, Y₄O₆, Y₄O₆⁺, Y₅O₇, Y₅O₇⁺, Y₆O₈, Y₆O₈⁺, Y₇O₁₀, Y₇O₁₀⁺, along with LaO, LaO₂, LaO₃, La₂O₃, La₂O₃⁺, La₃O₄, La₃O₄⁺, La₅O₇, and La₅O₇⁺. The minimum energy structures, energies, and vibrational frequencies were computed for each cluster, and these data are reported in the Supporting Information. Natural bond orbital (NBO) analysis, employing the Wiberg index [66], was used to investigate the possible occurrence of metal-metal bonding across the oxide cage structures.

3.4 Results and Discussion

The mass spectrum of Y_nO_m⁺ cation clusters produced is shown in Figure 3.1. As shown, oxide clusters are detected containing up to 13 or more metal atoms. The stoichiometries produced are not random. Instead, there is a strong tendency to form certain clusters preferentially. Species such as Y₃O₄⁺, Y₄O₆⁺, Y₅O₇⁺, Y₆O₈⁺, Y₇O₁₀⁺ and Y₉O₁₃⁺ are prominent. For convenience, these stoichiometries and others are designated

as 3/4, 4/6, 5/7, etc., from here on. This mass spectrum changes slightly in its relative peak intensities with pulsed nozzle-vaporization laser timing and gas conditions, but the same prominent clusters are always observed. The number of oxygen atoms, m , is always greater than or equal to the number of metal atoms, n . Beyond that, many of the intense mass peaks fit the formula $YO(Y_2O_3)_x^+$, and it is apparent that these odd-numbered species are usually somewhat more abundant than the even-numbered species. Little change in stoichiometry is observed upon changing the oxygen concentration. The mass spectrum in Figure 3.1 is obtained with 5% O_2 ; the overall signals decrease with lower oxygen concentration, but values down to about 1% still produce spectra with comparable overall intensities. The oxygen concentration has a small effect on the stoichiometry of the $n=4$ clusters, with $Y_4O_5^+$ (i.e. 4/5) the most prominent species at lower oxygen concentrations and 4/6 slightly more abundant at 5% oxygen or higher. The mass spectrum reported here is similar to the one reported by Bernstein and Kang using photoionization of neutral clusters [28i], although no preference was apparent in their work for the odd numbered species.

The mass spectrum of $La_nO_m^+$ cation clusters produced can be seen in Figure 3.2. Clusters containing up to about 15 metal atoms are detected here. Many stoichiometries similar to those seen for yttrium oxide are again found here, however, the preference to form $LaO(La_2O_3)_x^+$ clusters appears to be stronger. The mass spectrum in the top pane of Figure 2 is obtained with a 3% oxygen gas mixture. The strong preference for odd numbered cation clusters is apparent, and all of the prominent species fit the $LaO(La_2O_3)_x^+$ stoichiometry. In the small clusters, the 3/4 species stands out, while in the larger clusters 7/10 and 9/13 are prominent. The 7/10 cluster has 3-4 times the

intensity of its 6/9 or 8/12 neighbors, and it is also appreciably more intense than the 5/7 cation. At each metal atom increment, there is a limited number of oxide stoichiometries present, with some small intensity seen for the cation clusters containing only one oxygen more or less than the main cluster in that group. The two largest clusters observed, 13/19 and 15/22, both fit the $\text{LaO}(\text{La}_2\text{O}_3)_x^+$ stoichiometry, and have no adjacent peaks with other amounts of oxygen. The bottom pane of Figure 3.2 shows the mass spectrum measured with a 10% oxygen gas mixture. Here, a wider variety of cluster cations are observed, with some metal sizes having up to eight more oxygen atoms than the most prominent cluster stoichiometry. In the $n=4$ group, the 4/7 species is larger with 10% oxygen, but the 4/6 and 4/7 species have comparable intensities with 3% oxygen. There is also a slight preference for 8/13 with 10% oxygen instead of the 8/12 observed with 3% oxygen. These results generally agree with those seen by Gibson²³ and by van Stipdonk and coworkers [24], although both of these previous studies detected primarily the major $\text{LaO}(\text{La}_2\text{O}_3)_x^+$ peaks and little else. It is not obvious why the lanthanide species vary more with the oxygen concentration or why they exhibit a stronger preference for the $\text{MO}(\text{M}_2\text{O}_3)_n^+$ stoichiometry. The growth conditions are the same for these species, and their bonding energetics are similar (see below). However, the clusters produced in experiments such as these have likely undergone many addition/fragmentation steps in growth, in addition to ionization/neutralization processes in the plasma. The energy deposited into the plasma may vary substantially because of the different species present and their detailed states, spectra and energy transfer processes. Any further conclusions about the mass spectral intensities would therefore be highly speculative.

To investigate the relative stabilities of these clusters, we perform mass-selected photoexcitation experiments. Cation cluster masses with sufficient intensity are selected and then photodissociated by laser excitation in the reflectron at either 355 or 532 nm. The lists of yttrium and lanthanum oxide cation clusters studied and their photofragments are presented in Tables 3.1 and 3.2. We find that either 355 nm or 532 nm induces photofragmentation in some but not all yttrium oxide clusters. However, only 355 nm yields fragmentation in the lanthanum oxide species. Relatively high laser fluences (40-60 mJ/pulse) are necessary to give detectable fragmentation in either system. This indicates that multiple photon excitation is necessary to break bonds in these clusters, consistent with the conditions we have applied in the past to study other transition metal oxide species.²⁷ This suggests, as we suspect, that the bond energies in these systems are quite high. Armentrout and coworkers determined the dissociation energy for the yttrium oxide diatomic to be 7.14 eV using zero-kinetic-energy (ZEKE) photoelectron spectroscopy [33d]. Jackson and coworkers determined the dissociation energy for LaO to be 9.07 eV using CID [34]. Although DFT calculations like these are not expected to provide quantitative binding energies, the results of these calculations presented later indicate that the per-bond dissociation energies for many of the larger clusters are around 6 eV. It is therefore understandable that these larger oxide clusters would also have strong bonds, thus explaining why extreme laser conditions are required for photodissociation. Dissociation is never efficient, but 355 nm laser light produces the largest fragment yield here, and thus all data shown are using this wavelength. We cannot tell whether the greater efficiency at 355 nm is due to the larger photon energy or to an improved absorption spectrum at this shorter wavelength. At the extreme laser

powers employed here, it is conceivable that multiple photon processes could lead to doubly charged photofragments, via photoionization of singly charged fragment ions. However, no such species are detected.

Another observation in these photodissociation experiments supports the exceptional bond strength in these systems. The dissociation efficiency depends not only on the laser intensity used for dissociation; it also depends on the *vaporization* laser intensity. In the full mass spectra of both yttrium oxide and lanthanum oxide, little dependence on the vaporization laser was noticed other than a predictable decrease in signal when its power was too high or too low. However, upon mass selection, laser fluences of 15 mJ/pulse or greater lead to the production of signals for low-mass fragment peaks even without the photodissociation laser. These so-called metastable ion signals are familiar and are often seen with reflectron instruments when ions have significant internal energy. Even though we have collisional cooling via a supersonic expansion, the condensation energy from the formation of multiple metal oxide bonds, and perhaps the energy deposited into the metal-containing plasma upon vaporization, is too great to be cooled by collisions with the helium collision gas. Because of this unquenched internal energy, some prompt fragmentation likely occurs in the cluster source itself or in the transit time to the mass spectrometer, and we only detect the remnant of the internal energy which is still present at the mass spectrometer sampling position about 200 μ sec downstream. For metastable ions to be detected, fragmentation must occur in the time window between the ion acceleration at this point and the reflectron turning region, which is an additional 60-80 μ sec away from the source, depending on the mass. Such slow unimolecular dissociation like this is typically found

only for strongly bound ions. Reducing the vaporization laser power eliminates the metastable fragmentation, presumably because clusters are not produced with as much internal energy. However, too much reduction in the vaporization laser intensity makes the photodissociation more difficult. We find that vaporization laser pulse energies of about 12 mJ/pulse were required to observe detectable photodissociation, regardless of the fragmentation laser pulse energy. This suggests that residual internal energy from the cluster formation process is needed to aid in the photofragmentation process. In the reflectron configuration that we use, photodissociation must occur on a timescale of 1-3 μ sec to be detected. Apparently, the internal energy that these oxide clusters retain from their growth plus that imparted by photoexcitation makes it possible for the dissociation to occur within this time frame.

Figures 3.3 and 3.4 show typical photodissociation mass spectra for selected yttrium oxide clusters. These are shown in a difference mode, in which the mass spectrum with the fragmentation laser off is subtracted from that with it on. This gives a negative parent ion peak indicating its depletion and positive fragment peaks. In an ideal scenario, the integrated fragment peak intensities would equal the amount of depletion. However, mass discrimination in this photodissociation configuration makes it difficult to focus simultaneously on parent ions and their fragments [72]. We can therefore distinguish between strong and weak fragmentation channels but cannot give any quantitative branching ratios. In the present experiments, the fragmentation yield is so extremely small that the fragment signal often cannot be seen shot-by-shot on the oscilloscope, making it difficult to focus on these species. The parent ion is always at least partially focused, and its depletion is therefore more intense. It is conceivable that

fragment ion detection is affected by some translational energy release in these photofragments, but this is not generally expected to be prominent in multiphoton processes, which deposit energy non-specifically in many internal states. In each of the fragmentation spectra here, the parent ion depletion is offscale, and its intensity is therefore limited with a horizontal line.

Figure 3.3 shows a series of $n=4$ cluster cations and their fragments. This group of clusters showed no clear stoichiometric preference in the mass spectrum, with the most intense cluster in the group depending on the oxygen concentration. The $4/5$ cluster has a relatively efficient fragmentation to form the $3/4$ species. The $4/6$ species fragments to produce the smaller $2/2$, $2/3$, and $1/1$ ions. This cluster is the only one that leads to such small fragments. The $4/7$ cation fragments to produce $4/6$ and $4/5$ by losing one or two oxygen atoms, and also to a small amount of $3/4$. The fragmentation from $4/7 \rightarrow 4/6$ must occur by loss of atomic oxygen, while the production of $4/5$ could occur by the loss of either two atoms or the O_2 molecule. Likewise, the production of the $3/4$ charged fragment here could be accompanied by atomic or molecular neutrals. Unfortunately in this case and others below, we cannot identify the missing neutral(s) which would elucidate whether the mechanism of decomposition is sequential or concerted. We therefore indicate neutral losses in brackets, e.g. $[O_2]$, to emphasize this uncertainty. It is also true that we cannot distinguish between concerted and sequential fragmentation processes. The fragment ions seen here could be formed stepwise, or all in parallel. Laser power dependence does not reveal any change in relative ion intensities, but this is not a definitive way to identify the mechanism. Therefore, we focus on just the nature of the fragments formed and the neutral losses that must go along with these.

Figure 3.4 shows the fragmentation mass spectra for the $Y_7O_{10}^+$ and $Y_9O_{13}^+$ clusters. The $7/10$ species fragments to form $6/8$, $5/7$, and $3/4$, with the $3/4$ ion the most intense. Each of these fragments are immediately recognizable as the most intense stoichiometries seen in the mass spectrum coming out of the cluster source. The $9/13$ cluster fragments to produce $7/10$, and then the rest of the smaller fragment ions are the same for both parents. As noted above, we cannot determine what the specific neutral fragments are that go along with these ions. In every case, atomic or molecular neutral species are possible that would conserve mass. However, it is interesting to note the repeated occurrence of the $2/3$ interval in the neutrals. Except for the $6/8$ species, there is a common interval of $2/3$ for the apparent sequence $9/13 \rightarrow 7/10 \rightarrow 5/7 \rightarrow 3/4$. Y_2O_3 is of course the stoichiometry of the most common bulk oxide of yttrium [1-3].

These selected fragmentation mass spectra in Figures 3 and 4 already demonstrate the features common to all the yttrium oxide clusters that we have studied, as listed in Table 3.1. The $3/4$, $5/7$, $6/8$ and $7/10$ ions are produced many times from many parent ion dissociation processes. Except for the $6/8$ species, these all have an odd number of metal atoms and fit the general formula of $YO(Y_2O_3)_n^+$, where $n=1,2,3$. Except for the formation of the $6/8$ species, these ions often fragment by the loss of the $[2/3]$ neutral interval or some multiple of this. It is therefore tempting to view their fragmentation as a sequential loss of the $[2/3]$ neutral. Other ions that we have selected that are not one of these $YO(Y_2O_3)_n^+$ species tend to lose whatever group is necessary to produce one of these ions. The only even-numbered ion that is produced in multiple fragmentation events is $6/8$. There are no prominent two, four or eight-atom fragment ions.

Lanthanum oxide clusters fragment in much the same way that the yttrium species do. Here, fragmentation is extremely inefficient, even compared to the yttrium oxide systems. The fragmentation data shown was averaged for considerably longer than the yttrium oxide data, and still shows very low signals. The fragmentation channels for each mass selected cation cluster are shown in Table 3.2. Photofragmentation was attempted with both 355 and 532 nm, but fragmentation was only observed with 355 nm. Although different distributions of lanthanum oxide clusters are observed when the oxygen concentration is varied, there are no differences in the fragmentation channels observed when the same parent ion is studied.

Figure 3.5 shows the photofragmentation data for the 4/6 and 4/7 clusters. In the top frame, the fragmentation of 4/7 produces the 4/5 and 3/4 species. Again, the possible paths to 4/5 are via the loss of O₂ or two oxygen atoms. Unlike in yttrium oxide, no channel is observed for the loss of a single oxygen atom, suggesting that the 4/7 → 4/5 process occurs by the loss of O₂. The 3/4 fragment could be formed by a single loss of neutral [1/3] or by a sequential loss of [O₂] and then [1/1]. The latter seems more likely, as the [1/3] neutral should not be as stable as [1/1] because of the likely oxidation state of the metal. Theory was performed to investigate this, as discussed below. In the lower frame, the dissociation of the 4/6 species to produce 3/4 indicates a neutral loss of [1/2].

Figure 3.6 shows the photofragmentation data for several other representative La_nO_m⁺ clusters, chosen mainly by their availability with good intensity in the mass spectrum from the source. The top trace shows the fragmentation of 9/13, which produces the next smaller LaO(La₂O₃)_x cation, 7/10, with a neutral difference of [2/3]. The middle trace shows the fragmentation of 7/10, which again loses [2/3] to yield 5/7,

which is another $\text{LaO}(\text{La}_2\text{O}_3)_x^+$ cluster. Most of the other clusters are also found to fragment in this way, eliminating $[2/3]$ to form the next smallest $\text{LaO}(\text{La}_2\text{O}_3)_x$ cation cluster. The main exception to this pattern is the $6/8$ species, whose fragmentation is shown in the lower trace. The charged fragments here are $5/7$ and $3/4$, implying that $6/8$ loses $[1/1]$ and then the $5/7$ species produced fragments in exactly the way the selected $5/7$ ion does, by the elimination of $[2/3]$ to produce $3/4$. The $6/9$ cluster (not shown) has a single fragmentation channel to produce $5/7$, implying the loss of $[1/2]$.

The fragmentation in all these lanthanum oxide clusters seems to be driven by the strong tendency to form the $\text{LaO}(\text{La}_2\text{O}_3)_x^+$ stoichiometry. Other fragmentation channels are rare, and only observed for the clusters which are less intense in the mass spectrum. When the $\text{LaO}(\text{La}_2\text{O}_3)_x$ cation clusters fragment, they all lose units of neutral $[2/3]$, which is the bulk stoichiometry. Van Stipdonk and coworkers observed similar behavior in the metastable decay of $\text{LaO}(\text{La}_2\text{O}_3)_x^+$ clusters [24]. These particular clusters demonstrate considerably less efficient photofragmentation compared to the even numbered clusters. Given the dramatic preference for these clusters in the mass spectrum and how they dominate the fragmentation channels, it seems likely that they are significantly more stable than other cluster stoichiometries.

Some insight can be gained from comparing these yttrium and lanthanum oxides. Both have the same bulk stoichiometries, M_2O_3 . In the mass spectra for both systems, the $\text{MO}(\text{M}_2\text{O}_3)_x^+$ cations are more intense than the clusters with even numbers of metal atoms. For these odd-numbered metal species, there is little variation in the number of oxygen atoms. This is not the case for the even-numbered clusters, which demonstrate no clear preference for a specific number of oxygens. In the fragmentation processes of both

yttrium and lanthanum oxides, $\text{MO}(\text{M}_2\text{O}_3)_x$ cations are universally the most abundant, as is the loss of neutral [2/3]. For the even-numbered ions of both metals, the initial neutral loss varies as needed to produce the nearest $\text{MO}(\text{M}_2\text{O}_3)_x^+$ species as the highest mass charged fragment. Smaller fragments then follow the same $\text{MO}(\text{M}_2\text{O}_3)_x^+$ sequence seen for the other clusters. This indicates that the production of $\text{MO}(\text{M}_2\text{O}_3)_x$ cations is the strongest driving force behind these fragmentation processes. Another important tendency is the loss of the [2/3] neutral unit.

The similarities between these yttrium and lanthanum systems are striking, but there are also differences. In particular, the overall fragmentation processes for lanthanum are less efficient than those for yttrium, and fewer fragment channels are detected for lanthanum. This is consistent with a sequential fragmentation mechanism for both kinds of systems, which proceeds to a greater extent for the yttrium species. This suggests that the bond energies for the yttrium species are generally lower than those for the lanthanum species. The most common step in the sequential fragmentation appears to be the elimination of the [2/3] neutral corresponding to the bulk stoichiometry. Another noticeable difference is the importance of the 6/8 cluster for the yttrium oxides. This is a prominent species in the mass spectrum of the clusters produced by the source, and it is the only cluster with an even number of metal atoms produced as a common fragment ion. This particular cluster appears to be quite important for yttrium oxides, but not for lanthanum.

The stoichiometries seen in these yttrium and lanthanum oxide clusters are reasonable in light of the metal oxidation states known for these metals. As noted, both lanthanum and yttrium oxides take the form M_2O_3 in the bulk, where the metal oxidation

state is +3. If we average over all the atoms without regard to structural arrangements, the $\text{MO}(\text{M}_2\text{O}_3)_x^+$ cations seen throughout the data here for both metals indicate that the metal in these clusters has the same +3 oxidation state. This same $\text{MO}(\text{M}_2\text{O}_3)_x^+$ stoichiometry was observed previously for oxides clusters of aluminum [35c], and in those of antimony and bismuth [27a], where the +3 oxidation state is also expected. Apparently, this stoichiometry pattern is the best way for these clusters to maintain the +3 oxidation state while accommodating the single positive charge. Yttrium is also known to have a +2 oxidation state in metal-hydrides, as does lanthanum in hydrides, sulfides, tellurides and selenides [3]. The 1/1 neutral seen occasionally in the data here as a leaving group can be rationalized in this way, along with the 4/5 and 6/8 clusters, which would require a single metal atom in this lower oxidation state. However, there is no simple way to assign common oxidation states to some of the other even numbered metal clusters produced as minor species in the source distribution. At least one metal with a +4 oxidation state would be necessary in the 4/6, 6/9 and 8/12 clusters. Although some of these latter species deviate from this, it is clear that the most stable species produced for both of these metals follow the $\text{MO}(\text{M}_2\text{O}_3)_x^+$ formula and have the most common +3 oxidation state. This behavior is quite different from that seen previously for other transition metals. In our studies of the vanadium group (V, Nb, Ta) oxides, where the normal oxidation state is +5, we found evidence for lower oxidation states (average values of 4.5) in the smaller clusters [27b]. In the case of chromium oxides, where the most common oxidation state is +3 (as in Cr_2O_3), the small clusters preferred the higher +6 oxidation state, which is known, but less common, for chromium (as in CrO_3) [27c]. In the iron system, the small clusters preferred the +2 oxidation state, and 1:1 oxide

stoichiometries rather than the more common +3 value seen in Fe_2O_3 [27d]. Thus, we have seen significant variation in the oxidation states of small transition metal oxides compared to the most common bulk phases in other studies. However, the yttrium and lanthanum systems seen here follow the same oxidation state trend seen in the most common solids.

To further investigate the stability of the specific ions and neutrals identified here, we performed DFT calculations to find the lowest energy structure and binding energies, using the B3LYP functional. The prominent cations Y_2O_3^+ , Y_3O_4^+ , Y_4O_6^+ , Y_5O_7^+ , Y_6O_8^+ , and $\text{Y}_7\text{O}_{10}^+$ were investigated. Additionally, the possible neutral leaving groups YO , YO_2 , YO_3 , and Y_2O_3 were investigated. To investigate possible differences in structure between lanthanum oxide and yttrium oxide, selected lanthanum oxide clusters were also included in these computational studies (La_2O_3 , La_2O_3^+ , La_3O_4 , La_3O_4^+ , La_5O_7 , and La_5O_7^+). The schematic minimum energy structures found for these clusters are shown in Figures 3.7 and 3.8. The cations and neutrals have quite similar structures, only differing slightly in bond lengths and angle. In these figures, only one structure for each stoichiometry is shown; additional details are presented in the Supporting Information along with the calculated vibrational frequencies. For each of the stable cations, the corresponding neutral was investigated to explore the role of charge on the relative stability. The energetics for these systems are summarized in Table 3.3 and Table 3.4. For each cluster studied, numerous starting geometries and spin states were investigated in the search to locate the most likely structures for these species. Unfortunately, none of even the diatomic or triatomic species here have been studied with high resolution spectroscopy whereby we could test ground state bond distances or spin configurations.

As shown in Figures 3.7 and 3.8, the structures for these oxides are cage-like with alternating metal-oxygen-metal bonds. Each oxygen is bonded to two or three metal atoms and each metal forms at least three bonds, consistent with the +3 oxidation state. There are no terminal oxygens, i.e., oxygen atoms only attached to a single metal via a double bond. Terminal oxygens like this have been seen in the structures of all the previous transition metal oxide systems that we have studied (V, Nb, Ta, Cr) except iron [27], and are the result of higher metal oxidation states. No internal atoms are found for any of these clusters. NBO analysis shows that all the bonding occurs along the edges of these structures, with no significant metal-metal interactions across the interior of the cages. Lanthanum oxide clusters are calculated to have the same general structures as the corresponding yttrium species, but the bond distances are generally longer. For each stoichiometry, the neutral and cation have essentially the same structure, with only minor differences in bond lengths and angles. These structures presumably maximize the number of strong metal-oxygen bonds. Interestingly, the structures shown here for the smaller clusters are pretty much the same as those we proposed several years ago in our study of antimony and bismuth oxide clusters [27a]. At that time, we were not able to do any DFT calculations, but instead just used the expected oxidation states and connected the atoms to make structures that satisfied their bonding capacity. It is satisfying that the more sophisticated DFT calculations here arrive at the same qualitative conclusions for these structures. The NBO analysis also provides a charge on each atom, which is within ± 0.2 of +3 for each metal atom and -2 for each oxygen, consistent with the expected ionic bonding.

The bond energies in these clusters are all quite high, as is typical for metal oxides. Table 3.3 shows that the per bond dissociation energy varies from 59 kcal/mol to 155 kcal/mol (2.56 to 6.72 eV) for yttrium oxide, with the larger clusters having bond energies around 150 kcal/mol (6 eV). Lanthanum oxide clusters (Table 3.4) have per bond energies ranging from 100 to 142 kcal/mol (4.3-6.2 eV), with the larger clusters again having bond energies around 140 kcal/mol (6 eV). These bond energies are significantly greater than those for other transition metal oxides that we have studied [27]. For example, the per-bond energy computed for chromium oxide clusters with the same DFT methods were in the range of 70-90 kcal/mol [27c]. DFT is of course not reliable for quantitative energetics in clusters of this type, but the relative energies computed indicate that the yttrium and lanthanum clusters are quite strongly bound. We can investigate the effect of charge on bonding energetics as well. The atomization energies are relative to separated neutral atoms or to separated neutrals and one metal ion, respectively. Using this as a reference, the cations here are found to be slightly more stable than the corresponding neutrals. It is possible in principle to use the difference in atomization energies for neutrals and ions to derive ionization potentials for the neutral clusters. However, because DFT energetics are not quantitative even for the atomic metal species, such an exercise would not be useful. Although the atomization energy is generally higher for yttrium oxide, the lanthanum oxide clusters proved to be more difficult to fragment and had fewer fragmentation channels. However, the absorption cross sections for lanthanum and yttrium oxide are unknown, so lanthanum oxide may simply not absorb light at the wavelengths used as efficiently as yttrium oxide.

The calculated energetics prove somewhat useful in explaining the observed stabilities and fragmentation patterns. YO and YO₂ are strongly bound, but YO₃ does not converge to a stable structure. This suggests that the loss of [1,3] in our photodissociation experiments most likely represents the simultaneous, or rapid sequential, loss of YO and O₂. The same is seen with lanthanum clusters, where LaO₃ does not converge to a stable structure. The calculated atomization energy for YO (6.71 eV) is somewhat lower than the value measured by Armentrout (7.14 eV) [33d]. The calculated value for LaO (9.93 eV) compares somewhat less favorably to Jackson's measured value of 9.07 eV [34]. Although these comparisons are reasonable, some of the energetics computed for the larger clusters are somewhat troubling. Oddly, both the Y₄O₆ cation and neutral are calculated to be among the most stable clusters per bond, but these are not seen as fragments in any case other than the dissociation of 4/7. Y₃O₄⁺ and the Y₂O₃ are not calculated to be especially stable relative to other clusters, but these are seen to be the most intense cation fragment and the most common neutral leaving group, respectively, throughout our data. Y₂O₃ is not calculated to be more stable than the cation, despite having the same stoichiometry as bulk yttrium oxide. On the other hand, the Y₇O₁₀ cation is nearly 20 kcal/mol more stable per bond than the 5/7 cation, and this species is quite prominent in the mass spectrum and it appears in the fragmentation of all clusters with n > 7.

Another trend running through the data for both metal oxide systems is that the per-bond dissociation energies increase with cluster size. The 5/7 clusters for both metals have energies of about 140 kcal/mol, while the 7/10 value for yttrium is about 150 kcal/mol. These are significantly greater than the 2/3 and 3/4 values for both metals.

Apparently, the smaller cage structures are strained compared to the larger ones. It could then be speculated that the smaller cage species here are more reactive than their larger cage counterparts. Reaction kinetics studies on these systems would be interesting to test this possibility.

3.5 Conclusions

Yttrium and lanthanum oxide clusters produced by laser vaporization have been investigated with time-of-flight mass spectrometry and mass-selected photodissociation. Only a limited number of oxide stoichiometries are observed for each cluster size. There is a strong preference observed for odd numbered metal clusters in the mass spectrum. Dissociation produces mainly the same ions, mostly commonly those with the $\text{MO}(\text{M}_2\text{O}_3)_x^+$ stoichiometry. Yttrium oxide clusters are observed to have a variety of fragmentation channels. Photodissociation appears to be a sequential process, with the loss of the M_2O_3 neutral occurring throughout the data for both metals. In addition to the $\text{MO}(\text{M}_2\text{O}_3)_x^+$ ions and M_2O_3 neutrals, the Y_6O_8^+ cluster is also formed prominently by cluster growth and is a common photofragment. Lanthanum oxide clusters rarely have more than one fragmentation channel, with $\text{LaO}(\text{La}_2\text{O}_3)_x^+$ fragments produced almost exclusively. Unlike other transition metal oxide clusters studied previously, the +3 oxidation state implied by the data here for both of these cluster systems is exactly the same as that for the corresponding bulk oxides.

Density functional theory computations on these clusters produce structures that are visually and geometrically appealing, which lead to high bonding stability.

Examination of the per-bond energetics gives some insight into the stabilities of the clusters, but the picture is not as clear as in the experiment. Future theoretical investigations of these systems could be useful. These oxide systems have greater per-bond binding energies than many other transition metal oxide clusters. Due to this high intrinsic stability, these systems may be interesting for isolation in macroscopic quantities as nanocluster materials. Because several of these systems are closed-shell singlets with an overall single charge, they might be less reactive and produce more stable solids if co-condensed with negatively charged ligands.

3.6 Acknowledgements

We gratefully acknowledge generous support for this work from the Air Force Office of Scientific Research (Grant No. FA9550-06-1-0028).

Supporting Information

The Supporting Information for this manuscript includes the full citation for reference 66 as well as additional details for the density functional calculations on the clusters studied here. These details can be found in Appendix A.

3.7 References

- (1) Cox, P. A., *Transition Metal Oxides*, Clarendon Press, Oxford, 1992.
- (2) Rao, C. N.; Raveau, B. *Transition Metal Oxides*, John Wiley, New York, 1998.
- (3) Cotton, F. A.; Wilkinson, G.; Murillo, C. A.; Bochmann, M., *Advanced Inorganic Chemistry*, 6th edition, John Wiley & Sons, New York, 1999.
- (4) Hayashi, C.; Uyeda, R.; Tasaki, A., *Ultra-Fine Particles*; Noyes, Westwood, 1997.
- (5) Henrich, V. E.; Cox, P. A., *The Surface Science of Metal Oxides*; Cambridge University Press, Cambridge, 1994.
- (6) Somorjai, G. A., *Introduction to Surface Chemistry and Catalysis*; Wiley-Interscience, New York, 1994.
- (7) Gates, B. C. *Chem. Rev.* **1995**, *95*, 511.
- (8) a) Rainer, D. R.; Goodman, D. W. *J. Mol. Catal. A: Chem.* **1998**, *131*, 259. b) St. Clair, T. P.; Goodman, D. W. *Top. Catal.* **2000**, *13*, 5. c) Wallace, W. T.; Min, B. K.; Goodman, D. W. *Top. Catal.* **2005**, *34*, 17. d) Chen, M. S.; Goodman, D. W. *Acc. Chem. Res.* **2006**, *39*, 739.
- (9) a) Wachs, I. E.; Briand, L. E.; Jehng, J. M.; Burcham, L.; Gao, X. T. *Catal. Today* **2000**, *57*, 323. b) Chen, Y. S.; Wachs, I. E. *J. Catal.* **2003**, *217*, 468. c) Wachs, I. E. *Catal. Today* **2005**, *100*, 79. d) Wachs, I. E.; Jehng, J. M.; Ueda, W. *J. Phys. Chem. B* **2005**, *109*, 2275. e) Tian, H. J.; Ross, E. I.; Wachs, I. E., *J. Phys. Chem. B* **2006**, *110*, 9593.
- (10) Pope, M.T; Müller, A. *Polyoxyometalate Chemistry From Topology via Self-Assembly to Applications*; Kluwer: Boston, 2001.

- (11) Crans, D.C.; Smee, J.J.; Gaidamauskas, E.; Yang, L.Q. *Chem. Rev.* **2004**, *104*, 849.
- (12) a) Rockenberger, J.; Scher, E.C.; Alivisatos, A.P. *J. Am. Chem. Soc.* **1999**, *121*, 11595 b) Puentes, V.F.; Krishnan, K.M.; Alivisatos, A.P. *Science* **2001**, *291*, 2115. c) Nolting, F.; Luning, J.; Rockenberger, J.; Hu, J.; Alivisatos, A.P. *Surf. Rev. Lett.* **2002**, *9*, 437. d) Jun, Y.W.; Casula, M.F.; Sim, J.H.; Kim, S.Y.; Cheon, J.; Alivisatos, A.P. *J. Am. Chem. Soc.* **2003**, *125*, 15981. e) Casula, M.F.; Jun, Y.W.; Zaziski, D.J.; Chan, E.M.; Corrias, A.; Alivisatos, A.P. *J. Am. Chem. Soc.* **2006**, *128*, 1675.
- (13) Ayers, T.M.; Fye, J.L.; Li, Q.; Duncan, M.A. *J. Cluster Sci.* **2003**, *14*, 97.
- (14) Cushings, B.L.; Kolesnichenko, V.L.; O'Connor, C.J. *Chem. Rev.* **2004**, *104*, 3893.
- (15) Fernandez-Garcia, M.; Martinez-Arias, A.; Hanson, J.C.; Rodriguez, J.A. *Chem. Rev.* **2004**, *104*, 4063.
- (16) Stepanov, A.L.; Boura, G.; Gartzza, M.; Osinb, Yu.N.; Reinholdta, A.; Kreibig, U. *Vacuum* **2004**, *64*, 9.
- (17) a) Berkowitz, J.; Chupka, W. A.; Inghram, M. G. *J. Chem. Phys.* **1957**, *27*, 87. b) Inghram, M. G.; Chupka, W. A.; Berkowitz, J. *J. Chem. Phys.* **1957**, *27*, 569.
- (18) Farber, M.; Uy, O. M.; Srivastava, R. D., *J. Chem. Phys.* **1972**, *56*, 512.
- (19) Bennett, S. L.; Lin, S. S.; Gilles, P. W. *J. Phys. Chem.* **1974**, *78*, 266.
- (20) Kahwa, I.A.; Selbin, J. *Inorg. Chim. Acta* **1988**, *144*, 275
- (21) Knickelbein, M. *J. Chem. Phys.* **1995**, *102*, 1
- (22) Knickelbein, M. *Phys. Rev. B* **2005**, *71*, 1

- (23) Gibson, J.K. *J. Appl. Phys.* **1995**, 78, 1274
- (24) a) Van Stipdonk, M.J.; Schweikert, E.A. *Nuclear Instruments and Methods in Physics Research B* **1995**, 96, 530 b) Van Stipdonk, M.J.; Justes, D. R.; English, R. D.; Schweikert, E.A. *J. Mass Spectrom.* **1999**, 34, 677
- (25) a) Kooi, S. E.; Castleman, A. W. *J. Phys. Chem. A* **1999**, 103, 5671. b) Bell, R. C.; Zemski, K. A.; Justes, D. R.; Castleman, A. W. *J. Chem. Phys.* **2001**, 114, 798.
- (26) a) Deng, H. T.; Kerns, K. P.; Castleman, A. W. *J. Phys. Chem.* **1996**, 100, 13386. b) Bell, R. C.; Zemski, K. A.; Kerns, K. P.; Deng, H. T.; Castleman, A. W. *J. Phys. Chem. A* **1998**, 102, 1733. c) Bell, R. C.; Zemski, K. A.; Castleman, A. W. *J. Cluster Sci.* **1999**, 10, 509. d) Zemski, K. A.; Justes, D. R.; Castleman, A. W. *J. Phys. Chem. B* **2002**, 106, 6136. e) Justes, D. R.; Mitric, R.; Moore, N. A.; Bonacic-Koutecky, V.; Castleman, A. W. *J. Am. Chem. Soc.* **2003**, 125, 6289. f) Justes, D. R.; Moore, N. A.; Castleman, A. W. *J. Phys. Chem. B* **2004**, 108, 3855. g) Bergeron, D. E.; Castleman, A. W.; Jones, N. O.; Khanna, S. N. *Nano. Lett.* **2004**, 4, 261. h) p) Moore, N. A.; Mitric, R.; Justes, D. R.; Bonacic-Koutecky, V.; Castleman, A. W. *J. Phys. Chem. B* **2006**, 110, 3015. i) Reilly, N. M., Reveles, J. U., Johnson, G. E., Khanna, S. N., Castleman, A.W. *Chem. Phys. Lett.* **2007**, 435, 295.
- (27) a) France, M. R.; Buchanan, J. W.; Robinson, J. C.; Pullins, S. H.; Tucker, J. L.; King, R. B.; Duncan, M. A. *J. Phys. Chem. A* **1997**, 101, 6214. b) Molek, K. S.; Jaeger, T. D.; Duncan, M. A., *J. Chem. Phys.* **2005**, 123. c) Molek, K.S., Reed,

- Z.D., Ricks, A.M., Duncan, M.A. *J. Phys. Chem. A* **2007**, *111*, 8080 d) Molek, K. S.; Anfuso, C.; Duncan, M. A., *J. Phys. Chem. A*, submitted.
- (28) a) Foltin, M.; Stueber, G. J.; Bernstein, E. R. *J. Chem. Phys.* **1999**, *111*, 9577. b) Shin, D. N.; Matsuda, Y.; Bernstein, E. R. *J. Chem. Phys.* **2004**, *120*, 4150. c) Shin, D. N.; Matsuda, Y.; Bernstein, E. R. *J. Chem. Phys.* **2004**, *120*, 4157. d) Matsuda, Y.; Bernstein, E. R. *J. Phys. Chem. A* **2005**, *109*, 314. e) Matsuda, Y.; Bernstein, E. R. *J. Phys. Chem. A* **2005**, *109*, 3803. f) Kang, Y.; Bernstein, E.R. *Bull. Korean Chem. Soc.* 2005, *26*, 345. g) Dong, F.; Heinbuch, S.; He, S. G.; Xie, Y.; Rocca, J. J.; Bernstein, E. R. *J. Chem. Phys.* **2006**, *125*, 164318.
- (29) a) Harvey, J. N.; Diefenbach, M.; Schröder, D.; Schwarz, H. *Int. J. Mass. Spectrom.* **1999**, *183*, 85. b) Schröder, D.; Schwarz, H.; Shaik, S. *Struct. & Bonding* **2000**, *97*, 91. c) Jackson, P.; Fisher, K. J.; Willett, G. D. *Chem. Phys.* **2000**, *262*, 179. d) Jackson, P.; Harvey, J. N.; Schröder, D.; Schwarz, H. *Int. J. Mass. Spectrom.* **2001**, *204*, 233. e) Schroder, D.; Engeser, M.; Schwarz, H.; Harvey, J. N. *ChemPhysChem* **2002**, *3*, 584. Koszinowski, K.; Schlangen, M.; Schröder, D.; Schwarz, H. *Eur. J. Inorg. Chem.* **2005**, 2464. f) Feyel, S.; Dobler, J.; Schröder, D.; Sauer, J.; Schwarz, H. *Angew. Chem. Int. Ed. Eng.* **2006**, *45*, 4681. g) Feyel, S.; Schröder, D.; Rozanska, X.; Sauer, J.; Schwarz, H. *Angew. Chem. Int. Ed. Eng.* **2006**, *45*, 4677.
- (30) Wang, X.; Neukermans, S.; Vanhoutte, F.; Janssens, E.; Verschoren, G.; Silverans, R. E.; Lievens, P. *Appl. Phys. B: Lasers Opt.* **2001**, *73*, 417.
- (31) Fielicke, A.; Rademann, K. *Phys. Chem. Chem. Phys.* **2002**, *4*, 2621.
- (32) Aubriet, F.; Muller, J. F. *J. Phys. Chem. A* **2002**, *106*, 6053.

- (33) a) Griffin, J. B.; Armentrout, P. B. *J. Chem. Phys.* **1997**, *106*, 4448. b) Xu, J.; Rodgers, M. T.; Griffin, J. B.; Armentrout, P. B. *J. Chem. Phys.* **1998**, *108*, 9339. c) Griffin, J. B.; Armentrout, P. B. *J. Chem. Phys.* **1998**, *108*, 8062. d) Linton, C.; Simand, B.; Loock, H.P.; Wallin, S.; Rothschof, G.K.; Gunion, R.F.; Morse, M.D.; Armentrout, P.B. *J. Chem. Phys.* **1999**, *111*, 2017 e) Vardhan, D.; Liyanage, R.; Armentrout, P. B. *J. Chem. Phys.* **2003**, *119*, 4166. f) Liu, F. Y.; Li, F. X.; Armentrout, P. B. *J. Chem. Phys.* **2005**, *123*.
- (34) Jackson, G.P.; King, F.L.; Goeringer, D.E.; Duckworth, D.C. *Int. J. Mass Spectrom.* **2002**, *216*, 85.
- (35) a) Chertihin, G. V.; Bare, W. D.; Andrews, L. *J. Chem. Phys.* **1997**, *107*, 2798. b) Zhou, M. F.; Andrews, L. *J. Chem. Phys.* **1999**, *111*, 4230. c) Andrews, L.; Rohrbacher, A.; Laperle, C. M.; Continetti, R. E. *J. Phys. Chem. A* **2000**, *104*, 8173.
- (36) a) Fan, J. W.; Wang, L. S. *J. Chem. Phys.* **1995**, *102*, 8714. b) Wang, L. S.; Wu, H. B.; Desai, S. R. *Phys. Rev. Lett.* **1996**, *76*, 4853. c) Wu, H. B.; Desai, S. R.; Wang, L. S. *J. Am. Chem. Soc.* **1996**, *118*, 7434. d) Wang, Q.; Sun, Q.; Sakurai, M.; Yu, J. Z.; Gu, B. L.; Sumiyama, K.; Kawazoe, Y. *Phys. Rev. B* **1999**, *59*, 12672. e) Gutsev, G. L.; Rao, B. K.; Jena, P.; Li, X.; Wang, L.-S. *J. Chem. Phys.* **2000**, *113*, 1473. f) Sun, Q.; Sakurai, M.; Wang, Q.; Yu, J. Z.; Wang, G. H.; Sumiyama, K.; Kawazoe, Y. *Phys. Rev. B* **2000**, *62*, 8500. g) Gutsev, G. L.; Jena, P.; Zhai, H.-J.; Wang, L.-S. *J. Chem. Phys.* **2001**, *115*, 7935. h) Zhai, H.-J.; Wang, L.-S. *J. Chem. Phys.* **2002**, *117*, 7882. i) Gutsev, G. L.; Bauschlicher, C. W., Jr.; Zhai, H.-J.; Wang, L.-S. *J. Chem. Phys.* **2003**, *119*, 11135. j) Zhai, H.-J.;

- Kiran, B.; Cui, L.-F.; Li, X.; Dixon, D. A.; Wang, L.-S. *J. Am. Chem. Soc.* **2004**, *126*, 16134. k) Zhai, H. J.; Wang, L.-S. *J. Chem. Phys.* **2006**, *125*, 164315. l) Zhai, H. J.; Wang, L.-S. *J. Am. Chem. Soc.* **2007**, *129*, 3022.
- (37) a) Wenthold, P. G.; Jonas, K. L.; Lineberger, W. C. *J. Chem. Phys.* **1997**, *106*, 9961. b) Ramond, T. M.; Davico, G. E.; Hellberg, F.; Svedberg, F.; Salen, P.; Soderqvist, P.; Lineberger, W. C. *J. Mol. Spec.* **2002**, *216*, 1. c) Ichino, T.; Gianola, A. J.; Andrews, D. H.; Lineberger, W. C. *J. Phys. Chem. A* **2004**, *108*, 11307.
- (38) a) Yang, D. S.; Hackett, P. A. *J. Elec. Spectros. Relat. Phenom.* **2000**, *106*, 153. b) Yang, D. S. *Coord. Chem. Rev.* **2001**, *214*, 187.
- (39) Green, S. M. E.; Alex, S.; Fleischer, N. L.; Millam, E. L.; Marcy, T. P.; Leopold, D. G. *J. Chem. Phys.* **2001**, *114*, 2653.
- (40) a) Pramann, A.; Nakamura, Y.; Nakajima, A.; Kaya, K. *J. Phys. Chem. A* **2001**, *105*, 7534. b) Pramann, A.; Koyasu, K.; Nakajima, A.; Kaya, K. *J. Phys. Chem. A* **2002**, *106*, 4891. c) Pramann, A.; Koyasu, K.; Nakajima, A.; Kaya, K. *J. Chem. Phys.* **2002**, *116*, 6521.
- (41) Yoder, B. L.; Maze, J. T.; Raghavachari, K.; Jarrold, C. C. *J. Chem. Phys.* **2005**, *122*, 094313.
- (42) Zhai, H.-J.; Dobler, J.; Sauer, J.; Wang, L.-S. *J. Am. Chem. Soc.* **2007**, *129*, 13270.
- (43) a) von Helden, G.; Kirilyuk, A.; van Heijnsbergen, D.; Sartakov, B.; Duncan, M. A.; Meijer, G. *Chem. Phys.* **2000**, *262*, 31. b) van Heijnsbergen, D.; von Helden, G.; Meijer, G.; Duncan, M. A. *J. Chem. Phys.* **2002**, *116*, 2400. c) van

- Heijnsbergen, D.; Demyk, K.; Duncan, M. A.; Meijer, G.; von Helden, G. *Phys. Chem. Chem. Phys.* **2003**, *5*, 2515.
- (44) a) Fielicke, A.; Meijer, G.; von Helden, G. *J. Am. Chem. Soc.* **2003**, *125*, 3659. b) Fielicke, A.; Meijer, G.; von Helden, G. *Eur. Phys. J. D* **2003**, *24*, 69. c) Fielicke, A.; Mitric, R.; Meijer, G.; Bonacic-Koutecky, V.; von Helden, G. *J. Am. Chem. Soc.* **2003**, *125*, 15716. d) Demyk, K.; van Heijnsbergen, D.; von Helden, G.; Meijer, G. *Astron. & Astrophys.* **2004**, *420*, 547.
- (45) a) Asmis, K. R.; Bruemmer, M.; Kaposta, C.; Santambrogio, G.; von Helden, G.; Meijer, G.; Rademann, K.; Wöste, L. *Phys. Chem. Chem. Phys.* **2002**, *4*, 1101. b) Brummer, M.; Kaposta, C.; Santambrogio, G.; Asmis, K. R. *J. Chem. Phys.* **2003**, *119*, 12700. c) Asmis, K. R.; Meijer, G.; Bruemmer, M.; Kaposta, C.; Santambrogio, G.; Wöste, L.; Sauer, J. *J. Chem. Phys.* **2004**, *120*, 6461. d) Asmis, K. R.; Santambrogio, G.; Brummer, M.; Sauer, J., *Angew. Chem. Int. Ed. Eng.* **2005**, *44*, 3122. e) Janssens, E.; Santambrogio, G.; Brummer, M.; Wöste, L.; Lievens, P.; Sauer, J.; Meijer, G.; Asmis, K. R. *Phys. Rev. Lett.* **2006**, *96*.
- (46) a) Sambrano, J. R.; Andres, J.; Beltran, A.; Sensato, F.; Longo, E. *Chem. Phys. Lett.* **1998**, *287*, 620. b) Calatayud, M.; Silvi, B.; Andres, J.; Beltran, A. *Chem. Phys. Lett.* **2001**, *333*, 493. c) Calatayud, M.; Andres, J.; Beltran, A. *J. Phys. Chem. A* **2001**, *105*, 9760. d) Sambrano, J. R.; Gracia, L.; Andres, J.; Berski, S.; Beltran, A. *J. Phys. Chem. A* **2004**, *108*, 10850. e) Sambrano, J. R.; Andres, J.; Gracia, L.; Safont, V. S.; Beltran, A. *Chem. Phys. Lett.* **2004**, *384*, 56. f) Gracia, L.; Andres, J.; Safont, V. S.; Beltran, A. *Organometallics* **2004**, *23*, 730.

- (47) a) Veliah, S.; Xiang, K. H.; Pandey, R.; Recio, J. M.; Newsam, J. M. *J. Phys. Chem. B* **1998**, *102*, 1126. b) Xiang, K. H.; Pandey, R.; Recio, J. M.; Francisco, E.; Newsam, J. M. *J. Phys. Chem. A* **2000**, *104*, 990.
- (48) a) Reddy, B. V.; Khanna, S. N. *Phys. Rev. Lett.* **1999**, *83*, 3170. b) Morisato, T.; Jones, N. O.; Khanna, S. N.; Kawazoe, Y. *Comp. Mater. Sci.* **2006**, *35*, 366.
- (49) Chakrabarti, A.; Hermann, K.; Druzinic, R.; Witko, M.; Wagner, F.; Petersen, M. *Phys. Rev. B* **1999**, *59*, 10583.
- (50) Zimmermann, R.; Steiner, P.; Claessen, R.; Reinert, F.; Hufner, S.; Blaha, P.; Dufek, P. *J. Phys.: Condens. Matter* **1999**, *11*, 1657.
- (51) a) Vyboishchikov, S. F.; Sauer, J. *J. Phys. Chem. A* **2000**, *104*, 10913. b) Vyboishchikov, S. F.; Sauer, J. *J. Phys. Chem. A* **2001**, *105*, 8588. c) Vyboishchikov, S. F. *J. Mol. Struct. Theochem.* **2005**, *723*, 53.
- (52) Albaret, T.; Finocchi, F.; Noguera, C. *J. Chem. Phys.* **2000**, *113*, 2238.
- (53) Gutsev, G. L.; Andrews, L.; Bauschlicher, C. W. *Theo. Chem. Accts.* **2003**, *109*, 298.
- (54) Ayuela, A.; March, N.H.; Klein, D.J. *J. Phys. Chem. A* **2007**, *111*, 10162
- (55) a) Guo, B. C.; Kerns, K. P.; Castleman, A. W. *Science* **1992**, *255*, 1411. b) Guo, B. C.; Wei, S.; Purnell, J.; Buzza, S.; Castleman, A. W. *Science* **1992**, *256*, 515. c) Cartier, S. F.; May, B. D.; Castleman, A. W. *J. Phys. Chem.* **1996**, *100*, 8175.
- (56) a) Pilgrim, J. S.; Duncan, M. A. *J. Am. Chem. Soc.* **1993**, *115*, 9724. b) Pilgrim, J. S.; Duncan, M. A. *J. Am. Chem. Soc.* **1993**, *115*, 6958. c) Duncan, M. A. *J. Cluster Sci.* **1997**, *8*, 239.
- (57) Rohmer, M.-M.; Benard, M.; Poblet, J.-M. *Chem. Rev.* **2000**, *100*, 495.

- (58) a) van Heijnsbergen, D.; von Helden, G.; Duncan, M. A.; van Roij, A. J. A.; Meijer, G. *Phys. Rev. Lett.* **1999**, *83*, 4983. b) von Helden, G.; van Heijnsbergen, D.; Meijer, G. *J. Phys. Chem. A* **2003**, *107*, 1671.
- (59) a) Gueorguiev, G. K.; Pacheco, J. M. *Phys. Rev. Lett.* **2002**, *88*, 115504. b) Gueorguiev, G. K.; Pacheco, J. M. *Phys. Rev. B* **2003**, *68*, 241401.
- (60) a) Liu, P.; Rodriguez, J. A.; Hou, H.; Muckerman, J. T. *J. Chem. Phys.* **2003**, *118*, 7737. b) Liu, P.; Rodriguez, J. A.; Muckerman, J. T. *J. Chem. Phys.* **2004**, *121*, 10321. c) Liu, P.; Lightstone, J. M.; Patterson, M. J.; Rodriguez, J. A.; Muckerman, J. T.; White, M. G. *J. Phys. Chem. B* **2006**, *110*, 7449.
- (61) a) Varganov, S. A.; Gordon, M. S. *Chem. Phys.* **2006**, *326*, 97. b) Varganov, S. A.; Dudley, T. J.; Gordon, M. S. *Chem. Phys. Lett.* **2006**, *429*, 49.
- (62) Gutsev, G. L.; Andrews, L.; Bauschlicher, C. W. *Theo. Chem. Accts.* **2003**, *109*, 298.
- (63) *Clusters of Atoms and Molecules Vol. I*; Haberland, H., Ed., Springer, Berlin, 1995. *Clusters of Atoms and Molecules Vol. II*; Haberland, H., Ed., Springer, Berlin, 1995.
- (64) Johnston, R. L., *Atomic and Molecular Clusters*; Taylor & Francis, London, 2002.
- (65) a) Ticknor, B. W.; Duncan, M. A. *Chem. Phys. Lett.* **2005**, *405*, 214. b) Jaeger, J. B.; Jaeger, T. D.; Duncan, M. A. *J. Phys. Chem. A* **2006**, *110*, 9310.
- (66) Frisch, M. J. et al., *Gaussian 03 (Revision B.02)*; Gaussian, Inc.: Pittsburgh, PA, 2003.
- (67) Becke, A. D. *J. Chem. Phys.* **1993**, *98*, 5648.
- (68) Lee, C.; Yang, W.; Parr, R. G. *Phys. Rev. B* **1988**, *37*, 785.

- (69) Perdew, J. R.; Chevary, J. A.; Vosko, S. H.; Jackson, K. A.; Pederson, M. R.; Singh, D. J.; Fiolhais, C. *Phys. Rev. B* **1992**, *46*, 6671.
- (70) Dunning, T.H.; Hay, P. J. *Methods of Electronic Structure Theory*, Vol. 2, H. F. Schaefer, ed., Plenum Press, **1977**.
- (71) a) Hay, P. J.; Wadt, W. R. *J. Chem. Phys.* **1985**, *82*, 270. b) Hay, P. J.; Wadt, W. R. *J. Chem. Phys.* **1985**, *82*, 284. c) Hay, P. J.; Wadt, W. R. *J. Chem. Phys.* **1985**, *82*, 299.
- (72) Cornett, D. S.; Peschke, M.; LaiHing, K.; Cheng, P. Y.; Willey, K. F.; Duncan, M. A. *Rev. Sci. Instrum.* **1992**, *63*, 2177.
- (73) Sutton, L.E. *Table of interatomic distances and configuration in molecules and ions*, Supplement 1956-1959, Special publication No. 18, Chemical Society, London, UK, 1965.

Table 3.1. The stoichiometries of yttrium oxide photofragments ($Y_nO_m^+ = n/m$) detected using 355 nm. When multiple fragments are produced, especially prominent channels are indicated in bold.

Cation Clusters	Fragment Ions
4/5	3/4
4/6	1/1 , 2/2, 2/3, 3/4
4/7	3/4, 4/5, 4/6
5/7	3/4
6/9	3/4
7/10	3/4 , 5/7, 6/8
8/11	3/4 , 5/7, 6/8
9/13	3/4 , 5/7, 6/8, 7/10

Table 3.2. The stoichiometries of lanthanum oxide photofragments ($\text{La}_n\text{O}_m^+ = n/m$) detected using 355 nm. When multiple fragments are produced, especially prominent channels are indicated in bold.

Cation Cluster	Fragment Ions
4/5	3/4
4/6	3/4
4/7	3/4, 4/5
5/7	3/4
6/8	3/4, 5/7
6/9	5/7
7/10	5/7
8/12	7/10
9/13	7/10
11/16	9/13

Table 3.3: The energies computed using B3LYP for the yttrium oxide clusters studied here. All units are kcal/mol.

	Atomization Energy	Energy per Bond	Spin Multiplicity
YO	154.8	154.8	2
YO ₂	235.6	117.8	2
Y ₂ O ₃	815.3	135.6	1
Y ₂ O ₃ ⁺	819.5	136.6	2
Y ₃ O ₄	1175.6	130.6	2
Y ₃ O ₄ ⁺	1248.9	138.8	1
Y ₄ O ₆	1789.1	149.1	1
Y ₄ O ₆ ⁺	1790.9	149.2	2
Y ₅ O ₇	2126.0	141.7	2
Y ₅ O ₇ ⁺	2200.1	146.7	1
Y ₇ O ₁₀	3036.5	151.8	2
Y ₇ O ₁₀ ⁺	3101.9	155.1	1

Table 3.4: The energies computed using B3LYP for the lanthanum oxide clusters studied here. All units are kcal/mol.

	Atomization Energy	Energy per Bond	Spin Multiplicity
LaO	229.1	229.1	2
LaO ₂	400.9	200.5	2
La ₂ O ₃	652.1	108.7	1
La ₂ O ₃ ⁺	795.6	132.6	2
La ₃ O ₄	1153.0	128.1	2
La ₃ O ₄ ⁺	1210.4	134.5	1
La ₅ O ₇	2064.1	137.6	2
La ₅ O ₇ ⁺	2130.0	142.0	1

Figure Captions

Figure 3.1. Time of Flight Mass Spectrum for $Y_nO_m^+$ clusters formed in a He expansion with 5% O_2 .

Figure 3.2. Time-of-flight mass spectra for $La_nO_m^+$ clusters formed in a He expansion with 3% (top) versus 10% (bottom) O_2 concentration.

Figure 3.3. Photodissociation mass spectra for $Y_4O_m^+$ clusters at 355 nm. The parent ion depletion is marked as a off-scale negative-going peak.

Figure 3.4. Photodissociation mass spectra for $Y_7O_{10}^+$ and $Y_9O_{13}^+$ clusters at 355 nm. The parent ion depletion is marked as a off-scale negative-going peak.

Figure 3.5. Photodissociation mass spectra for $La_4O_m^+$ clusters at 355 nm. The parent ion depletion is marked as a off-scale negative-going peak.

Figure 3.6. Photodissociation mass spectra for $La_6O_8^+$, $La_7O_{10}^+$, and $La_9O_{13}^+$ clusters at 355 nm. The parent ion depletion is marked as a off-scale negative-going peak.

Figure 3.7. The structures computed for various Y_nO_m clusters.

Figure 3.8. The structures computed for various La_nO_m clusters.

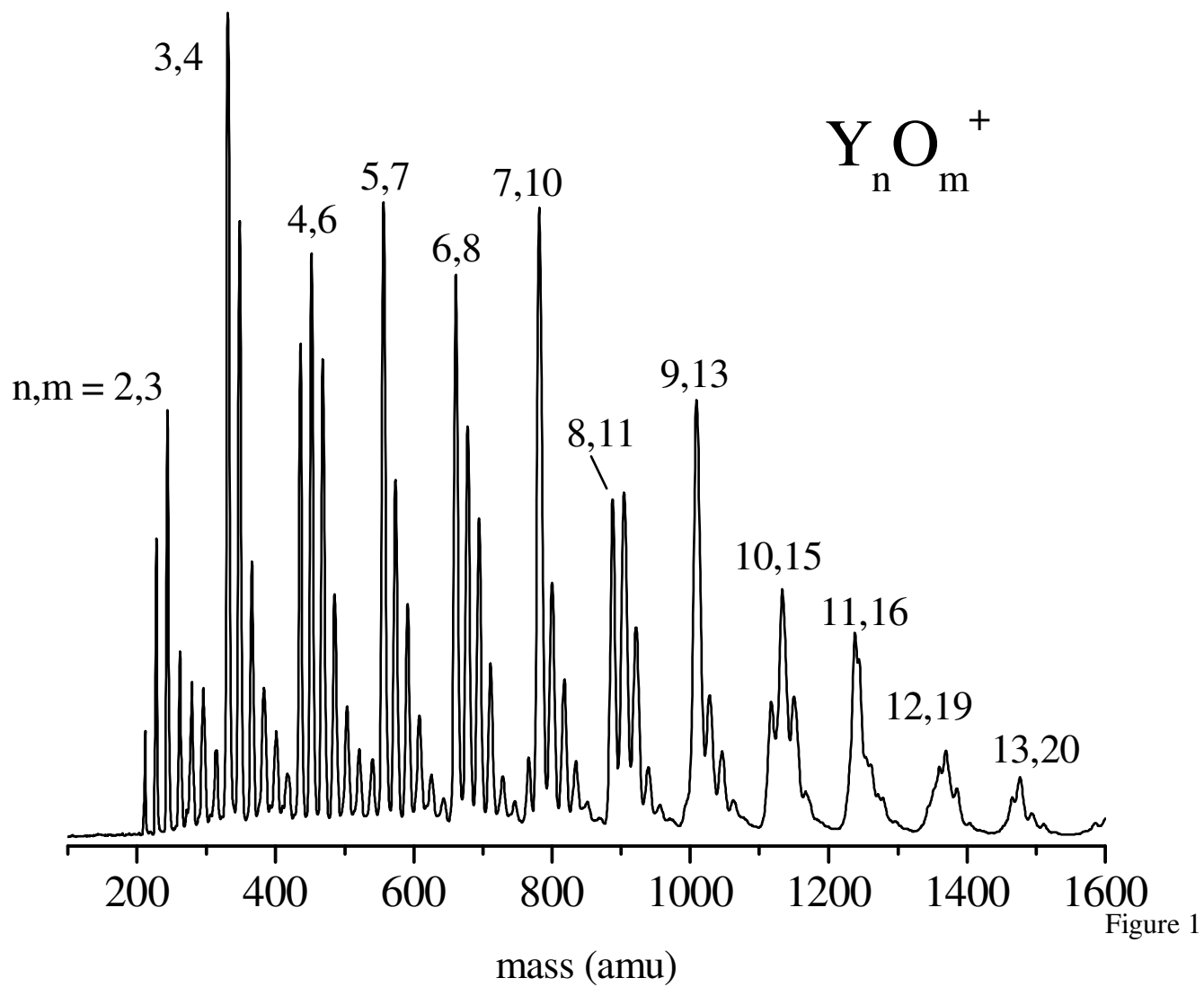


Figure 3.1.

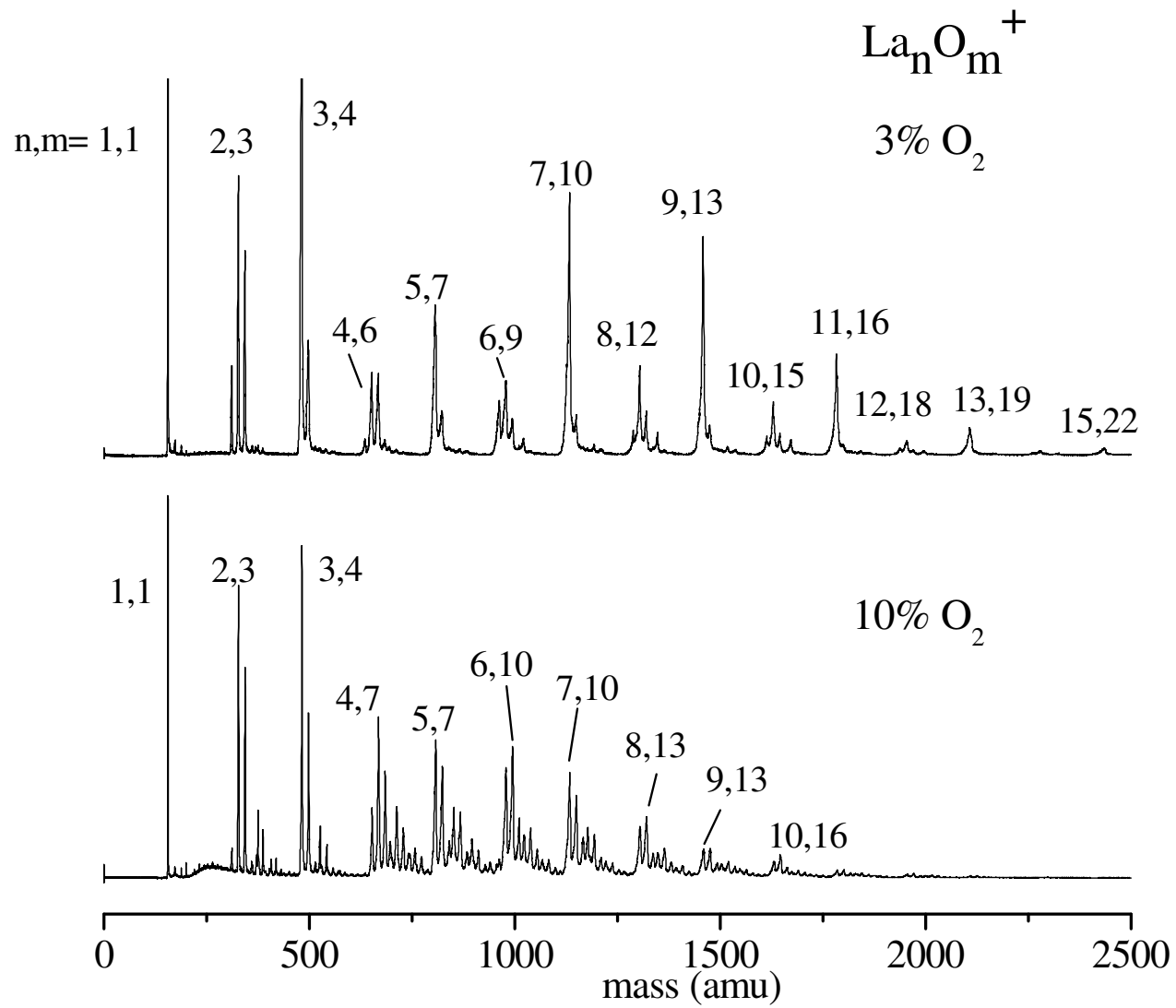


Figure 3.2.

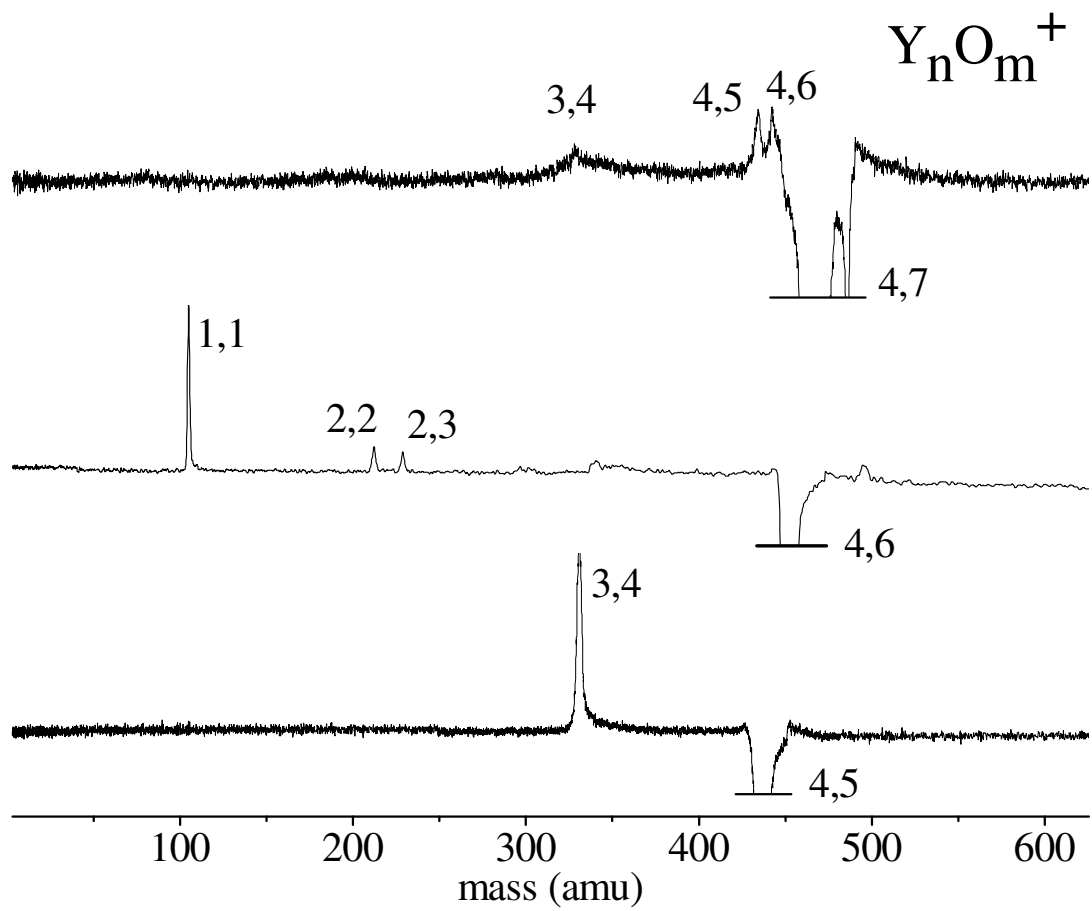


Figure 3.3.

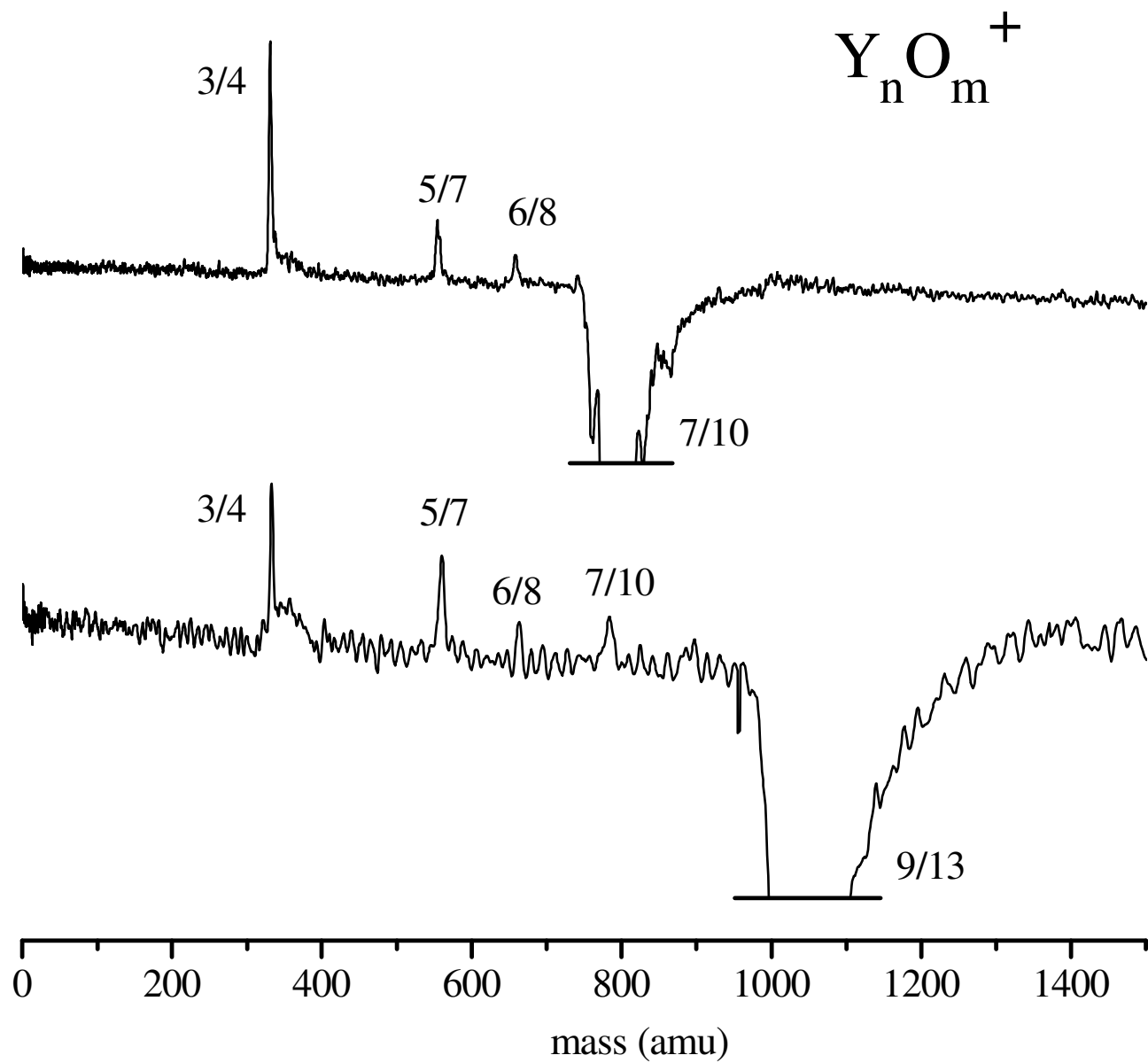


Figure 3.4.

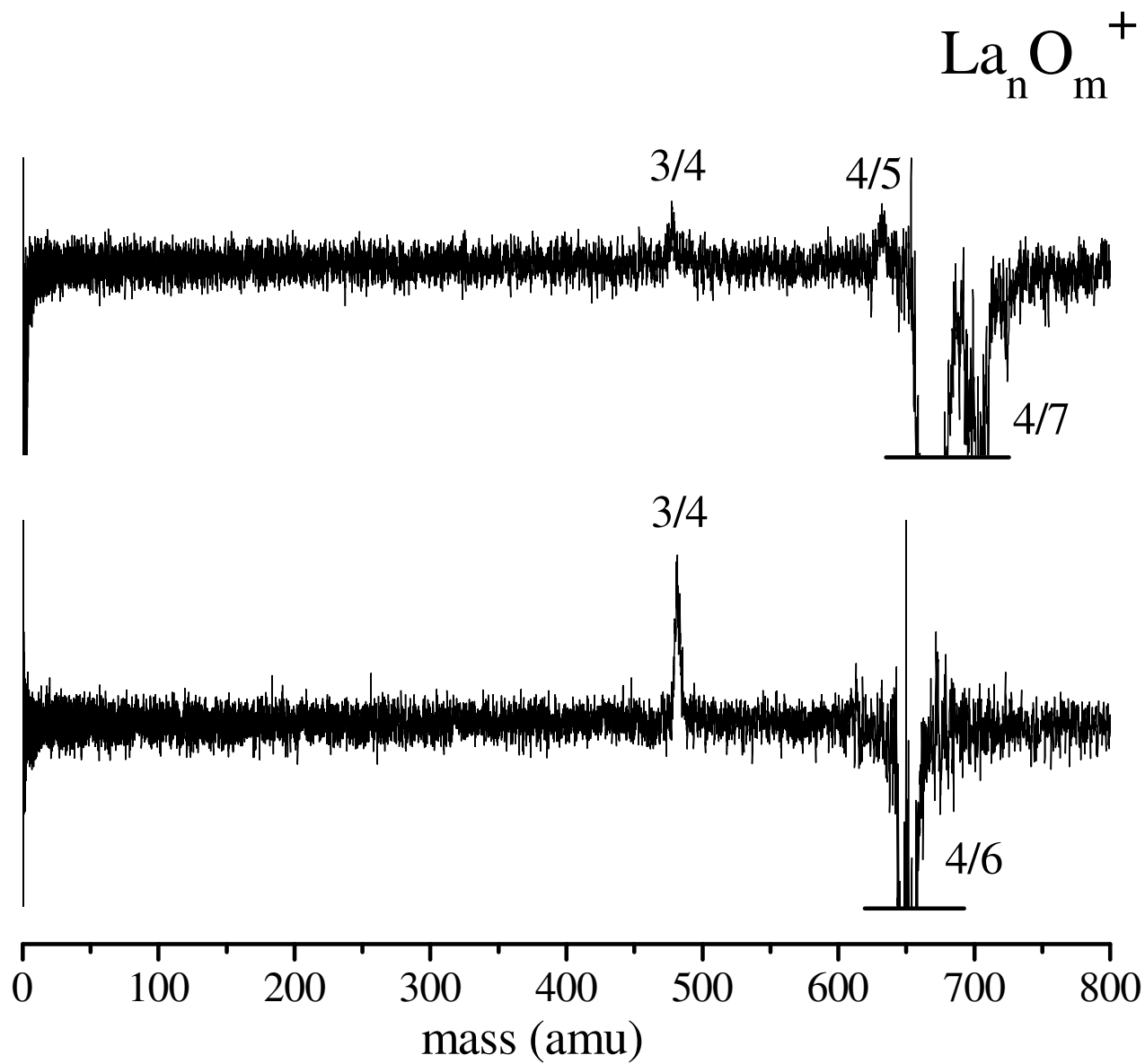


Figure 3.5.

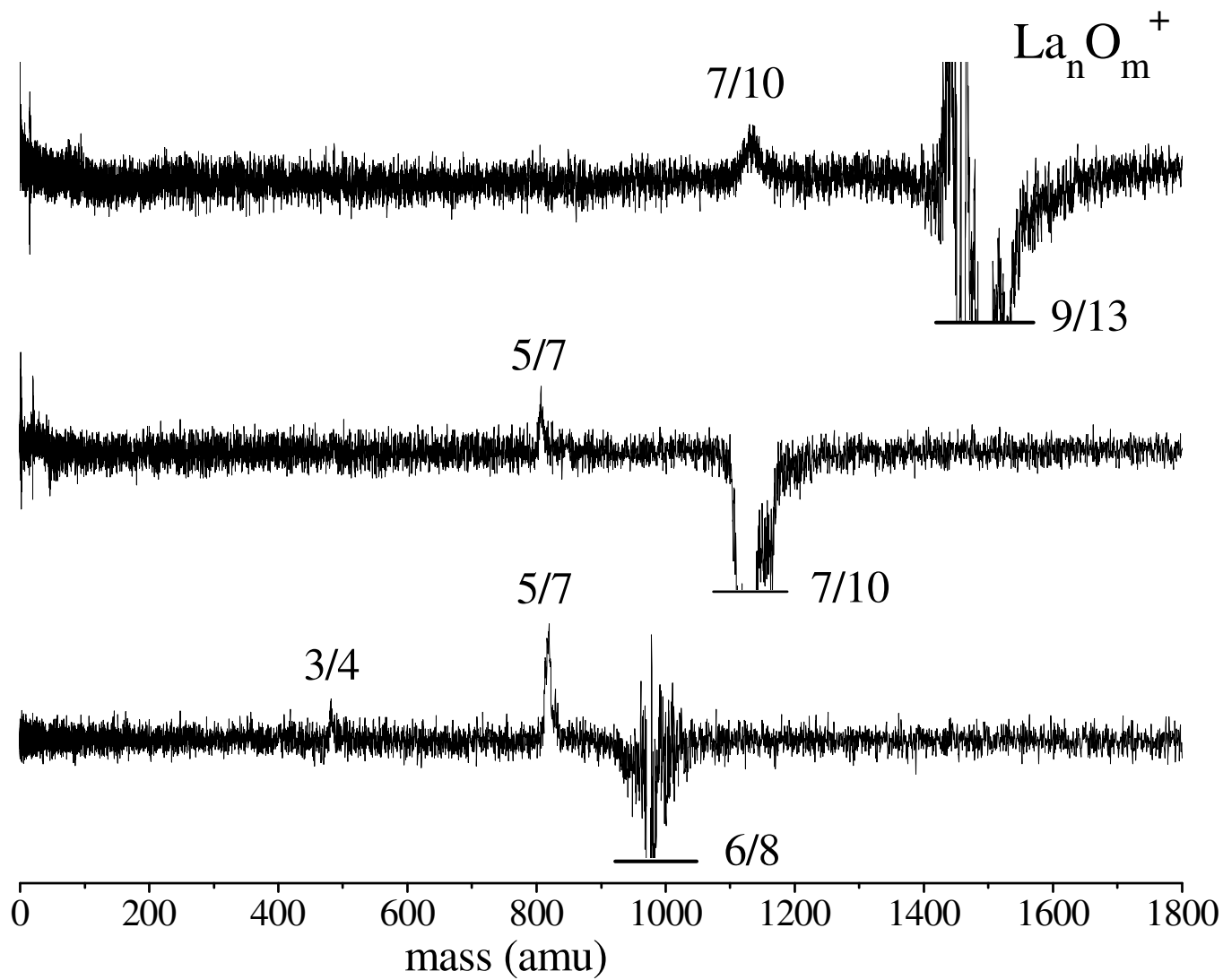
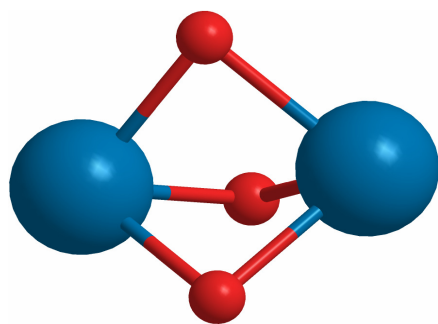
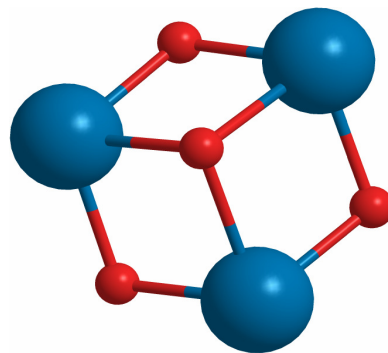


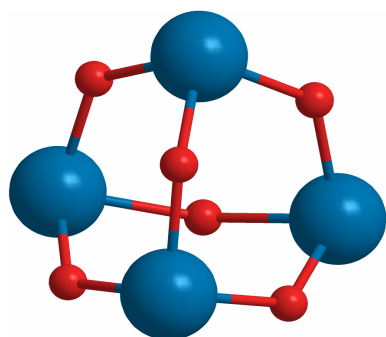
Figure 3.6.



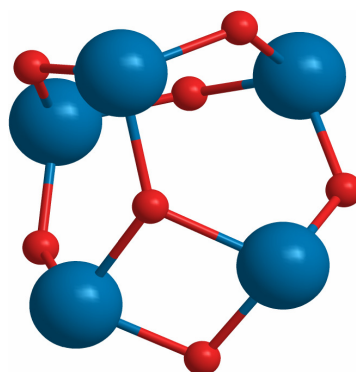
$Y_2O_3^+$



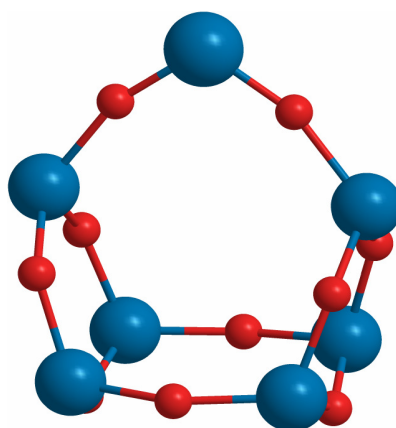
$Y_3O_4^+$



$Y_4O_6^+$



$Y_5O_7^+$



$Y_7O_{10}^+$

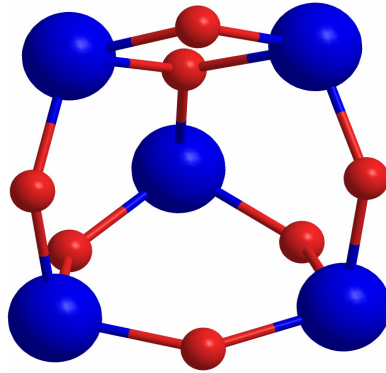
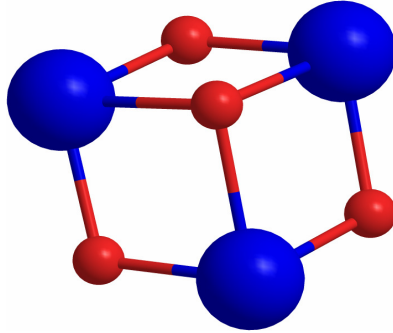
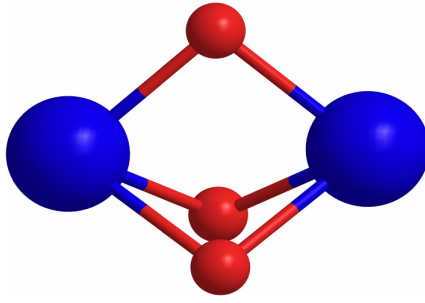


Figure 3.8.

CHAPTER 4

MASS SPECTRA AND PHOTODISSOCIATION OF INDIUM OXIDE (In_nO_m^+) CLUSTER CATIONS¹

¹Reed, Z.D., Anfuso, C.L., Molek, K.S., and Duncan, M.A. To be submitted to *Int. J. Mass Spec.*

4.1 Abstract

Indium oxide cations of the form In_nO_m^+ are produced by laser vaporization in a pulsed nozzle source and detected with time of flight mass spectrometry. Only a limited number of cluster stoichiometries for each value of n are formed. Cluster cations are mass selected and photodissociated using the third harmonic (355 nm) of an Nd:YAG laser. Cation clusters that are commonly produced are likely to be particularly stable. Several clusters that appear to be particularly stable are found to obey Wade's Rules, including In_5O_4^+ , In_5O_4^+ , and In_3O_2^+ . The In_3O_1^+ cluster is also found to be particularly stable. The evaporation of indium cation is a dominant loss channel for all cluster cations.

4.2 Introduction

Metal oxides have been demonstrated to have importance in electronics, magnetic materials, catalysis, and ceramics [1-9]. Metal oxide nanoparticles have applications that include magnetics, catalysis, and medicinal applications. Main group metal complexes have particular application in semiconductors and molecular devices. Main group metal complexes, including arsenides, phosphides, and oxides can have fascinating combinations of electrical and optical properties, and are known quantum dot systems [17]. Gas phase study of these compounds can help elucidate their fundamental properties. Mass spectroscopy experiments have shown significant intensity discontinuities in the relative ion abundances of Ga and In clusters and interesting trends in ionization potential for indium clusters [18]. Here we investigate indium oxide clusters. Indium oxides are used as n-type semiconductors, functioning as resistive

elements in integrated circuits [18]. Indium oxide nanowires have found application as high transparency metallic conductors [19], in molecular devices [20], and gas sensors [21].

Previous studies have investigated both pure indium clusters and indium oxides in the gas phase. The pure clusters have been probed using mass spectrometric methods [22-29], and ion mobility [30]. Mixed metal alloys of indium have been studied using mass spectrometric methods [31-33], and with theoretical calculations [34]. Indium oxide clusters have been studied using mass spectrometric methods [35,36], emission spectroscopy [37], electron spin resonance using matrix isolation [38], and theoretical calculation [39,40]. These studies have demonstrated that certain pure indium and indium alloy clusters are particularly stable.

Transition metal oxides clusters in the gas phase have been found to have localized bonding,[50-52] with conventional oxidation states and structures consisting of metal to oxygen bonds. Main group metal compounds rarely follow this scheme. Their electronic structures and bonding are usually understood with simple models based on electron counting. These rules were originally developed to explain the stabilities of Zintl ions, which are well known in inorganic chemistry [41-42]. Wade's Rules, as this system of electron counting is known, explains and predicts the stabilities of electron deficient clusters [42]. The clusters take on polyhedral structures to maximize the sharing of electron density in the interior of the cluster. This results in a system where closed shell species result from species with n metal atoms and $2n + 2$, $2n + 4$, and $2n+6$ valence p electrons, which correspond to *close*, *nido*, and *arachno* cluster forms respectively. Gas phase analogies to the condensed phase Zintl ions have been studied

for various main group metal alloy clusters, including Group IV/Group V binary clusters [43,44], In/Sb and In/Bi clusters [45], Bi/alkali clusters [46,47], and tin-bismuth alloy clusters [48]. These systems can all be explained using the Wade's Rules. These rules has not been demonstrated to work reliably on main group metal oxides, which can form particularly stable clusters that do not satisfy Wade's Rule and instead are driven by simple covalent bonding [49].

Previous work on various metal oxide clusters has revealed limitations in the determination of relative cluster stabilities [50-52]. Source and growth conditions can significantly affect the distribution of clusters observed. In mass spectrometric experiments, some form of ionization is always required. Photoionization and electron impact both suffer from unknown ionization potentials, size-dependent cross sections, and fragmentation processes. Identification of particularly stable clusters from a simple examination of mass spectrometric intensity has therefore proven to be unreliable. Our previous work has demonstrated that mass selected photodissociation of metal compound cluster ions can identify which stoichiometries are most stable. These stable clusters may or may not be prominent in the mass spectrum, but they are more likely to be resistant to decomposition and should be produced more frequently than other clusters during the fragmentation of larger clusters. We cannot detect stable neutrals directly, but they can be inferred using mass conservation and examination of the cation fragment loss channels. We have previously applied this methodology to study various metal carbides [53], metal silicon clusters [54], and several metal oxide systems [50-52] and demonstrated that it can identify the stoichiometries which are the most stable.

In this paper, we present the mass spectrum and mass selected photodissociation of some indium oxide clusters. We will examine clusters that appear to be particularly stable from mass spectrometric intensities and photodissociation data, and explain these results in the context of Wade's Rules.

4.3 Experimental

Metal oxide clusters are produced by laser vaporization using a pulsed nozzle source and are sampled using a time of flight mass spectrometer. This setup has been previously described. The third harmonic (355nm) of an Nd:YAG laser (Spectra Physics GCR-11) is used to vaporize metal from the surface of a rotating and translating indium rod. Helium gas seeded with either 1-5% O₂ or 1-5% N₂O is pulsed over the rod with a General Valve pulsed valve (60 psi backing pressure, 1mm orifice). The sample holder has a 5mm bore diameter and a 1 in growth channel to encourage larger cluster growth. The cluster cations grow directly in the laser plasma and are skimmed into the mass spectrometer as a molecular beam. A pulsed acceleration field time-of-flight mass spectrometer samples the clusters. Pulsed deflection plates on the first leg of the mass spectrometer allow for mass selection of cluster. The selected ions are crossed in the turning region of the reflection with another Nd:YAG operating at either 532nm or 355nm (DCR-3). The parent ions and any fragment ions produced from the photoexcitation process are mass analyzed in the second leg of the reflection and subsequently detected by an electron multiplier tube and digital oscilloscope (LeCroy 9310A). The data are transferred from the oscilloscope to a computer using an IEEE-488

interface. Studies were performed as a function of vaporization laser power, which ranged from 10 mJ to 60 mJ/pulse.

4.4 Results and Discussion

The mass spectrum of In_nO_m^+ cations produced is shown in Figure 4.1. Oxide clusters containing up to six metal atoms are produced. Clusters produced using helium seeded with oxygen are shown in the top pane, and clusters produced using helium seeded with N_2O are shown in the lower pane. Somewhat smaller clusters are produced with N_2O , and there is less variation in the number of oxygen atoms per metal atom. Clusters containing only a few metal atoms have a strong tendency to produce certain cluster stoichiometries, instead of a random distribution. As the cluster sizes increase, the stoichiometric preference appears to decrease, with three or more clusters having roughly equal intensity in the mass spectrum. The metal ion and the species In_2O_1^+ and In_3O_1^+ are very prominent in both spectra. These stoichiometries will be designated as 1/0, 2/1, 3/1 from now on for the sake of convenience. The 4/2 cluster is the first $n=4$ cluster produced, but the preference over $n=4$ clusters with more oxygens is not obvious. Production of clusters containing five or more metal atoms varies greatly with condition, and no preference can be discerned.

Mass-selected photo-fragmentation experiments were performed to investigate the relative stabilities of these clusters. Cluster cations with sufficient intensity are mass selected and then photodissociated by laser excitation at 355 nm in the reflectron region of the mass spectrometer. Fragmentation experiments were attempted with 532 nm light, but fragmentation was not nearly as efficient as with 355 nm for any cluster. The photon

energy may be too low to cause efficient fragmentation, or the absorption cross section at that wavelength may be too small. Studies of fragmentation yield versus laser fluence were also performed. Fragmentation was observed with fluences as low as 10 mJ/cm^2 at 355 nm. Most of the clusters fragment efficiently with 30 mJ/cm^2 . A complete list of fragmentation channels for each cluster cation studied can be found in Table 4.1.

Figure 4.2 shows the photofragmentation mass spectrum for In_3O_2^+ . This spectrum is shown in a difference mode, with the mass spectrum with the fragmentation laser off subtracted from the mass spectrum with the laser on. This gives a negative parent ion peak and positive going fragment ion peaks. Ideally, the integrated peak intensities would equal the amount of depletion. Unfortunately, mass discrimination effects make it difficult to focus equally on parent and fragment ions. Therefore, we cannot give any quantitative branching ratios and simply distinguish between strong and weak fragment channels.

The In_3O_2^+ cluster has three fragmentation channels. There is a small amount of fragmentation from $3/2 \rightarrow 3/1$. We cannot detect the neutral fragments, so the identity of the neutrals is inferred by the mass difference. In this case, the neutral loss must be atomic oxygen. The next fragment, $2/1$, could be produced several different ways. It could be a sequential loss from $3/1$, or a concerted loss from $3/2$. We cannot distinguish conclusively between these two alternatives, and the neutral loss is indicated in brackets, e.g. [1,1] to emphasize this uncertainty. Laser power dependence studies show no change in relative fragmentation yields, but this cannot conclusively identify the mechanism. The final fragment is the atomic indium cation, which can be produced from

$3/2 \rightarrow 1/0$, or from $2/1 \rightarrow 1/0$, with neutral losses of $[2/2]$ and $[1/1]$ respectively. This channel is by far the most intense, at any laser power.

The other $n=3$ cluster cations also fragment primarily to $1/0$, but the other loss channels show some variety. The $3/1$ cluster cation fragments to $2/1$, $2/0$, $2/1$, and $0/1$. It is interesting that the atomic oxygen cation and the diatomic metal would be produced, but there is no sign of the In_3^+ cluster. The oxygen atom has an IP of 13.6 eV, while the IP of the In atom is only 5.78 eV and the bulk work function is 4.12 eV [57]. Only a small amount of oxygen cation is produced, and it seems likely that it is a product of a sequential loss from the $2/1$ fragment instead of $3/1 \rightarrow 3/0$. The $3/3$ cluster cation fragments to $2/1$, $1/0$, and $0/1$. Here again we have the production of an oxygen atom, without any signs of either the $3/2$ or $2/0$ cations being produced. These species should have much lower IPs than the oxygen atom, so it is somewhat puzzling how this species is being produced.

Figure 4.3 shows the fragmentation mass spectrum of In_4O_3^+ with 355 nm photoexcitation. This cluster has quite a few fragmentation channels. The most intense channels are $3/2$, $2/1$, and $1/0$. Smaller amounts of $3/1$, $2/2$, and $2/0$ are produced. If we assume a concerted mechanism, the main neutral losses are $[1/1]$, $[2,3]$, and $[3,3]$. The $4/3$ cluster cation also fragments with 532 nm photoexcitation, but not nearly as efficiently as with 355 nm. The loss channels and relative intensities are the same as with 355 nm.

The other $n=4$ cations have similarly diverse fragmentation channels, but few loss channels appear for more than one cluster. The $4/2$ cluster cation fragments to $3/1$, $2/1$, $2/0$, and $1/0$. The $2/1$ channel is most intense, followed by the metal cation. The $4/2 \rightarrow$

2/1 channel would produce [2/1] as a neutral. It is somewhat tempting to view this as a simple fission process, splitting the 4/2 cluster in half. No atomic oxygen is observed as a fragment channel here. The diatomic metal cation is observed. The most prominent fragment channel from the 4/4 cluster cation is again 2/1, with a neutral loss of [2/3]. The metal cation and oxygen cation are also rather prominent, even at low laser powers. No metal cluster cations larger than the atom are observed here. It is again interesting that the loss channel of 4/4→4/2 with a neutral loss of [O₂] is observed, but no 4/3 is observed and the O⁺ species is produced.

Figure 4.4 shows the fragmentation mass spectrum of the 5/4 cluster cation. The n=5 clusters are somewhat more homogenous in their fragmentation than smaller cluster sizes. The 5/4 cluster has prominent channels to 3/2 (a neutral loss of [2/2]), 2/1 (a neutral loss of [3/3]), and 1/0 (a neutral loss of [4/4]). One bulk stoichiometry of indium oxide is known to be InO, so these neutral losses may be reassuring. If a sequential mechanism is considered, the neutral losses are [2/2] and [1/1], again, both with the same stoichiometry as the bulk. However, this trend is not reproduced across the n=5 clusters. The 5/2 cluster cation has a prominent neutral loss of [2/1], the 5/3 cluster cation has a prominent neutral loss of [2/2] again, and 5/5 has prominent neutral losses of [2/3] and [4/4]. Indium oxide is also known to take the In₂O₃ stoichiometry in the bulk, but the [2/1] neutral is anomalous. It is also interesting that 5/5 and 5/4 fragment primarily to 3/2, and 5/3 and 5/2 fragment primarily to 3/1. Also of note is the production of the oxygen cation for all four parent cations. Only in the 5/5 cation cluster is the In₅O_{m-1}⁺ channel observed.

The driving force behind the production of specific clusters is not at all obvious. We observe some enhanced intensity for 2/1 and 3/1 in the mass spectrum. Certain clusters are commonly produced as fragments, but their relative intensities can vary widely. The [1/1] and [2/3] neutral losses, both stoichiometries found in bulk indium oxide, are observed as fragments but not universally. The 3/2 cluster cation is commonly produced as a fragment, sometimes as the most intense channel and sometimes as an extremely weak channel. The same is true with the 3/1 cluster cation. It is produced from every cluster with $n \geq 4$, but only occasionally as a prominent channel. It is not produced at all from 3/3, which may have seemed plausible via a loss of neutral molecular oxygen channel. The 2/1 cluster cation is again produced from every parent, but is not especially prominent in all. The [2/1] neutral loss is again common but far from ubiquitous. The production of the metal cation is the only true constant; it is produced from every parent and with fairly high intensity for all. Rayane observed that the metal cation loss channel was the dominant process for fragmentation in pure indium clusters, which he rationalized in terms of the ion's relatively low ionization potential. This may explain the apparently ubiquitous fragmentation of the metal cation from indium oxide clusters as well.

Some insight may be gained into the stability of these certain cluster cations from the application Wade's Rules of electron counting for electron deficient clusters. Our previous study on In/Sb and In/Bi alloy clusters demonstrated that there is little s-p hybridization [44], so we will only consider the p-electron count for satisfying Wade's Rules. Additionally, work by Rayane et al. on charged pure indium clusters supports the assertion that there is little s-p mixing in small ($n < 15$) indium clusters [22].

In this context, we can see in Table 4.2 that many of our prominent clusters can be assigned to a Wade's Rule polyhedral structure. Each of the prominently observed $n=5$ clusters can be assigned to a particularly stable polyhedral framework. The $5/5$ cluster is nido, $5/4$ is closo, and $5/3$ has $4n$ electrons, which represents a capped polyhedron. Previous work from our group on indium sulfur clusters (paper in progress), which might be expected to follow the same electron counting rules, also found a particularly intense peak at $5/4$ in the mass spectrum. Among the $n=4$ clusters, none fit into the Wade's Rules framework. This may explain why no consistent fragmentation patterns were observed for $n=5$ going to $n=4$ clusters. If we consider the neutral clusters, which have one more electron than the cations, each of the observed $n=4$ stoichiometries should have increased stability. This may explain the loss of single metal cations in the $n=5$ clusters, as particularly stable neutral $n=4$ clusters could be formed as a result. When we consider the $n=3$ clusters, the $3/3$ cluster fits the criteria for a closo structure, $3/2$ fits a capped structure, and $3/1$ does not fit a Wade's Rule shell closing. The structure of In_3O^+ was previously calculated by Lievens, indicating a planar D_{3h} structure with a central oxygen. This provides a rationalization for why $3/1$ does not fit the Wade's Rules prediction; it is simply too small to form a viable polyhedron. It does, however, share electron density inside an inner cavity, albeit a two dimensional cavity. The Wade's Rules framework may provide an explanation for the relatively common production of $3/2$ as a fragment, but this is not conclusive.

4.5 Conclusions

Indium oxide clusters produced by laser vaporization have been investigated with time of flight mass spectrometry and mass selected photodissociation. We observe a non-statistical distribution of sizes for each cluster size. It appears that clusters with five metal atoms that satisfy Wade's Rules have some enhanced stability. No enhanced stability from Wade's Rules is found for cation clusters, but the neutral complexes could have enhanced stability and may provide explain some explanation for various fragmentation processes. The In_3O^+ cluster does not satisfy Wade's Rules, but is analogous in principle due to sharing electrons in a central cavity. This cluster is especially stable. The dominant fragmentation process is elimination of the metal cation, which may simply be due to its fairly low ionization potential.

4.6 Acknowledgements

We gratefully acknowledge generous support for this work from the Air Force Office of Scientific Research (Grant No. FA9550-06-1-0028).

4.7 References

- (1) P.A. Cox, Transition Metal Oxides, Clarendon Press, Oxford, 1992.
- (2) C.N. Rao, B. Raveau, Transition Metal Oxides, John Wiley, New York, 1998.
- (3) F.A. Cotton, G. Wilkinson, C.A. Murillo, M. Bochmann, Advanced Inorganic Chemistry, 6th edition, John Wiley & Sons, New York, 1999.
- (4) C. Hayashi, R. Uyeda, A. Tasaki, Ultra-Fine Particles; Noyes, Westwood, 1997.
- (5) V.E. Henrich, P.A. Cox, The Surface Science of Metal Oxides; Cambridge University Press, Cambridge, 1994.
- (6) G.A. Somorjai, Introduction to Surface Chemistry and Catalysis; Wiley-Interscience, New York, 1994.
- (7) B.C. Gates, Chem. Rev. 95 (1995) 511.
- (8) a) D.R. Rainer, D.W. Goodman, J. Mol. Catal. A: Chem. 131 (1998) 259. b) T.P. St. Clair, D.W. Goodman, Top. Catal. 13 (2000) 5. c) W.T. Wallace, B.K. Min, D.W. Goodman, Top. Catal. 34 (2005) 17. d) M.S Chen, D.W. Goodman, Acc. Chem. Res. 39 (2006) 739.
- (9) a) I.E. Wachs, L.E. Briand, J.M. Jehng, L. Burcham, X.T. Gao, Catal. Today 57 (2000) 323. b) Y.S. Chen, I.E.J. Wachs, J. Catal. 217 (2003) 468. c) I.E. Wachs, Catal. Today 100 (2005) 79. d) I.E. Wachs, J.M. Jehng, W. Ueda, J. Phys. Chem. B 109 (2005) 2275. e) H.J. Tian, E.I. Ross, I.E Wachs, J. Phys. Chem. B 110 (2006) 9593.
- (10) M.T. Pope, A. Müller, Polyoxyometalate Chemistry From Topology via Self-Assembly to Applications, Kluwer: Boston, 2001.

- (11) D.C. Crans, J.J. Smee, E. Gaidamauskas, L.Q. Yang, *Chem. Rev.* 104 (2004) 849.
- (12) a) J. Rockenberger, E.C Scher, A.P. Alivisatos, *J. Am. Chem. Soc.* 121 (1999) 11595 b) V.F. Puentes, K.M. Krishnan, A.P. Alivisatos, *Science* 291 (2001) 2115. c) F. Nolting, J. Luning, J. Rockenberger, J. Hu, A.P. Alivisatos, *Surf. Rev. Lett.* 9 (2002) 437. d) Y.W. Jun., M.F. Casula, J.H. Sim, S.Y. Kim, J. Cheon, A.P. Alivisatos, *J. Am. Chem. Soc.* 125 (2003) 15981. e) M.F. Casula, Y.W. Jun, D.J. Zaziski, E.M. Chan, A. Corrias, A.P. Alivisatos, *J. Am. Chem. Soc.* 128 (2006) 1675.
- (13) T.M. Ayers, J.L. Fye, Q. Li, M.A. Duncan, *J. Cluster Sci.* 14 (2003) 97.
- (14) B.L. Cushings, V.L. Kolesnichenko, C.J. O'Connor, *Chem. Rev.* 104 (2004) 3893.
- (15) M. Fernandez-Garcia, A. Martinez-Arias, J.C. Hanson, J.A. Rodriguez, *Chem. Rev.* 104 (2004) 4063.
- (16) A.L. Stepanov, G. Boura, M. Gartzza, Yu.N. Osinb, A. Reinholdta, U. Kreibig, *Vacuum* 64 (2004) 9.
- (17) G. Schmid, *Nanoparticles*, Wiley-VCH, Weinheim, 2004
- (18) H. Haberland, *Clusters of Atoms and Molecules I* Springer Series in Chemical Physics, Springer-Verlag, New York, 1995
- (19) Q. Wan, E.N. Dattolo, W.Y. Fung, W. Guo, Y. Chen, X. Pan, W. Lu, *Nano Letters* 6 (2006) 2909 "High-Performance Transparent Conducting Oxide Nanowires"

- (20) “Multilevel memory based on molecular devices” C. Li, W. Fan, B. Lei, D. Zhang, S. Han, T. Tang, X. Liu, Z. Liu, S. Asano, M. Meyyappan, J. Han, C. Zhou, *Appl. Phys. Lett.* 84 (2004) 1949.
- (21) D. Zhang, C. Li, X. Liu, S. Han, T. Tang, C. Zhou, *Appl. Phys. Lett.* 83 (2003) 1845-1847
- (22) D. Rayane, P. Melinon, B. Cabaud, A. Hoareau, B. Tribollet, M. Broyer, *J. Chem. Phys.* 90 (1989) 3295. “Electronic properties and fragmentation processes for singly and doubly charged indium clusters
- (23) F.L. King, M.M. Ross, *Chem. Phys. Lett.* 164 (1989) 131 “Abundance distributions and dissociations of sputtered aluminum, gallium, and indium cluster ions”
- (24) K.E. Schriver, J.L. Persson, E.C. Honea, R.L. Whetton, *Phys. Rev. Lett.* 64 (1990) 2539 “Electronic Shell Structure of Group-IIIA Metal Atomic Clusters”
- (25) B. Baguenard, M. Pellarin, C. Bordas, J. Lermé, J.L. Vialle, M. Broyer, *Chem. Phys. Lett.* 205 (1993) 13 “Shell structure of small indium clusters below $N \approx 200$ atoms”
- (26) Z. Ma, S. R. Coon, W. F. Calaway, M. J. Pellin, D. M. Gruen, and E. I. von Nagy-Felsobuki *J. Vac. Sci. Technol. A* 12 (1994) 2425-2430
- (27) Wucher, Z. Ma, W.F. Calaway, M.J. Pellin, *Surf. Sci. Lett.* 304 (1994) L439
- (28) E. Cottancin, M. Pellarin, J. Lermé, B. Palpant, B. Baguenard, J.-L. Vialle, M. Broyer, *Z. Phys. D* 40 (1997) 288 “Unimolecular dissociation of trivalent metal clusters ions (Al_n^+ , Ga_n^+ , In_n^+): evidence for a transition from covalent to metallic bonding”

- (29) C. Staudt, A. Wucher, S. Neukermans, E. Janssens, F. Vanhoutte, E. Vandeweert, R.E. Silverans, P. Lievens, Nucl. Instr. and Meth. in Phys. Res. B 193 (2002) 787
“Internal excitation of sputtered neutral indium clusters”
- (30) J. Lermé, P. Dugourd, R.R. Hudgins, M.F. Jarrold, Chem. Phys. Lett. 304 (1999)
19 “High-resolution ion mobility measurements of indium clusters: electron spill-
out in metal cluster anions and cations”
- (31) M.B. Bishop, K. LaiHing, P.Y. Cheng, M. Peschke, M.A. Duncan, J. Phys. Chem.
93 (1989) 1566
- (32) Y. Yamada, A.W. Castleman, Jr., J. Chem. Phys. 97 (1992) 4543
- (33) T. Lill, W.F. Calaway, Z. Ma, M.J. Pellin, Surf. Sci. 322 (1995) 361 “Sputtering
of Group III-A elements. Properties of the metal cluster formation mechanism”
- (34) D.W. Liao, K. Balasubramanian, J. Chem. Phys. 96 (1992) 8938 “Electronic
structure of the III-V tetramer clusters and their positive ions”
- (35) R. Middleton, Nuclear Instruments and Methods 144 (1977) 373 “A survey of
negative ions from a cesium sputter source”
- (36) F.L. King, B.I. Dunlap, D.C. Parent, J. Chem. Phys. 94 (1991) 2578
“Characterization of cluster ions produced by the sputtering or direct laser
vaporization of group 13 metal (Al, Ga, and In) oxides”
- (37) W.J. Balfour, M.D. Saksena, J. Mol. Spec. 143 (1990) 392 “An Emission
Spectrum of the InO^+ Molecular Ion”
- (38) L.B. Knight, Jr., T.J. Kirk, J. Herlong, J.G. Kaup, E.R. Davidson, J. Chem. Phys.
107 (1997) 7011 “Electron spin resonance matrix isolation studies of $^{27}\text{Al}^{16,17}\text{O}$,

$^{69,71}\text{Ga}^{16,17}\text{O}$ and $^{115}\text{In}^{16,17}\text{O}$: Observed hyperfine interactions compared with *ab initio* theoretical results”

- (39) P. Belanzoni, E. van Lenthe, E.J. Baerends, J. Chem. Phys. 114 (2001) 4421
- (40) E. Janssens, S. Neukermans, F. Vanhoutte, R.E. Silverans, P. Lievens, A. Navarro-Vásquez, P.v.R. Schleyer, J. Chem. Phys. 118 (2003) 5862
- (41) R.B. King Inorganic Chemistry of Main Group Elements; VCH New York, 1995.
- (42) K. Wade, K. Adv. Inorg. Chem. Radiochem. 18 (1976) 1
- (43) R.G. Wheeler, K. LaiHing, W.L. Wilson, M.A. Duncan J. Chem. Phys. 88 (1988) 2831 Growth Patterns in binary clusters of Group IV and V metals
- (44) R.G. Wheeler, K. LaiHing, W.L. Wilson, J.D. Allen, R.B. King, M.A. Duncan J. Am. Chem. Soc. 108 (1986) 8101 Neutral Gas Phase Analogs of Condensed Phase Post-Transition Metal Cluster Ions: Sn/Bi and Pb/Sb Alloys
- (45) M.B. Bishop, K. LaiHing, P.Y. Cheng, M. Peshke, M.A. Duncan J. Phys. Chem. 93 (1989) 1566 Growth Patterns of In/Sb and In/Bi Intermetallic Clusters
- (46) R.W. Farley, A.W. Castleman J. Am. Chem. Soc. 111 (1989) 2734 Observations of Gas-Phase Anionic Bismuth Zintl Ions
- (47) R.W. Farley, A.W. Castleman J. Chem. Phys 92 (1990) 1790 Reactions of Intermetallic Clusters
- (48) U. Gupta, A.C. Reber, P.A. Clayborne, J.J. Melko, S.N. Khanna, A.W. Castleman Inorg. Chem. 47 (2008) 10953 Effects of Charge and Composition on the Structural Fluxionality and Stability of Nine Atom Tin-Bismuth Zintl Analogues
- (49) M.R. France, J.W. Buchanan, J.C. Robinson, S.H. Pullins, J.L. Tucker, R.B. King, M.A. Duncan, J. Phys. Chem. 101 (1997) 6214

- (50) K.S. Molek, T.D. Jaeger, M.A. Duncan, *J. Chem. Phys.* 123 (2005) 144313
- (51) K.S. Molek, Z.D. Reed, A.M. Ricks, M.A. Duncan *J. Phys. Chem. A* 111 (2007) 8080
- (52) Z.D. Reed, M.A. Duncan *J. Phys. Chem. A* 112 (2008) 5354
- (53) a) B.W. Ticknor, M.A. Duncan, *Chem. Phys. Lett.* 405 (2005) 214. b) J.B. Jaeger, T.D. Jaeger, M.A. Duncan, *J. Phys. Chem. A* 110 (2006) 9310.
- (54) a) J.S. Pilgrim, M.A. Duncan, *J. Am. Chem. Soc.* 115 (1993) 9724. b) J.S. Pilgrim, M.A. Duncan, *J. Am. Chem. Soc.* 115 (1993) 6958. c) M.A. Duncan, *J. Cluster Sci.* 8 (1997) 239.
- (55) J.A. Dean (ed) *Lange's Handbook of Chemistry*, McGraw-Hill, New York, USA, 14th edition, 1992

Table 4.1. The stoichiometries of indium oxide photofragments ($\text{In}_n\text{O}_m^+ = n,m$) detected using 355 and 532 nm.

Parent Cation Cluster	Photofragments
3,1	2,1; 2,0; 1,0, 0,1
3,2	3,1; 2,1; 1,0
3,3	2,1; 1,0; 0,1
4,2	3,1; 2,1; 2,0; 1,0
4,3	3,2; 3,1; 2,2; 2,1; 2,0; 1,0
4,4	4,2; 3,2; 3,1; 2,1; 1,1; 1,0
5,2	3,2; 3,1; 2,1; 1,0; 0,1
5,3	3,2; 3,1; 2,1; 1,0; 0,1
5,4	4,3; 3,2; 3,1; 2,1; 1,0; 0,1
5,5	5,4; 5,3; 3,2; 3,1; 2,1; 1,0; 0,1

Table 4.2 : Wade's Rules electron counts and structural assignments for selected indium oxide stoichiometries

Cluster	p electron count	Wade's Rule structural assignment
In_5O_5^+	24	Nido
In_5O_4^+	20	Closo
In_5O_3^+	16	Capped
In_5O_2^+	12	None
In_4O_4^+	19	None
In_4O_3^+	15	None
In_4O_2^+	11	None
In_3O_3^+	14	Closo
In_3O_2^+	10	Capped
In_3O_1^+	6	None

Figure Captions

Figure 4.1. Time-of-flight mass spectra for In_nO_m^+ clusters formed in a helium expansion seeded with either 3 % O_2 (upper trace) or 3 % N_2O (lower trace).

Figure 4.2. Photodissociation mass spectra of In_3O_2^+ .

Figure 4.3. Photodissociation mass spectra of In_4O_3^+ .

Figure 4.4. Photodissociation mass spectra of In_5O_4^+ .

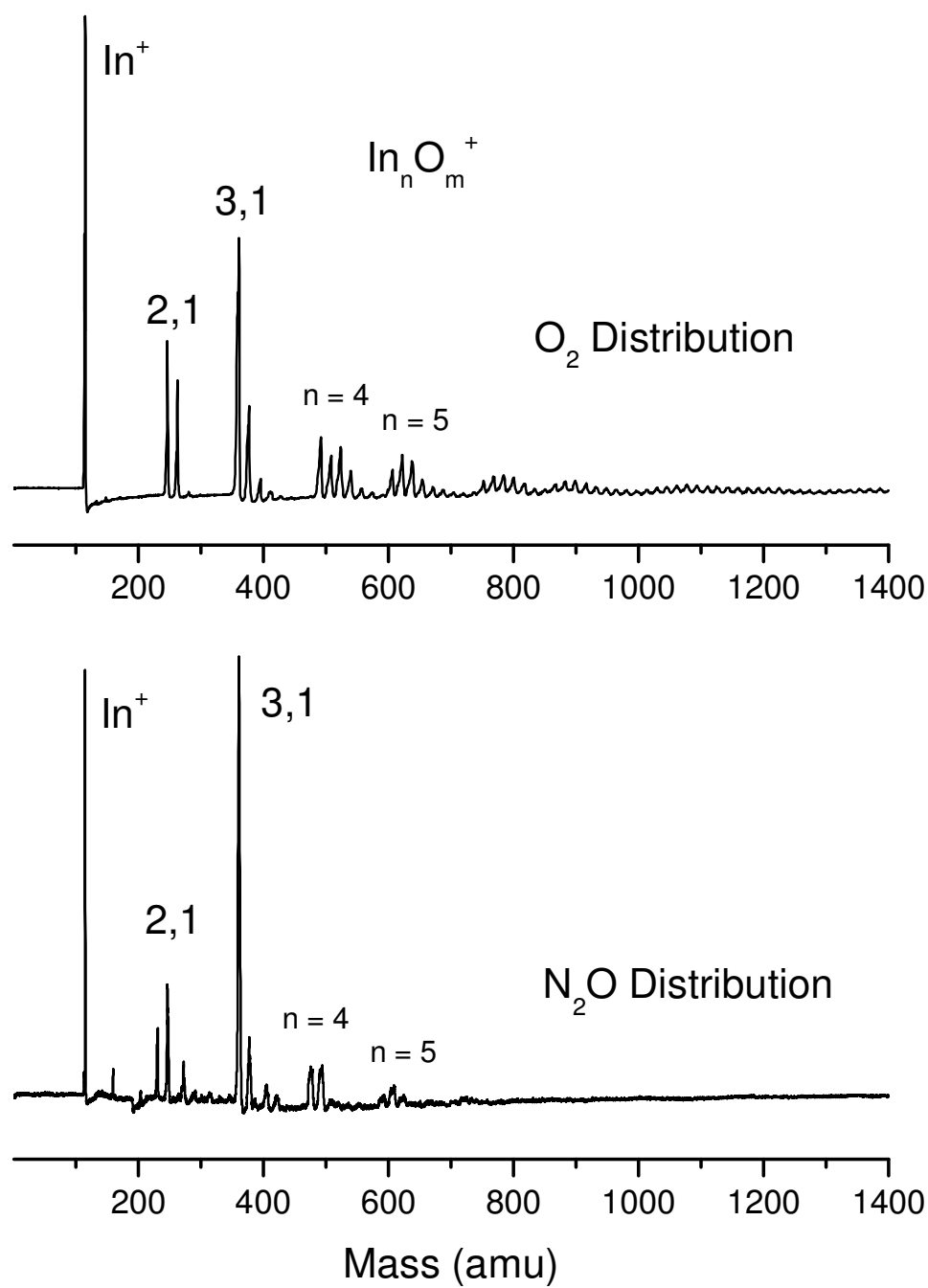


Figure 4.1.

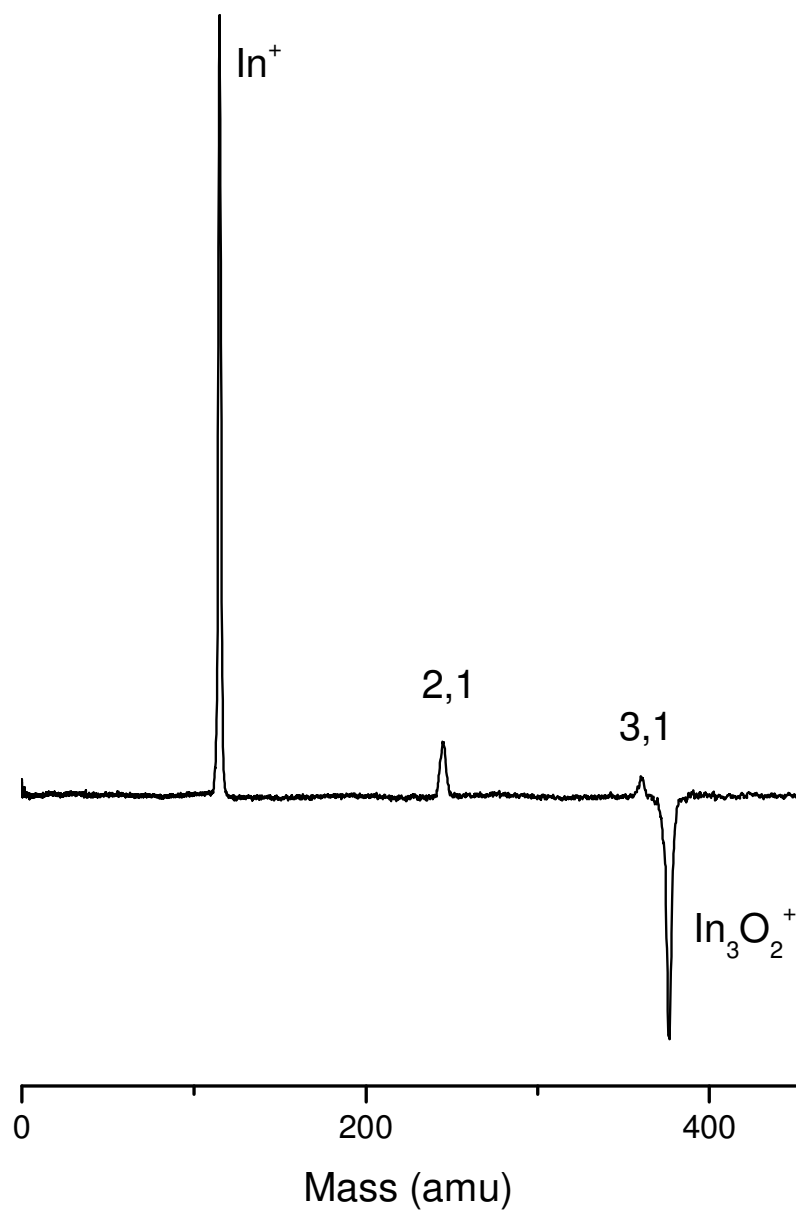


Figure 4.2.

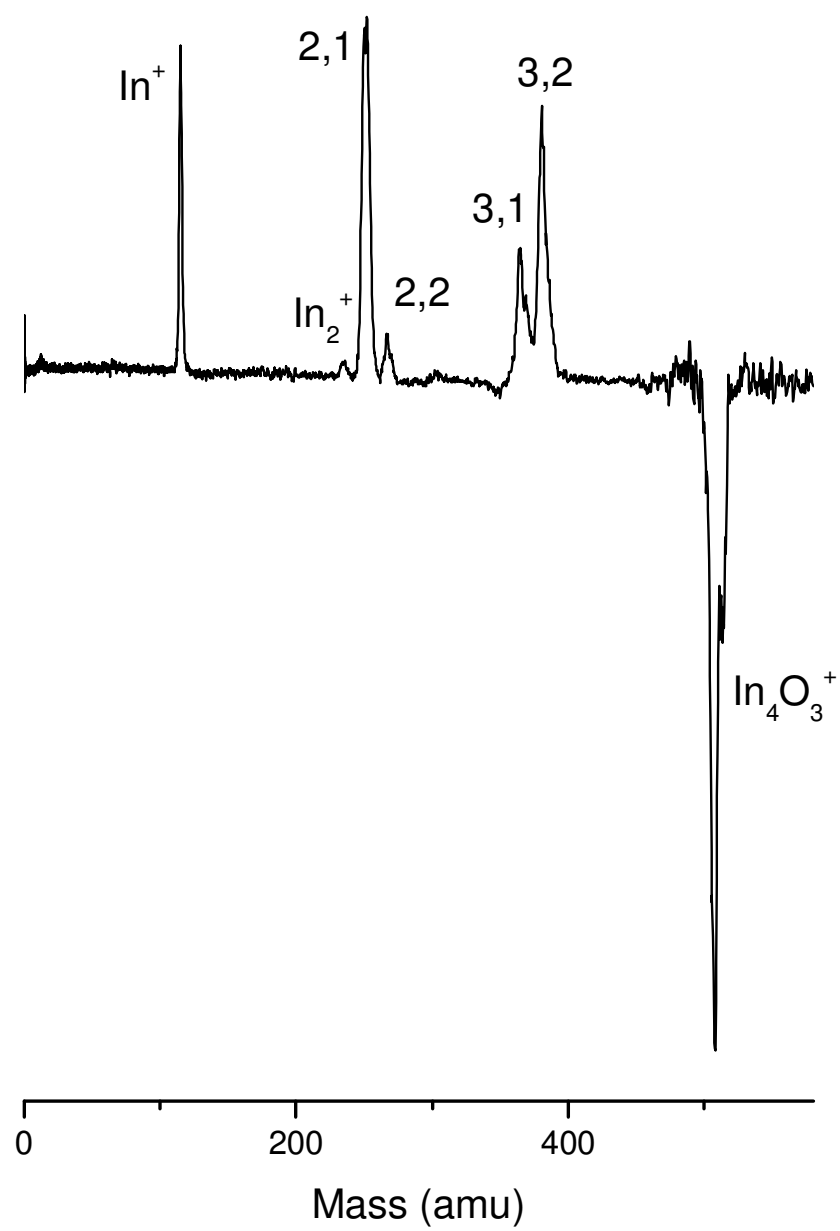


Figure 4.3.

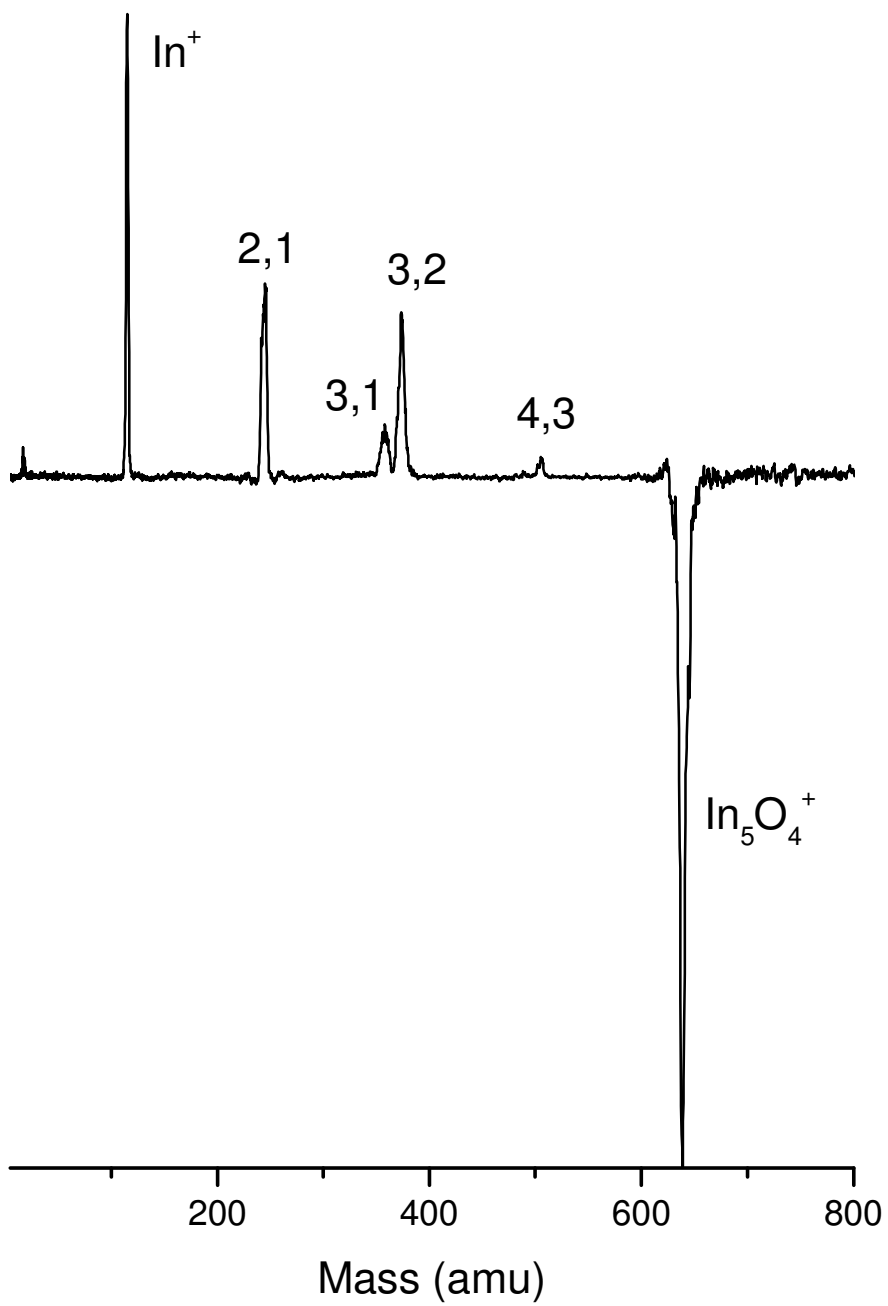


Figure 4.4.

CHAPTER 5
INFRARED SPECTROSCOPY AND STRUCTURES OF MANGANESE
CARBONYL CATIONS, $\text{Mn}(\text{CO})_n^+$ ($n=1-9$)¹

¹Reed, Z.D. and Duncan, M.A. 2008. Submitted to *J. Am. Soc. Mass Spec.* 11/23/09

5.1 Abstract

Manganese carbonyl cations of the form $\text{Mn}(\text{CO})_n^+$ ($n=1-9$) are produced in a molecular beam by laser vaporization in a pulsed nozzle source. Mass selected infrared photodissociation spectroscopy in the carbonyl stretching region is used to study these complexes and their "argon-tagged" analogues. The geometries and electronic states of these complexes are determined by comparing their infrared spectra to theoretical predictions. $\text{Mn}(\text{CO})_6^+$ has a completed coordination sphere, consistent with its predicted 18-electron stability. It has an octahedral structure in its singlet ground state, similar to its isoelectronic analogue $\text{Cr}(\text{CO})_6$. Charge-induced reduction in π backbonding leads to a decreased red-shift in $\text{Mn}(\text{CO})_6^+$ ($\nu_{\text{CO}}=2106 \text{ cm}^{-1}$) compared to $\text{Cr}(\text{CO})_6$ ($\nu_{\text{CO}}=2003 \text{ cm}^{-1}$). The spin multiplicity of $\text{Mn}^+(\text{CO})_n$ complexes gradually decreases with progressive ligand addition. MnCO^+ is observed as both a quintet and a septet, $\text{Mn}(\text{CO})_2$ is observed only as a quintet, while $\text{Mn}(\text{CO})_{3,4}^+$ are both observed as triplets. $\text{Mn}(\text{CO})_5^+$ has a singlet ground state, and $\text{Mn}(\text{CO})_6^+$ is observed predominantly as a singlet but with some triplet population. All larger complexes are observed exclusively as singlets.

5.2 Introduction

Transition metal carbonyls are significant in organometallic and inorganic chemistry and provide classic examples of metal-ligand bonding [1-3]. Metal carbonyl complexes are used in synthesis and catalysis and as models for chemisorption on metal surfaces [4]. Infrared and Raman vibrational spectroscopy provides information about the structure and bonding in these systems [1-8]. In particular, the number of IR- or

Raman-active vibrations and their frequencies reveals the symmetry of carbonyl complexes and their electronic structure. On surfaces, the geometrical arrangement of CO bonding can be determined from the vibrational frequency [4]. The free molecule C-O stretch occurs at 2143 cm^{-1} [9], which is well-removed from most other molecular vibrations, and provides a convenient and sensitive indicator of bonding interactions. Vibrational spectroscopy has therefore been employed to study a wide variety of metal carbonyl complexes. In the present study, we use new IR spectroscopy methods to study the carbonyl stretch of manganese carbonyl cations in the gas phase.

The bonding interactions in transition metal carbonyls are usually described with the Dewar-Chatt-Duncanson (DCD) complexation model [1,7,8,10,11]. The metal-carbonyl bond involves a synergistic interaction between a σ -type donation and π -type back-bonding. Electron density is contributed from the occupied orbitals of the carbonyl to empty orbitals on the metal, removing electron density from the partially bonding carbonyl orbitals and forming the σ bond. π -type backbonding stems from donation of electron density from the partially filled d-shells into the antibonding π^* orbital of the CO. In "classical" carbonyls, the C-O stretching frequency (ν_{CO}) is lowered compared to its value in the free-CO molecule due to a net decrease in bonding electron density and an increase in antibonding electron density in the π^* orbitals. The majority of transition metal carbonyl complexes exhibit a resulting red-shift in the carbonyl stretch. In rare cases, a blue-shift of this vibration is observed. The interplay of these σ and π type interactions in metal carbonyl bonding has been recognized for many years. However, recent work suggests that electrostatic interactions can provide interesting additional effects in ionized systems. Calculations suggest that metal charge may play an important

role in the polarization and electron density distribution of the CO orbitals [12,13].

Unfortunately, there are few studies of isolated gas phase metal carbonyl ions with which to investigate these predictions.

Stable neutral transition metal carbonyl complexes have been studied extensively in both the condensed phase and the gas phase [6,7,14-17]. Neutral chromium hexacarbonyl, which is isoelectronic with manganese hexacarbonyl cation, is stable at room temperature and has been investigated spectroscopically [18,19]. Charged transition metal carbonyl complexes have been produced and studied in the condensed phase as salts with counterions to study isoelectronic analogues [20-23]. Various small neutral carbonyls have been studied using photoelectron spectroscopy of mass selected anions [24-26]. The electronic structure and bonding in these systems causes systematic shifts in the carbonyl stretching frequency and theory has investigated these effects extensively [12,13,27,28].

Mass spectrometry has been used to study a number of ionic metal carbonyl complexes [29,30]. Ion-molecule reactions have been characterized and ion-ligand dissociation energies have been measured [31,34]. Rare gas matrix isolation techniques have been employed to study neutral, cationic, and anionic carbonyls, including those of manganese neutrals and anions [8,35]. Gas phase studies of carbonyl cations are limited. Free electron lasers have been used to study metal cluster ions with attached CO ligands using resonance enhanced multiphoton photodissociation [36-39]. Our research group has recently employed mass-selected infrared photodissociation to study various metal cation-carbonyl complexes in the gas phase [40-41], including $\text{Au}(\text{CO})_n^+$ [42], $\text{Pt}(\text{CO})_n^+$ [43], $\text{Co}(\text{CO})_n^+$ [44], and the vanadium group systems [45]. In the present work, we use

these same techniques to investigate the manganese carbonyl cation complexes $\text{Mn}(\text{CO})_n^+$ ($n=1-9$).

Manganese complexes are of particular interest both because of the high spin in the isolated atomic ion, which has a ^7S configuration, and the existence of the stable saturated binuclear carbonyl complex $\text{Mn}_2(\text{CO})_{10}$. $\text{Mn}_2(\text{CO})_{10}$ is a stable complex at room temperature, and can dissociate into $\text{Mn}(\text{CO})_5$ radicals [46]. Spectroscopy for both the binuclear and mononuclear neutral and anionic complexes has been reported [35j]. Photolysis of $\text{HMn}(\text{CO})_5$ gives a $\text{Mn}(\text{CO})_5$ radical with C_{4v} structure [46]. When the cations are considered, $\text{Mn}(\text{CO})_6^+$ should be stable, as it satisfies the 18-electron rule and is isoelectronic to $\text{Cr}(\text{CO})_6$. The salt of $\text{Mn}(\text{CO})_6^+$ was isolated as $\text{Mn}(\text{CO})_6^+(\text{PF}_6)^-$ and ν_{CO} was measured at 2095 cm^{-1} [23]. The binding energies of $\text{Mn}(\text{CO})_n^+$ ($n=1-6$) have been determined by measuring the kinetic energy release distributions [53]. The MnCO^- ground state has been investigated by theory [27], and various neutrals and anions have been studied theoretically and compared to experiment [35j]. The present study examines the infrared spectroscopy in the gas phase of both the small unsaturated $\text{Mn}^+(\text{CO})_n$ ($n=1-5$) complexes and larger species at or above the filled coordination ($n=6-9$). The experimental infrared spectra are interpreted using density functional theory (DFT) computations to probe the structure and bonding in these systems.

5.3 Experimental Section

$\text{Mn}(\text{CO})_n^+$ ions are produced in a pulsed-nozzle laser vaporization source using the third harmonic of a pulsed Nd:YAG laser (355 nm; Spectra-Physics DCR-11). The laser is focused onto a rotating and translating $\frac{1}{4}$ inch diameter manganese rod, which is

mounted with a $\frac{3}{4}$ inch horizontal offset in front of a pulsed nozzle (General Valve Series 9). The apparatus has been described in detail elsewhere [40]. The expansion gas is pure carbon monoxide (National Specialty Gases) at a backing pressure of 150 psi. Mixed clusters containing argon, i.e., $\text{Mn}^+(\text{CO})_n\text{Ar}_m$, are produced using a mixture of carbon monoxide and argon. The expansion is skimmed into a second chamber and pulse extracted into a homemade Wiley-McLaren time-of-flight mass spectrometer. Ions of interest can be mass selected using pulsed deflection plates located in the first flight tube. These ions are then excited with tunable infrared light produced in an optical parametric oscillator/amplifier system (LaserVision) pumped by the fundamental (1064 nm) of a pulsed Nd:YAG (Spectra Physics Pro 230). This system provides continuously tunable light in the region of 2000-4000 cm^{-1} with about 1 cm^{-1} linewidth. When cluster cations are excited on resonance with a molecular vibration, intramolecular vibrational energy relaxation (IVR) occurs on a time-scale faster than the time scale of the experiment (1-2 μs), leading to dissociation of the complex provided the binding energies are low enough. Infrared spectra are obtained by monitoring the yield of a particular fragment as a function of the laser wavelength.

Density functional theory (DFT) computations were performed to investigate the structures and spin configurations of the complexes studied. Calculations were performed for several isomers each for $\text{Mn}(\text{CO})_n^+$ ($n=1-7$) and $\text{Mn}(\text{CO})_n^+\text{Ar}$ ($n=1-6$), considering the singlet, triplet, and quintet spin states for each complex. The calculations were performed using the B3LYP functional [48-49], as implemented in the Gaussian 2003 computational package [50], using the Def 2-TZVPP basis set on all atoms [51,52].

5.4 Results and Discussion

A mass spectrum of the $\text{Mn}(\text{CO})_n^+$ complexes produced is shown in Figure 5.1, along with selected examples of infrared photofragmentation mass spectra. The most intense peak in the mass spectrum produced by the cluster source corresponds to $\text{Mn}(\text{CO})_6^+$, indicating that this cluster cation is produced preferentially and likely has some enhanced stability. This cluster is expected to be stable as it satisfies the 18-electron rule and is isoelectronic to the well-known neutral $\text{Cr}(\text{CO})_6$. The addition of carbonyls beyond $n=6$ would likely result in "external" CO's, that is, ligands not bound directly to the metal ion but coordinated to other carbonyls through weaker electrostatic forces. These clusters are produced efficiently due to the cold supersonic expansion, and are not likely to survive at room temperature.

The ligand binding energies in these complexes can be investigated further by their fragmentation tendencies upon infrared excitation. Small $\text{Mn}^+(\text{CO})_n$ clusters ($n=1-5$) do not fragment in this experiment. This is consistent with the binding energies measured previously by Bowers for these clusters, which range from 0.69 eV to 1.39 eV [53]. IR photons in the CO stretching region near 2100 cm^{-1} have energies of about 0.26 eV, so it is not surprising that fragmentation is not observed. The fragmentation mass spectra for $\text{Mn}(\text{CO})_n^+$ ($n=6-8$) are shown in the inset of Figure 5.1. These spectra are accumulated with a difference method by recording the mass spectrum with the fragmentation laser "on" versus "off," resulting in a negative-going parent ion (showing its depletion) and positive fragment ions. The laser was set to the wavelength that produced the maximum fragmentation yield for each parent complex. At $n=6$, only a small amount of fragmentation is detected. The low signal here indicates a poor

fragmentation yield, consistent with the relatively high binding energy expected for this ion which should have complete coordination. The small amount of fragmentation is likely coming from multiphoton absorption or from a small fraction of ions containing residual internal energy from the growth process. At the low laser energy energies used here (about 1 mJ/pulse), we do not expect efficient multiphoton absorption. Residual internal energy could add to the photon energy and allow for fragmentation below the one-photon threshold. There is relatively little signal, simply because few hot ions are produced. If we change conditions, we find that hotter plasmas lead to increased fragmentation, supporting the idea that internal energy contributes to the fragmentation. As shown in the figure, clusters larger than $n=6$ fragment efficiently, and their fragmentation terminates at $n=6$. This is consistent with the presence of weakly bound external ligands beyond this size, confirming our expectation that the six-coordinate complex is most stable.

To investigate the spectroscopy of these systems, we measure the wavelength dependence of the fragmentation. The smaller clusters do not fragment with IR excitation, so we use the “rare gas tagging” technique to study these systems [40,41]. We produce mixed complexes of the form $\text{Mn}(\text{CO})_n\text{Ar}_m^+$, which can fragment by eliminating argon when excited on vibrational resonances. The Mn^+-Ar binding energy has not been measured, but is calculated to be 0.131 eV (1056 cm^{-1}) [54], and should be low enough to allow efficient fragmentation when the IR laser is in the CO stretching region. As shown in Figure 5.2, this method allows spectra to be measured for the small ($n=1-5$) manganese carbonyl complexes. It is of course a valid question whether or not these spectra of tagged complexes represent the desired spectra of the bare carbonyl species. Experience

with previous systems indicates that tagging usually has a negligible effect on the structure and spectrum of the complex, but argon can bind strongly in some systems and cause a significant perturbation. With this in mind, we exercise caution in interpreting the resultant spectra and use computations on complexes with versus without argon to investigate this.

Fragmentation of the $\text{Mn}(\text{CO})^+$ complex cannot be detected when it is tagged with a single argon, presumably because the argon binding is still too strong, and even a second argon cannot be eliminated efficiently. The addition of a third argon leads to efficient fragmentation, producing the spectrum shown in the lower trace of Figure 5.2. In a similar way, the $\text{Mn}(\text{CO})_2^+$ complex fragments inefficiently with a single argon, but acceptable signal is obtained with two. The $\text{Mn}(\text{CO})_2\text{Ar}^+$ spectrum (not shown) is not significantly shifted in frequency from that of $\text{Mn}(\text{CO})_2\text{Ar}_2^+$, indicating that the second argon is a minor perturbation on the system. All the larger complexes in the $n=3-6$ size range fragment efficiently when tagged with a single argon. All of the spectra of these small complexes feature a strong primary band that is red shifted from the free CO frequency of 2143 cm^{-1} (indicated with the vertical dashed line in the figure), and the $n=1,3,4$ and 5 spectra contain small secondary bands. The interpretations of these spectra are discussed later, using DFT calculations to investigate the spin states, structure and spectra.

Complexes containing more than five CO ligands can be dissociated without the addition of an argon tag. Spectra were obtained for $n=6$ both with and without argon, allowing for a direct comparison of the perturbation caused by the argon. The neat spectrum can be seen in the bottom trace of Figure 5.3 and the argon tagged spectrum is

in the top trace of Figure 5.2. The band for the tagged complex is blue shifted by 4 cm^{-1} and is much sharper than that for the untagged species. The untagged complex would not be expected to fragment with a single photon unless it had substantial internal energy, so the broadness of the $\text{Mn}(\text{CO})_6^+$ spectral feature is not unexpected. The tagged complex is also observed to lose CO and Ar simultaneously, and this loss channel yields a slightly different spectrum, which will be discussed later.

The spectra measured for the $n=6-9$ complexes in the CO-loss channel are shown in Figure 5.3. Each features one primary spectral feature, red-shifted by roughly 20 cm^{-1} from the free-CO frequency. This band does not significantly change position as more ligands are added. The increased dissociation yield after $n=6$ and the lack of further change in the vibrational spectrum are both consistent with the presence of a six coordinate $\text{Mn}(\text{CO})_6^+$ core ion, which becomes solvated by weakly bound external CO's. A second weaker spectral feature near 2174 cm^{-1} gradually becomes prominent as additional CO ligands are added past the $n=6$ species, and its position also does not change as more ligands are added. We assign this band to the vibration of the external carbonyls in the second sphere, which are bound only to other carbonyls and not directly to the metal ion. This behavior has been seen in other metal ion-CO complexes we have studied. The presence of this band only after the $n=6$ complex size again supports the conclusion of a six-coordinate $\text{Mn}(\text{CO})_6^+$.

To gain further insight into these spectra, we have performed DFT calculations on the $\text{Mn}(\text{CO})_n^+$ complexes for $n=1-7$. Complete details on all the calculated structures, energetics, and spin states are provided in the Supporting Information for this paper. We have investigated various isomers and spin states for each complex, and have also

investigated the corresponding argon complexes at the same level of theory to help determine the perturbation caused by tagging. Table 5.1 summarizes the structures, electronic states, and relative energetics of the computed species. The addition of the argon causes a significant geometry perturbation in the $n=3$ complex, but has only a minor effect on all other cluster sizes. The excellent signal to noise observed in this experiment can also be understood from these theoretical results. The computed intensities of the CO stretches are generally >500 km/mol, with some in excess of 1000 km/mol (see Supporting Information). Also, second-sphere CO molecules are calculated to be bound by about 600 cm^{-1} . Although the van der Waals binding in this situation is not expected to be handled particularly well by DFT, the weak binding suggested is low enough to allow for efficient photodissociation for the larger complexes.

We find that $\text{Mn}^+(\text{CO})$ is linear for all spins states, and DFT predicts a septet ground state, although this is favored by only 0.75 kcal/mol over the quintet. The triplet lies another 33 kcal/mol higher in energy from the quintet. For the bare cation, the ^7S state is 9472.97 cm^{-1} (27 kcal/mol) lower in energy than the ^5S state [58]. The addition of a single argon only minimally perturbs the geometry of the $\text{Mn}^+(\text{CO})$ system and results in an overall linear structure. Addition of a second argon leads to a small geometric distortion and a C_{2v} structure. The $\text{Mn}^+(\text{CO})_2$ complex has a linear triplet ground state, with a higher energy singlet state. The argon binds on the side of this, producing a slightly bent C_{2v} structure. $\text{Mn}^+(\text{CO})_3$ has a triplet D_{3h} structure, with a C_{2v} singlet species lying 10 kcal/mol higher in energy. The triplet is deformed significantly by the addition of argon, into a structure resembling that of the singlet. For $\text{Mn}^+(\text{CO})_4$, a C_{2v} singlet structure is predicted to be more stable than a triplet C_{3v} species by about 9

kcal/mol. The singlet is only slightly perturbed by the addition of argon, while the triplet again distorts towards the singlet geometry. The energy difference is nearly the same for $\text{Mn}^+(\text{CO})_5$, but the singlet is predicted to be more stable with a C_{4v} structure. The distortion caused by argon is again small for this complex. $\text{Mn}^+(\text{CO})_6$ is predicted to be an octahedral singlet, some 48 kcal more stable than the triplet configuration. This complex is also virtually unchanged by the addition of argon. No minimum structure could be found for a seven-coordinate $\text{Mn}(\text{CO})_7^+$ complex; all starting geometries converged to structures with a central octahedral core and an external CO ligand capping the octahedron. This is consistent with the previous conclusion that six carbonyl molecules complete the coordination sphere around Mn^+ .

Table 5.2 gives a comparison between the computed frequencies and the experimentally measured frequencies, for neat and argon tagged complexes. The calculated frequencies are scaled by 0.9679 and given a 3 cm^{-1} FWHM Lorentzian line shape to produce computed spectra to compare to the experimental data. The scaling factor was chosen to make the calculated CO stretching frequency match the experimental free molecule value. Figure 5.4 shows the computed and experimental spectra for the n=1-2 complexes, along with their computed ground state geometries. $\text{Mn}^+(\text{CO})$ has two experimental IR bands, indicating the presence of two spin states. The septet and quintet configurations are nearly equivalent in energy, with the triplet lying some 33 kcal/mol higher in energy. Considering solely the neat calculated spectra, we might be tempted to exclude the septet, which is predicted to have ν_{CO} at 2210 cm^{-1} . However, the addition of a single argon shifts this band to 2158 cm^{-1} , and to 2141 cm^{-1} with a second. The neat quintet lies at 2130 cm^{-1} , the singly tagged at 2120 cm^{-1} , and the

doubly tagged at 2114 cm^{-1} . The doubly tagged triplet configuration shifts down to 2080 cm^{-1} , from 2107 cm^{-1} for the neat variant. We were unable to find a stable minima on the triply argon tagged potential energy surface, likely due to the extremely flat argon potential. However, we do have a noisy experimental spectrum for the doubly tagged (not shown), which is not significantly shifted from the triply tagged, so we are reasonably confident that the theoretical calculations for doubly tagged complex serve as an adequate representation. We must take the frequency positions with some skepticism due to the argon perturbation, but due to the overall ordering of the frequencies and the significant energy difference of the triplet, we can reasonably say that the quintet and septet are present in our experiment. The majority of the population is in the quintet state. The oscillator strengths are nearly identical, around 544 km/mol , so the observed intensities should roughly reflect the relative populations. It appears that theory somewhat overestimates the stability of the septet.

In the $n=2$ complex, the quintet is 28 kcal more stable than the triplet, which is predicted to be roughly 28 kcal/mol more stable than the singlet. There are two stable structures for the monoargon complex, a linear structure with the argon binding to the oxygen in a carbonyl, and a bent C_{2v} structure with the argon bound to the metal. There is fairly minimal perturbation in the linear structure for either the singlet or triplet due to the argon, and the predicted triplet frequency matches up well to our measured value. We could not find a stable minima on the potential energy surface of the quintet for this linear configuration. We found stable minima for all three spin states in the bent configuration. The quintet is the lowest energy, by 25 kcal over the triplet. The bent triplet configuration is nearly identical in energy to the linear triplet configuration. The

calculated frequency for the bent quintet is 2115 cm^{-1} , which matches quite well with our experiment spectrum's band position of 2116 cm^{-1} . The bent triplet is calculated to be at 2096 cm^{-1} , and the linear triplet is calculated to be at 2112 cm^{-1} . The bent quintet is significantly lower in energy, and so we assign this complex as a quintet. We successfully measured a very low signal to noise spectrum for the singly argon tagged spectrum (not shown), and its band position was identical to that of the doubly argon tagged. We were not able to calculate the doubly tagged complex, but our experimental data gives us some confidence that our singly argon tagged experimental spectra are reasonable reflections of the true $\text{Mn}(\text{CO})_2^+$ spectrum.

The experimental and calculated spectra and structures for $n=3,4$ can be found in Figure 5.5. For $n=3$, we have some ambiguity in the assignment of the electronic state. The triplet state is predicted to be around 10 kcal/mol more stable. The predicted spectrum for the neat triplet is well off our observed values, but it is significantly perturbed by the addition of Ar, from a D_{3h} structure to a C_{2v} structure. The Ar tagged triplet fits somewhat well to the observed spectrum, but there is a small band around 2135 cm^{-1} that we cannot clearly resolve in our measured spectrum. The singlet spectrum is only minimally perturbed by the addition of argon, and our peak is wide enough for the red-shaded shoulder to mask the predicted doublet of peaks. The singlet does predict a single small band to the blue, although the position is not an exact match. We cannot draw a concrete assignment for this complex from these data.

For the $n=4$ complexes, the predicted triplet structure features two bands with positions that nearly match our measured frequencies. The intensity ratio, however, is reversed between the theory and experiment. The singlet has three major bands, with

sufficient separation that we should be able to resolve them if they were present. We can conclude we do not have the triplet, despite it being more stable. When the triplet calculation was performed with a different basis set, 6-31+G* on C, O, and Ar and LANL2DZ on Mn, the predicted neat spectrum was nearly identical to that calculated with TZVPP, but the Ar tagged complex swapped intensity ratios as seen in our experimental spectrum. It appears here that the deformation due to argon is not fully described when using TZVPP. If we assume that n=4 is in fact a triplet, then the n=3 complex should also be a triplet. There is no obvious reason that a smaller complex would have a lower spin.

Figure 5.6 shows the experimental and calculated spectra for n=5 and 6, along with their ground state geometries. Neither the singlet or triplet configuration is deformed significantly by the addition of argon. Here, the singlet is predicted to be more stable by 8.8 kcal/mol. The singlet has two bands, at 2097 and 2114 cm^{-1} . The positions and intensity ratio matches quite neatly with our observed spectra. The triplet is predicted to have a 2095 cm^{-1} band, and a doublet split by 0.5 cm^{-1} at 2148 cm^{-1} . We do not observe a band in this higher region, and can exclude the triplet and assign the n=5 complex as a singlet.

We obtained neat and Ar tagged versions of the n=6 complex, which can be compared to theory. Figure 5.6 shows the Ar tagged spectra, as measured by the loss of Ar and CO. The spectra as measured by loss of Ar can be found in Figure 5.3, bottom pane. The main band position is identical between the two spectra. Here we can see excellent agreement with both the argon tagged and neat calculated spectra. As we were able to measure experimentally the neat and argon tagged complex, we have some direct

confirmation of the degree of shift induced. For this complex, the band centers are nearly identical at 2114 cm^{-1} . The untagged complex has a much broader band, likely due to the degree of internal energy required for fragmentation. Subsequent comparisons will use the argon tagged complex as representative of the correct spectrum. We can see excellent agreement between the O_h singlet configuration and the measured spectra, adding additional confirmation that this is indeed a hexacoordinate system. The $\text{Mn}(\text{CO})_6^+$ complex ground state has previously been determined to be a singlet by various methods [53,56,57], and we reaffirm that conclusion here. The top panel of Figure 5.6 shows the $\text{Mn}(\text{CO})_6\text{Ar}^+$ complex measured by the loss of $\text{Ar} + \text{CO}$. This is a weaker channel than the loss of argon in the experiment, and thus the signal to noise is somewhat poor. However, we can see two clearly resolved bands along with the main band we previously identified as the singlet CO stretch. The calculated spectra for the triplet, predicted to be some 46 kcal/mol higher in energy, matches these two bands quite well in position and intensity ratio. It seems that, while the majority of the ion population here is in the singlet state, some population exists as a triplet despite the significantly higher energy. It was experimentally noted that these bands increased in intensity as the source plasma temperature was increased, and could be eliminated entirely.

The $\text{Mn}(\text{CO})_6^+$ core ion identified here, with a CO stretching frequency at 2114 cm^{-1} , varies by some 20 cm^{-1} from the solution phase $[\text{Mn}(\text{CO})_6^+][\text{PF}_6^-]$ salt value. The chromium hexacarbonyl, isoelectronic to $\text{Mn}(\text{CO})_6^+$, has a stretching frequency of 2003 cm^{-1} [19]. This significant redshift from the cation to neutral analogue mirrors the trend previously observed between $\text{Co}(\text{CO})_5^+$ and $\text{Fe}(\text{CO})_5$. $\text{Co}(\text{CO})_5^+$ has ν_{CO} at 2140 and 2150 cm^{-1} , while $\text{Fe}(\text{CO})_5$ has ν_{CO} at 2013 and 2034 cm^{-1} [46,55]. It is likely due to

increased π backbonding into the antibonding π^* orbital in the neutral analogue. The charged manganese has more tightly bound d electrons than the neutral chromium, which inhibits backbonding and leads to a lessened red-shift in the cation. This has also been demonstrated for the isoelectronic series of $\text{Ni}(\text{CO})_4$, $\text{Co}(\text{CO})_4^-$, and $\text{Fe}(\text{CO})_4^{2-}$, which have CO stretching frequencies of 2094, 1946, and 1799 cm^{-1} respectively [15,20,22]. The negatively charged complexes have increased back bonding, and thus weaker C-O bonds. The results observed here are consistent with those previous experiments.

The effect of charge on oscillator strength has also been investigated. Table 5.3 shows the calculated frequencies and oscillators strengths compared to the experimental frequencies for the isoelectronic pairs of $\text{Mn}(\text{CO})_6^+$ and $\text{Cr}(\text{CO})_6$, and $\text{Co}(\text{CO})_5^+$ and $\text{Fe}(\text{CO})_5^+$, respectively. We can see reasonably good band position agreement between theory and experiment for each system. Interestingly, the oscillator strengths are significantly higher for the neutral analogues. This may be due to the cation withdrawing more charge from the CO, leading to a more even charge distribution between carbon and oxygen. This would lead to a lessened red-shift for the cations, which is indeed seen experimentally, and a lower oscillator strength due to decreased change in dipole.

With the six-coordinate octahedral ion identified as the “core” ion of this system, we can interpret subsequent complexes as CO solvated versions of this. No stable seven-coordinate complex could be found, and $n=7$ invariably converged to a six-coordinate core with an external CO ligand. The spectra and calculated structure can be found in the Supporting Information. The agreement between the theoretical calculation and experiment is excellent, with the blue-shifted “surface” CO reproduced quite nicely. The main ν_{CO} stretch moves slightly as additional CO ligands are added, reaching 2119 cm^{-1}

by the third external CO, $n=9$. The surface CO band also shifts slightly to the red, from 2175 cm^{-1} for $n=7$ to 2172 cm^{-1} for $n=9$. These frequencies are some 30 cm^{-1} from the free CO stretch at 2143 cm^{-1} . We have previously partially interpreted this blue shift in terms of the polarization effects described by Goldman and Krogh-Jespersen [12]. However, the magnitude of the shift cannot fully be explained in this context. We have now observed this effect for several systems, and some further theoretical study may be necessary.

5.5 Conclusion

Manganese carbonyl cations of the form $\text{Mn}(\text{CO})_n^+$ ($n=1-9$) and their corresponding “argon-tagged” analogues $\text{Mn}(\text{CO})_n(\text{Ar})_m^+$ were produced and studied using mass selected infrared photodissociation spectroscopy and density functional theory. Comparison of the number of infrared bands, along with their positions and intensities, allows us to assign the electronic configuration and geometry for these complexes. A gradual spin change is observed as sequential carbonyl ligands are added. The MnCO^+ complex has both quintet and septet population, with a quintet ground state. $\text{Mn}^+(\text{CO})_2$ also has a quintet ground state, while $\text{Mn}(\text{CO})_{3-4}^+$ complexes are triplets. The $\text{Mn}(\text{CO})_5^+$ complex is a singlet, and the ground state of $\text{Mn}(\text{CO})_6^+$ is also a singlet. Some triplet population is observed for $\text{Mn}(\text{CO})_6^+$. $\text{Mn}(\text{CO})_6^+$ has a completed coordination shell, in line with its expected 18 electron stability, and shares an octahedral structure with its isoelectronic analogue, $\text{Cr}(\text{CO})_6^+$. The carbonyl stretches for $\text{Mn}(\text{CO})_6^+$ are *less* red-shifted than in $\text{Cr}(\text{CO})_6^+$, as expected due to lessened π backbonding due to the

charge. However, the oscillator strengths of the neutral analogues are *greater* than the cations, potentially due to polarization effects on the carbonyl.

5.6 Acknowledgements

We acknowledge generous support for this work from the U.S. Department of Energy (grant no. DE-FG02-96ER14658) and the Air Force Office of Scientific Research (Grant No. FA95509-1-0166).

Supporting Information

The Supporting Information for this manuscript contains the full details of the DFT computations done in support of the spectroscopy here, including the structures, energetics and vibrational frequencies for each of the structures considered. The complete reference for Ref 50 is also included in the Supporting Information.

5.7 References

- (1) Cotton, F. A. *Advanced Inorganic Chemistry*, 6th ed., John Wiley and Sons, Inc., New York, 1999.
- (2) Huheey, J. E.; Keiter, E. A.; Keiter, R. L. *Inorganic Chemistry Principles of Structure and Reactivity*, Harper Collins, New York, 1993.
- (3) Wrighton, M. The Photochemistry of Metal Carbonyls. *Chem. Rev.* **1974**, *74*, 401.
- (4) Somorjai, G. A. *Introduction to Surface Chemistry and Catalysis*, John Wiley and Sons, Inc., New York, 1994.
- (5) Bertini, I.; Gray, H. B.; Stiefel, E. I.; Valentine, J. S. *Biological Inorganic Chemistry Structure and Reactivity*, University Science Books, Sausalito California, 2007.
- (6) Nakamoto, K. *Infrared and Raman Spectra of Inorganic and Coordination Compounds*, John Wiley, New York, 1997.
- (7) Frenking, G.; Fröhlich, N. The Nature of the Bonding in Transition-Metal Compounds. *Chem. Rev.* **2000**, *100*, 717.
- (8) Zhou, M.; Andrews, L.; Bauschlicher, C. W. Spectroscopic and Theoretical Investigations of Vibrational Frequencies in Binary Unsaturated Transition-Metal Carbonyl Cations, Neutrals, and Anions. *Chem. Rev.* **2001**, *101*, 1931.
- (9) Huber, K. P.; Herzberg, G. *Molecular Spectra and Molecular Structure IV. Constants of Diatomic Molecules*, Van Nostrand Reinhold Co., **1979**.
- (10) Chatt, J.; Duncanson, L.A. Olefin coordination compounds. III. Infrared spectra and structure: attempted preparation of acetylene compounds. *J. Chem. Soc.* **1953**, 2939.

- (11) Dewar, M.J.S.S “A review of the π -complex theory,” *Bull. Soc. Chim. Fr.* **1951**, 18, C79
- (12) Goldman, A. S.; Krogh-Jespersen, K. Why do cationic carbon monoxide complexes have high CO stretching force constants and short CO bonds? Electrostatic effects, not σ bonding. *J. Am. Chem. Soc.* **1996**, 118, 12159.
- (13) a) Lupinetti, A. J.; Frenking, G.; Strauss, S. H. Nonclassical Metal Carbonyls. *Angew. Chem. Int. Ed.* **1998**, 37, 2113. b) Lupinetti, A. J.; Jonas, V.; Thiel, W.; Strauss, S. H.; Frenking, G. Trends in Molecular Geometries and Bond Strengths of the Homoleptic d10 Metal Carbonyl Cations: A Theoretical Study. *Chem. Eur. J.* **1999**, 5, 2573. c) Lupinetti, A. J.; Fau, S.; Frenking, G.; Strauss, S. H. Theoretical Analysis of the Bonding between CO and Positively Charged Atoms. *J. Phys. Chem.* **1997**, 101, 9551.
- (14) O’Dwyer, M. F. Infrared Spectra and Normal Coordinate Analysis of Iron Pentacarbonyl. *J. Molec. Spectroscopy* **1958**, 2, 144.
- (15) Jones, L. H.; McDowell, R. S.; Goldblatt, M. Infrared spectra of $\text{Cr}(\text{CO})_6$, $\text{Mo}(\text{CO})_6$ and $\text{W}(\text{CO})_6$ Gas phase. *Inorg. Chem.* **1969**, 28, 2349.
- (16) Boquet, G.; Birgone, M. Infrared spectra of $\text{Ni}(\text{CO})_4$ in gas phase. *Spectrochim. Acta.* **1971**, 27, 139.
- (17) Beagley, B.; Schmidling, D. G. A Re-evaluation of the molecular structure of iron pentacarbonyl. *J. Molec. Struct.* **1974**, 22, 5466.
- (18) Shufler, S.L.; Sternberg, H.W.; Friedel, R.A. Infrared spectrum and structure of chromium hexacarbonyl, $\text{Cr}(\text{CO})_6$. *J. Am. Chem. Soc.* **1956**, 78, 2687
- (19) Hansford, G.M.; Davies, P.B. Infrared laser spectroscopy of jet-cooled chromium hexacarbonyl in the 5 micron region. *J. Mol. Spec.* **1994**, 168, 540

- (20) Stammerich, H.; Kawai, K.; Tavares, Y.; Krumholz, P.; Behmoiras, J.; Bril, S. Infrared spectra of $\text{Fe}(\text{CO})_4^{2-}$ in aqueous solution. *J. Chem. Phys.* **1960**, *32*, 1482.
- (21) Abel, E. W.; McLean, A. N.; Tyfield, S. P.; Braterman, P. S.; Walker, A. P.; Hendra, P. J. Infrared spectra of $\text{V}(\text{CO})_6^-$ and $\text{Re}(\text{CO})_6^+$ in CH_3CN solution. *J. Mol. Spec.* **1969**, *30*, 29.
- (22) Edgell, W. F.; Lyford, J. I. Infrared spectra of $\text{Co}(\text{CO})_4^-$ in DMF solution. *J. Chem. Phys.* **1970**, *52*, 4329.
- (23) McLean, R. A. N. Infrared and Raman spectra of $\text{Mn}(\text{CO})_6^+$ in CH_3CN solutions and solids. *Can. J. Chem.* **1974**, *52*, 213.
- (24) Engelking, P. C.; Lineberger, W. C. Laser Photoelectron spectrometry of the negative ions of iron and iron carbonyls. Electron affinity determination for the series $\text{Fe}(\text{CO})_n$ $n=0,1,2,3,4$. *J. Am. Chem. Soc.* **1979**, *101*, 5579.
- (25) a) Villalta, P. W.; Leopold, D. G. A study of the FeCO and the s and s states of FeCO by negative ion photoelectron spectroscopy. *J. Chem. Phys.* **1993**, *98*, 7730. b) Bengali, A. A.; Casey, S. M.; Cheng, C. L.; Dick, J. P.; Fenn, P. T.; Villalta, P. W.; Leopold, D. G. Negative ion photoelectron spectroscopy of the coordinatively unsaturated Group VI metal carbonyls of chromium, molybdenum and tungsten. *J. Am. Chem. Soc.* **1992**, *114*, 5257.
- (26) Butcher, C. P.; Johnson, B. F. G.; McIndoe, J. S.; Yang, X.; Wang, X. B.; Wang, L. S. Collision-Induced Dissociation and Photodetachment of Singly and Doubly Charged Anionic Polynuclear Transition Metal Carbonyl Clusters $\text{Ru}_3\text{CO}(\text{CO})_{13}^-$, $\text{Ru}_6\text{CO}(\text{CO})_{16}^{2-}$, $\text{Ru}_6\text{CO}(\text{CO})_{18}^{2-}$. *J. Chem. Phys.* **2002**, *116*, 6560.

- (27) Barnes, L.A.; Rosi, M.; Bauschlicher, C.W. Theoretical studies of the first- and second-row mono- and di-carbonyl positive ions. *J. Chem. Phys.* **1990**, *93*, 609.
- (28) Huo, C.-H.; Li, Y.-W.; Wu, G.-S.; Beller, M.; Jiao, H. Structures and energies of $[\text{Co}(\text{CO})_n]^m$ ($m=0, 1+, 1-$) and $\text{HCo}(\text{CO})_n$: Density functional studies. *J. Phys. Chem. A* **2002**, *106*, 12161.
- (29) Russell, D.H. *Gas Phase Inorganic Chemistry*, Plenum, New York, 1989.
- (30) Freiser, B. S. *Organometallic Ion Chemistry*, Kluwer, Dordrecht, The Netherlands, 1996.
- (31) a) Khan, F. A.; Clemmer, D. E.; Schultz, R. H.; Armentrout, P. B. Sequential bond energies of chromium carbonyls ($\text{Cr}(\text{CO})_x^+$, $x=1-6$). *J. Phys. Chem.* **1993**, *97*, 7978. b) Sievers, M. R.; Armentrout, P. B. Collision-Induced Dissociation Studies of $\text{V}(\text{CO})_x$, $x=1-7$: Sequential Bond Energies and the Heat of formation of $\text{V}(\text{CO})_6$. *J. Phys. Chem.* **1995**, *99*, 8135. c) Meyer, F.; Chen, Y. M.; Armentrout, P.B. Sequential Bond Energies of $\text{Cu}(\text{CO})_x^+$ and $\text{Ag}(\text{CO})_x^+$ ($x=1-4$). *J. Am. Chem. Soc.* **1995**, *117*, 4071. d) Goebel, S.; Haynes, C. L.; Khan, F. A.; Armentrout, P. B. Collision-Induced Dissociation Studies of $\text{Co}(\text{CO})_x^+$, $x=1-5$: Sequential Bond Energies and Heats of Formation of $\text{Co}(\text{CO})_4$. *J. Am. Chem. Soc.* **1995**, *117*, 6994. e) Meyer, F.; Armentrout, P. B. Sequential bond energies of $\text{Ti}(\text{CO})_x^+$, $x=1-7$. *Mol. Phys.* **1996**, *88*, 187. f) Zhang, X. G.; Armentrout, P. B. Sequential Bond Energies of $\text{Pt}(\text{CO})_x^+$ ($x=1-4$) Determined by Collision-Induced Dissociation. *Organometallics* **2001**, *20*, 4266.
- (32) a) Grushow, A.; Ervin, K. M. Ligand and metal binding energies in platinum carbonyl cluster anions: Collision-induced dissociation of Pt_m^- and $\text{Pt}_m(\text{CO})_n^-$. *J.*

- Chem. Phys.* **1997**, *106*, 9580. b) Spasov, V. A.; Ervin, K. M. Binding energies of palladium carbonyl cluster anions: Collision-induced dissociation of $\text{Pd}_3(\text{CO})_n^-$ ($n = 0-6$). *J. Chem. Phys.* **1998**, *109*, 5344.
- (33) Le Caër, S.; Heninger, M.; Maitre, P.; Mestdagh, H. Accurate measurement of the relative bond energies of CO and H_2O ligands in Fe^+ mono- and bis-ligated complexes. *Rapid Commun. Mass Spectrom.* **2003**, *17*, 351.
- (34) Schwartz, H. Relativistic Effects in Gas-Phase Ion Chemistry: An Experimentalist's View. *Angew. Chem. Int. Ed.* **2003**, *42*, 4442.
- (35) a) Zhou, M.; Andrews, L. Infrared Spectra of RhCO^+ , RhCO , and RhCO^- in solid neon: a scale for charge support in catalyst systems. *J. Am. Chem. Soc.* **1999**, *121*, 9171. b) Zhou, M.; Andrews, L. Infrared Spectra and density functional calculations of CuCO_n^+ ($n=1-4$), CuCO_n ($n=1-3$), and CuCO_n^- ($n=1-3$), in solid neon. *J. Chem. Phys.* **1999**, *111*, 4548. c) Zhou, M.; Andrews, L. Infrared spectra and density functional calculations of RuCO^+ , OsCO^+ , $\text{Ru}(\text{CO})_x$, $\text{Os}(\text{CO})_x$, $\text{Ru}(\text{CO})_x^-$, and $\text{Os}(\text{CO})_x^-$ ($x=1-4$) in solid neon. *J. Phys. Chem. A* **1999**, *103*, 6956. d) Zhou, M.; Andrews, L. Reactions of laser-ablated iron atoms and cations with carbon monoxide: Infrared spectra of FeCO^+ , $\text{Fe}(\text{CO})_2^+$, $\text{Fe}(\text{CO})_x$ and $\text{Fe}(\text{CO})_x^-$ ($x=1-4$) in solid neon. *J. Chem. Phys.* **1999**, *110*, 10370. e) Zhou, M.; Andrews, L. Matrix infrared spectra and density functional calculations of ScCO , ScCO^- , and ScCO^+ . *J. Phys. Chem. A* **1999**, *103*, 2964. f) Zhou, M.; Andrews, L. Infrared spectra and density functional calculations for OMCO , and $\text{OM}-(\eta^2\text{-CO})^-$, OMCO^+ and OMOC^+ ($M=\text{V}, \text{Ti}$) in solid argon. *J. Phys. Chem. A* **1999**, *103*, 5259. g) Zhou, M.; Andrews, L. Reactions of laser ablated Co, Rh, and Ir with

- CO: Infrared spectra and density functional calculations of the metal carbonyl molecules, cations and anions in solid neon. *J. Phys. Chem. A.* **1999**, *103*, 7773.
- h) Liang, B.; Andrews, L. Reactions of Laser-Ablated Ag and Au atoms with carbon monoxide: Matrix Infrared Spectra and Density Functional Calculations on $\text{Au}(\text{CO})_n$ ($n=2,3$), $\text{Au}(\text{CO})_n^-$ ($n=1,2$), and $\text{M}(\text{CO})$ ($n=1-4$), ($\text{M}=\text{Ag}, \text{Au}$). *J. Phys. Chem. A.* **2000**, *104*, 9156. i) Liang, B.; Zhou, M.; Andrews, L. Reactions of Laser-Ablated Ni, Pd, and Pt atoms with carbon monoxide: Matrix Infrared Spectra and Density Functional Calculations on $\text{M}(\text{CO})_n$ ($n=1-4$), $\text{M}(\text{CO})_n^-$ ($n=1-3$), and $\text{M}(\text{CO})_n^+$ ($n=1-2$), ($\text{M}=\text{Ni}, \text{Pd}, \text{Pt}$). *J. Phys. Chem. A.* **2000**, *104*, 3905. j) Andrews, L.; Zhou, M.; Wang, X.; Bauschlicher, C.W. Matrix Infrared Spectra and DFT Calculations of Manganese and Rhenium Carbonyl Neutral and Anion Complexes. *J. Phys. Chem. A* **2000**, *104*, 8887
- (36) Fielicke, A.; von Helden, G.; Meijer, G.; Pedersen, D. B.; Simard, B.; Rayner, D. M. Size and Charge Effects on Binding of CO to Small Isolated Rhodium Clusters. *J. Phys. Chem. B.* **2004**, *108*, 14591.
- (37) Moore, D. T.; Oomens, J.; Eyler, J. R.; Meijer, G.; von Helden, G.; Ridge, D. P. Gas-Phase IR Spectroscopy of Anionic Iron Carbonyl Clusters. *J. Am. Chem. Soc.* **2004**, *126*, 14726.
- (38) a) Fielicke, A.; von Helden, G.; Meijer, G.; Simard, B.; Rayner, D. M. Gold Cluster Carbonyls: Vibrational Spectroscopy of the Anions and the Effects of Cluster Size, Charge, and Coverage on the CO Stretching Frequency. *J. Phys. Chem. B.* **2005**, *109*, 23935. b) Fielicke, A.; von Helden, G.; Meijer, G.; Pedersen, D. B.; Simard, B.; Rayner, D. M. Gold Cluster Carbonyls: Saturated

- Adsorption of CO on Gold Cluster Cations, Vibrational Spectroscopy, and Implications for Their Structures. *J. Am. Chem. Soc.* **2005**, *127*, 8416.
- (39) Fielicke, A.; von Helden, G.; Meijer, G.; Pedersen, D. B.; Simard, B.; Rayner, D. M. Size and charge effects on the binding of CO to late transition metal clusters. *J. Chem. Phys.* **2006**, *124*, 194305.
- (40) Duncan, M. A. Infrared spectroscopy to probe structure and dynamics in metal ion-molecule complexes. *Intl. Rev. Phys. Chem.* **2003**, *22*, 407.
- (41) Walker, N. R.; Walters, R. S.; Duncan, M. A. Frontiers in the infrared spectroscopy of gas phase metal ion complexes. *New J. Chem.* **2005**, *29*, 1495.
- (42) Velasquez III, J.; Njagic, B.; Gordon, M. S.; Duncan, M. A. IR Photodissociation Spectroscopy and Theory of $\text{Au}^+(\text{CO})_n$ Complexes: Nonclassical Carbonyls in the Gas Phase. *J. Phys. Chem. A.* **2008**, *112*, 1907.
- (43) Velasquez III, J.; Duncan, M. A. IR Photodissociation Spectroscopy of Gas Phase $\text{Pt}^+(\text{CO})_n$ ($n=4-6$). *Chem. Phys. Lett.* **2008**, *461*, 28.
- (44) Ricks, A.M.; Bakker, J.M.; Douberly, G.E.; Duncan, M.A. Infrared Spectroscopy and Structures of Cobalt Carbonyl Cations. *J. Phys. Chem. A.* **2009**, *113*, 4701
- (45) Ricks, A.M.; Reed, Z.D.; Duncan, M.A. Seven-Coordinate Homoleptic Metal Carbonyls in the Gas Phase. *J. Am. Chem. Soc.*, 2009, *131*, 9176–9177
- (46) Seder, T.A.; Church, S.P.; Weitz, E. Gas-phase infrared spectroscopy and recombination kinetics for pentacarbonylmanganese radical generated via xenon fluoride laser photolysis of decacarbonyldimanganese. *J. Am. Chem. Soc.* **1986**, *108*, 1084

- (47) Bauschlicher, C.W. On the ground state of MnCO^- . *Chem. Phys. Lett.* **1996**, *249*, 244
- (48) Becke, A. D. 3 term correlation functional. *J. Chem. Phys.* **1993**, *98*, 5648.
- (49) Lee, C.; Yang, W.; Parr, R. G. Lee Yang Parr, Correlation functional. *Phys. Rev B.* **1998**, *98*, 5648.
- (50) Frisch, M. J. et al., *Gaussian 03 (Revision B.02)*; Gaussian, Inc.: Pittsburgh, PA, 2003.
- (51) Weigend, F.; Ahlrichs, R. Balanced basis sets of split valence, triple zeta valence and quadruple zeta valence quality for H to Rn: Design and assessment of accuracy. *Phys. Chem. Chem Phys.* **2005**, *7*, 3297
- (52) Schaefer, A.; Huber, R.; Ahlrichs, J. Fully optimized contracted Gaussian basis sets of triple zeta valence quality for atoms Li to Kr. *J. Chem. Phys.* **1994**, *100*, 5829
- (53) Dearden, D.V.; Hayashibara, K.; Beauchamp, J.L.; Kirchner, N.J.; van Koppen, P.A.M.; Bowers, M.T. Fundamental studies of the energetics and dynamics of ligand dissociation and exchange processes at transition-metal centers in the gas phase: $\text{Mn}(\text{CO})_x^+$, $x = 1-6$. *J. Am. Chem. Soc.* **1989**, *111*, 2401
- (54) Partridge, H.; Bauschlicher, C.W.; Langhoff, S.R. Theoretical study of metal ions bound to helium, neon, and argon. *J. Phys. Chem.* **1992**, *96*, 5350
- (55) Jang, J. H.; Lee, G. J.; Lee, H.; Xie, Y.; Schaefer, F. H. Molecular Structures and Vibrational Frequencies of Iron Carbonyls: $\text{Fe}(\text{CO})_5$, $\text{Fe}_2(\text{CO})_9$, and $\text{Fe}_3(\text{CO})_{12}$. *J. Phys. Chem. A.* **1998**, *102*, 5298.

- (56) Beach, N. A.; Gray, H. B. Electronic structures of metal hexacarbonyls. *J. Am. Chem. Soc.* **1968**, *90*, 5713-5721.
- (57) Burdett, J. K. Calculation of the geometries of binary transition metal carbonyl and dinitrogen complexes. *J. Chem. Soc. Faraday Trans. 2* **1974**, *70*, 1599-1693.
- (58) Ralchenko, Yu., Kramida, A.E., Reader, J. and [NIST ASD Team](#) (2008). *NIST Atomic Spectra Database* (version 3.1.5), [Online]. Available: <http://physics.nist.gov/asd3> [2009, November 19]. National Institute of Standards and Technology, Gaithersburg, MD.

Table 5.1: The structures, electronic ground states, and energetics computed for $\text{Mn}(\text{CO})_n$ with DFT. No stable quintet configurations could be found for $n=3-6$.

complex	state/structure	relative energy (kcal/mol)
$\text{Mn}(\text{CO})^+$	$^7\text{C}_{\infty\text{v}}$	0.0
	$^5\text{C}_{\infty\text{v}}$	+0.7
$\text{Mn}(\text{CO})_2^+$	$^5\text{D}_{\infty\text{h}}$	0.0
	$^3\text{D}_{\infty\text{h}}$	+24.9
	$^1\text{D}_{\infty\text{h}}$	+51.6
$\text{Mn}(\text{CO})_3^+$	$^3\text{D}_{3\text{h}}$	0.0
	$^1\text{C}_{2\text{v}}$	+9.8
$\text{Mn}(\text{CO})_4^+$	$^1\text{C}_{2\text{v}}$	0.0
	$^3\text{C}_{3\text{v}}$	+8.8
$\text{Mn}(\text{CO})_5^+$	$^1\text{C}_{4\text{v}}$	0.0
	$^3\text{C}_{2\text{v}}$	+8.7
$\text{Mn}(\text{CO})_6^+$	$^1\text{O}_\text{h}$	0.0
	$^3\text{C}_{4\text{h}}$	48.0

Table 5.2: The vibrational frequencies computed (Scaled by 0.9679) and measured for $\text{Mn}(\text{CO})_n^+$ and $\text{Mn}(\text{CO})_n(\text{Ar})_m^+$ complexes

Complex		theory (neat)	theory (argon-tagged)	experiment
$\text{Mn}(\text{CO})^+$	septet	2210.1	2158.2 (m=1), 2141.5 (m=2)	2106, 2148
	quintet	2132.8	2122.3 (m=1), 2106.4 (m=2)	
$\text{Mn}(\text{CO})_2^+$	quintet	2127.4	2114.6	2115
$\text{Mn}(\text{CO})_3^+$	triplet	2146.1	2091.1, 2130.3, 2170.1	2110, 2188
$\text{Mn}(\text{CO})_4^+$	triplet	2077.0, 2150.1,	2072.6, 2138.6,	2081, 2148
		2150.3	2138.7, 2172.8	
$\text{Mn}(\text{CO})_5^+$	singlet	2099.9, 2119.3	2097.0, 2114.2	2086, 2114
$\text{Mn}(\text{CO})_6^+$	singlet	2118.5	2119.4	2114

Table 5.3: comparison of experimental frequencies to calculated frequencies and oscillator strengths of the isoelectronic analogues $\text{Mn}(\text{CO})_6^+$, $\text{Cr}(\text{CO})_6^+$ and $\text{Co}(\text{CO})_5^+$, $\text{Fe}(\text{CO})_5$.

Species	Experimental Frequency	Calculated Frequency	Oscillator Strength
$\text{Mn}(\text{CO})_6^+$	2114	2118.5	1061
$\text{Cr}(\text{CO})_6$	2002.9 ^a	2001.2	1861
$\text{Co}(\text{CO})_5^+$	2140, 2150 ^b	2140.0, 2154.1	644, 761
$\text{Fe}(\text{CO})_5$	2013, 2034 ^c	2008, 2036	1268, 1456

a) Ref 19

b) Ref 44

c) Ref 55

Figure Captions

Figure 5.1. The mass spectrum of $\text{Mn}(\text{CO})_n^+$ clusters produced by our cluster source.

Inset: the photofragmentation mass spectra of $n=6-8$.

Figure 5.2. The infrared photodissociation spectra of small $\text{Mn}(\text{CO})_n^+(\text{Ar})_m$ complexes measured by the elimination of argon. The dashed vertical line shows the vibrational frequency of isolated CO in the gas phase, at 2143 cm^{-1} .

Figure 5.3. The infrared photodissociation spectra of larger $\text{Mn}(\text{CO})_n^+$ complexes measured by the elimination of CO. The dashed vertical line shows the vibrational frequency of isolated CO in the gas phase, at 2143 cm^{-1} .

Figure 5.4. Infrared spectra of $\text{Mn}(\text{CO})_n\text{Ar}_m^+$ ($n=1,2$) compared to the spectra predicted by theory, along with calculated ground state structures.

Figure 5.5. Infrared spectra of $\text{Mn}(\text{CO})_n\text{Ar}_m^+$ ($n=3,4$) compared to the spectra predicted by theory, along with calculated ground state structures.

Figure 5.6. Infrared spectra of $\text{Mn}(\text{CO})_n\text{Ar}_m^+$ ($n=5,6$) compared to the spectra predicted by theory, along with calculated ground state structures. The $\text{Mn}(\text{CO})_6\text{Ar}^+$ spectra was measured by loss of $\text{Ar} + \text{CO}$, the $\text{Mn}(\text{CO})_5\text{Ar}^+$ spectra was measured by loss of CO.

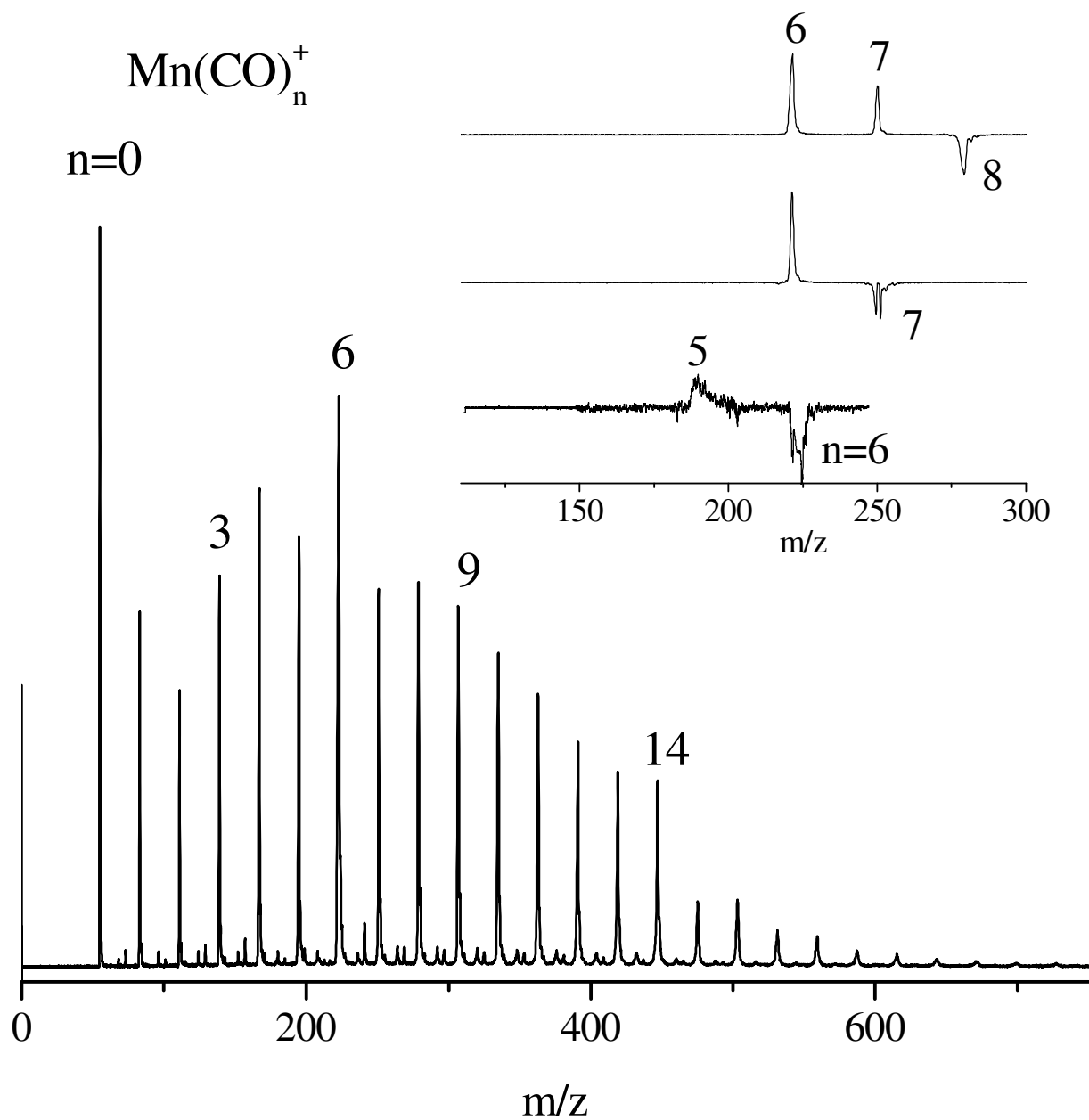


Figure 5.1.

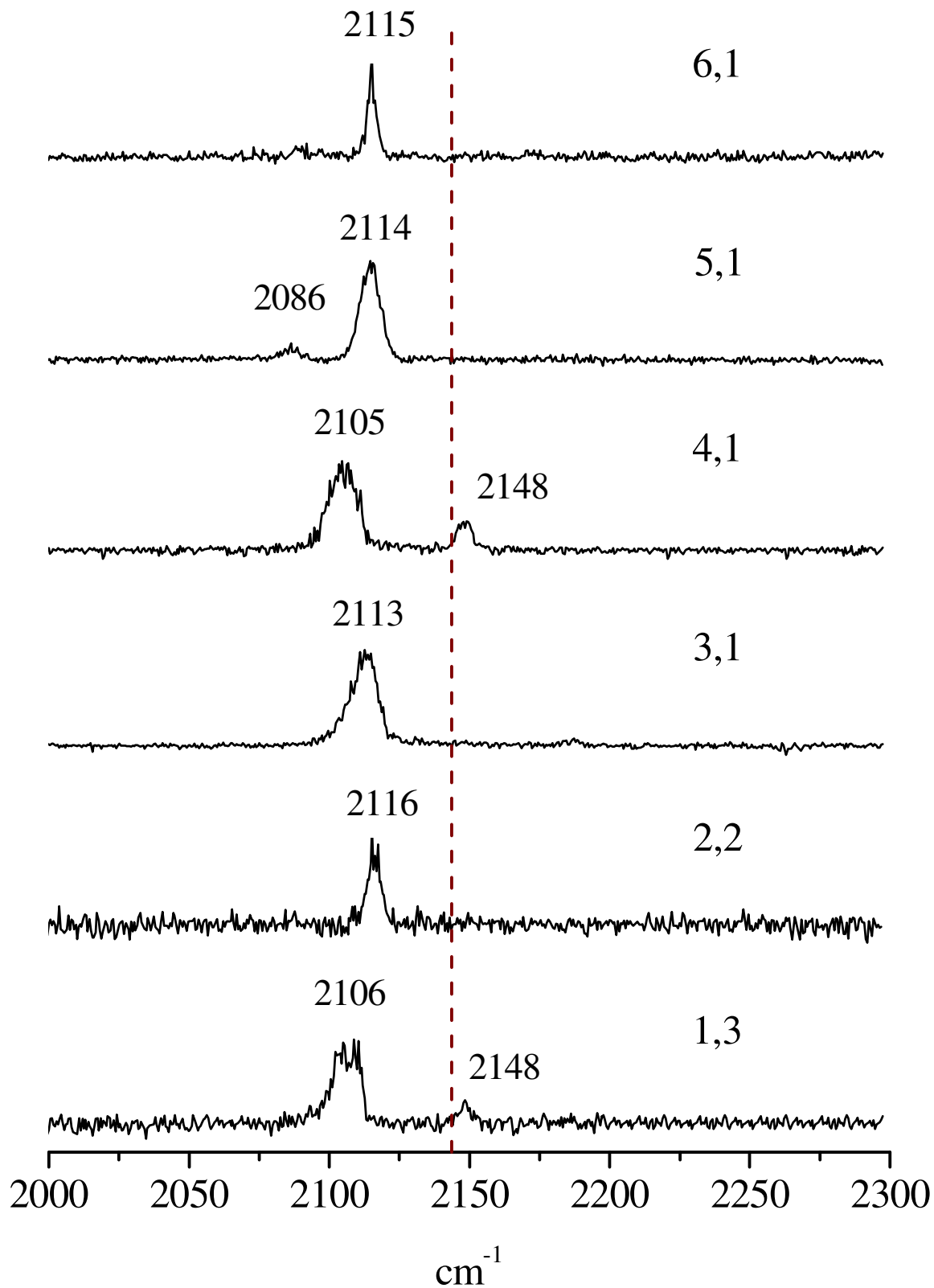


Figure 5.2.

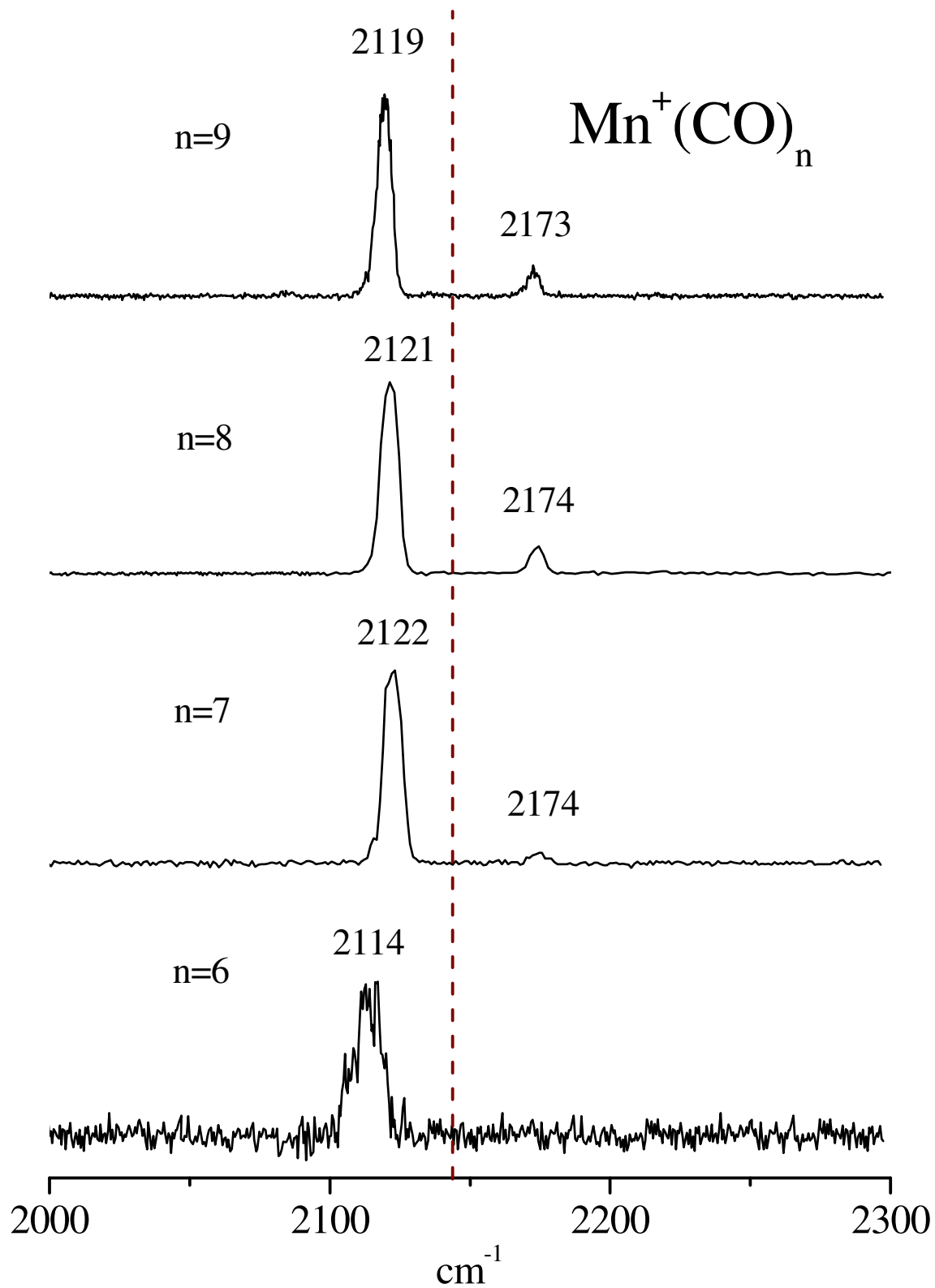


Figure 5.3.

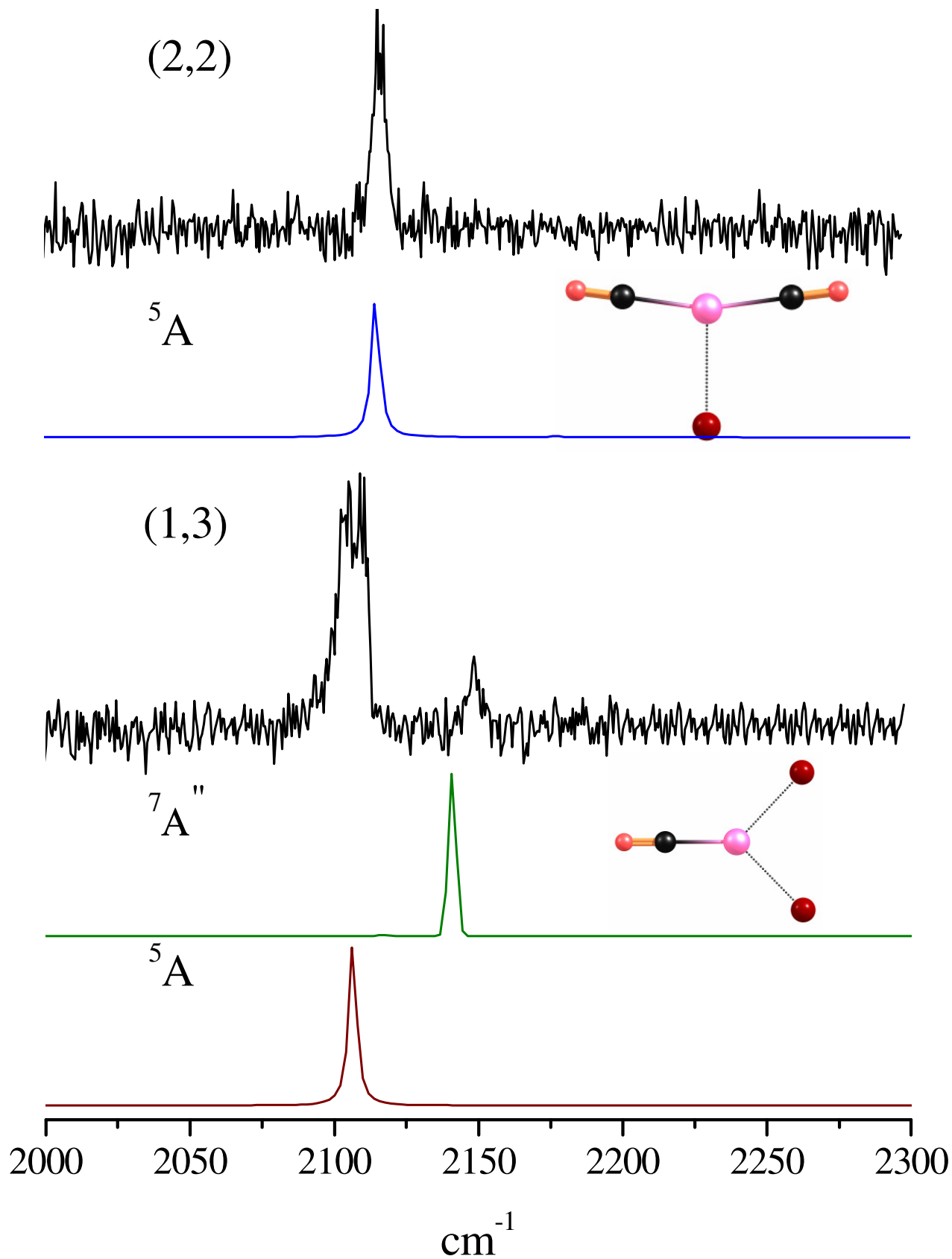


Figure 5.4.

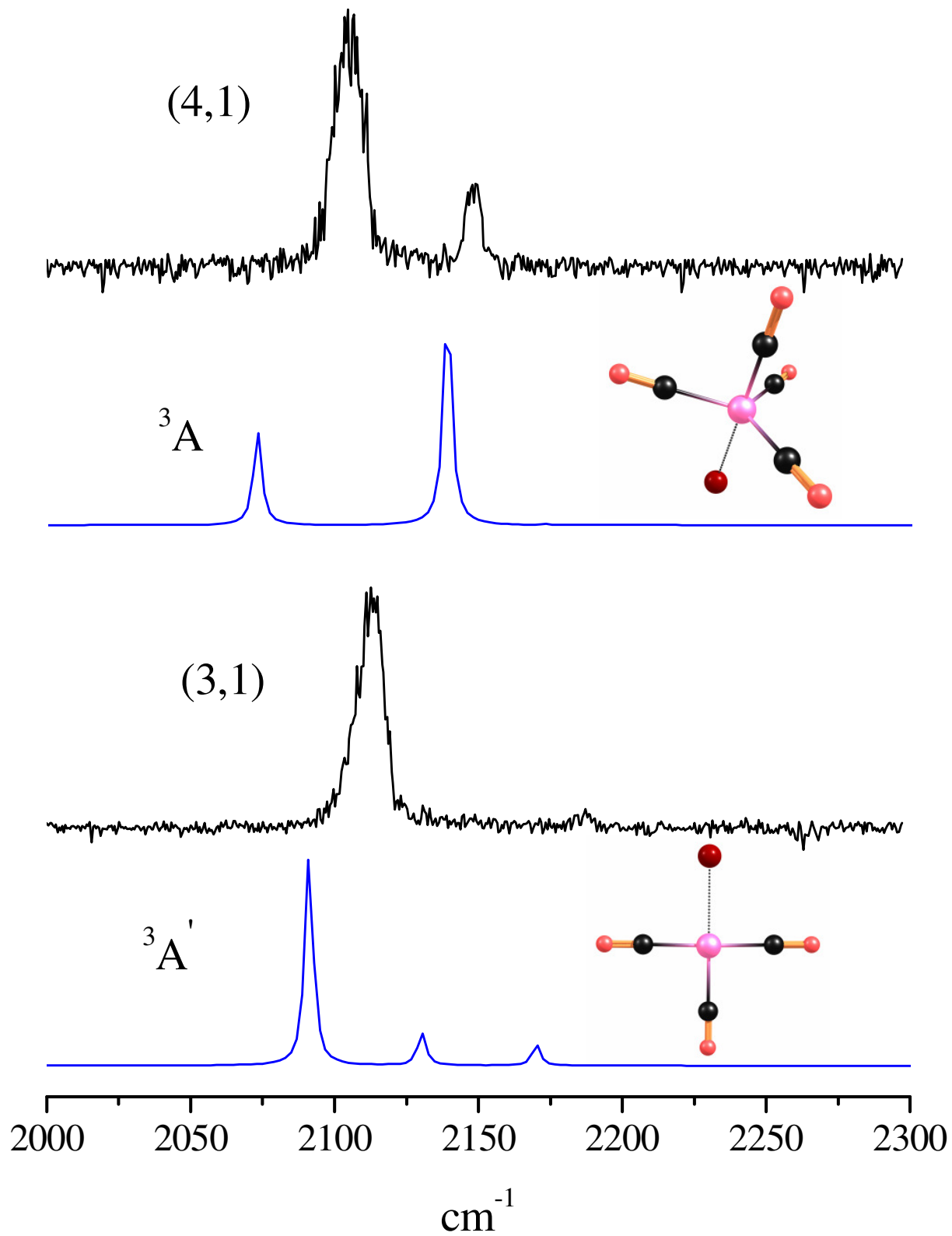
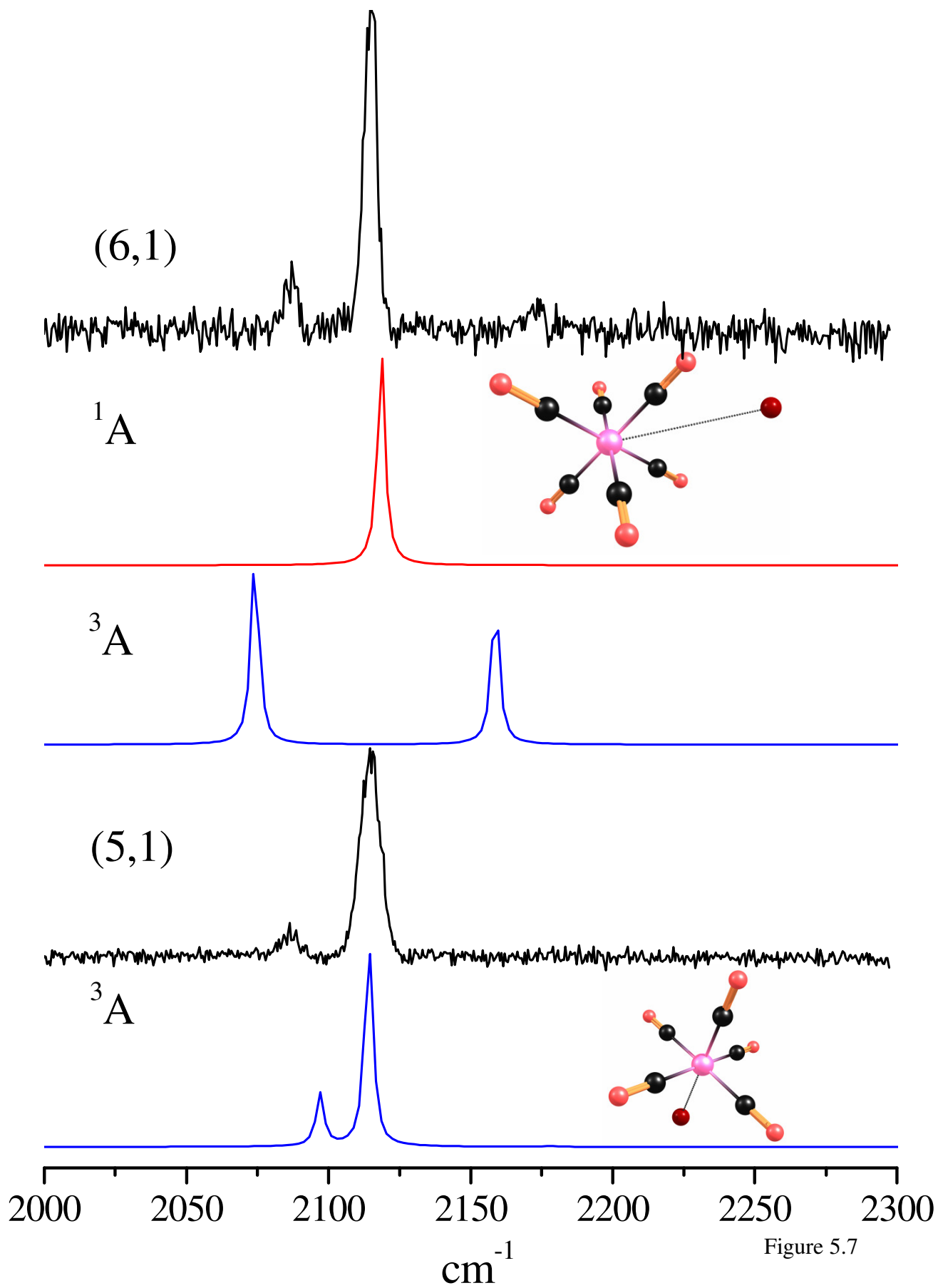


Figure 5.5.



CHAPTER 6

INFRARED SPECTROSCOPY OF COPPER AND GOLD CARBONYL CATIONS: NONCLASSICAL CARBONYLS¹

¹Reed, Z.D. and Duncan, M.A. To be submitted to *J. Phys. Chem. A*

6.1 Abstract

Copper carbonyl and gold carbonyl cations of the forms $\text{Cu}(\text{CO})_n^+$ and $\text{Au}(\text{CO})_n^+$ are produced in the gas phase via pulsed laser vaporization and are analyzed in a time of flight mass spectrometer. Copper carbonyl cation clusters containing up to 15 carbonyls are produced, and gold carbonyl cations containing up to 30 carbonyls are produced. Individual complexes are mass selected and studied by infrared photodissociation spectroscopy and the copper complexes are compared to density functional theory calculations. The argon tagged analogues of small copper carbonyl cation complexes ($n=2-4$) are studied, and feature blue-shifted carbonyl stretches (ν_{CO}). The larger complexes, $\text{Cu}(\text{CO})_n^+$ $n=4-8$, also feature blue-shifted ν_{CO} . These blue-shifts indicate copper carbonyl cation is a non-classical carbonyl. $\text{Cu}(\text{CO})_4^+$ has a completed coordination sphere, consistent with its expected 18 electron stability. The carbonyl stretch in gold carbonyl cations ($n=3-7$) is also blue-shifted and $\text{Au}(\text{CO})_4^+$ has a completed coordination sphere, but the third and fourth carbonyls are weakly bound.

6.2 Introduction

Carbon monoxide has been one of the most important ligands in transition metal chemistry for over 100 years. Many different transition metal carbonyls have been synthesized and characterized, and some of these are important in homogeneous and heterogeneous catalysis [1,2]. Transition metal complexes and carbon monoxide are

involved in hydroformylation, the Fischer-Tropsch synthesis, the synthesis of acetic acid, and the water-gas shift reaction, among other catalytic reactions [3]. More fundamentally, gas phase transition metal carbonyl systems are valuable models for complicated systems like chemisorption on metal surfaces [4], or the binding of carbon monoxide on the active sites of proteins [5].

Metal carbonyls are conveniently probed with Raman and infrared spectroscopy [1-5,6-8]. Stable neutral metal carbonyls have been studied in both the condensed phase and the gas phase [9-12]. Various charged metal carbonyls have been studied in the condensed phase as salts, including noble metal carbonyls [13-17]. Mass spectrometry has been used extensively to study metal carbonyl ions in the gas phase [18,19]. The structures and bonding of these systems have been investigated with theoretical calculations [20-24]. Reactions and bond energies have been reported [25-26]. Matrix isolation studies have been reported of anions, neutrals, and some cations [8,27]. Infrared photodissociation spectroscopy of metal cluster cations using a free electron laser has been reported [28-31]. Our group has studied several transition metal carbonyl systems using infrared photodissociation spectroscopy [32-35]. In the present study, we examine the copper carbonyl cation and gold carbonyl cation systems through infrared photodissociation spectroscopy in the gas phase.

Transition metal carbonyl bonding is usually understood in terms of the Dewar-Chatt-Duncanson complexation model [1,7,8,36,37]. Two separate interactions form the metal-CO bond. The carbonyl contributes electron density from its HOMO, forming a σ bond and reducing the electron density of the carbonyl orbitals. The metal donates electron density from its partially filled d-orbitals into the LUMO of CO through π

backbonding. This LUMO is antibonding, and thus π backbonding weakens the C-O bond. In the majority of carbonyl complexes, π backbonding predominates and the C-O bond is weaker, longer, and the C-O stretching frequency (ν_{CO}) is reduced. These are so-called “classical” carbonyls.

An increasing number of complexes have been found that do not follow this scheme, and these systems are known as “non-classical” carbonyls [37-42]. These species have ν_{CO} higher than the gas phase CO value of 2143 cm^{-1} . The very first carbonyl complex synthesized, $\text{Pt}(\text{CO})_2\text{Cl}_2$, is actually non-classical [42]. Non-classical carbonyls usually involve filled metal d-shells which cannot efficiently donate or accept charge. In these systems, σ donation dominates over π backbonding. Nonclassical carbonyl bonding was originally described in terms of electron density being moved out of the partially antibonding σ orbitals on CO, which would lead to an increased bond strength and blue shifted vibrations [7]. However, more recent theoretical work by Lupinetti explains the blue-shift in terms of an electrostatic polarization effect [21]. Noble metal atomic ions are known to form non-classical carbonyls in the condensed phase. Non-classical carbonyls have been studied theoretically by several groups [23,43-46]. Armentrout and coworkers measured the binding energy of the copper and silver carbonyls [25]. Noble metal carbonyls have been studied in strong protic acids and as salts [47-50]. Solid compounds have been prepared using highly fluorinated anions and have been structurally characterized [17]. Andrews and coworkers have studied some neutral, anionic, and cationic noble metal carbonyls in rare gas matrices, including gold and copper [27]. Meijer and coworkers have recorded the infrared spectra of CO bound to cationic and anionic gold clusters, with 3 to 20 gold atoms [30]. Our group has

published a preliminary report on the infrared spectroscopy of gold carbonyl complexes and compared them to theory [32].

Copper carbonyl complexes have been studied experimentally and theoretically. The neutrals have been characterized by EPR [51,52], IR spectroscopy [53], and by theory [24]. The binding energies of $\text{Cu}(\text{CO})_n^+$ complexes have been measured by collision induced dissociation (CID) [25]. The cations have also been investigated by theory [24,27]. Matrix isolation spectroscopy has been reported for $\text{Cu}(\text{CO})_n$ neutrals and cations [27]. These systems have also been studied in strong acids and prepared as solids [17,42]. Copper carbonyl cations in strong acids have been noted to have high catalytic activity towards various hydrocarbons [17]. There have been some discrepancies in the spectra for $\text{Cu}(\text{CO})_n^+$ complexes. Acid media studies demonstrated a red-shift in the CO stretching frequencies as sequential carbonyls are added [17], while argon matrix studies demonstrate a blue-shift [27]. Here we report infrared photodissociation spectroscopy for both small unsaturated $\text{Cu}(\text{CO})_n^+$ ($n=2-4$) complexes, and complexes beyond the coordination sphere, $n=5-9$. The experimental spectra are compared to density functional calculations to probe the structure and bonding in these systems. We also report new data on $\text{Au}(\text{CO})_n^+$ complexes, $n=3-8$ and determine the completion of the coordination sphere through spectroscopic measurements.

6.3 Experimental

Copper and gold carbonyl cations are produced in a pulsed nozzle laser vaporization source using the third harmonic of a pulsed Nd:YAG laser (355 nm;

Continuum Surelite). The laser is focused on a rotating and translating ¼ inch diameter copper or gold rod, which is mounted with a ¾ inch horizontal offset in front of a pulsed nozzle (General Valve Series 9). This general apparatus has been described in detail elsewhere [54]. The expansion gas is either pure CO, or 20% CO in Ar or Ne, by partial pressure. Backing pressures range from 200 to 300 psi. The expansion is skimmed into a second chamber and sampled by pulse extraction into a home-built Wiley McLaren reflectron time of flight mass spectrometer. Mass spectra are recorded with a digital oscilloscope (LeCroy “Waverunner”) connected to a computer via a GPIB interface. Ions of interest can be mass selected using pulsed deflection plates in the first leg of the reflectron. Mass selected complexes can be crossed with tunable infrared light in the turning region of the reflectron. The infrared light is generated in an optical parametric oscillator/amplified (OPO/OPA) system (LaserVision) pumped by the fundamental of an Nd:YAG (1064 nm; Continuum 8010). The tuning range is approximately 2000 cm⁻¹ to 4500 cm⁻¹. The laser energy in the carbonyl stretching region is 1-2 mJ/pulse with about 1 cm⁻¹ linewidth. Complexes with sufficiently weakly bound ligands dissociation via IVR upon excitation with infrared light tuned to a molecular vibration. Spectra are generated by monitoring fragment yield as a function of laser wavelength.

Density functional theory calculations were performed to investigate the structures and spin configurations of the complexes studied. Various geometries and spin states were calculated for each Cu(CO)_n⁺ (n=2-7) and Cu(CO)_n⁺Ar (n=2-4) complex studied experimentally. The calculations were performed using the B3LYP functional [54,56] as implemented in the Gaussian 2003 computational package [57]. We investigated all complexes using the Def 2 TZVPP basis set on all atoms [58-59]. A

scaling factor of 0.9679 was applied to all calculated frequencies, in line with literature values [24].

6.4 Results and Discussion

A mass spectrum of the $\text{Cu}(\text{CO})_n^+$ complexes produced is shown in Figure 6.1. The main peaks in the series are $\text{Cu}(\text{CO})_n^+$ complexes. The width of the peaks is due to the isotopes on copper, which can be resolved on an expanded view. There is some enhanced intensity to the $n=4$ peaks. The $n=4$ complex has 18 electrons and would be expected to have enhanced stability. Previous acid matrix and fluororacid counterion studies have indicated that copper carbonyl is stable with four ligands [17,42]. All carbonyls beyond $n=4$ are likely to be “external”, bound only to other carbonyls and not directly to the metal cation. These clusters are produced in our experiment because of the cold conditions of the supersonic expansion, and likely would not be stable at room temperature.

We can investigate the binding energies and coordination number further through their fragmentation patterns upon infrared excitation. These photofragmentation mass spectra can be seen in Figure 6.2. These mass spectra are shown as the difference of the laser on minus the laser off. The result is a negative going parent ion and positive going fragment channels. The smallest clusters, $n=1-3$, do not fragment at any wavelength of infrared excitation. The bonding energies for these complexes has previously been measured by Armentrout to be 1.54 eV, 1.78 eV, 0.78 eV, and 0.55 eV for $n=1-4$, respectively [25c]. Our photons have only about 0.27 eV of energy, so we would not

expect fragmentation for these strongly bound complexes. Interestingly, the $n=4$ complex does fragment weakly. Multiphoton excitation is possible, but unlikely due to the low laser power at this wavelength. Our cluster source produces a distribution of internal energies, and some clusters are produced with relatively high internal energy. We are likely seeing the “hot fraction” of complexes dissociate with a single photon, which adds to their internal energy and allows them to fragment. All complexes above $n=4$ fragment more efficiently, although not nearly as efficiently as other M-CO systems we have investigated. The fragmentation channels are also somewhat broad compared to other M-CO systems we have investigated. This effect will be discussed later in this paper. All complexes larger than $n=5$ are observed to lose two carbonyl units as the primary fragmentation channel. These fragmentation patterns suggest that copper carbonyl is likely four coordinate, but we must investigate the spectroscopy to be sure.

Figure 6.3 shows the spectra obtained for the smaller $\text{Cu}(\text{CO})_n^+$ clusters, $n=2-4$. The dashed line is the free CO vibrational frequency of 2143 cm^{-1} . These clusters do not fragment efficiently, so we investigate their argon tagged analogues, of the form $\text{Cu}(\text{CO})_n^+\text{Ar}$, and the neon tagged analogues, $\text{Cu}(\text{CO})_n^+\text{Ne}$. The $\text{Cu}^+\text{-Ar}$ binding energy has been calculated to be 0.504 eV , or 4065 cm^{-1} [60], and the argon binding energy should decrease as additional ligands or argons bind to copper. Experimentally, the binding energies of argon and neon are low enough to allow for fragmentation with a single photon in these complexes. We can see that all of these complexes are blue-shifted from the free-CO value, indicating that they are non-classical complexes.

The $n=1$ complex was not observed to fragment, even when tagged with three argon atoms or two neon atoms. We would not expect the singly tagged argon analogue

to fragment, but the per-argon binding energy should decrease as additional argons are added and we would expect fragmentation if no additional complications are present. Neon should be even more weakly bound. This may be a coupling issue, where the rate of IVR is too small due to low state density to allow for fragmentation through the rare gas coordinate to occur on the timescale of the experiment. The $n=2$ complex fragments weakly with a single argon or neon, with the two rare gas tags producing roughly equal signal to noise levels. Both spectra feature a single band, at 2225 cm^{-1} for the argon tagged version and at 2195 cm^{-1} for neon. The $n=3$ complex fragments much more efficiently, and the argon and neon tagged vibrations are at 2210 cm^{-1} and 2191 cm^{-1} , respectively. The $n=4$ complex also fragments efficiently with tagging, and has bands at 2202 cm^{-1} and 2198 cm^{-1} for argon and neon, respectively. The untagged $\text{Cu}(\text{CO})_4^+$ complex has one broad spectral feature at 2198 cm^{-1} . This width is not surprising, since fragmentation should only occur here for the complexes with residual internal energy. The tagged complexes are likely a better representation of the true spectrum.

Strauss observed a *blue-shift* in fluoroanion salts with the addition of carbonyls [49], while Andrews observed a *red-shift* in rare-gas matrices [27b]. We observe a *red-shift* in the argon tagged complexes as additional CO ligands are added. Our gas phase measurements, with only a single argon interaction, should be the closest to the true vibrational frequencies. It appears then that the fluoroanions have a significant solvation interaction in the structures of these copper carbonyl cation complexes. Andrews measured the carbonyl stretching frequency of $\text{Cu}(\text{CO})_2^+$ at 2233 cm^{-1} , of $\text{Cu}(\text{CO})_3^+$ at 2211 cm^{-1} , and of $\text{Cu}(\text{CO})_4^+$ at 2200 cm^{-1} in solid neon. These are quite close to our argon tagged frequencies, indicating the matrix and the argon tag have similar

perturbations on the system. The degree of perturbation is investigated further with theoretical calculations. Interestingly, the neon tagged analogues in our experiment are significantly shifted from either the argon tagged species and Andrew's neon matrix studies. Andrews observes a 60 cm^{-1} red-shift for CuCO^+ in Ar versus Ne matrices. Even if we consider the neon species, we still see a red-shift from $n=2$ to $n=3$, although a smaller one than with argon. There is a blue-shift from $n=3$ to $n=4$ in the neon analogues. We cannot fully explain this odd perturbation, but it indicates that neon may cause more significant frequency shifts than argon in some systems.

Figure 6.4 shows the larger $\text{Cu}(\text{CO})_n^+$ ($n=4-8$) complexes. Each has a single main feature, which gradually red-shifts from 2201 cm^{-1} to 2196 cm^{-1} as additional carbonyl ligands are added. This band is blue shifted from free CO, like those in the small CuCO_n^+ complexes. We also see the growth of a secondary feature around 2165 cm^{-1} as the complexes become larger. We have determined previously that this feature corresponds to "external" CO's, that is, carbonyls outside the first coordination sphere [32-36]. This band is weakly present for $n=5$ and grows larger with each additional carbonyl. This confirms our previous determination that the fourth carbonyl completes the first coordination sphere of copper. We also see some small features appear to the red of these main bands on $n=7,8$. These weak features will be investigated through theory. It was experimentally noted that they could be eliminated by varying the source conditions. Decreased laser power or altering the placement of the laser spark to produce an apparently "cooler" plasma eliminated these peaks.

To further elucidate the structural and bonding details of this system, we have performed DFT calculations on $\text{Cu}(\text{CO})_n^+$ complexes, $n=2-7$. The structures, electronic

states, and relative energetics of the computed species are summarized in Table 6.1. These complexes have been previously investigated by several groups, and our results are generally comparable to the previous results [24,27]. Detailed comparisons to previous theory can be found in Table 6.2. We find the ground state of each complex to be a closed shell singlet. The $n=2$ complex has a linear structure, $n=3$ is trigonal planar, and $n=4$ is tetrahedral. There are two calculated configurations for $n=5$, a D_{3h} structure with all carbonyls bonded directly to the metal, and a tetrahedral core with an externally bound CO. The D_{3h} structure lies much higher in energy, some 309 kcal/mol higher than the T_h structure and has a negative frequency, and can thus be excluded from consideration. Any additional carbonyls added past this point coordinate to the first carbonyl coordination sphere and not directly to the metal ion, confirming our previous conclusion that copper carbonyl cation has a coordination number of four.

Figure 6.5 shows the spectra of the small $CuCO_n^+$ complexes ($n=2-4$) and compares them to the predictions of theory. The calculated frequencies for these small complexes are compared to our experimentally measured vibrational bands and previous theoretical work in Table 6.2. The calculated spectrum for the neat linear singlet for the $n=2$ complex matches our experimental data, measured by loss of argon, fairly well. The CO stretch for this complex is at 2230 cm^{-1} , and our measured band position is 2225 cm^{-1} . The neon tagged spectrum is shifted by nearly 30 cm^{-1} from both the Ar tagged spectrum and the calculated neat spectrum. The calculated argon tagged complex is bent, and has a vibrational band at 2221 cm^{-1} . Apparently the theory slightly overestimates the perturbation caused by the argon, but the neat and tagged frequencies are quite close. The calculated triplet has a slightly bent structure, and lies 107.5 kcal/mol higher in

energy. The triplet is strongly red-shifted, with a band position at 1964 cm^{-1} . We can confidently assign our measured spectrum to the singlet state, and conclude that it is the ground state for this complex.

We also see excellent agreement between the calculated trigonal planar singlet spectrum for $n=3$ and our measured one. The calculated CO stretching frequency is 2208.5 cm^{-1} and our experimental value, measured by loss of argon, is 2210 cm^{-1} . Here again the spectrum measured by loss of neon is shifted, by some 19 cm^{-1} from that with the argon loss. The calculated argon tagged complex shows a somewhat significant perturbation, resulting in two vibrational bands at 2080 and 2210 cm^{-1} . Again, the theory appears to overestimate the deformation due to the argon binding.

The spectra for $n=4$ measured by loss of argon and neon are almost identical, and both agree well with predictions for the calculated tetrahedral singlet structure. The predicted value for $n=4$ is 2199 cm^{-1} , our neon tagged complex has a band at 2198 cm^{-1} , and that for the argon tagged complex appears at 2202 cm^{-1} . The Ar tagged analogue has a calculated ν_{CO} at 2198.5 cm^{-1} , which is a very minimal perturbation. We also have a spectrum for the neat complex, measured by the loss of CO, which features a broad spectral feature centered around 2198 cm^{-1} . This gives us some confidence that neither of the rare gases substantially perturbs this complex, but does not provide much insight into the disparity between the argon and neon loss channel in the previous two complexes. We can reasonably assign the $n=2-4$ complexes as singlets.

The experimental spectra for $n=5,6$ and the comparison to theory can be found in Figure 6.6. Here we can see the main spectral feature around 2200 cm^{-1} for both complexes and very weak band appearing around 2165 cm^{-1} for $n=5$ complex, and then

growing in intensity for the n=6 complex. This band is reproduced fairly accurately in our calculated spectra, and can be assigned to “external” CO’s, bound to the first coordination sphere and not directly to the metal. Again, we have fairly good agreement between our calculated spectra and the measured spectra. The n=5 structure is calculated to have a tetrahedral core with an externally bound CO. It features one main band at 2198 cm^{-1} , and a weaker band at 2171 cm^{-1} . The measured spectrum has bands at 2202.6 cm^{-1} and 2167 cm^{-1} . We can therefore be reasonably confident that this complex is a singlet with a tetrahedral core and an externally bound CO. The n=6 calculated structure is quite similar to that of n=5, with an added external carbonyl. The calculated spectrum again features two bands. The main band here is at 2194 cm^{-1} , red-shifted from that of n=5 and also somewhat red-shifted from our experimental value of 2199 cm^{-1} . The calculated secondary band here is at 2174 cm^{-1} , blue-shifted slightly from both the calculated n=5 band and our experimental value of 2167 cm^{-1} . However, both bands are sufficiently close for us to assign this complex as being a singlet with a tetrahedral core and two externally bound CO ligands.

Figure 6.7 shows the experimental spectrum of n=7 and compares it to the predictions of theory. The calculated structure for the singlet configuration features a tetrahedral core and externally bound ligands, and the spectra reproduces the main band and the external CO band well. However, we see a weak red-shifted peak around 2117 cm^{-1} , and the calculated spectra for the singlets does not account for these bands. We calculated the *triplet* configurations and found that these low frequency bands likely represent low lying excited triplet states. The triplet features a D_{4h} core, with externally bound CO ligands. Their vibrations fall around 2090 cm^{-1} , making them a reasonable fit

for our experimental spectral features. The multiple peaks in $n=8$ can be accounted for by the multiple possible configurations of carbonyl ligands. With the planar $\text{Cu}(\text{CO})_4^+$ core, four additional CO ligands can either be arranged with two above the plain of the core molecule and two below, or three above and one below. The triplet configurations are significantly higher in energy than the singlets, by 80 kcal/mol or more. However, the oscillator strengths are *much* greater than the singlets. The singlet oscillator strengths are generally around 250 km/mol, while the triplets are 1400-1900 km/mol (full details are reported in the Supporting Information). We likely have a very small amount of triplet population, trapped in the excited state during the cooling process in our source, but they are represented in our spectrum due to their extremely high oscillator strengths. It is also interesting to note that the fragmentation channel associated with bands assigned as singlets were rather broad, while those associated with triplets were quite sharp. The increased oscillator strength or the increased internal energy of the triplets compared to the singlets may lead to more discrete fragmentation.

We do not observe any triplet associated bands in complexes smaller than $n=7$. The theoretical calculations for the $n=2$ triplet indicate a severe red-shift, down to 1964 cm^{-1} , below the range scanned in this experiment. This complex was 107 kcal/mol higher in energy. We were unable to find a stable minima on the triplet potential energy surface for $n=3,4,5$. The $n=6$ triplet has two stable configurations with nearly identical energy, one with two carbonyls above the D_{4h} core, and one with a carbonyl above and below the core. Both are some 81 kcal/mol higher in energy than the singlet. The complex with both carbonyls above the core has a vibrational band at 2067 cm^{-1} , and the other configuration has its vibrations at 2068 and 2074 cm^{-1} . The $n=7$ complex has three

stable configurations, and their calculated vibrations are slightly less red-shifted again, up to around 2090 cm^{-1} . Our laser power decreased rapidly as the wavelength is decreased in this region, and it is likely we simply do not have enough laser power to observe the $n=6$ triplet complex, which presumably has a very small population like that observed for $n=7,8$.

Strauss and coworkers have previously discussed the bonding in $\text{Cu}(\text{CO})_n^+$ in terms of the σ -bond and π -back bonding [17]. They observed a blue-shift in the carbonyl stretch between $\text{Cu}(\text{CO})_2^+$ and $\text{Cu}(\text{CO})_3^+$. Their explanation focused on the relative decreases in electron density which leads to σ - and π -bonds. They concluded that the loss of π -backbonding going from $\text{Cu}(\text{CO})_2^+$ to $\text{Cu}(\text{CO})_3^+$ had a large effect than the loss of σ -bonding. However, their analysis was based on acid matrix studies. Our work here, and Andrews and coworkers work [28], clearly indicates that there is actually a red-shift between these two complexes, and thus the acid matrix studies overestimate the effect of π bonding. Silver and gold carbonyl cations in rare gas matrices follow an identical trend to our observed copper trend [27]. We can conclude here that copper follows trends more similar to those of other non-classical carbonyls, and not that of classical carbonyls.

We have also obtained new data for gold carbonyl cations, a known non-classical carbonyl system. The mass spectrum obtained from our cluster source for $\text{Au}(\text{CO})_n^+$ can be seen in Figure 6.8. Here we produce an excellent distribution of carbonyl ligands attached to gold, making complexes with 30 or more carbonyl ligands. The $n=2$ and 4 complexes have particularly high intensity. The $\text{Au}(\text{CO})_2^+$ core ion is known to be stable in the condensed phase [49] and the spectrum of these complexes has been measured

[29,32] and investigated by theory [21,27]. The tricarbonyl complex has been formed under high CO pressures [17].

The photofragmentation mass spectra can be found in Figure 6.9. From these patterns, we see additional support for the strongly bound $n=2$ complex. This complex does not fragment, the $n=3$ complex strongly loses a carbonyl to produce $\text{Au}(\text{CO})_2^+$, and $n=4$ fragments strongly to $n=3$ and weakly to $n=2$. Larger complexes fragment to produce the $n=4$ complex, strongly for $n=5$ and $n=6$, and weakly from $n=7$. This gives us some indication that $n=4$ has enhanced stability compared to the larger complexes, but each additional CO is bound much more weakly than the first two. This has previously been explained in terms of an $s-d(\sigma)$ hybridization model [17]. The hybridization minimizes the σ repulsion between the filled ligand orbitals and the metal orbitals, strongly enhancing the bonding for the first two ligands. The addition of more ligands makes the $s-d$ hybridization much less effective and produces weaker bonds.

To further investigate the bonding in this system, we measured the infrared photodissociation spectra. The measured spectra can be seen in Figure 6.10, with the free CO frequency indicated as a dashed line. The main band for each complex is blue-shifted, confirming previous observations that gold is a non-classical carbonyl. The spectra for the $n=3$ and $n=4$ complexes show only a single band, which corresponds well to calculations performed by Gordon predicting a trigonal planar complex for the $n=3$ complex and a tetrahedral structure for the $n=4$ complex [32]. The spectra for the $n>4$ complexes have a smaller secondary feature at 2170 cm^{-1} , which is assigned to the external CO band. This band gains intensity as more CO ligands are added. This confirms that there is a core $\text{Au}(\text{CO})_4^+$ ion, and additional ligand solvate this core. This

leads to the possibility of producing a stable four-coordinate gold carbonyl complex in the solid phase.

We were unable to obtain spectra for either $\text{Au}(\text{CO})^+$ or $\text{Au}(\text{CO})_2^+$, despite producing significant signal for both the neon and multiply argon tagged analogues. The Ar-Au⁺ binding energy has been calculated to be 2600 cm^{-1} [61], which is too strong for efficient single photon fragmentation. However, the per-ligand binding energies should decrease with multiple argons and should be low enough to allow fragmentation, but none is observed. The neon binding energy should also be lower than the argon value, but fragmentation is not observed. This same phenomena was observed for $\text{Cu}(\text{CO})^+$. There may be an issue with the coupling of the rare gas tag to the molecular framework, or it may be that fragmentation does not occur on the timescale of the experiment. We were able to measure argon and neon tagged spectra for $\text{Au}(\text{CO})_3^+$, which fragmented efficiently by eliminating the rare gas. The band positions were nearly unchanged for both tagged analogues compared to those of the neat complexes.

Bonding in non-classical systems has been discussed extensively in the literature [37-42]. Copper, silver and gold carbonyls are all non-classical, but their bond lengths and strengths vary significantly. One proposed reason is variation in the σ -repulsion from the filled CO 5σ MOs with the filled z^2 (d_σ) atomic orbital. Decreasing the σ -repulsion by s- d_σ mixing shifts electron density off the metal-ligand axis and allows for shorter, stronger bonds. The amount of s- d_σ mixing depends on the s- d_σ energy gap, which varies for each element. Gold is estimated to have the lowest energy gap of the noble metals (1.9 eV), and silver the largest (4.9 eV), with copper in the middle (2.7 eV) [17]. The bond dissociation energies for the first two carbonyls follow the inverse of that

trend, with gold having the most strongly bound carbonyls and silver the weakest. However, there are some interesting patterns in the molecular vibrations. Larger gold carbonyl complexes ($n > 2$) have nearly identical frequencies as the equivalent copper carbonyl systems, but the bond energy is significantly greater for $\text{Cu}(\text{CO})_3^+$ than $\text{Au}(\text{CO})_3^+$, and roughly equal for the tetracarbonyl complexes. $\text{Cu}(\text{CO})_3^+$ and $\text{Cu}(\text{CO})_4^+$ have bond dissociation energies of 0.78 eV, and 0.55 eV, respectively, while $\text{Au}(\text{CO})_3^+$ and $\text{Au}(\text{CO})_4^+$ have values of 0.54 eV and 0.58 eV, respectively [26,33]. The ν_{CO} for $\text{Cu}(\text{CO})_3^+$ is 2211 cm^{-1} , $\text{Cu}(\text{CO})_4^+$ is 2203, $\text{Au}(\text{CO})_3^+$ is 2208 cm^{-1} , and $\text{Au}(\text{CO})_4^+$ is 2199 cm^{-1} . Unfortunately, we were not able to measure the band positions of $\text{Au}(\text{CO})_{1,2}^+$, which are bound by 2.2 eV and 2.5 eV, respectively [32]. Following the bond dissociation energy trend, we would expect these complexes to be significantly blue-shifted from $n=3,4$ and this would have given us some additional insight into the bonding of these systems. We were also not able to measure any spectra for $\text{Ag}(\text{CO})_n^+$ despite significant effort, as none of the complexes were observed to fragment. Silver carbonyl cations are known to have very long C-O bonds and very low bond dissociation energies. It is possible that these long, weak bonds lead to a low rate of IVR, which would explain why no fragmentation is observed on the timescale of our experiment, although this is speculative.

6.5 Conclusion

Complexes of $\text{Cu}(\text{CO})_n^+$ and $\text{Au}(\text{CO})_n^+$ have been produced in the gas phase by laser vaporization and investigated using infrared photodissociation spectroscopy and density function theory calculations. The mass spectra and photodissociation patterns

indicate that copper carbonyl cation is a four-coordinate system with four strongly bound ligands. Gold carbonyl cation is a four-coordinate system, but the third and fourth ligands are only weakly bound due to s-d(σ) hybridization. A linear singlet ground state was observed for $\text{Cu}(\text{CO})_2^+$, a trigonal planar singlet for $\text{Cu}(\text{CO})_3^+$, and a tetrahedral singlet for $\text{Cu}(\text{CO})_4^+$. Larger complexes have a tetrahedral core and externally bound CO ligands. For the n=7,8 complexes, we observe a small population of triplets, which have a four coordinate D_{4h} core and externally bound CO's. These are observed due to their extremely high oscillator strengths compared to relatively those for the singlets. Smaller triplets, if present, are not observed in this experiment due to a significant red-shift in ν_{CO} , which gradually decreases as additional carbonyls are added.

6.6 Acknowledgements

We acknowledge generous support for this work from the U.S. Department of Energy (grant no. DE-FG02-96ER14658) and the Air Force Office of Scientific Research (Grant No. FA95509-1-0166).

Supporting Information

The Supporting Information for this manuscript contains the full details of the DFT computations done in support of the spectroscopy here, including the structures, energetics and vibrational frequencies for each of the structures considered. The complete reference for Ref 57 is also included in the Supporting Information.

6.7 References

- (1) Cotton, F. A.; Wilkinson, G.; Murillo, C. A.; Bochmann, M. *Advanced Inorganic Chemistry*, 6th ed.; John Wiley & Sons, Inc: New York, 1999.
- (2) Heck, R. F. *Organotransition Metal Chemistry*; Academic Press: New York, 1974.
- (3) (a). E.I. Solomon, P.M. Jones and J.A. May. *Chem. Rev.* **93** (1993), p. 2623. (b). A. Sen. *Accounts Chem. Res.* 1993, 26, p. 303. (c). K.C. Waugh. *Catal. Today* 1992, 15, p. 51 (d). M.A. Vannice. *Catal. Today* **1992**, 12, 255. (e). L. Guzzi, Editor, *Studies in Surface Science and Catalysis, Vol. 64: New Trends in CO Activation*, Elsevier Science B.V., Amsterdam **1991** (f). G. Henrici-Olivé and S. Olivé, *The Chemistry of the Catalyzed Hydrogenation of Carbon Monoxide.*, Springer-Verlag, Berlin **1983**. (g). P.C. Ford, Editor, *ACS Symposium Series, Vol. 152: Catalytic Activation of Carbon Monoxide*, American Chemical Society, Washington, DC **1981**.
- (4) Somorjai, G. A. *Introduction to Surface Chemistry and Catalysis*; Wiley-Interscience: New York, 1994.
- (5) Bertini, I.; Gray, H. B.; Stiefel, E. I.; Valentine, J. S. *Biological Inorganic Chemistry Structure and Reactivity*, University Science Books, Sausalito California, 2007.
- (6) Nakamoto, K. *Infrared and Raman Spectra of Inorganic and Coordination Compounds*, John Wiley, New York, 1997.

- (7) Frenking, G.; Fröhlich, N. "The Nature of the Bonding in Transition-Metal Compounds," *Chem. Rev.* **2000**, *100*, 717.
- (8) Zhou, M.; Andrews, L.; Bauschlicher, C. W. "Spectroscopic and Theoretical Investigations of Vibrational Frequencies in Binary Unsaturated Transition-Metal Carbonyl Cations, Neutrals, and Anions," *Chem. Rev.* **2001**, *101*, 1931.
- (9) O'Dwyer, M. F. "Infrared Spectra and Normal Coordinate Analysis of Iron Pentacarbonyl," *J. Molec. Spectroscopy* **1958**, *2*, 144.
- (10) Jones, L. H.; McDowell, R. S.; Goldblatt, M. "Infrared spectra of $\text{Cr}(\text{CO})_6$, $\text{Mo}(\text{CO})_6$ and $\text{W}(\text{CO})_6$ Gas phase," *Inorg. Chem.* **1969**, *28*, 2349.
- (11) Boquet, G.; Birgone, M. "Infrared spectra of $\text{Ni}(\text{CO})_4$ in gas phase," *Spectrochim. Acta.* **1971**, *27*, 139.
- (12) Beagley, B.; Schmidling, D. G. "A Re-evaluation of the molecular structure of iron pentacarbonyl," *J. Molec. Struct.* **1974**, *22*, 5466.
- (13) Stammerich, H.; Kawai, K.; Tavares, Y.; Krumholz, P.; Behmoiras, J.; Bril, S. "Infrared spectra of $\text{Fe}(\text{CO})_4^{2-}$ in aqueous solution," *J. Chem. Phys.* **1960**, *32*, 1482.
- (14) Abel, E. W.; McLean, A. N.; Tyfield, S. P.; Braterman, P. S.; Walker, A. P.; Hendra, P. J. "Infrared spectra of $\text{V}(\text{CO})_6^-$ and $\text{Re}(\text{CO})_6^+$ in CH_3CN solution," *J. Mol. Spec.* **1969**, *30*, 29.
- (15) Edgell, W. F.; Lyford, J. I. "Infrared spectra of $\text{Co}(\text{CO})_4^-$ in DMF solution," *J. Chem. Phys.* **1970**, *52*, 4329.
- (16) McLean, R. A. N. "Infrared and Raman spectra of $\text{Mn}(\text{CO})_6^+$ in CH_3CN solutions and solids," *Can. J. Chem.* **1974**, *52*, 213.

- (17) Rack, J.J.; Strauss, S.H.; "Polycarbonyl cations of Cu(I), Ag(I), and Au(I): $[M(CO)_n]^+$ " *Catal. Today* **1997**, *36*, 99
- (18) Russell, D.H. *Gas Phase Inorganic Chemistry*, Plenum, New York, 1989.
- (19) Freiser, B. S. *Organometallic Ion Chemistry*, Kluwer, Dordrecht, The Netherlands, 1996.
- (20) Goldman, A. S.; Krogh-Jespersen, K. "Why do cationic carbon monoxide complexes have high CO stretching force constants and short CO bonds? Electrostatic effects, not σ bonding," *J. Am. Chem. Soc.* **1996**, *118*, 12159.
- (21) a) Lupinetti, A. J.; Frenking, G.; Strauss, S. H. "Nonclassical Metal Carbonyls," *Angew. Chem. Int. Ed.* **1998**, *37*, 2113. b) Lupinetti, A. J.; Jonas, V.; Thiel, W.; Strauss, S. H.; Frenking, G. "Trends in Molecular Geometries and Bond Strengths of the Homoleptic d10 Metal Carbonyl Cations: A Theoretical Study," *Chem. Eur. J.* **1999**, *5*, 2573. c) Lupinetti, A. J.; Fau, S.; Frenking, G.; Strauss, S. H. "Theoretical Analysis of the Bonding between CO and Positively Charged Atoms," *J. Phys. Chem.* **1997**, *101*, 9551.
- (22) Barnes, L.A.; Rosi, M.; Bauschlicher, C.W. "Theoretical studies of the first- and second-row mono- and di-carbonyl positive ions," *J. Chem. Phys.* **1990**, *93*, 609.
- (23) Huo, C.-H.; Li, Y.-W.; Wu, G.-S.; Beller, M.; Jiao, H. "Structures and energies of $[Co(CO)_n]^m$ ($m=0, 1+, 1-$) and $HCo(CO)_n$: Density functional studies," *J. Phys. Chem. A* **2002**, *106*, 12161.

- (24) Wu, G.; Li, Y-W.; Xiang, H-W.; Xu, Y-Y.; Sun, Y-H.; Jiao, H. "Density functional investigation on copper carbonyl complexes," *Journal of Molecular Structure (Theochem)* 2003, 637,101–107
- (25) a) Khan, F. A.; Clemmer, D. E.; Schultz, R. H.; Armentrout, P. B. "Sequential bond energies of chromium carbonyls ($\text{Cr}(\text{CO})_x^+$, $x=1-6$)," *J. Phys. Chem.* **1993**, 97, 7978. b) Sievers, M. R.; Armentrout, P. B. "Collision-Induced Dissociation Studies of $\text{V}(\text{CO})_x$, $x=1-7$: Sequential Bond Energies and the Heat of formation of $\text{V}(\text{CO})_6$ " *J. Phys. Chem.* **1995**, 99, 8135. c) Meyer, F.; Chen, Y. M.; Armentrout, P.B. "Sequential Bond Energies of $\text{Cu}(\text{CO})_x^+$ and $\text{Ag}(\text{CO})_x^+$ ($x=1-4$)," *J. Am. Chem. Soc.* **1995**, 117, 4071. d) Goebel, S.; Haynes, C. L.; Khan, F. A.; Armentrout, P. B. "Collision-Induced Dissociation Studies of $\text{Co}(\text{CO})_x^+$, $x=1-5$: Sequential Bond Energies and Heats of Formation of $\text{Co}(\text{CO})_4$," *J. Am. Chem. Soc.* **1995**, 117, 6994. e) Meyer, F.; Armentrout, P. B. "Sequential bond energies of $\text{Ti}(\text{CO})_x^+$, $x= 1-7$," *Mol. Phys.* **1996**, 88, 187. f) Zhang, X. G.; Armentrout, P. B. "Sequential Bond Energies of $\text{Pt}(\text{CO})_x^+$ ($x=1-4$) Determined by Collision-Induced Dissociation," *Organometallics* **2001**, 20, 4266.
- (26) Schwartz, H. "Relativistic Effects in Gas-Phase Ion Chemistry: An Experimentalist's View," *Angew. Chem. Int. Ed.* **2003**, 42, 4442.
- (27) a) Zhou, M.; Andrews, L. "Infrared Spectra of RhCO^+ , RhCO , and RhCO^- in solid neon: a scale for charge support in catalyst systems," *J. Am. Chem. Soc.* **1999**, 121, 9171. b) Zhou, M.; Andrews, L. "Infrared Spectra and density functional calculations of CuCO_n^+ ($n=1-4$), CuCO_n ($n=1-3$), and CuCO_n^- ($n=1-$

3), in solid neon,” *J. Chem. Phys.* **1999**, *111*, 4548. c) Zhou, M.; Andrews, L. “Infrared spectra and density functional calculations of RuCO^+ , OsCO^+ , $\text{Ru}(\text{CO})_x$, $\text{Os}(\text{CO})_x$, $\text{Ru}(\text{CO})_x^-$, and $\text{Os}(\text{CO})_x^-$ ($x=1-4$) in solid neon,” *J. Phys. Chem. A* **1999**, *103*, 6956. d) Zhou, M.; Andrews, L. “Reactions of laser-ablated iron atoms and cations with carbon monoxide: Infrared spectra of FeCO^+ , $\text{Fe}(\text{CO})_2^+$, $\text{Fe}(\text{CO})_x$ and $\text{Fe}(\text{CO})_x^-$ ($x=1-4$) in solid neon,” *J. Chem. Phys.* **1999**, *110*, 10370. e) Zhou, M.; Andrews, L. “Matrix infrared spectra and density functional calculations of ScCO , ScCO^- , and ScCO^+ ,” *J. Phys. Chem. A* **1999**, *103*, 2964. f) Zhou, M.; Andrews, L. “Infrared spectra and density functional calculations for OMCO , and $\text{OM}(\eta^2\text{-CO})^-$, OMCO^+ and OMOC^+ ($M=\text{V}, \text{Ti}$) in solid argon,” *J. Phys. Chem. A* **1999**, *103*, 5259. g) Zhou, M.; Andrews, L. “Reactions of laser ablated Co, Rh, and Ir with CO: Infrared spectra and density functional calculations of the metal carbonyl molecules, cations and anions in solid neon,” *J. Phys. Chem. A* **1999**, *103*, 7773. h) Liang, B.; Andrews, L. “Reactions of Laser-Ablated Ag and Au atoms with carbon monoxide: Matrix Infrared Spectra and Density Functional Calculations on $\text{Au}(\text{CO})_n$ ($n=2,3$), $\text{Au}(\text{CO})_n^-$ ($n=1,2$), and $\text{M}(\text{CO})_n$ ($n=1-4$), ($M=\text{Ag}, \text{Au}$),” *J. Phys. Chem. A* **2000**, *104*, 9156. i) Liang, B.; Zhou, M.; Andrews, L. “Reactions of Laser-Ablated Ni, Pd, and Pt atoms with carbon monoxide: Matrix Infrared Spectra and Density Functional Calculations on $\text{M}(\text{CO})_n$ ($n=1-4$), $\text{M}(\text{CO})_n^-$ ($n=1-3$), and $\text{M}(\text{CO})_n^+$ ($n=1-2$), ($M=\text{Ni}, \text{Pd}, \text{Pt}$),” *J. Phys. Chem. A* **2000**, *104*, 3905. j) Andrews, L.; Zhou, M.; Wang, X.; Bauschlicher, C.W. “Matrix Infrared Spectra and DFT Calculations of

- Manganese and Rhenium Carbonyl Neutral and Anion Complexes” *J. Phys. Chem. A* **2000**, *104*, 8887
- (28) Fielicke, A.; von Helden, G.; Meijer, G.; Pedersen, D. B.; Simard, B.; Rayner, D. M. “Size and Charge Effects on Binding of CO to Small Isolated Rhodium Clusters,” *J. Phys. Chem. B* **2004**, *108*, 14591.
- (29) Moore, D. T.; Oomens, J.; Eyler, J. R.; Meijer, G.; von Helden, G.; Ridge, D. P. “Gas-Phase IR Spectroscopy of Anionic Iron Carbonyl Clusters,” *J. Am. Chem. Soc.* **2004**, *126*, 14726.
- (30) a) Fielicke, A.; von Helden, G.; Meijer, G.; Simard, B.; Rayner, D. M. “Gold Cluster Carbonyls: Vibrational Spectroscopy of the Anions and the Effects of Cluster Size, Charge, and Coverage on the CO Stretching Frequency,” *J. Phys. Chem. B* **2005**, *109*, 23935. b) Fielicke, A.; von Helden, G.; Meijer, G.; Pedersen, D. B.; Simard, B.; Rayner, D. M. "Gold Cluster Carbonyls: Saturated Adsorption of CO on Gold Cluster Cations, Vibrational Spectroscopy, and Implications for Their Structures," *J. Am. Chem. Soc.* **2005**, *127*, 8416.
- (31) Fielicke, A.; von Helden, G.; Meijer, G.; Pedersen, D. B.; Simard, B.; Rayner, D. M. “Size and charge effects on the binding of CO to late transition metal clusters,” *J. Chem. Phys.* **2006**, *124*, 194305.
- (32) Velasquez III, J.; Njagic, B.; Gordon, M. S.; Duncan, M. A. “IR Photodissociation Spectroscopy and Theory of Au⁺(CO)_n Complexes: Nonclassical Carbonyls in the Gas Phase,” *J. Phys. Chem. A* **2008**, *112*, 1907.

- (33) Velasquez III, J.; Duncan, M. A. "IR Photodissociation Spectroscopy of Gas Phase $\text{Pt}^+(\text{CO})_n$ ($n=4-6$)," *Chem. Phys. Lett.* **2008**, *461*, 28.
- (34) Ricks, A.M.; Bakker, J.M.; Douberly, G.E.; Duncan, M.A. "Infrared Spectroscopy and Structures of Cobalt Carbonyl Cations," *J. Phys. Chem. A.* **2009**, *113*, 4701
- (35) Ricks, A.M.; Reed, Z.D.; Duncan, M.A. "Seven-Coordinate Homoleptic Metal Carbonyls in the Gas Phase" *J. Am. Chem. Soc.*, 2009, *131*, 9176–9177
- (36) Chatt, J.; Duncanson, L.A. "Olefin coordination compounds. III. Infrared spectra and structure: attempted preparation of acetylene compounds." *J. Chem. Soc.* **1953**, 2939.
- (37) Dewar, M.J.S. *Bull. Soc. Chim. Fr.* "A review of the π -complex theory," **1951**, *18*, C79
- (38) Schroeder, D.; Hrusak, J.; Hertwig, R. H.; Koch, W.; Schwerdtfeger, P.; Schwarz, H. *Organometallics* **1995**, *14*, 312.
- (39) Schroeder, D.; Schwarz, H.; Hrusak, J.; Pyykkoe, P. "Cationic Gold(I) Complexes of Xenon and of Ligands Containing the Donor Atoms Oxygen, Nitrogen, Phosphorus, and Sulfur," *Inorg. Chem.* **1998**, *37*, 624.
- (40) Willner, H.; Aubke, F. *Inorg. Chem.* "Reaction of carbon monoxide in the super acid $\text{HSO}_3\text{F}-\text{Au}(\text{SO}_3\text{F})_3$, and the gold(I)bis(carbonyl)cation $[\text{Au}(\text{CO})_2]^+$. Isolation and characterization of gold(I) carbonyl fluorosulfate, $\text{Au}(\text{CO})\text{SO}_3\text{F}$," **1990**, *29*, 2195

- (41) Aubke, F. "The generation of unusual noble-metal cations in fluoro acids and super acids, and their spectroscopic properties." *J. Fluorine Chem.* **1995**, *72*, 195.
- (42) Strauss, S.H. "Copper(I) and silver(I) carbonyls. To be or not to be nonclassical" *J. Chem. Soc. Dalton Trans.* **2000**, 1-6
- (43) Barnes, L. A.; Rosi, M.; Bauschlicher, C. W., Jr. "Theoretical studies of the first- and second-row transition metal mono- and dicarbonyl positive ions." *J. Chem. Phys.* **1990**, *93*, 609.
- (44) Veldkamp, A.; Frenking, G. "Theoretical studies of organometallic compounds. 6. Structures and bond energies of $M(CO)_n^+$, MCN , and $M(CN)_2^-$ ($M = \text{silver, gold}; n = 1-3$)," *Organometallics* **1993**, *12*, 4613.
- (45) Dargel, T. K.; Hertwig, R. H.; Koch, W.; Horn, H. *J. Chem. Phys.* **1998**, *108*, 3876.
- (46) Jonas, V.; Thiel, W. "Towards an accurate gold carbonyl binding energy in $AuCO^+$: basis set convergence and a comparison between density-functional and conventional methods," *J. Phys. Chem. A* **1999**, *103*, 1381.
- (47) a.) Hurlburt, P. K.; Anderson, O. P.; Strauss, S. H. "Ag(CO)B(OTeF₅)₄: the first isolatable silver carbonyl," *J. Am. Chem. Soc.* **1991**, *113*, 6277. b.) Hurlburt, P. K.; Rack, J. J.; Dec, S. F.; Anderson, O. P.; Strauss, S. H. "Bis(carbonyl)silver tetrakis(pentafluorooxotellurato)borate: the first structurally characterized $M(CO)_2$ complex," *Inorg. Chem.* **1993**, *32*, 373. c.) Hurlburt, P. K.; Rack, J. J.; Luck, J. S.; Dec, S. F.; Webb, J. D.; Anderson, O.

- P.; Strauss, S. H. "Nonclassical Metal Carbonyls: $[\text{Ag}(\text{CO})]^+$ and $[\text{Ag}(\text{CO})_2]^+$," *J. Am. Chem. Soc.* **1994**, *116*, 10003.
- (48) Rack, J. J.; Moasser, B.; Gargulak, J. D.; Gladfelter, W. L.; Hochheimer, H. D.; Strauss, S. H. "Infrared and manometric evidence for the formation of the $[\text{Ag}(\text{CO})_3]^+$ complex ion at high PCO ," *J. Chem. Soc., Chem. Commun.* **1994**, 685. Rack, J. J.; Polyakov, O. G.; Gaudinski, C. M.; Hammel, J. W.; Kasperbauer, P.; Hochheimer, H. D.; Strauss, S. H. "Use of 0.1 mm pathlength gas cell to eliminate $\text{CO}(\text{g})$ absorbance from high- CO -pressure solid-state IR spectra of nonclassical metal carbonyls," *Appl. Spectrosc.* **1998**, *52*, 1035. Rack, J.J.; Strauss, S.H. "Polycarbonyl cations of $\text{Cu}(\text{I})$, $\text{Ag}(\text{I})$, and $\text{Au}(\text{I})$: $[\text{M}(\text{CO})_n]^+$," *Catal. Today* **1997**, *36*, 99
- (49) Willner, H.; Schaebs, J.; Hwang, G.; Mistry, F.; Jones, R.; Trotter, J.; Aubke, F. "Bis(carbonyl)gold(I) undecafluorodiantimonate(V), $[\text{Au}(\text{CO})_2][\text{Sb}_2\text{F}_{11}]$: synthesis, vibrational, and carbon-13 NMR study and the molecular structure of bis(acetonitrile)gold(I) hexafluoroantimonate(V), $[\text{Au}(\text{NCCH}_3)_2][\text{SbF}_6]$," *J. Am. Chem. Soc.* **1992**, *114*, 8972
- (50) Xu, Q.; Imamura, Y.; Fujiwara, M.; Souma, Y. " A New Gold Catalyst: Formation of Gold(I) Carbonyl, $[\text{Au}(\text{CO})_n]^+$ ($n = 1, 2$), in Sulfuric Acid and Its Application to Carbonylation of Olefins " *J. Org. Chem.* **1997**, *62*, 1594
- (51) Howard, J. A.; Mile, B.; Morton, J. R.; Preston, K. F.; Sutcliffe, R. "The EPR spectrum and structure of copper tricarbonyl," *Chem. Phys. Lett.* **1985**, *117*, 115.

- (52) a) Kasai, P. H.; Jones, P.M. "Copper carbonyls, Cu(CO) and Cu(CO)₃: matrix isolation ESR study," *J. Am. Chem. Soc.* **1985**, *107*, 813 b)
- (53) Chenier, J. H. B.; Hampson, C.A.; Howard, J.A.; Mile, B. "A spectroscopic study of the reaction of copper atoms with carbon monoxide in a rotating cryostat: evidence for the formation of monocarbonylcopper, tricarbonylcopper, and hexacarbonyldicopper," *J. Phys. Chem.* **1989**, *93*, 114
- (54) Duncan, M. A. "Infrared spectroscopy to probe structure and dynamics in metal ion-molecule complexes," *Intl. Rev. Phys. Chem.* **2003**, *22*, 407.
- (55) Becke, A. D. "3 term correlation functional," *J. Chem. Phys.* **1993**, *98*, 5648.
- (56) Lee, C.; Yang, W.; Parr, R. G. Lee Yang Parr, "Correlation functional," *Phys. Rev B.* **1998**, *98*, 5648.
- (57) Frisch, M. J. et al., *Gaussian 03 (Revision B.02)*; Gaussian, Inc.: Pittsburgh, PA, 2003.
- (58) Weigend, F.; Ahlrichs, R. "Balanced basis sets of split valence, triple zeta valence and quadruple zeta valence quality for H to Rn: Design and assessment of accuracy," *Phys. Chem. Chem Phys.* **2005**, *7*, 3297
- (59) Schaefer, A.; Huber, R.; Ahlrichs, J. "Fully optimized contracted Gaussian basis sets of triple zeta valence quality for atoms Li to Kr," *J. Chem. Phys.* **1994**, *100*, 5829
- (60) Shen, Y.; BelBruno, J.J. "Studies of Neutral and Ionic CuAr and CuKr van der Waals Complexes," *J. Phys. Chem. A* **2005**, *109*, 10077-10083
- (61) Pyykko, P. "Predicted Chemical Bonds between Rare Gases and Au⁺," *J. Am. Chem. Soc.* **1995**, *117*, 2067

Table 6.1 The structures, electronic ground states, and energetics computed for $\text{Cu}(\text{CO})_n$ with DFT. No stable triplet configurations could be found for $n=3-5$.

complex	state/structure	relative energy (kcal/mol)
$\text{Cu}(\text{CO})_2^+$	$^1\text{C}_{\infty v}$	0.0
	$^3\text{C}_{2v}$	107.5
$\text{Cu}(\text{CO})_3^+$	$^1\text{D}_{3h}$	0.0
$\text{Cu}(\text{CO})_4^+$	$^1\text{T}_d$	0.0
$\text{Cu}(\text{CO})_5^+$	$^1\text{C}_{2v}$	0.0
$\text{Cu}(\text{CO})_6^+$	$^1\text{C}_{2v}$	0.0
	$^3\text{C}_s$	+81.4
	$^3\text{C}_{4v}$	+81.4
$\text{Cu}(\text{CO})_7^+$	$^1\text{C}_{3v}$	0.0
	$^3\text{C}_s$	+81.6

Table 6.2: The vibrational frequencies computed (Scaled by 0.9679) and measured for $\text{Cu}(\text{CO})_n^+$ and $\text{Cu}(\text{CO})_n(\text{Ar})_m^+$ complexes, along with comparisons to previous theoretical work. All frequencies are in wavenumbers.

Complex	theory ^a	theory ^b	theory ^c	experiment ^a
$\text{Cu}(\text{CO})_2^+$	2230	2228	2230.2	
$\text{Cu}(\text{CO})_2^+\text{Ar}$	2221			2225
$\text{Cu}(\text{CO})_3^+$	2208.5	2203.0	2211.6	
$\text{Cu}(\text{CO})_3^+\text{Ar}$	2090, 2210			2210
$\text{Cu}(\text{CO})_4^+$	2199	2195.9	2202.1	2198
$\text{Cu}(\text{CO})_4^+\text{Ar}$	2198.5			2202

a) This work

b) Reference 27a

c) Reference 24

Figure Captions

Figure 6.1: The mass spectrum of $\text{Cu}(\text{CO})_n^+$ clusters produced by our cluster source.

Figure 6.2: The photofragmentation mass spectra of $\text{Cu}(\text{CO})_n^+$, $n=4-8$.

Figure 6.3: The infrared photodissociation spectra of small $\text{Cu}(\text{CO})_n^+(\text{Ar})_m$ complexes, measured by the elimination of argon.

Figure 6.4: The infrared photodissociation spectra of larger $\text{Cu}(\text{CO})_n^+$ complexes, measured by the elimination of CO.

Figure 6.5: Infrared spectra of $\text{Cu}(\text{CO})_n\text{Ar}_m^+$, $n=1-4$ compared to the spectra predicted by theory, along with calculated ground state structures.

Figure 6.6: Infrared spectra of $\text{Cu}(\text{CO})_n^+$, $n=5,6$ compared to the spectra predicted by theory, along with calculated ground state structures.

Figure 6.7: Infrared spectra of $\text{Cu}(\text{CO})_n^+$, $n=7,8$ compared to the spectra predicted by theory, along with calculated structures.

Figure 6.8: The mass spectrum of $\text{Au}(\text{CO})_n^+$ clusters produced by our cluster source.

Figure 6.9: The photofragmentation mass spectra of $\text{Au}(\text{CO})_n^+$, $n=3-7$.

Figure 6.10: The infrared photodissociation spectra of $\text{Au}(\text{CO})_n^+$ complexes, measured by the elimination of CO.

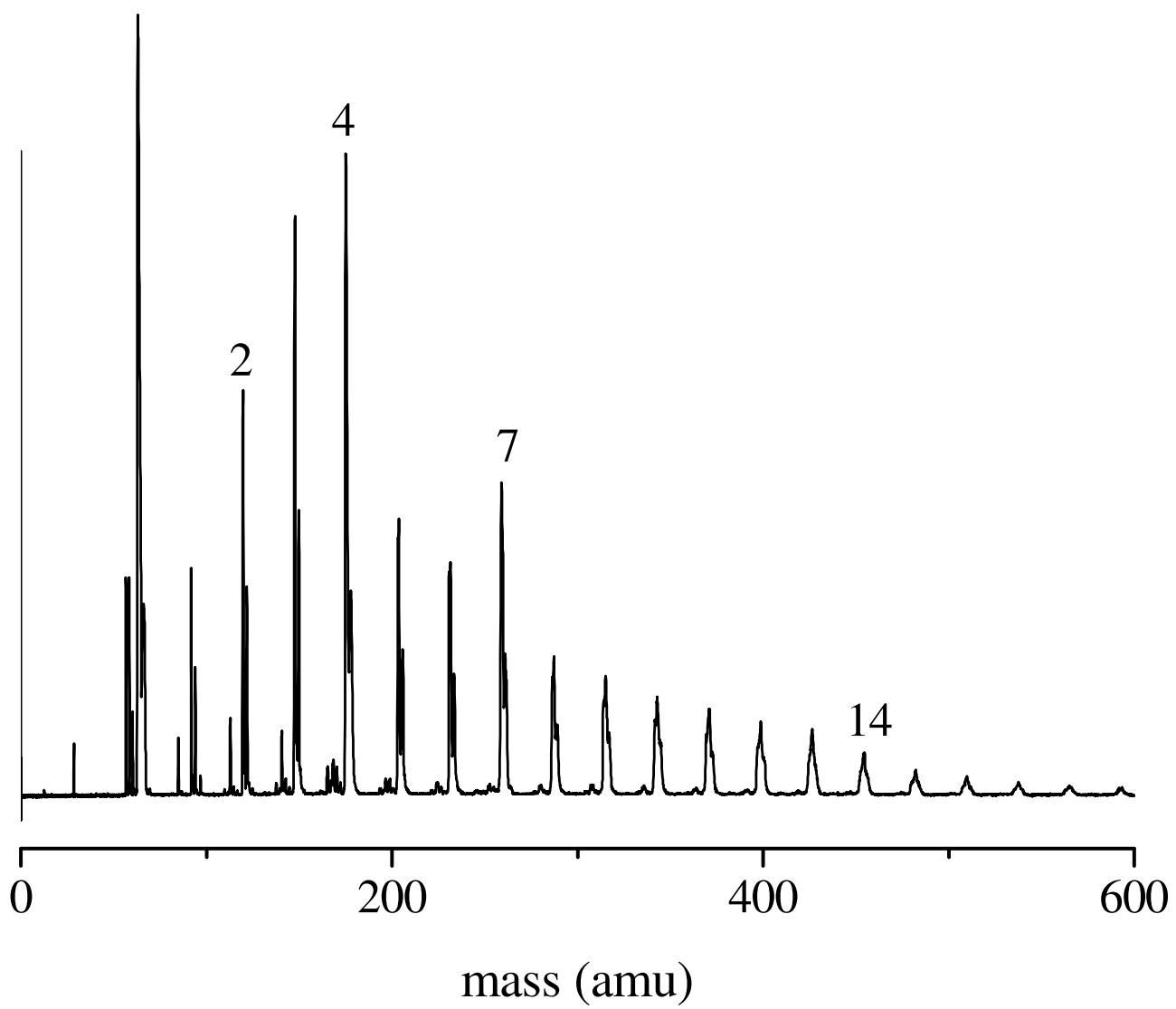


Figure 6.1.

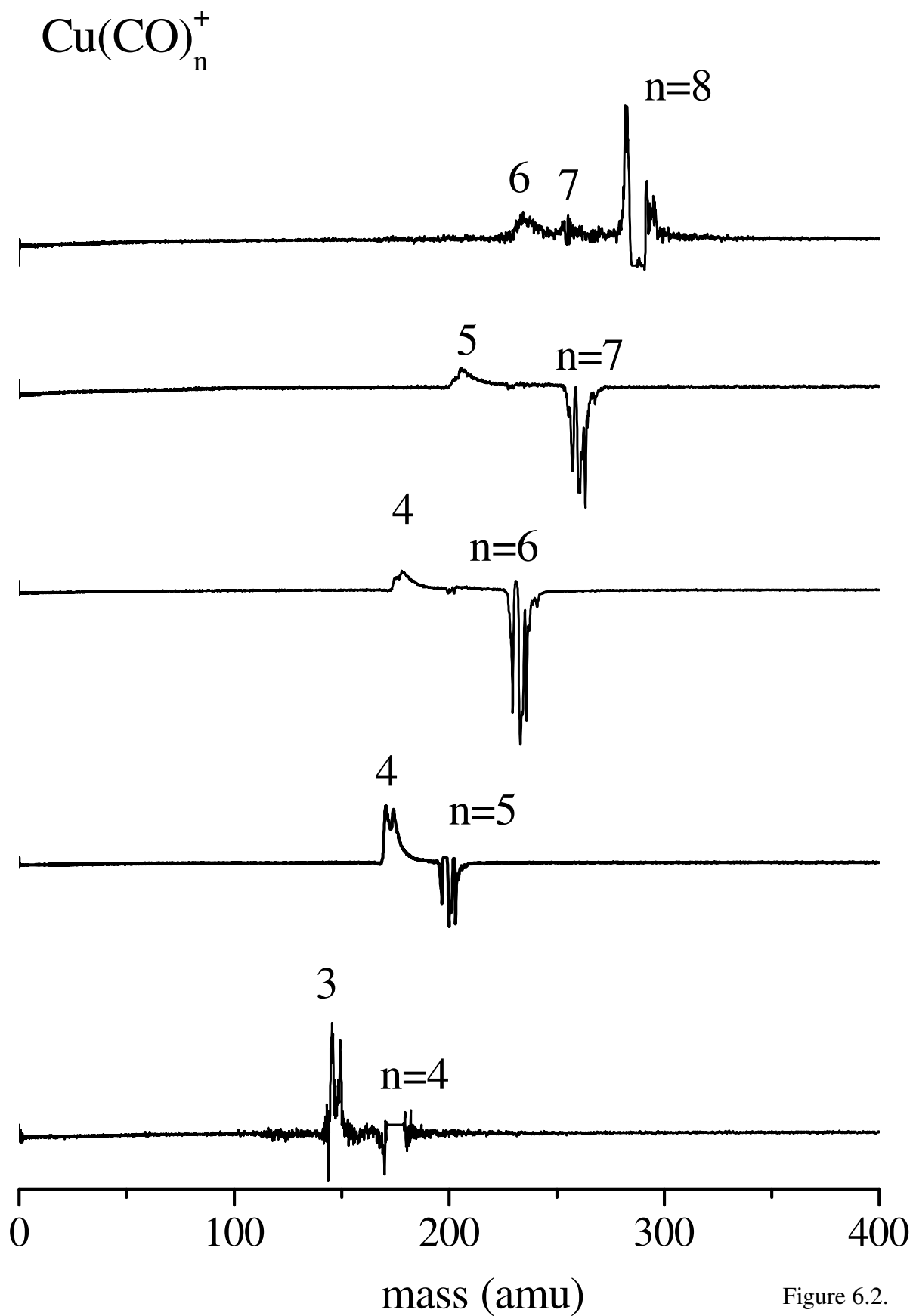


Figure 6.2.

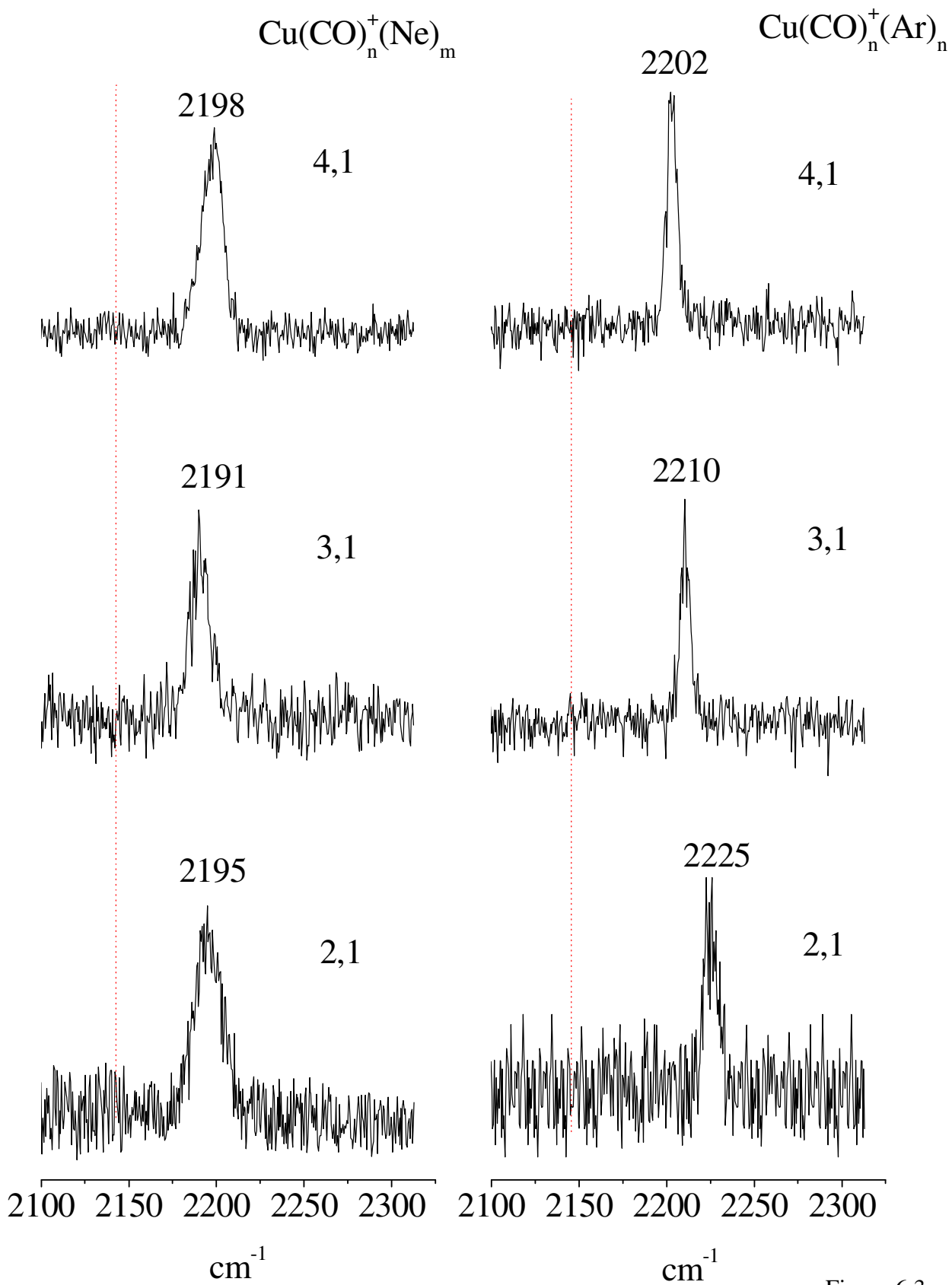


Figure 6.3.

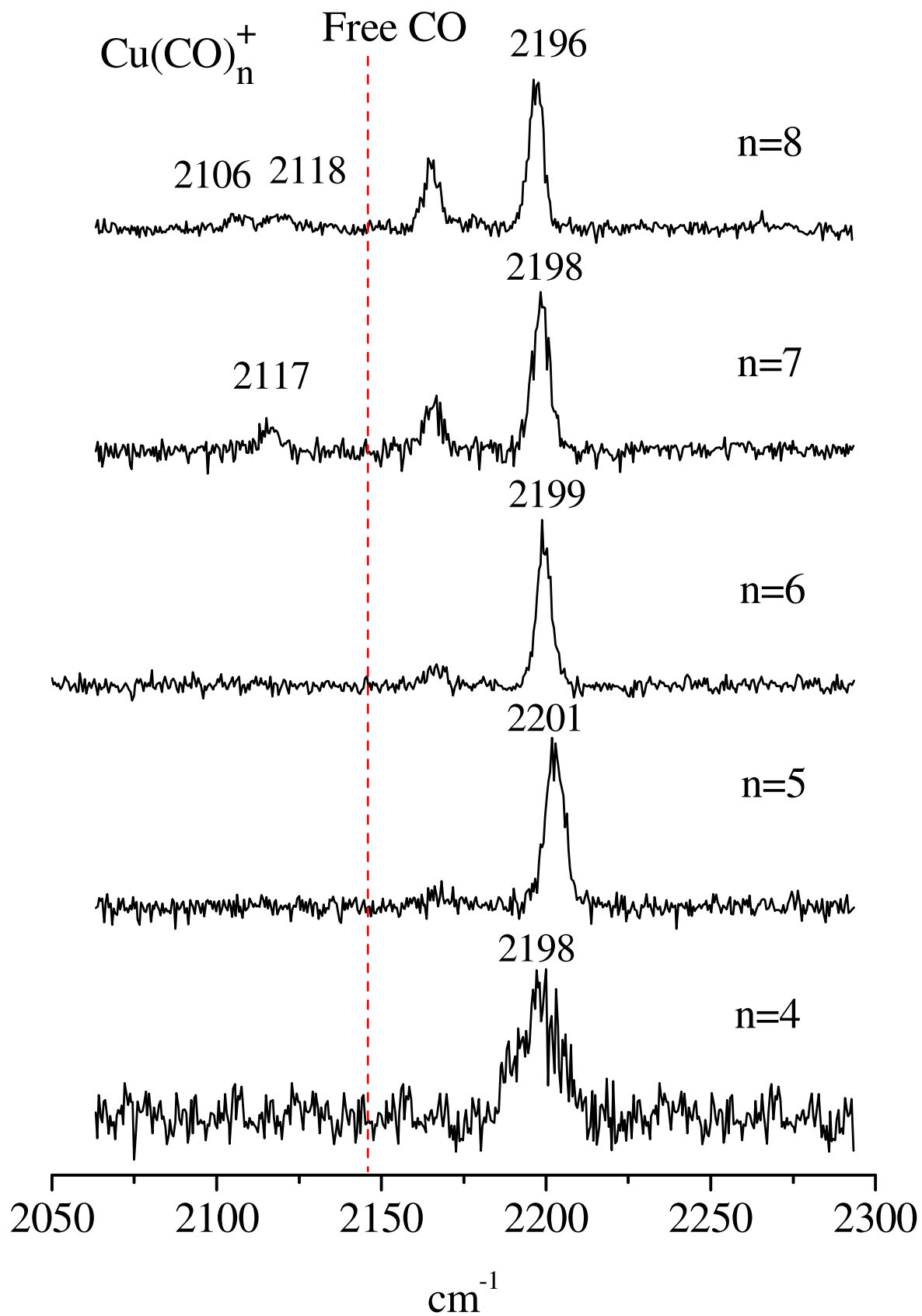


Figure 6.4.

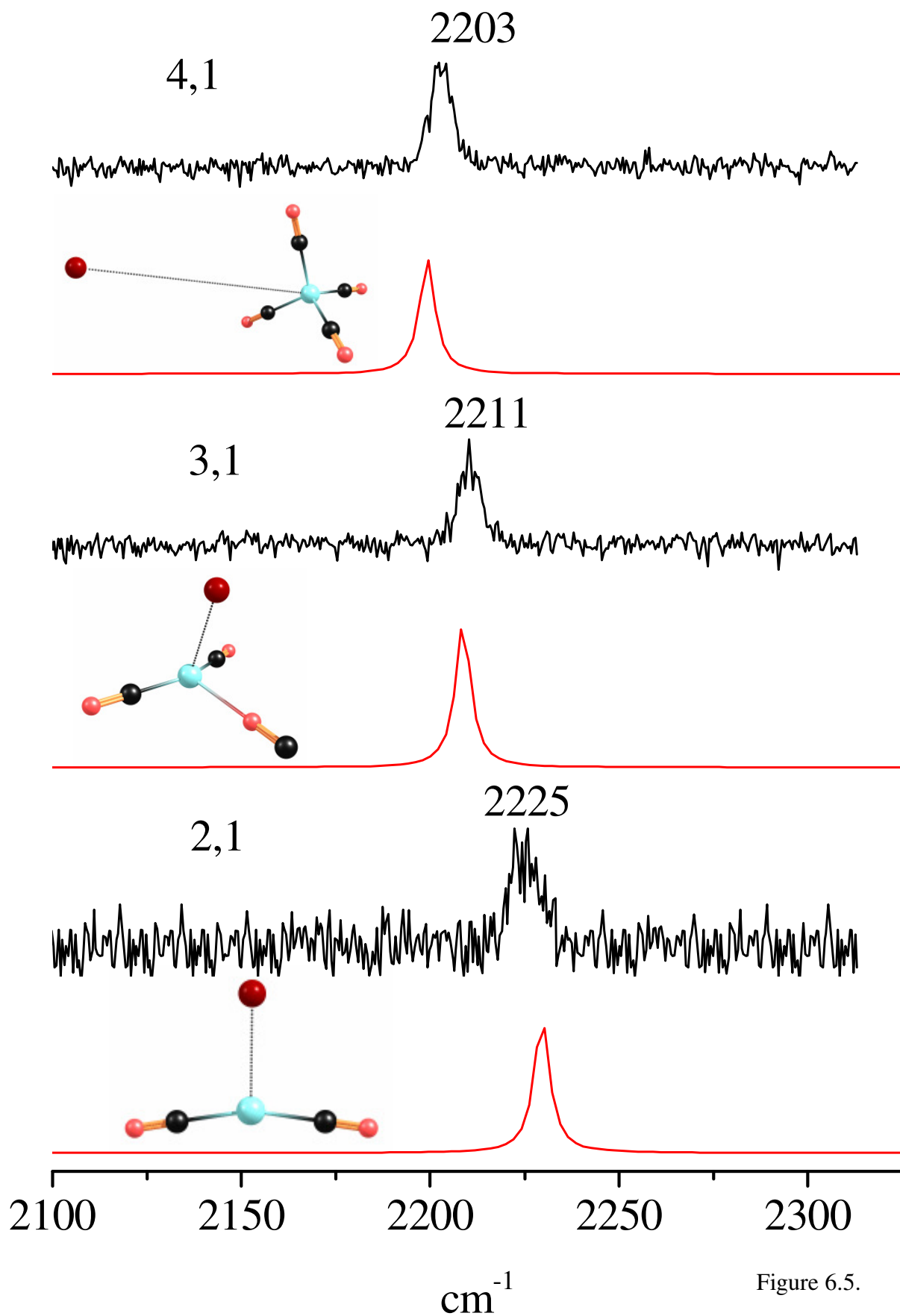


Figure 6.5.

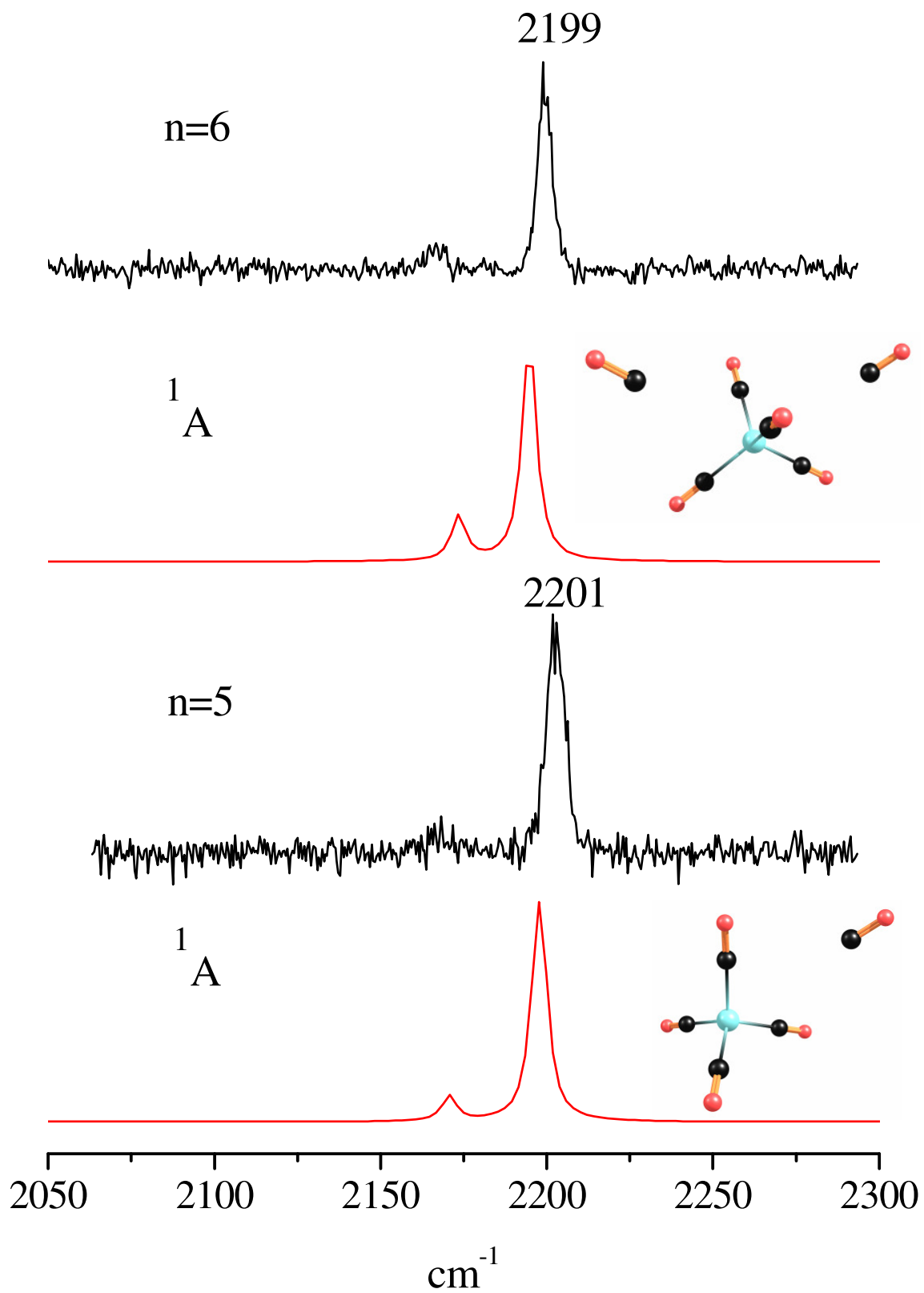


Figure 6.6.

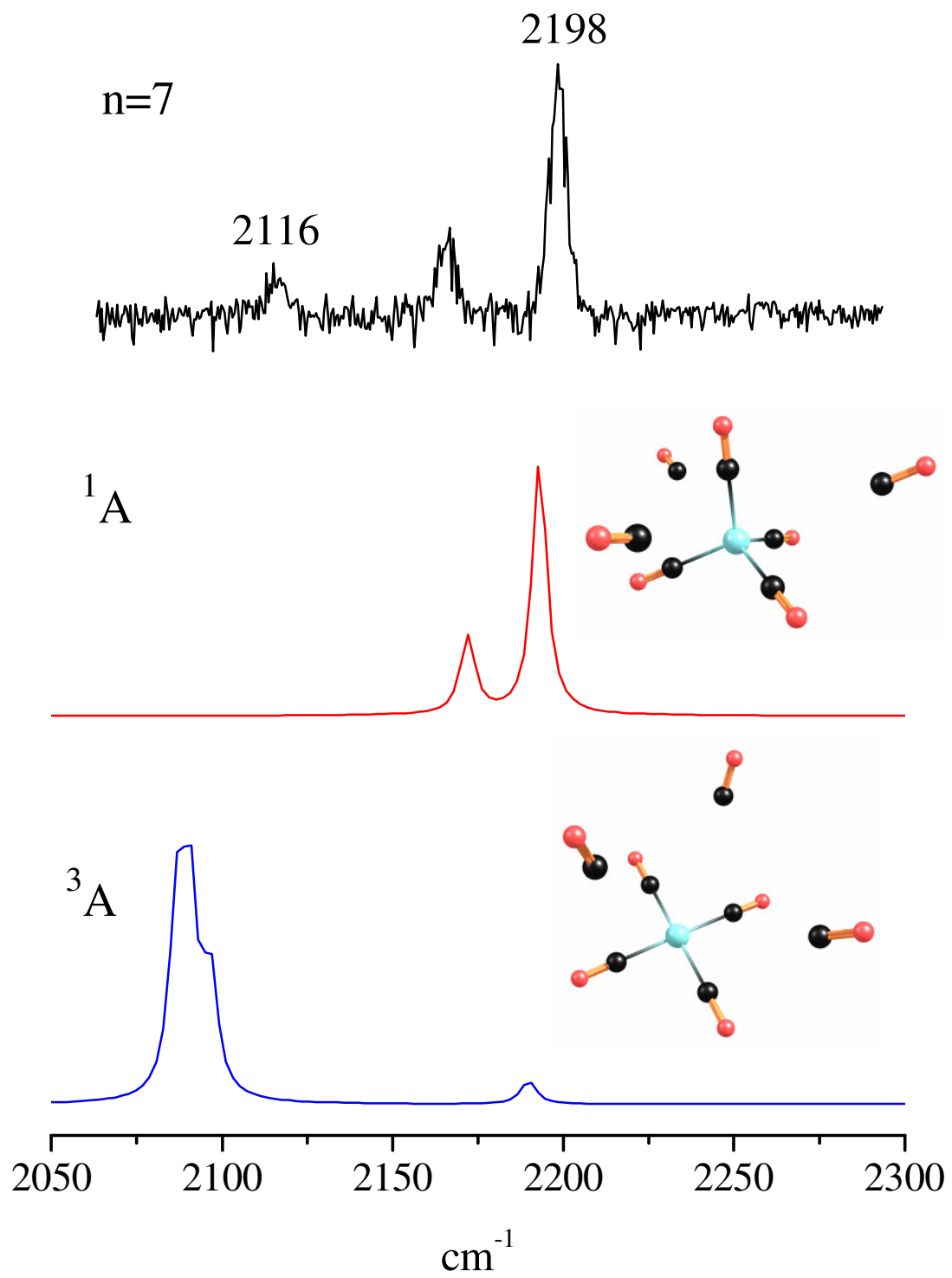


Figure 6.7.

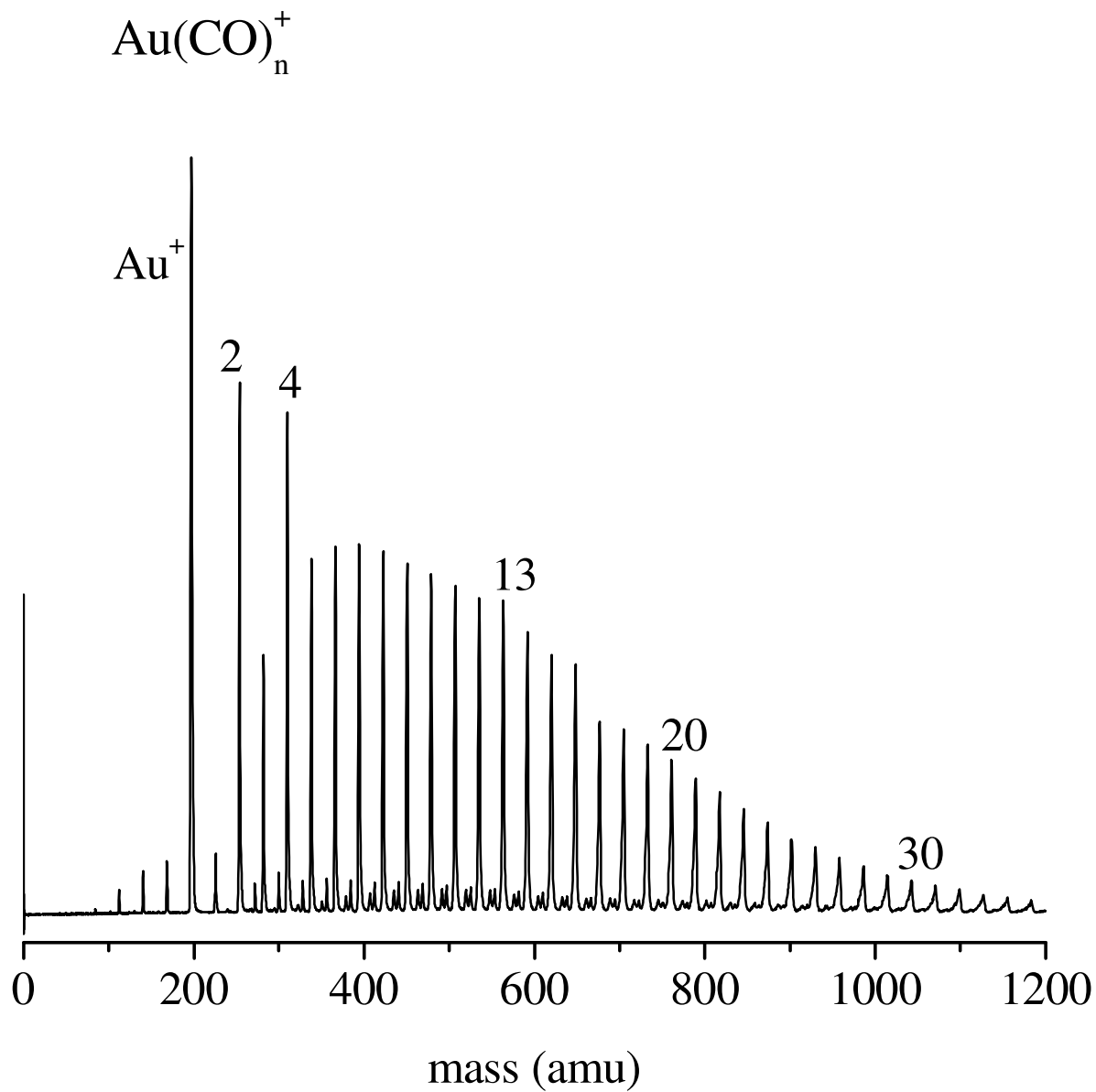


Figure 6.8.

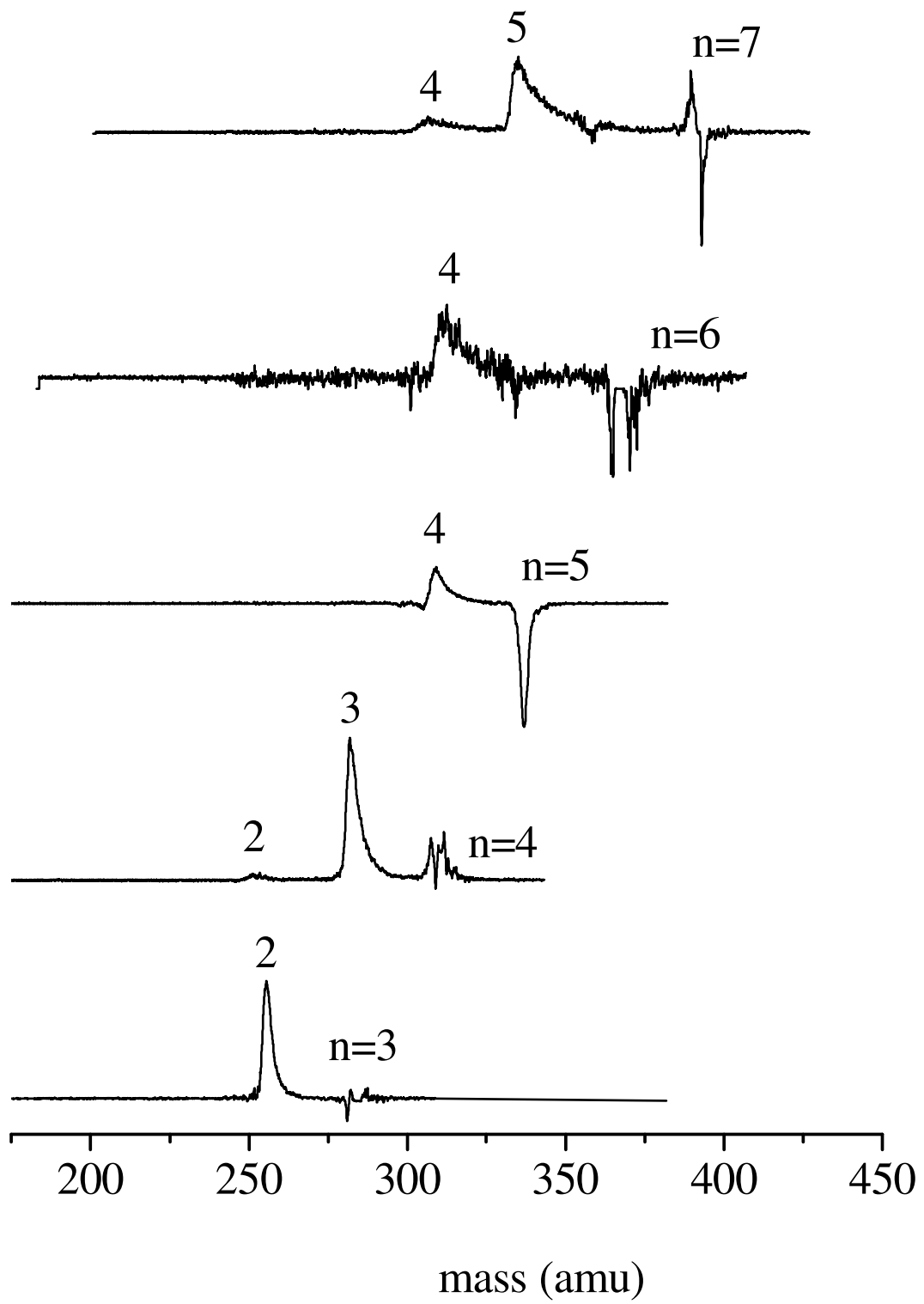


Figure 6.9.

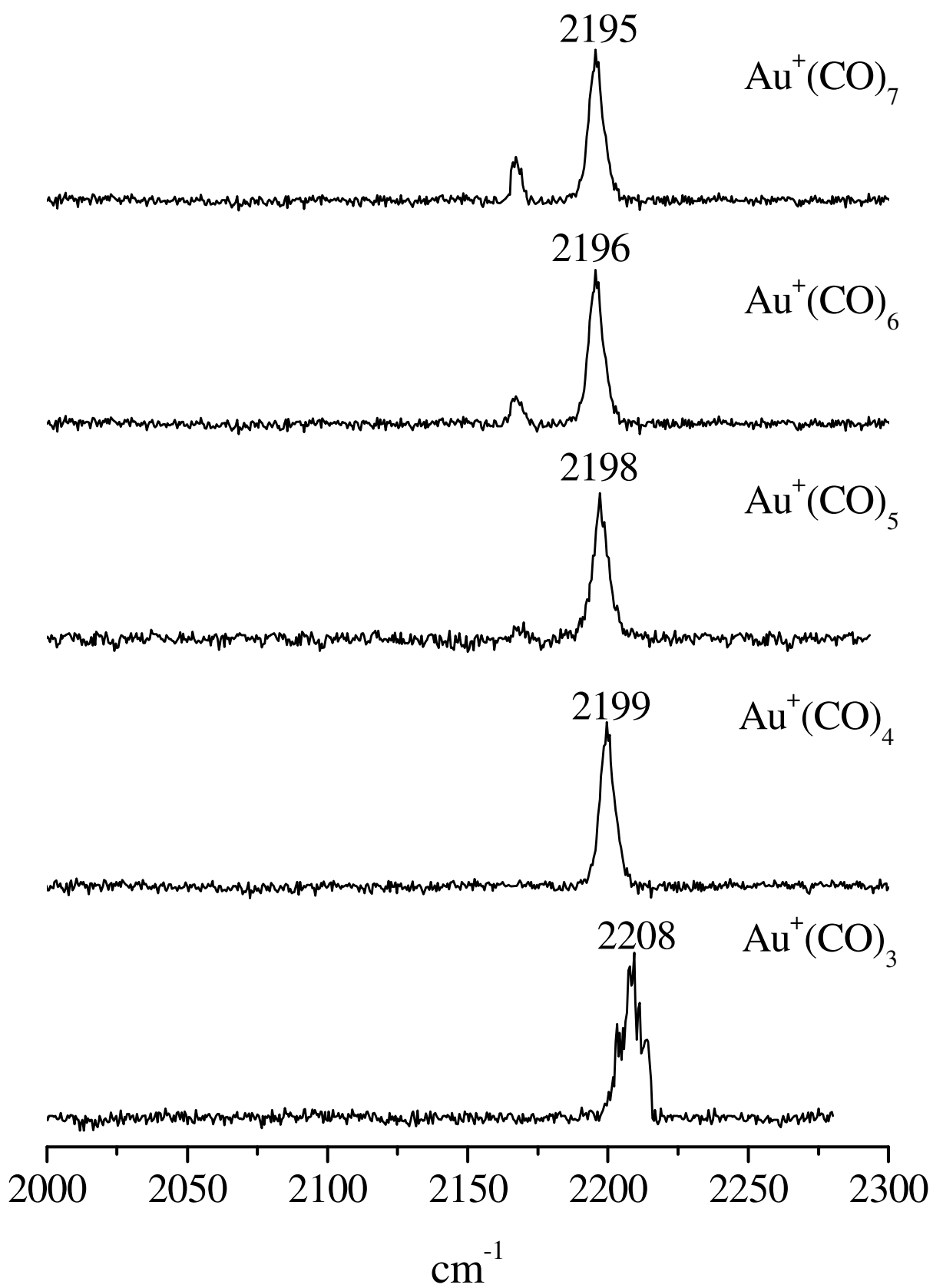


Figure 6.10.

CHAPTER 7

INFRARED PHOTODISSOCIATION SPECTROSCOPY OF BENZENE VANADIUM CARBONYL CATIONS, $\text{bz-V}^+(\text{CO})_n$

¹Reed, Z.D. and Duncan, M.A. To be submitted to *J. Phys. Chem. A*

7.1 Abstract

Benzene vanadium carbonyl cations of the form $(bz)V^+(CO)_n$ are produced in a pulsed nozzle laser vaporization source and studied by infrared photodissociation spectroscopy and density functional theory. Photofragmentation patterns indicate a stable tricarbonyl core ion. Further infrared spectroscopy and comparison to the predictions of DFT indicates that *two* stable configurations are present, a triplet tricarbonyl core and a singlet tetracarbonyl core. The tetracarbonyl complex is calculated to be more stable, but a greater population of the tricarbonyl complex is observed in our experiment. The benzene strongly activates the symmetric C-O stretches in these complexes. The asymmetric carbonyl stretch is red-shifted from that of gas-phase vanadium carbonyl.

7.2 Introduction

Aromatic organometallic carbonyl molecules have been a topic of interest since the discovery of ferrocene more than 50 years ago [1]. These “piano stool” molecules, with a planar aromatic molecule acting as the “seat” and carbonyl “legs” with a metal atom at the core, have applications in synthesis and catalysis, and have been used in various applications such as gasoline additives [2-4]. Fischer introduced cyclopentadienyl vanadium tetracarbonyl and cyclopentadienyl manganese tricarbonyl in 1954 [6,7]. Benzene metal carbonyls have also been synthesized. (η^6 -benzene) chromium tricarbonyl was synthesized by Fischer in 1957 by reacting dibenzene chromium with chromium hexacarbonyl in a heated sealed tube [8]. The formation of η^6 or η^5 complexes between arenes and metal carbonyl moieties significantly alters the

chemical reactivities of the arene. Among benzene complexes, the complexation of $\text{Cr}(\text{CO})_3$ to benzene activates the benzene to nucleophilic attack, due to electron withdrawing effects from the metal carbonyl [3]. The resulting compounds are useful intermediates for organic synthesis [4]. Here we report infrared photodissociation spectroscopy for benzene vanadium carbonyl cations and investigate their structure, electronic states, and coordination chemistry.

The structure of benzene chromium tricarbonyl has been determined by x-ray crystallography, neutron diffraction, and microwave spectroscopy [8-11]. The infrared and electronic spectra have also been measured [12-15]. The vanadium organometallic analogue, $\text{Cp-V}(\text{CO})_4$, has been studied by x-ray crystallography [16]. Its reactions have been studied by mass spectroscopy and Fourier transform ion cyclotron resonance experiments [17-21]. The cyclopentadienyl vanadium carbonyl system has been observed to form clusters of the form $(\text{CpV})_n(\text{CO})_m$ ($m=1-4$) [22]. Vanadium benzene famously forms multidecker sandwich complexes. These multidecker complexes have been studied by mass spectrometry [23-26], atomic force microscopy [27], ion mobility experiments [28], infrared spectroscopy, magnetic deflection [29,30], and theoretical calculations [31-34].

Inorganic coordination chemistry is often understood in terms of the 18 electron rule [1]. $\text{Cp-V}(\text{CO})_4$, $\text{Cp-Mn}(\text{CO})_3$, and $(\text{bz})\text{Cr}(\text{CO})_3$ all have 18 electrons. However, $\text{V}(\text{CO})_6$ is stable with 17 electrons [1]. Theoretical calculations predicted that a seven-coordinate vanadium carbonyl cation would be stable [35] and collision induced dissociation measurements found some evidence for a seven-coordinate homoleptic vanadium carbonyl cation [36]. We have recently reported infrared spectroscopy of gas

phase vanadium group carbonyl cations, and found no evidence for a seven coordinate vanadium carbonyl cation complex [37]. However, Nb formed both six and seven coordinate complexes and Ta was exclusively seven coordinate. This trend may be caused by the ionic radius of the metal. The benzene ligand is smaller than three carbonyl ligands [11] and this may allow for the formation of a seven coordinate mixed system with vanadium cation. The (bz)V(CO)_n⁺ system presents an interesting test case for coordination chemistry. Benzene typically contributes one more electron than cyclopentadienyl, and the positive charge removes an electron. A tricarbonyl or tetracarbonyl species may be expected, analogous to either V(CO)₆⁺ or Cp-V(CO)₄.

Gas phase infrared photodissociation spectroscopy provides a sensitive probe of the coordination number and the bonding in metal ligand systems. We have previously applied this technique to various metal-benzene and metal-carbonyl systems and have learned much about the bonding, geometries, and electronic structures of those systems [38,39]. Here we apply this technique to a novel mixed benzene-vanadium-carbonyl cation system and determine its coordination number and explore the detail of its binding. The infrared spectra are compared to density functional theory calculations to further elucidate the structure and bonding of this system.

7.3 Experimental

Benzene vanadium carbonyl complexes are produced in a pulsed nozzle laser vaporization source using the third harmonic of a pulsed Nd:YAG laser (355 nm; Continuum Surelite), which is focused on a rotating and translating ¼ inch diameter

vanadium rod. The rod is mounted with a $\frac{3}{4}$ inch horizontal offset in front of a pulsed nozzle (General Value Series 9). The general apparatus has been described in detail elsewhere [40]. The expansion gas is pure carbon monoxide seeded with benzene, which is introduced via a reservoir placed in the gas line. The nozzle backing pressure was 300 psi. The expansion is skimmed and pulse extracted into a home-built reflectron time of flight mass spectrometer. Ions of interest can be mass selected with a pulsed deflection plate and crossed with tunable infrared light in the turning region of the reflectron. The infrared light is generated by an optical parametric oscillator/amplifier (OPO/OPA; LaserVision) pumped by the fundamental of an Nd:YAG (Continuum 8010). The tuning range is from 2000-4500 cm^{-1} , and the pulse energy is about 1-2 mJ/pulse in the carbonyl stretching region, and 8-10 mJ/pulse in the C-H stretching region. Complexes with sufficiently weakly bound ligands dissociate via IVR upon resonant excitation with infrared light, and spectra are generated as a function of the fragment yield versus laser wavelength.

Density functional theory calculations were performed to investigate the structures and spin configurations of the complexes studied. A variety of geometries and spin states were examined for each $(\text{bz})\text{V}^+(\text{CO})_n$ complex studied experimentally. All calculations were performed in Gaussian 2003 [41] using the B3LYP functional [42,43]. The 6-31+G(d) basis set was used on all atoms [44]. A scaling factor of 0.9732 was applied.

7.4 Results and Discussion

A mass spectrum of the $(bz)V^+(CO)_n$ complexes produced is shown in Figure 7.1. The main series is $V(CO)_n^+$. $bzV^+(CO)_n$ is a smaller secondary series, which can be seen on the expanded view (inset). The other small secondary series is $(H_2O)V^+(CO)_n$. Some water is present along with the benzene, and we find experimentally that some water is necessary to produce the desired complexes. We produce $(bz)V^+(CO)_n$ complexes containing up to 10 carbonyls. We are able to mass select only the $(bz)V^+(CO)_n$ complexes and exclude the $V(CO)_n^+$ and $(H_2O)V^+(CO)_n$ complexes. Many of the complexes we produce are not likely to be stable at room temperature and are observed due to the cold conditions of the supersonic expansion. No $(bz)V^+(CO)_n$ complex has obviously enhanced intensity, and we must investigate the photofragmentation patterns to gain clues about the coordination of these complexes.

The photofragmentation mass spectra of the $(bz)V^+(CO)_n$ complexes can be seen in Figure 2. These are shown as the difference of the mass spectra with the fragmentation laser on minus the laser off. The result is a negative going parent ion and positive going fragments. The laser wavelength is selected to maximize fragmentation of each complex. We do not observe any fragmentation for the $(bz)V^+(CO)_{1-3}$ complexes (e.g., $n=1-3$). The $n=4$ complex fragments readily on excitation with 2070 cm^{-1} light, and loses a single carbonyl. Large complexes lose multiple carbonyls and have several loss channels. The $n=5$ complex loses one or two carbonyls to produce $n=3$ and $n=4$. The loss of two carbonyl channel is much more intense. The $n=6$ and $n=7$ complexes lose two carbonyls as their primary decay channel, but the loss of one and three carbonyl channels are also

present. Taken all together, these results suggest that the $n=3$ complex has a completed coordination sphere and additional carbonyls are externally bound.

The vibrational spectra of these complexes are measured by recording the fragmentation yield versus the wavelength. The measured spectra of $n=4-7$ are shown in Figure 3. The $n=4$ complex is measured by loss of one carbonyl, and all the larger complexes by the loss of two carbonyls. The $n=4$ and $n=5$ complexes have three major vibrational bands, two large ones around 2070 cm^{-1} and 2120 cm^{-1} , and a smaller one at 2165 cm^{-1} . The gas phase $V(\text{CO})_n^+$ system has carbonyl stretches around 2100 cm^{-1} [37]. Larger complexes, those with a filled coordination sphere and externally bound carbonyls, have a “free CO” stretch around 2165 cm^{-1} . Here we see two bands in the carbonyl stretch region, and a third band that may be the free carbonyl band. This gives support to the idea that $n=3$ represents a filled coordination sphere. The larger complexes, $n=6,7$, have the same three bands, with the 2165 cm^{-1} growing in intensity. We would expect this band to gain intensity as more external CO's are added. We also see two smaller bands develop, at 2030 cm^{-1} and 2090 cm^{-1} . This hints that some other isomer or spin state may be present. This will be investigated further with theoretical calculations.

We performed DFT calculations for the singlet, triplet, and quintet configuration for the $(\text{bz})V^+(\text{CO})_3$ core complex. The triplet is most stable, and the singlet and quintet are 10 and 26 kcal/mol higher in energy, respectively. The energetics for all calculated complexes can be found in Table 7.1. When a fourth carbonyl is added, it can bind to the metal center to form a tetracarbonyl core ion, to the $V^+(\text{CO})_3$ moiety as an “external” carbonyl, or to the benzene ring. For convenience, we will use the notation (n,m) to refer

to “n” directly bound carbonyls and “m” externally bound carbonyls, eg the $V^+(CO)_3$ core with an externally bound carbonyl is (3,1) and the $V^+(CO)_4$ core is (4,0). The various electronic states must also be considered here. When another CO is placed near the metal on (3,0), the singlet converges to form the (4,0) core. The triplet, however, converges as (3,1), with the external carbonyl binding to the first carbonyl coordination sphere. The (3,1) triplet is 18.5 kcal/mol higher in energy than the (4,0) singlet. The (4,0) triplet configuration has significant imaginary frequencies and is 43 kcal/mol higher in energy than the $V^+(CO)_3$ core and is not likely to be stable. The (3,1) quintet is 43 kcal/mol higher in energy than the singlet, and 24.5 kcal/mol higher in energy than the triplet. It has a distorted (3,1) geometry, with one elongated M-CO bond and the external CO on the $V^+(CO)_3$ moiety. The metal carbonyl group is also slipped from the center of the benzene ring. When the carbonyl is placed near the benzene on the singlet (3,0), it binds to the edge of the benzene ring. This (3,1) singlet configuration is some 28 kcal/mol higher than the (4,0) singlet, and 9.6 kcal/mol higher than the (3,1) triplet.

We have calculated the binding energy for sequential carbonyl addition, and the results can be found in Table 7.2. We can readily see that all external carbonyls are quite weakly bound, by 1 or 2 kcal/mol in most cases. The fourth carbonyl in the singlet (4,0) complex is bound by 30.1 kcal/mol, and we would not expect to observe fragmentation for this complex. Armentrout has previously measured the binding energy for the homoleptic $V(CO)_n^+$ system, and found the binding energy to be around 20 kcal/mol for $n=1-7$, with some variation for each complex [36]. Our binding energy here for the singlet (4,0) complex is generally in line with those measurements, and indicates that the carbonyl is directly coordinated to the metal ion. The predicted spectra for $n=4$ are

compared to our measured spectra in Figure 4. The geometries of each complex are also shown there. Each has two main bands and a smaller band corresponding to the external CO stretch. We see good agreement between the predicted (3,1) triplet band positions and our experimental data. The predicted doublet at 2080 cm^{-1} also coincides well with the broadened 2072 cm^{-1} experimental band. The (3,1) quintet also agrees fairly well, and there are no significant spectral difference to rule out one or the other, although the quintet is computed to be substantially higher in energy. The (4,0) complex not does match well with our experiment, and we would not expect to be able to fragment this complex anyway based on its high computed binding energy (see Table 7.2). The (3,1) singlet has similar band positions to the (4,0) complex. Therefore, the $n=4$ complex is likely a triplet with a $\text{V}(\text{CO})_3^+$ core and an externally bound carbonyl, but we cannot exclude the higher energy (3,1) quintet. It is also possible that we have some population of both spin states present.

In the (3,0) and (3,1) triplets, the 2070 cm^{-1} band corresponds to two asymmetric carbonyl stretches, split by some 6 cm^{-1} . The 2120 cm^{-1} band is a symmetrical carbonyl stretch. These two bands are respectively red shifted and blue shifted relative to the $\text{V}(\text{CO})_6^+$ gas phase values, which has a single vibrational band at 2102 cm^{-1} , assigned to the nearly degenerate asymmetric CO stretches in that complex [37]. The (4,0) singlet band at 2030 cm^{-1} is a doubly degenerate asymmetrical carbonyl vibration, and the 2090 cm^{-1} band is a symmetric carbonyl stretch. This fully symmetric mode has low oscillator strengths (generally $<1\text{ km/mol}$) in our previous metal carbonyl cation studies [37,39], and seems to be activated by the benzene in the present systems, as the computed oscillator strengths here are $>500\text{ km/mol}$.

The bonding in metal carbonyl systems has been well described in previous work [1,44-48]. The red-shift observed for ν_{CO} in most carbonyl systems is attributed to the dominance of π -back-bonding over σ -bonding. π -back-bonding leads to an increased population in the antibonding orbitals of C-O, and thus causes red-shifted carbonyl vibrations. In this system, we see a greater red-shift than in the homoleptic vanadium carbonyl cation. It seems that the π bonding between the vanadium cation and the benzene either increases the amount of π backbonding to the carbonyls or decreases the amount of σ -bonding, either of which would result in a further red-shift. The vanadium cation-benzene binding energy has been previously measured to be 55.8 kcal/mol [49]. This is much greater than the energy of a single carbonyl bond (roughly 20 kcal/mol), but slightly less than three carbonyls [36]. Given the similar bond energies for a single benzene and three carbonyls to vanadium, the cause of the additional red-shift is not obvious. The charge transfer between the vanadium and the benzene likely plays a role, but we cannot fully explain this effect.

To investigate the extra bands appearing in the spectra of larger complexes, we performed calculations on various $n=5$ complexes. The calculated and experimentally measured spectra for $n=5$ are shown in Figure 5. All the calculated vibrational frequencies are compared to the experimental values in Table 7.3. For this complex, we have two different experimental spectra, one measured by the loss of 1 CO and one measured by the loss of 2 CO. The spectra shown here is from the loss of 1 channel. The spectrum from the loss of 2 CO, shown in Figure 3, looks nearly identical to that of $n=4$, while the spectrum from loss of 1 CO has two extra vibrational bands, one at 2032 cm^{-1} and a very weak one at 2094 cm^{-1} . The spectrum of calculated (4,1) singlet agrees quite

well with the positions of these two additional bands, with the calculated vibrations at 2035 and 2090 cm^{-1} . The (3,2) triplet agrees rather well with the other band two positions. If we examine the $n=6$ spectrum in Figure 3, we see evidence for the same two bands at 2032 and 2094 cm^{-1} associated with the singlet (4,1) configuration. It appears that two separate core isomers are present in our experiment, a triplet $(\text{bz})\text{V}^+(\text{CO})_3$ and a singlet $(\text{bz})\text{V}^+(\text{CO})_4$. All larger complexes have one of these two cores, with externally bound carbonyls.

The oscillator strengths of the two core ion configurations are similar, with computed IR intensities around 1000 km/mol . From the relative band intensities, we can conclude that the population of complexes with the (3,0) core is greater than that with a (4,0) core. This is interesting on several levels. The triplet (3,1) is calculated to be 18.5 kcal/mol higher in energy than the singlet (4,0). The $(\text{bz})\text{V}^+(\text{CO})_4$ complex would have 18 electrons, and the $(\text{bz})\text{V}^+(\text{CO})_3$ complex has 16 electrons. Despite this, we see a greater population of the tricarbonyl core ion. This is in some ways expected in light of our study of $\text{V}(\text{CO})_n^+$, which was found to be exclusively six coordinate [37]. Here though, we seem to at least some seven coordinate complexes.

Several separate factors leading to the production of six over seven coordinate vanadium species were discussed in our work on the vanadium group carbonyl cations [37]. The vanadium cation is smaller than both niobium and tantalum cations, and was apparently less able to accommodate seven carbonyl ligands. In this work, however, the benzene ligand is smaller than three carbonyls, and this diminished steric crowding may allow for the formation of seven coordination species. Additionally, greater spin-orbit coupling was determined to decrease the inhabitation towards insertion of the seventh

carbonyl. The benzene may allow for greater spin orbit coupling in these mixed systems compared to the homoleptic system. We see a significantly greater population of triplet (3,0) core ions than singlet (4,0) ions, despite the calculation of a singlet ground state. We have observed similar behavior in $V^+(bz)_2$ complexes, where DFT predicted a triplet ground state, but we observed a quintet state. Interestingly, the equivalent complex to $V^+(bz)_2$ in this work, $(bz)V^+(CO)_3$, is a triplet, not a quintet, supporting the idea that carbonyls encourage lower spin configurations than pure benzene. The cold growth conditions of our source may prevent the majority of complexes from overcoming energy or spin activation barriers to reach the seven coordinate singlet ground state in this system. However, the computed energetics of different spin states are often misjudged by DFT/B3LYP calculations [50], and the computed energies here may simply not be reliable.

We also measured the spectroscopy of these complexes in the C-H stretching region. Again, no fragmentation was observed for $n \leq 3$. All complexes $n \geq 4$ fragmented very weakly over a broad region, some 200 cm^{-1} wide and centered around 3100 cm^{-1} . Our theoretical calculations predict a number of very weak (oscillator strengths from 1-10 km/mol) bands in this region, which explains the weak fragmentation. It is unclear why the fragmentation occurs over such a broad region. Previous electron diffraction and microwave spectroscopy experiments on $(bz)Cr(CO)_3$ predicted that the benzene could freely rotate at elevated temperatures (some 400K for that system) [11]. We noted experimentally that high vaporization laser power was necessary to produce the desired complexes and the laser plasma appeared quite hot. It is certainly possible that our complexes were hot and this contributed to the very wide fragmentation. High

fragmentation laser power (~10 mJ/pulse) was also required to observe any fragmentation in the C-H stretching region, and may have caused some broadening.

7.5 Conclusions

We have produced (bz)V⁺(CO)_n complexes in the gas phase using laser vaporization and investigated them using infrared photodissociation. Different spectra are obtained by recording different loss channels. The spectra feature two main bands. These bands are assigned to degenerate asymmetric carbonyl stretching modes and a symmetric carbonyl stretch of the triplet V⁺(CO)₃ core ion. This symmetric carbonyl stretch is strongly activated by the benzene. Smaller bands in the n_≥5 complexes are assigned to the asymmetric and symmetric carbonyl stretches of a singlet V⁺(CO)₄ core ion. The spectra for all complexes with n_>4 are a mix of both complexes. The addition of carbonyls past either of these coordination numbers leads to externally bound ligands, which appear as a “free” CO vibration. A greater population of the tricarbonyl complex is observed, which could be due to preferential trapping of the higher energy isomer in our source. The relative energetics may also be incorrectly predicted by DFT. This organometallic carbonyl cation system apparently has stable tricarbonyl and tetracarbonyl forms, and may be interesting to study in the condensed phase with counterions.

7.6 Acknowledgements

We acknowledge generous support for this work from the U.S. Department of Energy (grant no. DE-FG02-96ER14658) and the Air Force Office of Scientific Research (Grant No. FA95509-1-0166).

Supporting Information

The Supporting Information for this manuscript contains the full details of the DFT computations done in support of the spectroscopy here, including the structures, energetics and vibrational frequencies for each of the structures considered. The complete reference for Ref 41 is also included in the Supporting Information.

7.7 References

- (1) Cotton, F. A. *Advanced Inorganic Chemistry*, 6th ed., John Wiley and Sons, Inc., New York, 1999.
- (2) Huheey, J. E.; Keiter, E. A.; Keiter, R. L. *Inorganic Chemistry Principles of Structure and Reactivity*, Harper Collins, New York, 1993.
- (3) Pearson, A.J. *Metallo-Organic Chemistry* Wiley, New York, 1985
- (4) Semmeihack, M.F. *Tetrahedron* **1981**, *37*, 3956.
- (5) Fischer, E.O.; Jira, R. "Cyclopentadienyl-mangan-tricarbonyl," *Z. Naturforsch. B* **1954**, *9*, 618.
- (6) Fischer, E.O.; Hafner, W. "Cyclopentadienyl-vanadin-tetracarbonyl," *Z. Naturforsch. B* **1954**, *9*, 503

- (7) Fisher, E.O.; Ofele, K. "Benzene-chromium-tetracarbonyl," *Chem. Ber.* **1957**, *90*, 2532
- (8) Rees, B.; Coppens, P. "Electronic structure of benzene chromium tricarbonyl by x-ray and neutron diffraction at 78 degrees K," *Acta Crystallogr. B* 1973, *29*, 2515.
- (9) Byers, B.P.; Hall, M.B. "Comparison of isolobal fragments- photoelectron spectra and molecular orbital calculations of (arene) tricarbonylchromium (arene) tricarbonylmolybdenum, and (arene)tricarbonyltungsten complexes," *Organometallics* **1987** *6*, 2319.
- (10) Chiu, N.-S.; Schafer, L.; Seip, R. "Internal rotation in gaseous benzenechromium tricarbonyl," *J. Organomet. Chem.* **1975**, *101*, 331
- (11) Kukolich, S.G.; Sickafoose, S.M.; Flares, L.D.; Breckenridge, S.M. "Measurements of the microwave spectrum and structural parameters for benzene chromium tricarbonyl," *J. Chem. Phys.* **1994**, *100*, 6125.
- (12) Schafer, L. "Raman Spectrum of Benzene-Chromium Tricarbonyl," *Spectrochim. Acta. A* **1972**, *28*, 803
- (13) Guest, M.F.; Hillier, I.H.; Higginson, B.R.; Lloyd, D.R. "Electronic structure of transition metal complexes containing organic ligands, Low-energy photoelectron spectra and ab-initio SCF-MO calculations of dibenzene chromium and benzene chromium tricarbonyl," *Mol. Phys.* **1975**, *29*, 113
- (14) Lichtenberger, D.L.; Fenske, R.F. "Helium (I) photoelectron spectra and electron structure of (eta 5-cyclopentadienyl) d6 metal carbonyls," *J. Am. Chem. Soc.* **1976**, *98*, 50

- (15) Field, C.N.; Green, J.C.; Moody, A.G.J.; Siggel, M.R.F. "A photoelectron study of the electronic structure of (η -C₆H₆) Cr(CO)₃ and (η -C₅H₅) Mn(CO)₃ using variable photon energy," *Chem. Phys.* **1996**, *206*, 211
- (16) Wilford, J.B.; Whitla, A.; Powell, H.M. "The Crystal and Molecular Structure of η -cyclopentadienylvanadium tetracarbonyl" *J. Organometal. Chem.* **1967**, *8*, 495
- (17) Winters, R.E.; Kiser, R.W. "Ion produced in a mass spectrometer from cyclopentadienylmetal carbonyl compounds of cobalt, manganese, and vanadium," *J. Organomet. Chem.* **1965**, *4*, 190.
- (18) Allison, J. "The gas phase chemistry of transition metal ions with organic molecules," *Prog. Inorg. Chem.* **1986**, *34*, 627.
- (19) Armentrout, P.B.; Halle, L.F.; Beauchamp, J.L. "Periodic trends in transition metal hydrogen, metal-carbon, and metal-oxygen bond dissociation energies-correlation with reactivity and electronic structure," *J. Am. Chem. Soc.* **1981**, *103*, 6501.
- (20) Armentrout, P.B. *Gas Phase Inorganic Chemistry*, D.H. Russell (Ed.), Plenum, 1989, pp. 1-42.
- (21) Taylor, S.M.; Comisarow, M.B. "Gas phase ion molecule chemistry of tetracarbonyl (η -cyclopentadienyl) vanadium by Fourier transform ion cyclotron resonance," *Int. J. Mass. Spec.* **1999**, *182*, 139
- (22) Fischer, E.O.; Schneider, R.J.J. "Reactions of cp-V carbonyl" *Chem. Ber.* **1970**, *103*, 3584.

- (23) Hoshino, K.; Kurikawa, T.; Takeda, H.; Nakajima, A.; Kaya, K. "Structures and Ionization Energies of Sandwich Clusters (Vn(benzene)m)," *J. Phys. Chem.* **1995**, *99*, 3053.
- (24) Hoshino, K.; Kurikawa, T.; Takeda, H.; Nakajima, A.; Kaya, K. "Structures of organometallic clusters: V-n(benzene)(m) and Co-n(benzene)(m)," *Surf. Rev. Lett.* **1996**, *3*, 183.
- (25) Yasuike, T.; Nakajima, A.; Yabushito, S.; Kaya, K. "Why Do Vanadium Atoms Form Multiple-Decker Sandwich Clusters with Benzene Molecules Efficiently?," *J. Phys. Chem. A* **1997**, *101*, 5360.
- (26) Nakajima, A.; Kaya, K. "A Novel Network Structure of Organometallic Clusters in the Gas Phase," *J. Phys. Chem. A* **2000**, *104*, 176.
- (27) Nagaoka, S.; Ikemoto, K.; Fujio, K. "An atomic force microscope study of vanadium benzene sandwich clusters soft-landed on self-assembled monolayers," *Eur. Phys. J. D* **2009**, *1-3*, 103
- (28) Weis, P.; Kemper, P.R.; Bowers, M.T. "Structures and Energetics of $V_n(C_6H_6)_m^+$ Clusters: Evidence for a Quintuple-Decker Sandwich," *J. Phys. Chem. A* **1997**, *101*, 8207.
- (29) Judai, K.; Sera, K.; Amatsutsumi, S.; Yagi, K.; Yasuike, T.; Yabushita, S.; Nakajima, A.; Kaya, K. "A soft-landing experiment on organometallic cluster ions: infrared spectroscopy of V(benzene)(2) in Ar matrix," *Chem. Phys. Lett.* **2001**, *334*, 277.

- (30) Nagaoka, S.; Okada, E.; Doi, S.; Mitsui, M.; Nakajima, A. "Trapping of V(benzene)(2) sandwich clusters in a n-alkanethiol self-assembled monolayer matrix," *Eur. Phys. J. D* **2005**, *34*, 239.
- (31) Kurikawa, T.; Takeda, H.; Hirano, M.; Judai, K.; Arita, T.; Nagoa, S.; Nakajima, A.; Kaya, K. "Electronic Properties of Organometallic Metal–Benzene Complexes $[M_n(\text{benzene})_m]$ ($M = \text{Sc–Cu}$)," *Organometal.* **1999**, *18*, 1430.
- (32) Kandalam, A.K.; Rao, B.K.; Jena, P. "Geometry and electronic structure of V-n(Bz)(m) complexes," *J. Chem. Phys.* **2004**, *120*, 10414.
- (33) Wang, J.; Acioli, P.H.; Jellinek, J. "Structure and Magnetism of $V_n\text{Bz}_{n+1}$ Sandwich Clusters," *J. Am. Chem. Soc.* **2005**, *127*, 2812.
- (34) Kua, J.; Tomlin, K.M. "Computational Study of Multiple-Decker Sandwich and Rice-Ball Structures of Neutral Titanium–Benzene Clusters," *J. Phys. Chem. A* **2006**, *110*, 11988.
- (35) Dicke, J.W.; Stibrich, N.J.; Schaefer, H.F. "V(CO)(7)(+): A capped octahedral structure completes the 18-electron rule," *Chem. Phys. Lett.* **2008**, *456*, 13
- (36) Sievers, M.R.; Armentrout, P.B. "Collision-Induced Dissociation Studies of V(CO)_x⁺, x = 1-7: Sequential Bond Energies and the Heat of Formation of V(CO)₆," *J. Phys. Chem.* **1995**, *99*, 8135.
- (37) Ricks, A.M.; Reed, Z.D.; Duncan, M.A. "Seven- Coordinate Homoleptic Metal Carbonyls in the Gas Phase," *J. Am. Chem. Soc.* **2009**, *131*, 9176.
- (38) a) Jaeger, T. D.; Pillai, E. D.; Duncan, M. A. *J. Phys. Chem. A* **2004**, *108*, 6605.
b) Jaeger, T. D.; Duncan, M. A. *J. Phys. Chem. A* **2005**, *109*, 3311. c) Jaeger, J. B.; Pillai, E. D.; Jaeger, T. D.; Duncan, M. A. *J. Phys. Chem. A* **2005**, *109*, 2801.

- (39) a) Ricks, A.M.; Bakker, J.M.; Douberly, G.E.; Duncan, M.A. *J. Phys. Chem. A.* **2009**, *113*, 4701 b) Ricks, A.M.; Reed, Z.D.; Duncan, M.A. *J. Am. Chem. Soc.*, **2009**, *131*, 9176–9177
- (40) Duncan, M. A. "Infrared spectroscopy to probe structure and dynamics in metal ion-molecule complexes," *Intl. Rev. Phys. Chem.* **2003**, *22*, 407.
- (41) Frisch, M. J. et al., *Gaussian 03 (Revision B.02)*; Gaussian, Inc.: Pittsburgh, PA, 2003.
- (42) Becke, A. D. "3 term correlation functional," *J. Chem. Phys.* **1993**, *98*, 5648.
- (43) Lee, C.; Yang, W.; Parr, R. G. Lee Yang Parr, "Correlation functional," *Phys. Rev B.* **1998**, *98*, 5648.
- (44) Rassolov, V.; Pople, J.A.; Ratner, M.; Redfern, P.C.; Curtiss, L.A. "6-31G* Basis Set for Third-Row Atoms," *J. Comp. Chem.* **2001**, *22*, 976.
- (45) Frenking, G.; Fröhlich, N. "The Nature of the Bonding in Transition-Metal Compounds," *Chem. Rev.* **2000**, *100*, 717.
- (46) Zhou, M.; Andrews, L.; Bauschlicher, C. W. "Spectroscopic and Theoretical Investigations of Vibrational Frequencies in Binary Unsaturated Transition-Metal Carbonyl Cations, Neutrals, and Anions," *Chem. Rev.* **2001**, *101*, 1931.
- (47) Chatt, J.; Duncanson, L.A. *J. Chem. Soc.* **1953**, 2939.
- (48) Dewar, M.J.S. *Bull. Soc. Chim. Fr.* **1951**, *18*, C79
- (49) Meyer, F.; Khan, F.A.; Armentrout, P.B. "Thermochemistry of Transition Metal Benzene Complexes: Binding Energies of $M(C_6H_6)_x$ ($x = 1, 2$) for $M = Ti$ to Cu ," *J. Am. Chem. Soc.* **1995**, *117*, 9740.

- (50) Koch, W. and Holthausen, M. C. *A Chemist's Guide to Density Functional Theory*, 2nd ed.; Wiley-VCH: Weinheim, Germany, 2001

Table 7.1: The electronic ground states and energetics computed for (bz)V⁺(CO)_n with DFT.

complex	state	relative energy (kcal/mol)
(bz)V ⁺ (CO) ₃	singlet	+10.1
	triplet	0.0
	quintet	+26.4
(bz)V ⁺ (CO) ₄	singlet	0.0
	triplet	+18.5
	quintet	+40.8
(bz)V ⁺ (CO) ₅	singlet	0.0
	triplet	+19.4

Table 7.2: Calculated sequential carbonyl binding energies for $(bz)V^+(CO)_n$. All binding energies are in kcal/mol.

Complex	$D_0 (bz)V^+(CO)_{n-1}$
$(bz)V^+(CO)_4$ singlet	30.1 kcal/mol
$(bz)V^+(CO)_4$ triplet	1.46 kcal/mol
$(bz)V^+(CO)_4$ quintet	5.6 kcal/mol
$(bz)V^+(CO)_5$ singlet	2.1 kcal/mol
$(bz)V^+(CO)_5$ triplet	1.3 kcal/mol

Table 7.3: The vibrational frequencies computed (scaled by 0.9732) and measured for $(bz)V(CO)_n^+$. All frequencies are in wavenumbers.

Complex		theory	experiment
$(bz)V^+(CO)_4$			2072, 2120, 2164
	singlet	2036, 2038, 2091	
	triplet	2054, 2060, 2110, 2168	
	quintet	2080, 2088, 2127, 2169	
$(bz)V^+(CO)_5$			2032, 2067, 2094
			2128, 2164
	singlet	2034, 2035, 2090, 2173	
	triplet	2056, 2071, 2120, 2164, 2170	

Figure Captions

Figure 7.1. The mass spectrum of $(bz)V^+(CO)_n$ clusters produced by our cluster source.

Inset, expanded view of the mass spectrum with several series labeled.

Figure 7.2. The photofragmentation mass spectra of $(bz)V^+(CO)_n$, $n=4-7$.

Figure 7.3. The infrared photodissociation spectra of $(bz)V^+(CO)_n$, $n=4-7$

Figure 7.4. Infrared spectra of $(bz)V^+(CO)_4$ compared to the spectra predicted by theory, along with calculated structures. Complexes are indicated as (n,m) with n directly coordinated carbonyls and m external carbonyls.

Figure 7.5. Infrared spectra of $(bz)V^+(CO)_5$ compared to the spectra predicted by theory, along with calculated structures. Complexes are indicated as (n,m) with n directly coordinated carbonyls and m external carbonyls.

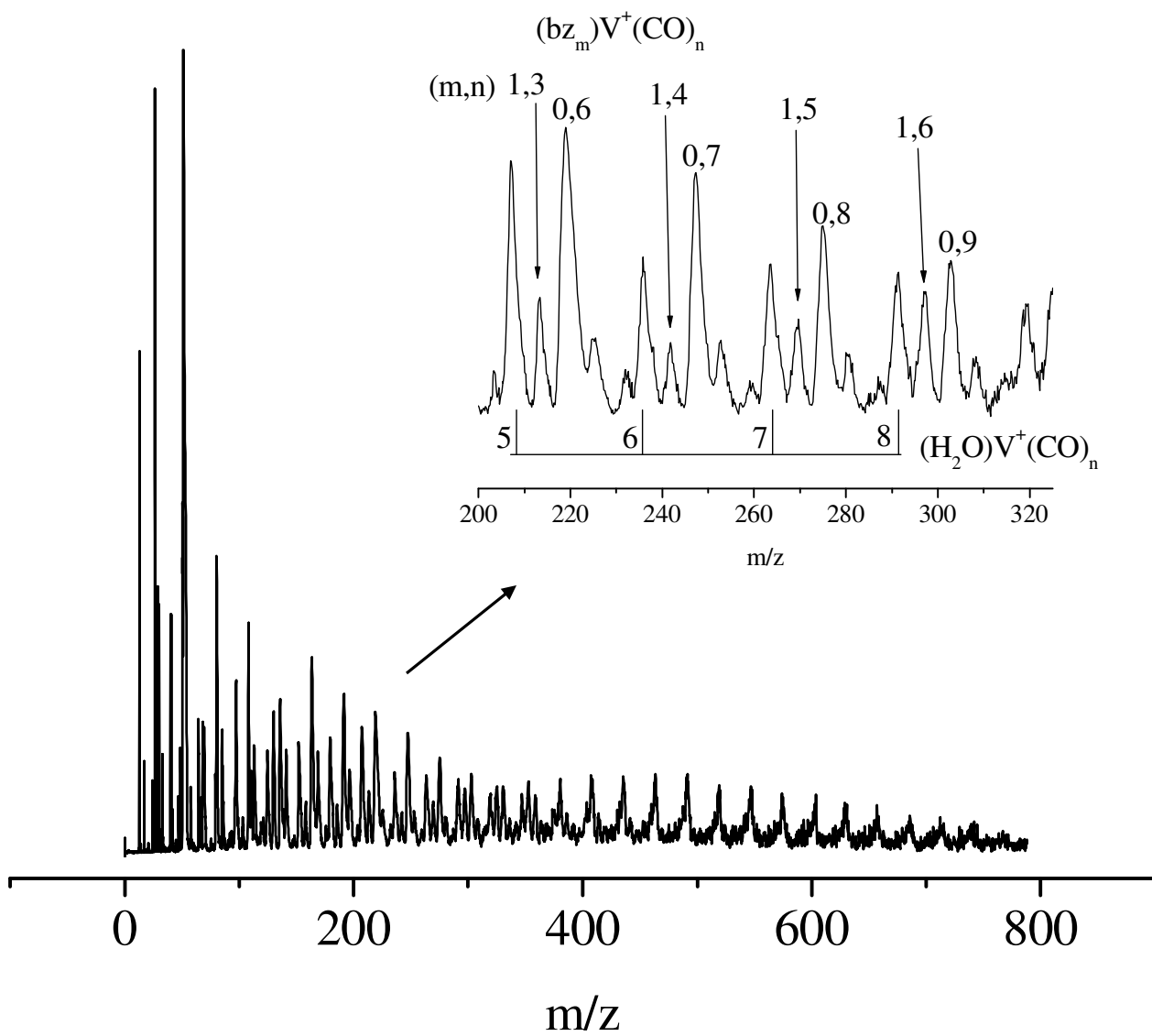


Figure 7.1.

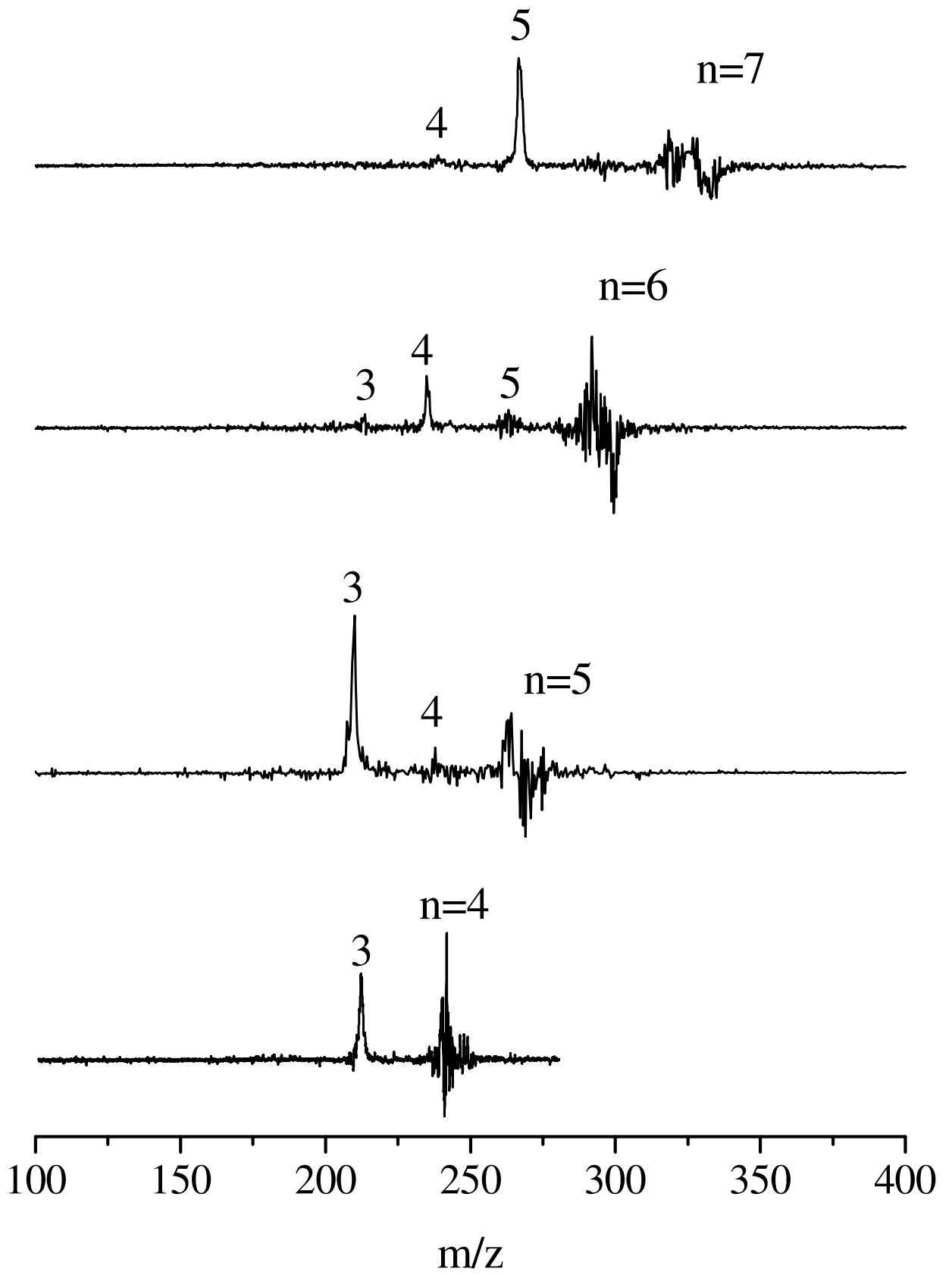


Figure 7.2

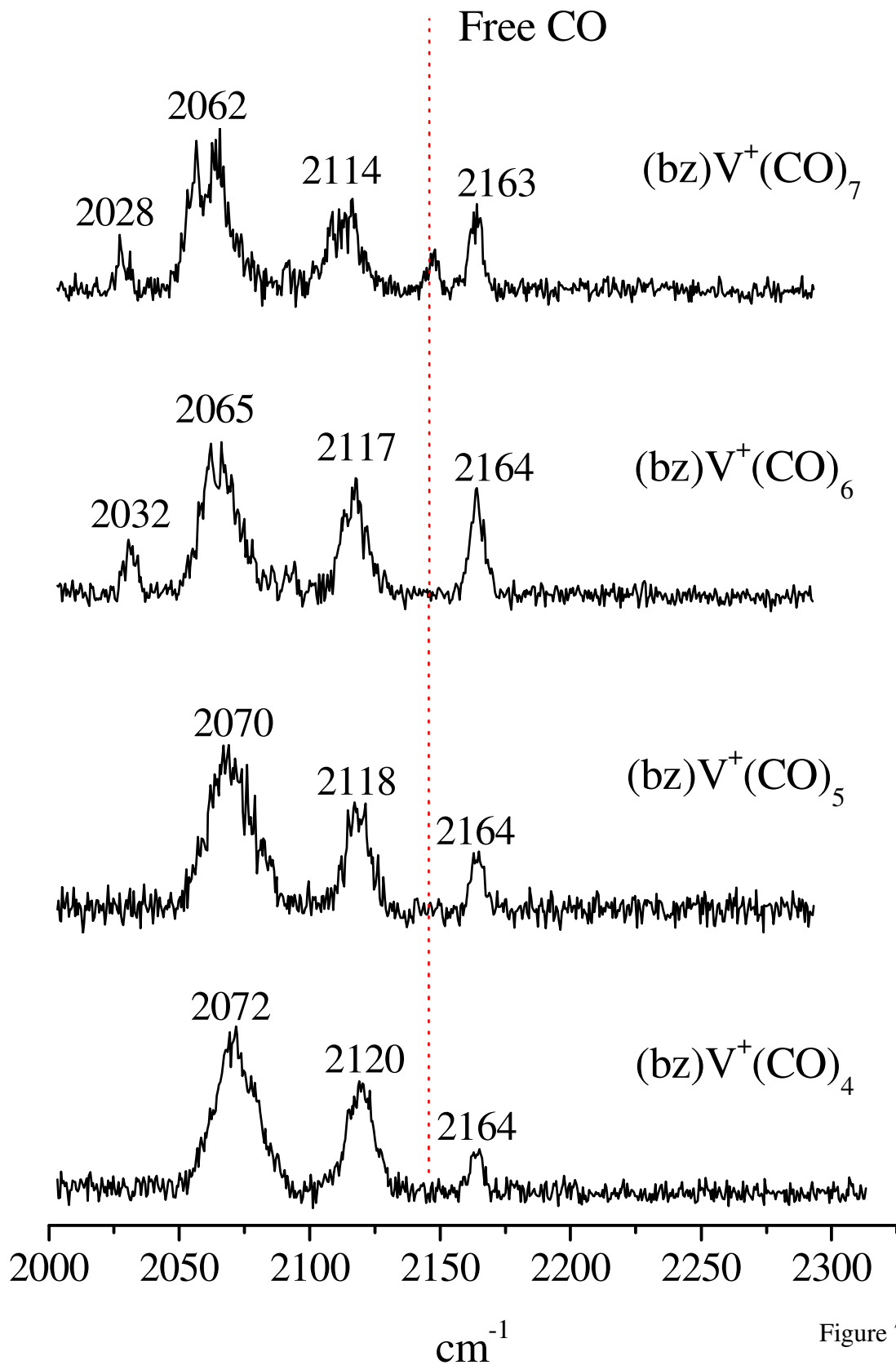


Figure 7.3

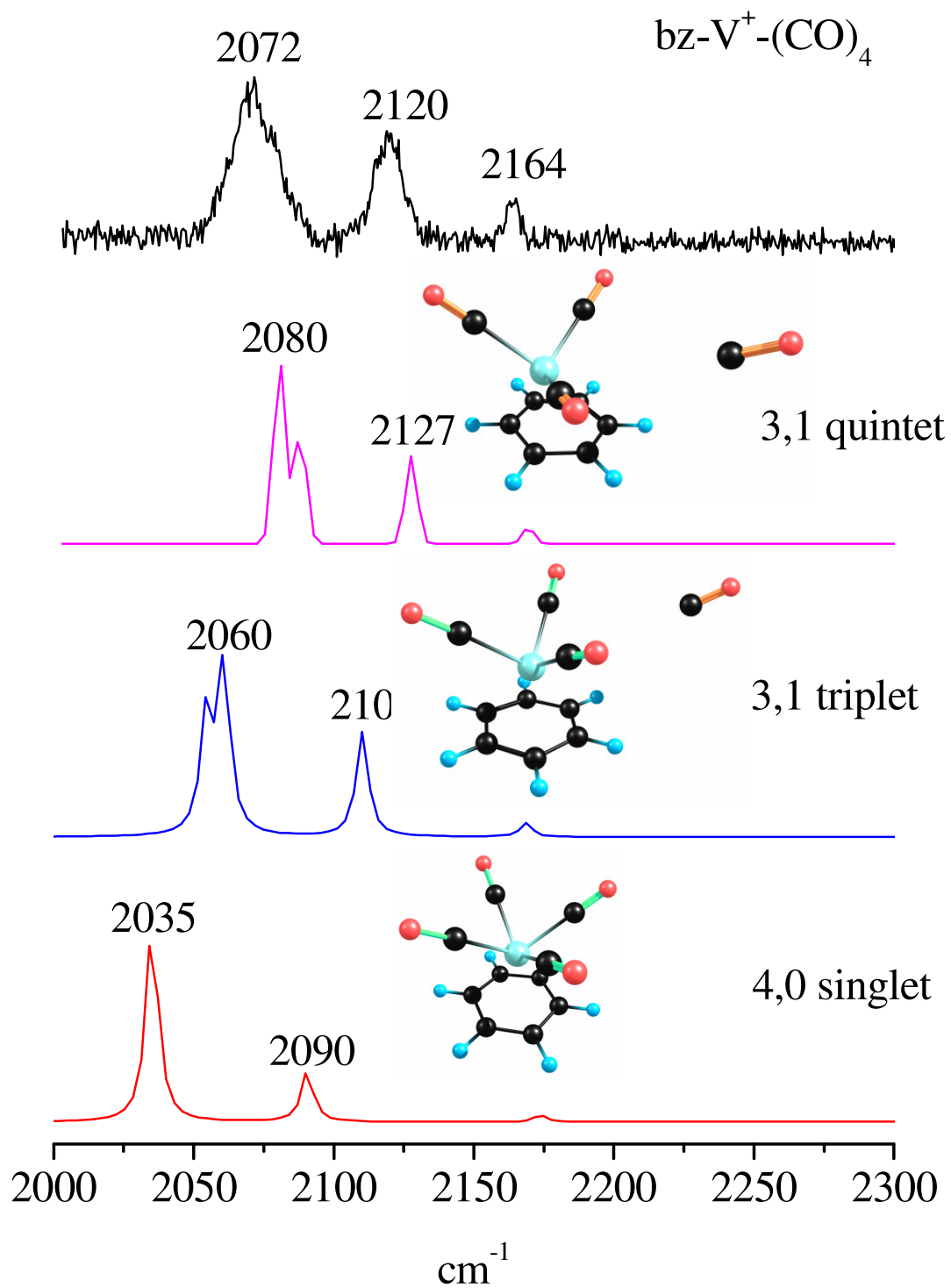


Figure 7.4

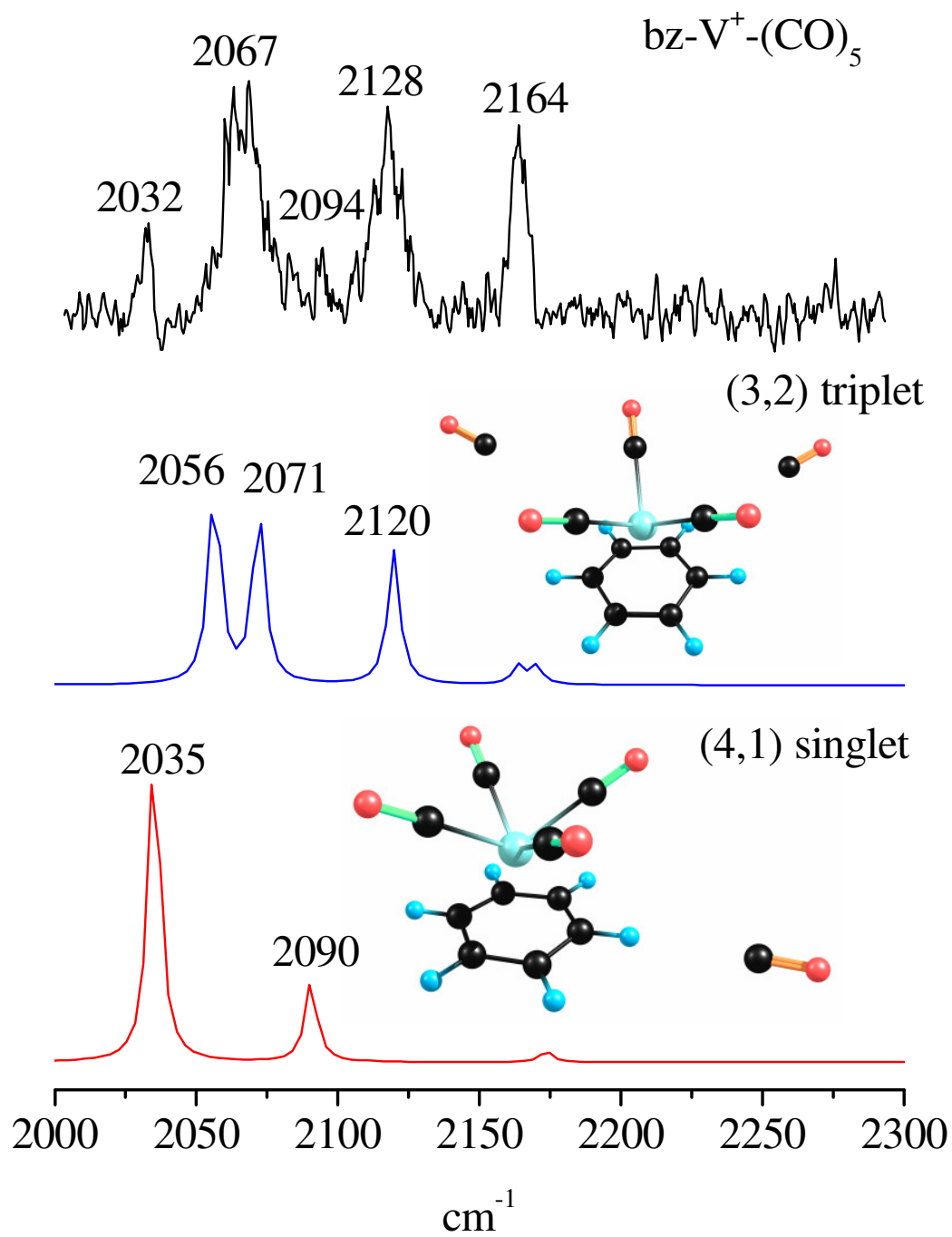


Figure 7.5

Chapter 8

Conclusions

Metal oxide cations of the form $M_nO_m^+$ ($M=La, Y, In$), transition metal carbonyl cations of the form $TM-(CO)_n^+$ ($TM=Mn, Cu, Au$), and mixed vanadium benzene-carbonyls of the form $(bz)V^+(CO)_n$ are produced by laser vaporization and analyzed in a time of flight mass spectrometer. Density functional theory calculations were employed in support of the experimental work. The bonding and structure of these systems is understood through their fragmentation patterns and spectroscopy. This work has particular application to catalytic systems. Stable metal oxide clusters that may be interesting for isolation as nanoparticles have been identified and their bonding examined. Significant details are revealed about the coordination chemistry of metal carbonyls, both homoleptic and mixed arene systems. The details of metal carbonyl bonding have been probed by investigating both classical and non-classical carbonyl systems.

The metal oxide systems demonstrate only a limited number of stoichiometries for each cluster size. Lanthanum and yttrium oxides show a preference in the mass spectrum for clusters of the form $MO(M_2O_3)_n^+$. The metal oxides are studied further using fixed frequency photodissociation. Certain clusters are produced repeatedly from the fission of larger clusters, and are deduced to be stable. Yttrium and lanthanum oxide cation clusters often fragment to produce cluster of the form $MO(M_2O_3)_n^+$. $Y_6O_8^+$ is also commonly produced. These clusters appear to be particularly stable. Density functional

theory calculations were performed to investigate the structures and bonding of these clusters. The clusters form cage structures with alternating M-O bonds. The bonding is almost exclusively ionic, and the metals have the oxidation state of the bulk metals, +3. These systems have a high per-bond energy, and may be interesting for future isolation on the macroscale as nanoparticles.

The mass spectrum of indium oxide shows enhanced signal for In_2O^+ and In_3O^+ . Photodissociation indicates some preference for certain clusters, but more variety is observed. Clusters with five metals atom that satisfy Wade's Rules appear to have enhanced stability. The In_3O^+ cluster does not satisfy Wade's Rules, but is analogous in principle due to sharing electrons in a central cavity. The dominant fragmentation process is elimination of the metal cation, which may simply be due to its fairly low ionization potential.

Manganese carbonyl cations and their argon tagged analogues are studied using gas phase infrared photodissociation spectroscopy (IRPD) and density functional theory. Comparison of the number of infrared bands, along with their positions and intensities, allows us to assign the electronic configuration and geometry for these complexes. There is a gradual decrease in spin as sequential ligands are added. The MnCO^+ complex is observed as both a quintet and a septet, with a quintet ground state. $\text{Mn}(\text{CO})_2^+$ has a quintet ground state. $\text{Mn}(\text{CO})_{3,4}^+$ are both triplets. $\text{Mn}(\text{CO})_5^+$ is a singlet, while $\text{Mn}(\text{CO})_6^+$ is observed as both a singlet and a triplet, with a singlet ground state. $\text{Mn}(\text{CO})_6^+$ has a completed coordination sphere, in line with its expected 18 electron stability and shares an octahedral structure with isoelectronic $\text{Cr}(\text{CO})_6$. The carbonyl stretch for $\text{Mn}(\text{CO})_6^+$ is less red-shifted than that of $\text{Cr}(\text{CO})_6$ due to lessened π

backbonding. This follows the trends in other metal carbonyl systems. However, the oscillator strengths of the neutrals are actually stronger than that of the cations, potentially due to polarization effects caused by the positive charge.

Copper carbonyl cations are demonstrated to be non-classical. $\text{Cu}(\text{CO})_4^+$ has a completed coordination sphere, as expected from the 18 electron rule. Previous theoretical predictions of the ground state of $\text{Cu}(\text{CO})_{1-4}^+$ have been confirmed, and this work's theory has been compared to previous theoretical work. All complexes have singlet ground states, with triplets lying much higher in energy (80-100 kcal). However, some triplet population is observed in the larger ($n=7,8$) complexes. These complexes have very high oscillator strengths compared to the singlets. A gradual red-shift is observed in the triplets as additional CO ligands are added.

Gold carbonyl cations are again demonstrated to be non-classical. Here we discover that gold carbonyl cation has a completed coordination sphere at $\text{Au}(\text{CO})_4^+$. Studies of condensed phase gold carbonyl complexes and theoretical calculations have previously determined that only the first two carbonyls are strongly bound, so this coordination number is of interest and indicates that four coordinate gold carbonyl complexes may be possible in the condensed phase under certain conditions.

Novel benzene-vanadium-carbonyl complexes of the form $\text{bz-V}^+(\text{CO})_n$ have been studied. These systems are demonstrated to have two different coordination numbers, a triplet tricarbonyl and a singlet tetracarbonyl. The tetracarbonyl is calculated to be more stable, but a greater population of the tricarbonyl is observed. This may be due to various effects caused by our cold source, or may be an artifact of density functional theory. The asymmetric carbonyl stretch is observed to be red-shifted in these complexes relative to

that of gas phase homoleptic vanadium carbonyl. The symmetric carbonyl stretch is strongly activated in these complexes. These details provide valuable information on the bonding in organometallic carbonyl complexes.

This work presents several directions for future work. The fixed frequency fragmentation techniques in this work cannot determine the structures of these metal oxides, but the spectroscopy of metal oxides would provide invaluable details on their bonding. Metal oxides are too strongly bound to fragment with a single infrared photon, and we are currently unable to tag them due to the high amount of internal energy generation in their growth. The development of tagging techniques for these systems would enable their study by IRPD.

Silver carbonyl cations present an interesting case of non-classical carbonyls, with extremely long and weak bonds. Their spectroscopy would provide fascinating details on metal carbonyl bonding, filling in the gaps left after the study of gold and copper. Silver provides an example of a system with very minimal π backbonding, and determining the gas phase coordination number and vibrational frequencies would help answer outstanding questions about the nature of π backbonding, σ donation, and electrostatic effects in carbonyl bonding. The very small gold carbonyls, $n=1,2$, would likewise provide crucial details on carbonyl bonding, but we were unable to measure their spectra. These very strongly bound complexes have a high degree of s-d mixing and bonding details could be determined from the effect on the position of their vibrational bands. Multiple metal carbonyl systems, like $\text{Mn}_2(\text{CO})_n^+$ would also help resolve outstanding bonding questions. The effect of sharing metal-metal electrons on carbonyl bonding has not been well described, and investigating systems with known mononuclear

spectroscopy, like manganese carbonyl, would help describe these interactions. Larger mixed metal carbonyl benzene systems would also be fascinating. Multidecker metal-benzene sandwich complexes of the form $M_n b z_m$ are of great interest due to the work of Nakajima, and the addition of carbonyls to these complexes could prove to be a sensitive probe of changes in the electronic structure as additional sandwich layers were added. IRPD studies, or other novel spectroscopy techniques, of these various complexes would further refine the understanding of metal-molecule chemistry.

APPENDIX A

PHOTODISSOCIATION OF YTTRIUM AND LANTHANUM OXIDE

CLUSTER CATIONS

STRUCTURES, ENERGIES, AND FREQUENCIES

The complete citation for reference number 66 is :

Gaussian 03, Revision B.02, M. J. Frisch, G. W. Trucks, H. B. Schlegel, G. E. Scuseria, M. A. Robb, J. R. Cheeseman, J. A. Montgomery, Jr., T. Vreven, K. N. Kudin, J. C. Burant, J. M. Millam, S. S. Iyengar, J. Tomasi, V. Barone, B. Mennucci, M. Cossi, G. Scalmani, N. Rega, G. A. Petersson, H. Nakatsuji, M. Hada, M. Ehara, K. Toyota, R. Fukuda, J. Hasegawa, M. Ishida, T. Nakajima, Y. Honda, O. Kitao, H. Nakai, M. Klene, X. Li, J. E. Knox, H. P. Hratchian, J. B. Cross, C. Adamo, J. Jaramillo, R. Gomperts, R. E. Stratmann, O. Yazyev, A. J. Austin, R. Cammi, C. Pomelli, J. W. Ochterski, P. Y. Ayala, K. Morokuma, G. A. Voth, P. Salvador, J. J. Dannenberg, V. G. Zakrzewski, S. Dapprich, A. D. Daniels, M. C. Strain, O. Farkas, D. K. Malick, A. D. Rabuck, K. Raghavachari, J. B. Foresman, J. V. Ortiz, Q. Cui, A. G. Baboul, S. Clifford, J. Cioslowski, B. B. Stefanov, G. Liu, A. Liashenko, P. Piskorz, I. Komaromi, R. L. Martin, D. J. Fox, T. Keith, M. A. Al-Laham, C. Y. Peng, A. Nanayakkara, M. Challacombe, P. M. W. Gill, B. Johnson, W. Chen, M. W. Wong, C. Gonzalez, and J. A. Pople, Gaussian, Inc., Pittsburgh PA, 2003.

Table A.1: The energies computed using B3LYP for the yttrium oxide clusters studied here. All units are kcal/mol.

	Atomization Energy	Energy per Bond	Spin Multiplicity
YO	154.8	77.4	2
YO ₂	235.6	58.9	2
Y ₂ O ₃	815.3	135.6	1
Y ₂ O ₃ ⁺	819.5	136.6	2
Y ₃ O ₄	1175.6	130.6	2
Y ₃ O ₄ ⁺	1248.9	138.8	1
Y ₄ O ₆	1789.1	149.1	1
Y ₄ O ₆ ⁺	1790.9	149.2	2
Y ₅ O ₇	2126.0	141.7	2
Y ₅ O ₇ ⁺	2200.1	146.7	1
Y ₇ O ₁₀	3036.5	151.8	2
Y ₇ O ₁₀ ⁺	3101.9	155.1	1

Table A.2: The energies computed using B3LYP for the lanthanum oxide clusters studied here. All units are kcal/mol.

	Atomization Energy	Energy per Bond	Spin Multiplicity
LaO	229.1	114.5	2
LaO ₂	400.9	100.2	2
La ₂ O ₃	652.1	108.7	1
La ₂ O ₃ ⁺	795.6	132.6	2
La ₃ O ₄	1153.0	128.1	2
La ₃ O ₄ ⁺	1210.4	134.5	1
La ₅ O ₇	2064.1	137.6	2
La ₅ O ₇ ⁺	2130.0	142.0	1

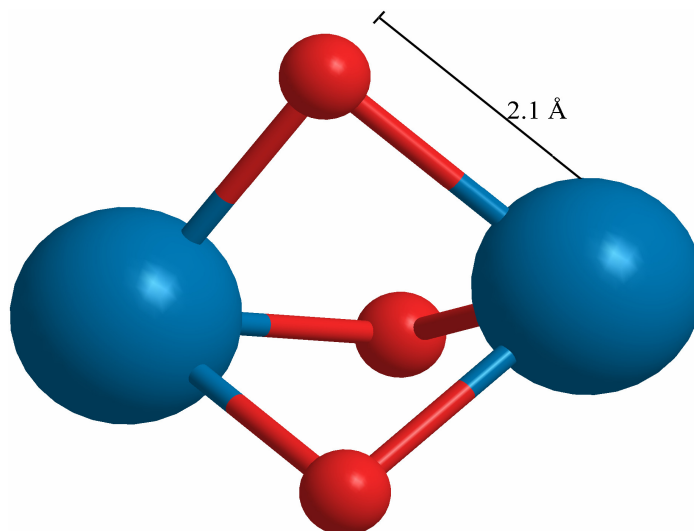


Figure A.1: Y_2O_3 optimized geometry using B3LYP.

Spin multiplicity: $2S+1=1$

B3LYP vibrational frequencies, in cm^{-1} , with IR intensities in parenthesis:
 294.8039(0.0157), 299.4594(0.0163), 341.4095(75.6776), 566.5360(184.0426),
 597.5202(269.2738), 648.3731(0.3777)

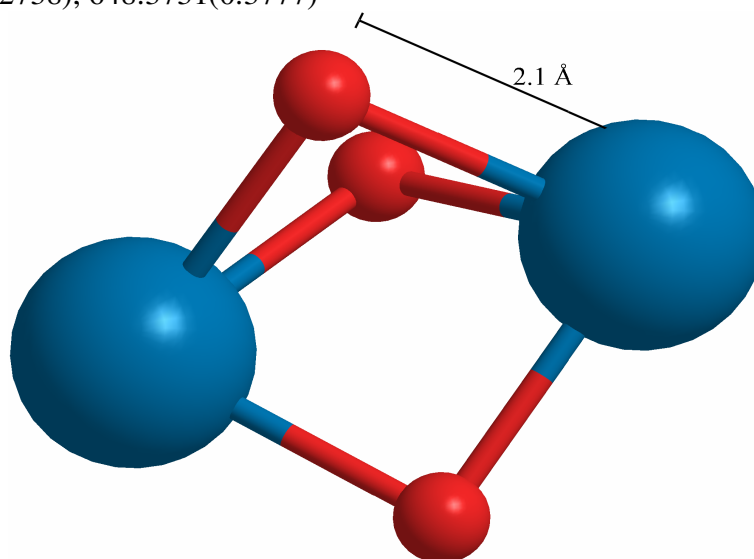


Figure A.2: Y_2O_3^+ optimized geometry using B3LYP.

Spin multiplicity: $2S+1=2$

B3LYP vibrational frequencies, in cm^{-1} , with IR intensities in parenthesis:
 198.6455(26.5821), 271.8808(34.5386), 320.0166(0.8591), 357.7280(2.7811),
 371.3711(0.0020), 397.4199(8.5321), 555.8618(148.3452), 614.1757(314.6896),
 640.7352(11.6385)

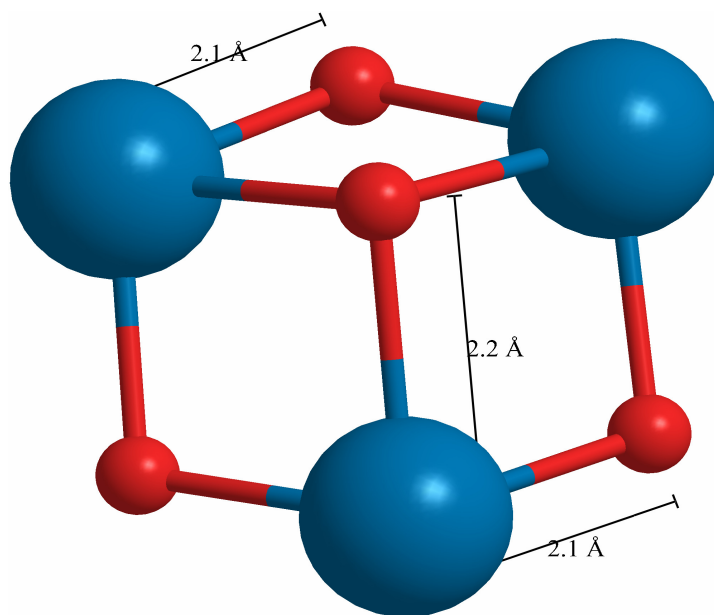


Figure A.3: Y₃O₄ optimized geometry using B3LYP.

Spin multiplicity: $2S+1=2$

B3LYP vibrational frequencies, in cm^{-1} , with IR intensities in parenthesis:
160.7167(6.3201), 164.8690(8.4815), 201.2802(21.7829), 202.0939(23.0606),
231.7138(22.0452), 289.8302(1.0630), 394.6674(81.2620), 395.8605(62.0081),
443.7018(78.4104), 454.2994(0.7941), 525.8355(840.7029), 530.7597(763.9568),
558.1876(895.0876), 563.4924(820.3416), 569.6911(95.6066)

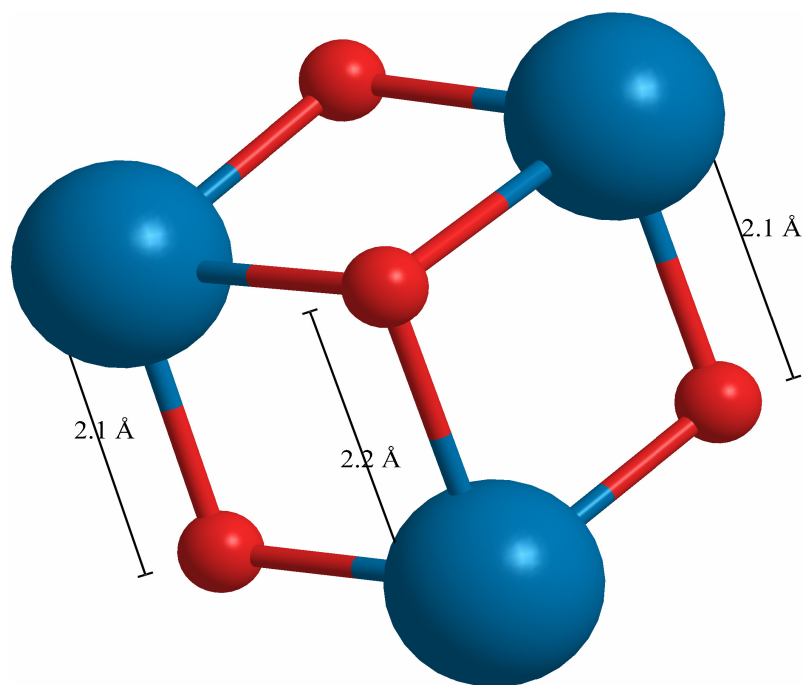


Figure A.4: $Y_3O_4^+$ optimized geometry using B3LYP.

Spin multiplicity: $2S+1=1$

B3LYP vibrational frequencies, in cm^{-1} , with IR intensities in parenthesis:
171.0158(14.4232), 171.6685(15.0620), 207.0475(4.1160), 208.1120(3.9595),
239.7684(30.1523), 308.1105(0.3474), 402.9077(33.1014), 404.4799(31.8857),
459.4788(200.1613), 473.7377(0.0002), 564.7200(144.9724), 568.6168(140.8275),
586.3768(39.9730), 683.4920(355.0992), 685.7982(360.8064)

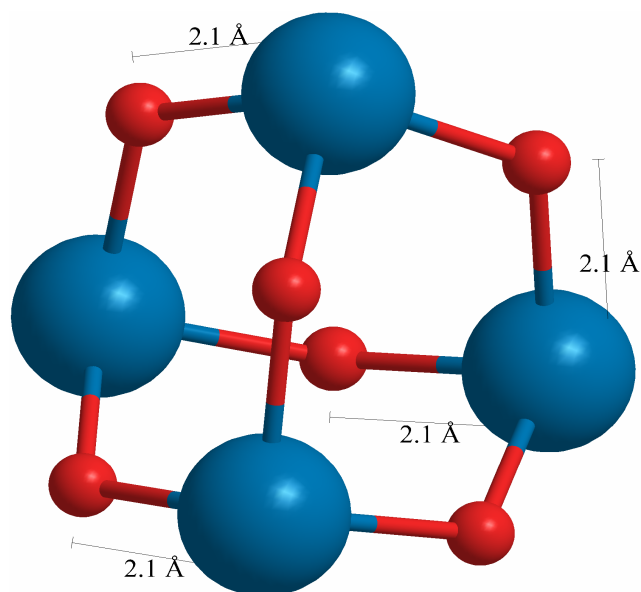


Figure A.5: Y_4O_6 optimized geometry using B3LYP.

Spin multiplicity: $2S+1=1$

B3LYP vibrational frequencies, in cm^{-1} , with IR intensities in parenthesis:
110.6454(0.0076), 112.4751(0.0155), 150.2576(35.3206), 150.7689(35.0455),
153.3657(34.8651), 171.7288(0.2006), 174.6992(0.1706), 174.7896(0.0053),
258.8313(0.0195), 280.3299(17.3793), 283.2706(18.8815), 283.9628(16.8762),
433.8690(135.9641), 435.0273(112.2697), 435.3698(245.1470), 437.4279(174.4619),
438.4888(142.6090), 447.8378(2.5463), 534.4511(0.0335), 536.6153(0.0209),
537.4455(0.0200), 739.8130(455.0830), 740.7677(454.8219), 742.1775(455.0861)

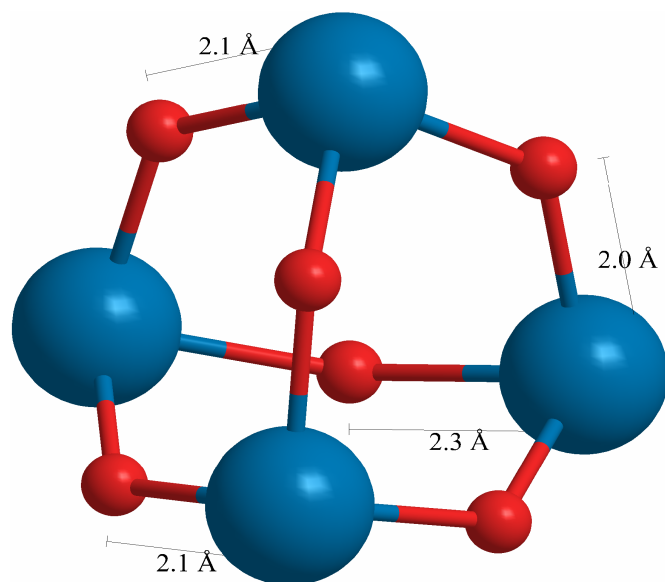


Figure A.6: $Y_4O_6^+$ optimized geometry using B3LYP.

Spin multiplicity: $2S+1=2$

B3LYP vibrational frequencies, in cm^{-1} , with IR intensities in parenthesis:
123.6213(43.2243), 144.2867(25.6132), 153.9291(31.0470), 166.8512(7.6139),
230.7769(2.8042), 252.6904(20.3983), 266.1160(22.2624), 274.1908(1.0557),
281.9409(30.1744), 409.3986(0.0123), 411.8085(237.8755), 417.5174(154.5669),
428.7791(96.3250), 436.6043(43.3367), 450.2424(2.0817), 564.8861(11.6553),
723.9996(292.1589), 774.0870(508.0853), 781.0462(372.6725)

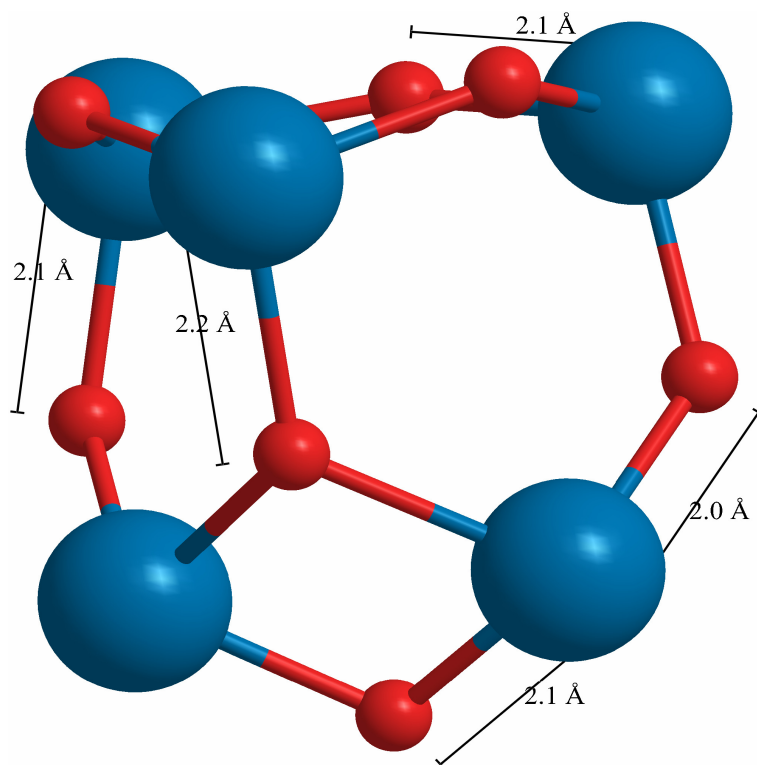


Figure A.7: Y_5O_7 optimized geometry using B3LYP.

Spin multiplicity: $2S+1=2$

B3LYP vibrational frequencies, in cm^{-1} , with IR intensities in parenthesis:
 63.2228(1.0841), 74.6943(0.1478), 86.3628(1.1010), 105.0323(0.1613),
 111.7353(5.8884), 126.7732(1.8083), 135.3959(9.7447), 142.3541(2.1686),
 184.8963(10.5619), 187.2212(21.3760), 211.5441(30.3618), 230.6135(1.7742),
 231.3851(0.1538), 259.3868(1.6744), 274.0294(7.9879), 279.9099(6.8439),
 381.8586(97.0849), 389.2091(121.6377), 424.5336(63.6249), 432.2804(2.2453),
 433.5691(115.7593), 438.1549(11.1653), 508.7560(257.8439), 518.8439(1.0287),
 552.0331(10.4442), 565.7620(0.0450), 601.7653(489.7289), 623.1031(780.9187),
 736.4154(190.0429), 760.1646(172.7955)

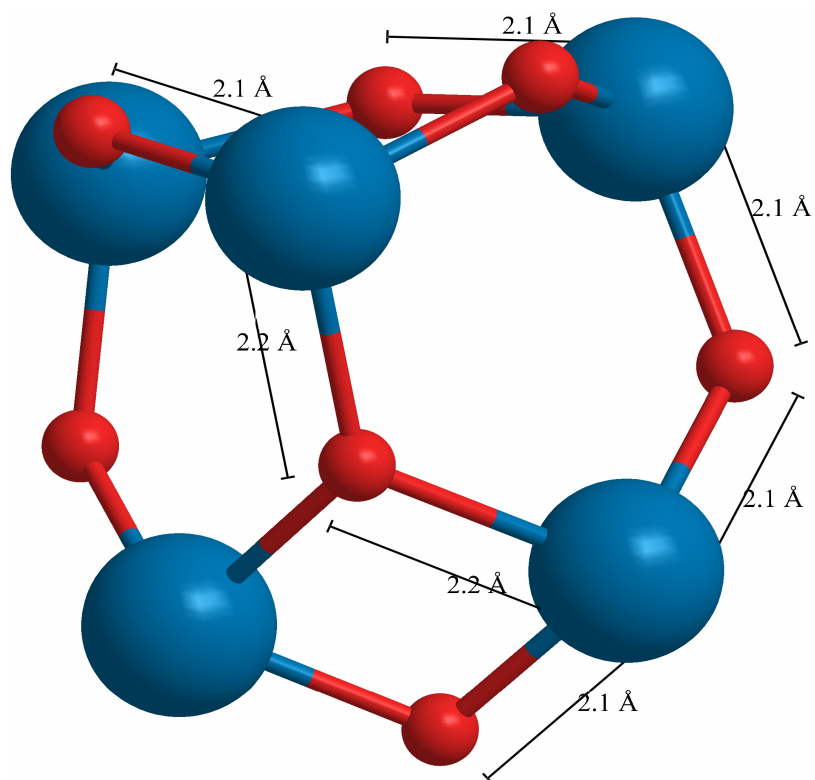


Figure A.8: $Y_5O_7^+$ optimized geometry using B3LYP.

Spin multiplicity: $2S+1=1$

B3LYP vibrational frequencies, in cm^{-1} , with IR intensities in parenthesis:
 65.8693(1.1104), 68.6503(0.4280), 91.0806(7.1661), 109.4180(19.2475),
 115.4146(0.4415), 128.9486(10.7479), 144.7740(4.5577), 146.7391(14.3253),
 198.1332(16.7467), 199.7415(65.6676), 226.8546(38.6982), 235.1523(0.6374),
 239.8445(3.0046), 275.0473(4.7165), 283.6132(43.8554), 326.8087(41.0345),
 380.1023(10.3007), 389.7676(105.7278), 417.6228(64.8793), 427.4296(243.6482),
 431.8291(117.2529), 437.3921(8.7710), 513.3560(130.9789), 546.5586(44.9815),
 570.5118(21.9943), 572.8869(90.8212), 702.7067(403.5465), 722.8652(409.8438),
 780.4021(730.3512), 794.3694(372.7628)

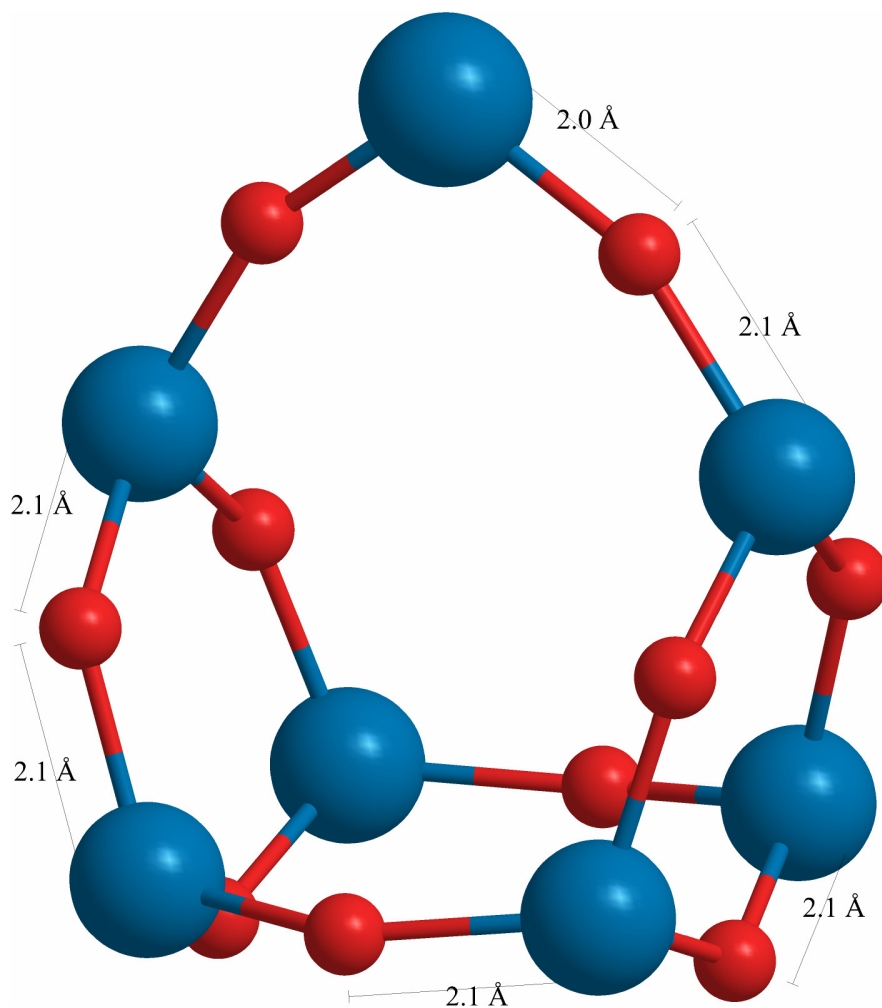


Figure A.9: Y_7O_{10} optimized geometry using B3LYP.

Spin multiplicity: $2S+1=2$

B3LYP vibrational frequencies, in cm^{-1} , with IR intensities in parenthesis:
 30.2867(0.0074), 32.1966(0.0021), 79.6521(2.2556), 79.8782(1.3555), 80.2610(7.1193),
 118.2271(2.6355), 120.6364(0.0053), 126.5755(17.8516), 126.8562(23.7572),
 165.1122(32.7123), 168.8652(8.2721), 186.2637(1.6694), 193.9274(10.7677),
 200.8347(123.9105), 209.4968(30.4598), 221.3915(32.4618), 238.6737(103.1465),
 251.3926(14.5975), 276.9752(20.5310), 286.5914(82.0513), 312.1875(0.0689),
 330.5310(122.3069), 342.9908(31.4138), 392.0752(135.3759), 398.5755(0.4969),
 401.0130(0.0513), 403.8454(0.0005), 411.8669(142.3215), 414.2357(200.6474),
 577.3760(0.0853), 613.5149(12.3265), 746.4628(1847.0594), 758.0708(824.2671),
 771.4560(1333.8643), 789.5962(25.1799), 816.4267(154.7381)

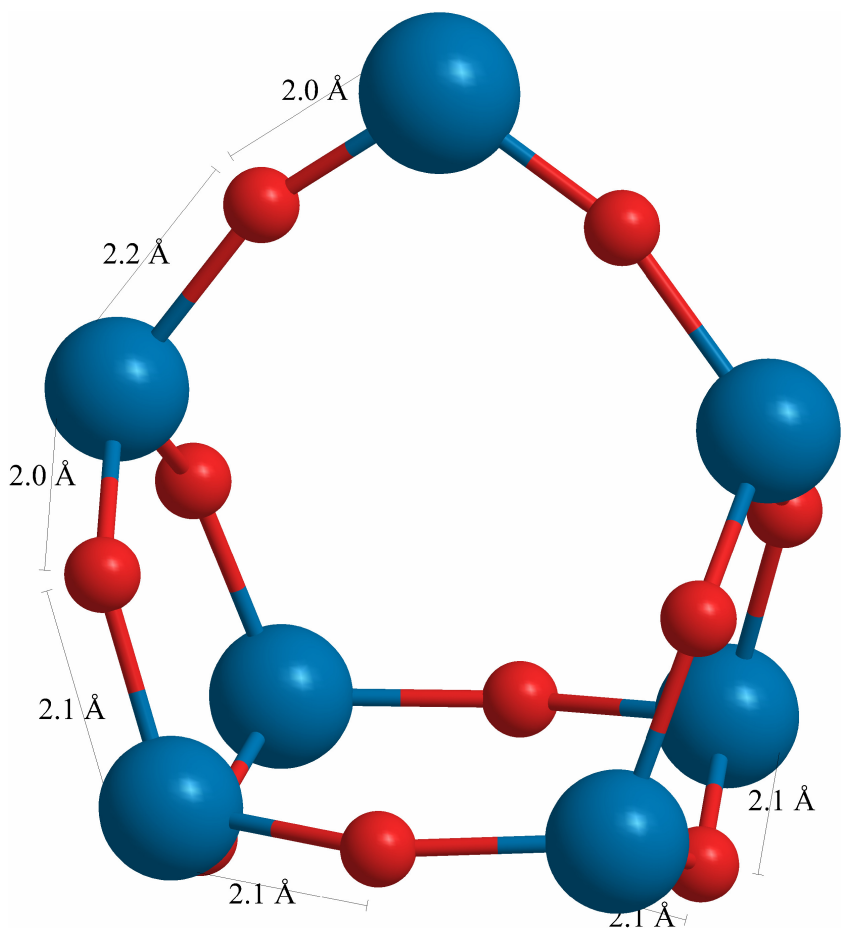


Figure A.10: $\text{Y}_7\text{O}_{10}^+$ optimized geometry using B3LYP.

Spin multiplicity: $2S+1=1$

B3LYP vibrational frequencies, in cm^{-1} , with IR intensities in parenthesis:

20.4043(6.3823), 32.8643(0.7528), 34.4230(0.6295), 41.4499(0.4106), 58.4914(0.0242),
 81.9362(2.0555), 85.0374(8.2873), 103.5836(4.2272), 114.7710(4.0344),
 122.8409(1.7613), 126.5363(0.0641), 129.8166(13.7768), 132.5674(21.3976),
 148.7156(0.7101), 171.6498(7.8738), 176.7056(78.6620), 186.1138(0.8033),
 187.9726(0.6411), 203.0566(9.3694), 208.6533(112.5018), 223.3141(21.8360),
 229.0545(63.3510), 235.6569(141.3745), 255.8196(25.1034), 273.8482(66.4015),
 289.0706(9.6461), 300.7516(0.2364), 330.4272(121.1584), 339.3907(26.8906),
 389.8722(101.0078), 395.3065(26.3685), 401.3236(1.9558), 402.4519(0.4881),
 411.0243(187.8365), 411.9433(193.1899), 587.0284(0.3757), 587.5016(7.7723),
 603.1403(0.0041), 641.5789(9.4449), 764.5565(1333.4317), 774.0577(992.8578),
 789.4271(1701.6095), 804.6659(14.4902), 808.5565(0.1683), 844.0737(185.8964)

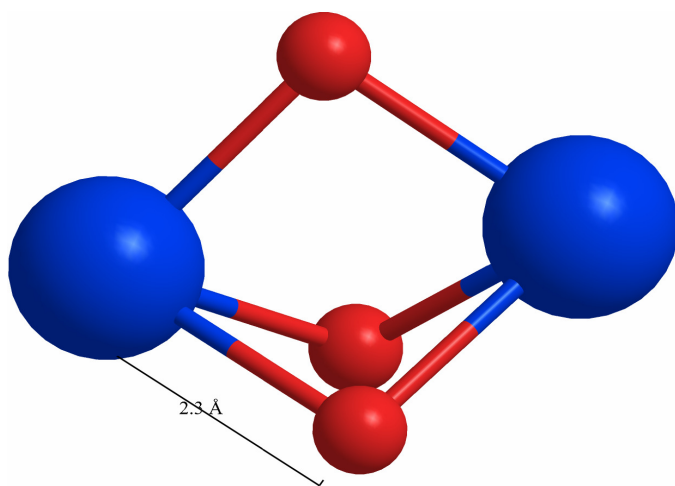


Figure A.11: La_2O_3 optimized geometry using B3LYP.

Spin multiplicity: $2S+1=1$

B3LYP vibrational frequencies, in cm^{-1} , with IR intensities in parenthesis:
 167.5632(26.8922), 263.4842(31.0534), 323.6255(2.0809), 347.2468(10.4297),
 491.4919(140.9536), 567.6181(339.3676), 568.8000(5.8649)

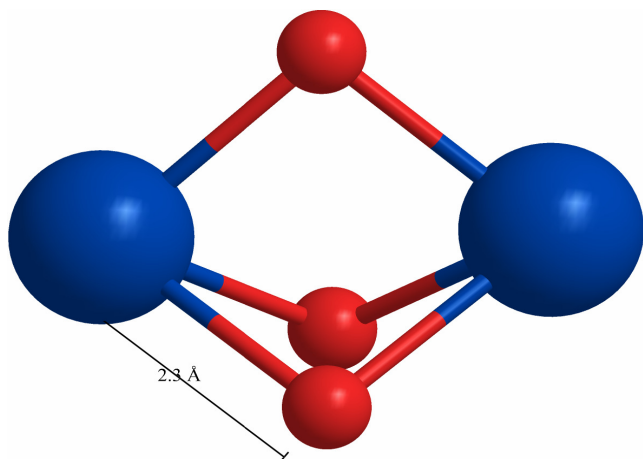


Figure A.12: La_2O_3^+ optimized geometry using B3LYP.

Spin multiplicity: $2S+1=2$

B3LYP vibrational frequencies, in cm^{-1} , with IR intensities in parenthesis:
 166.9270(26.6712), 242.9748(0.0044), 262.8196(30.9289), 323.6344(2.1067),
 347.1358(10.5245), 491.2794(140.8980), 567.6604(340.0399), 568.7613(5.3160)

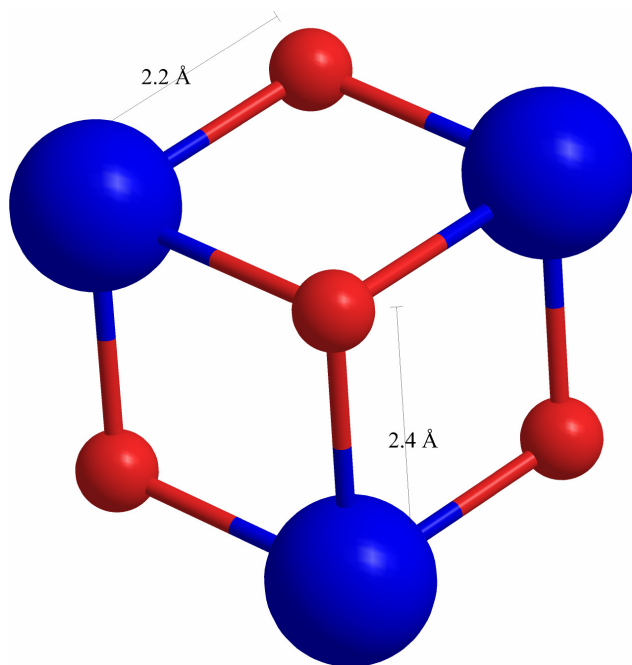


Figure A.13: La_3O_4 optimized geometry using B3LYP.

Spin multiplicity: $2S+1=2$

B3LYP vibrational frequencies, in cm^{-1} , with IR intensities in parenthesis:
136.0055(9.5563), 143.1994(7.8869), 151.4840(13.1210), 155.0574(20.5174),
20.5174(14.6867), 231.5125(6.11060), 349.0396(84.4080), 353.1341(32.5051),
388.9950(44.5382), 403.3043(0.1262), 471.5872(398.1967), 473.3951(328.6216),
505.1591(260.5793), 506.6895(619.4531), 513.3034(1466.7457)

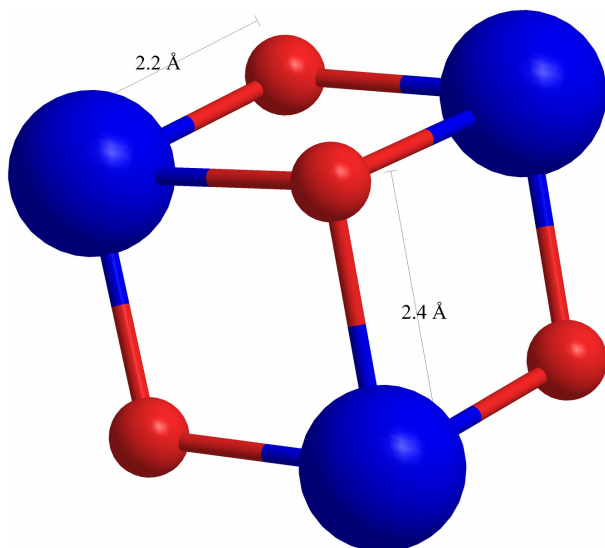


Figure A.14: La_3O_4^+ optimized geometry using B3LYP.

Spin multiplicity: $2S+1=1$

B3LYP vibrational frequencies, in cm^{-1} , with IR intensities in parenthesis:
142.5763(14.0078), 147.5126(13.1457), 156.2897(0.0628), 158.4294(0.2382),
197.8976(20.7218), 247.5325(4.7252), 354.1634(34.4754), 357.8271(35.3853),
405.0050(176.4316), 419.8530(0.0494), 494.5141(119.3488), 496.7493(124.1908),
519.8272(33.3674), 629.3541(385.2355), 631.4367(389.1194)

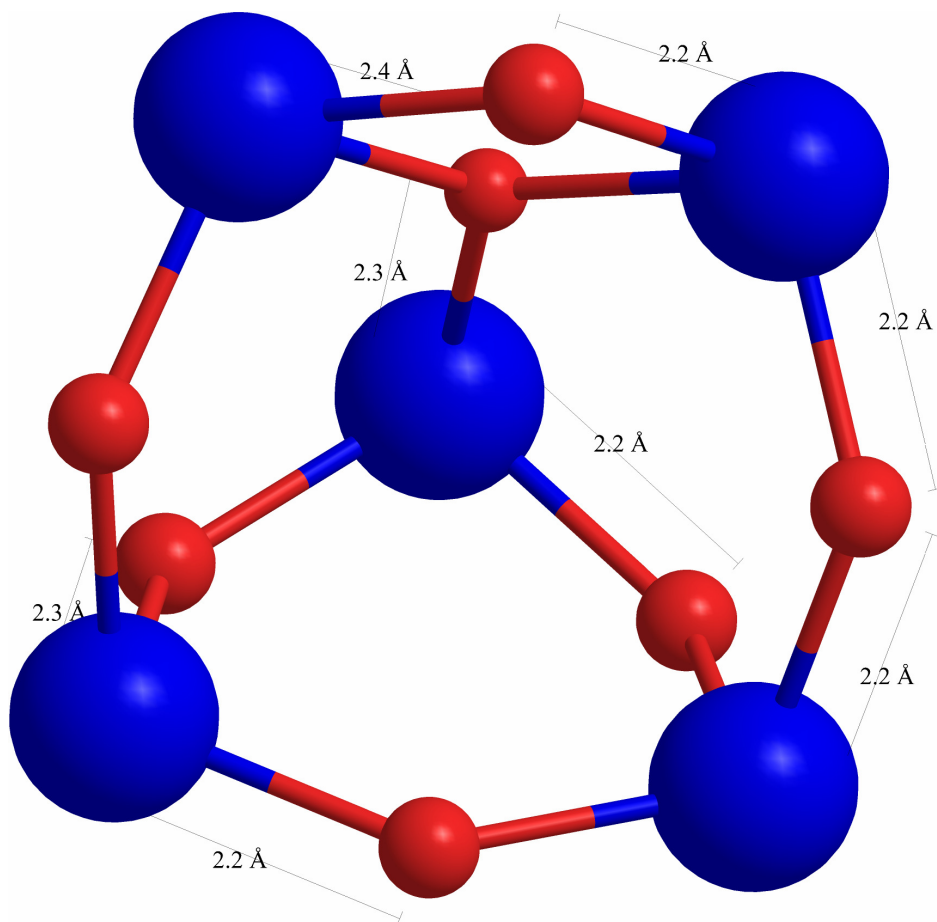


Figure A.15: La_5O_7 optimized geometry using B3LYP.

Spin multiplicity: $2S+1=2$

B3LYP vibrational frequencies, in cm^{-1} , with IR intensities in parenthesis:
 46.3856(0.3351), 73.4708(2.9240), 77.2667(0.7847), 86.5122(5.4300),
 107.7506(2.3236), 109.0530(1.3631), 109.5000(4.0924), 159.0927(0.5173),
 161.4495(26.4621), 170.8673(30.0019), 184.9751(0.6382), 196.5761(1.1629),
 214.0435(1.9554), 229.6036(15.0566), 254.2335(2.7640), 324.5605(91.2516),
 338.1484(28.2712), 348.5204(8.9029), 355.0812(96.0741), 356.0609(64.0841),
 364.9583(27.5007), 450.1933(2.1290), 455.4572(212.5729), 488.2359(10.6885),
 500.9340(0.1742), 548.6781(713.4319), 570.3196(970.8342), 682.7667(206.7483),
 706.1183(179.8960)

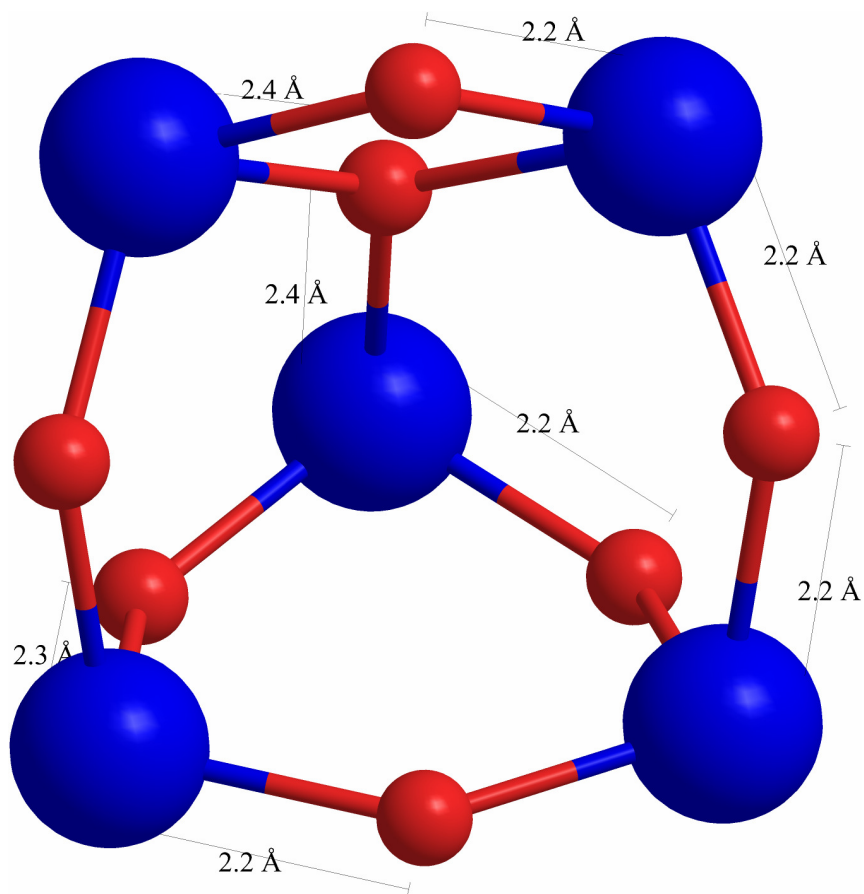


Figure A.16: La_5O_7^+ optimized geometry using B3LYP.

Spin multiplicity: $2S+1=1$

B3LYP vibrational frequencies, in cm^{-1} , with IR intensities in parenthesis:
 33.4722(1.0415), 48.4372(0.0316), 71.4277(15.0271), 85.2487(0.1249),
 87.0380(6.0675), 108.6134(4.0638), 110.9814(5.9819), 113.6725(5.8061),
 169.8986(28.9079), 170.8137(0.8695), 183.1009(18.8932), 186.6745(9.3914),
 199.1222(13.8450), 232.5688(40.0183), 237.2914(27.3339), 286.0936(28.5825),
 321.5828(89.1415), 336.0071(24.5147), 338.8096(0.9026), 346.5673(188.5083),
 350.6324(143.0878), 363.4988(20.5335), 442.5164(123.1444), 486.2670(34.5443),
 505.7770(12.2290), 505.9767(83.1256), 644.9193(481.2439), 661.9667(468.8717),
 721.8592(804.6682), 733.9625(367.0247)

APPENDIX B

INFRARED SPECTROSCOPY AND STRUCTURES OF MANGANESE

CARBONYL CATIONS, $\text{Mn}(\text{CO})_n^+$ ($n=1-9$)

CALCULATED STRUCTURES, ENERGETICS, AND VIBRATIONS

The complete citation for reference number 50 is :

Gaussian 03, Revision B.02, M. J. Frisch, G. W. Trucks, H. B. Schlegel, G. E. Scuseria, M. A. Robb, J. R. Cheeseman, J. A. Montgomery, Jr., T. Vreven, K. N. Kudin, J. C. Burant, J. M. Millam, S. S. Iyengar, J. Tomasi, V. Barone, B. Mennucci, M. Cossi, G. Scalmani, N. Rega, G. A. Petersson, H. Nakatsuji, M. Hada, M. Ehara, K. Toyota, R. Fukuda, J. Hasegawa, M. Ishida, T. Nakajima, Y. Honda, O. Kitao, H. Nakai, M. Klene, X. Li, J. E. Knox, H. P. Hratchian, J. B. Cross, C. Adamo, J. Jaramillo, R. Gomperts, R. E. Stratmann, O. Yazyev, A. J. Austin, R. Cammi, C. Pomelli, J. W. Ochterski, P. Y. Ayala, K. Morokuma, G. A. Voth, P. Salvador, J. J. Dannenberg, V. G. Zakrzewski, S. Dapprich, A. D. Daniels, M. C. Strain, O. Farkas, D. K. Malick, A. D. Rabuck, K. Raghavachari, J. B. Foresman, J. V. Ortiz, Q. Cui, A. G. Baboul, S. Clifford, J. Cioslowski, B. B. Stefanov, G. Liu, A. Liashenko, P. Piskorz, I. Komaromi, R. L. Martin, D. J. Fox, T. Keith, M. A. Al-Laham, C. Y. Peng, A. Nanayakkara, M. Challacombe, P. M. W. Gill, B. Johnson, W. Chen, M. W. Wong, C. Gonzalez, and J. A. Pople, Gaussian, Inc., Pittsburgh PA, 2003.

Table B.1: The electronic states calculated for $\text{Mn}(\text{CO})^+$ with the B3LYP functional using Gaussian03. The Def 2 TZVPP basis set was used for all atoms.

Isomer	Total Energy (Hartrees)	Relative Energy (kcal/mol)
$^3\text{Mn}(\text{CO})^+$	-1264.0568491	+33.6
$^5\text{Mn}(\text{CO})^+$	-1264.1104673	+0.74
$^7\text{Mn}(\text{CO})^+$	-1264.1116475	0.0

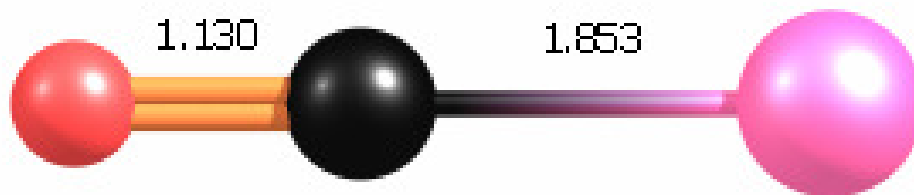


Figure B.1: The optimized geometry of the triplet MnCO^+ calculated with the B3LYP functional using Gaussian2003. The Def 2 TZVPP basis set was used for all atoms.

Table B.2: The unscaled normal mode frequencies and intensities (km/mol) are reported from this same level of theory.

Frequency	Intensity
351.5175	1.5568
351.5176	1.5568
454.0709	9.6207
2176.9108	402.1439

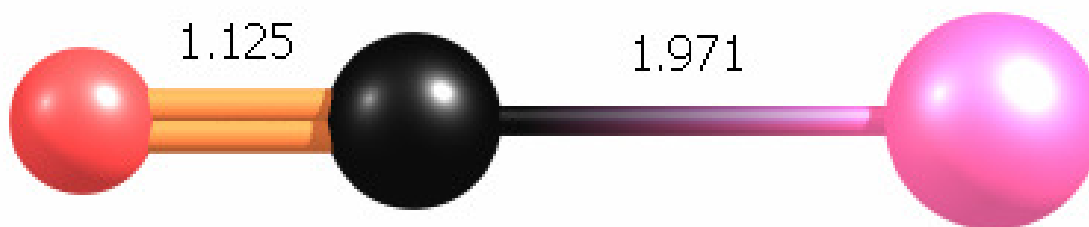


Figure B.2: The optimized geometry of the quintet MnCO^+ calculated with the B3LYP functional using Gaussian2003. The Def 2 TZVPP basis set was used for all atoms.

Table B.3: The unscaled normal mode frequencies and intensities (km/mol) are reported from this same level of theory.

Frequency	Intensity
279.474	0.5224
296.3447	3.592
387.4012	1.4532
2203.5303	409.6587

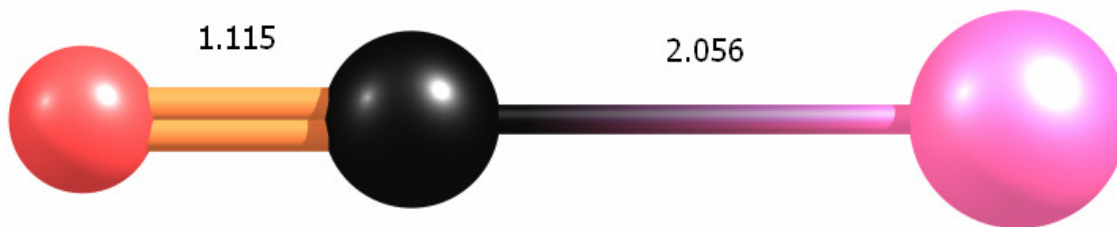


Figure B.3: The optimized geometry of the septet MnCO^+ calculated with the B3LYP functional using Gaussian2003. The Def 2 TZVPP basis set was used for all atoms.

Table B.4: The unscaled normal mode frequencies and intensities (km/mol) are reported from this same level of theory.

Frequency	Intensity
116.83554939	4.5931
116.83554939	4.5931
149.71820784	35.3764
2283.17409708	19.8158

Table B.5: The electronic states calculated for $\text{Mn}(\text{CO})^+\text{Ar}$ with the B3LYP functional using Gaussian03. The Def 2 TZVPP basis set was used for all atoms.

Isomer	Total Energy (Hartrees)	Relative Energy (kcal/mol)
$^3\text{Mn}(\text{CO})^+\text{Ar}$	-1791.624557	+33.5
$^5\text{Mn}(\text{CO})^+\text{Ar}$	-1791.6779615	+0.75
$^7\text{Mn}(\text{CO})^+\text{Ar}$	-1791.679162	0.0



Figure B.4: The optimized geometry of the triplet MnCO^+Ar calculated with the B3LYP functional using Gaussian2003. The Def 2 TZVPP basis set was used for all atoms.

Table B.6: The unscaled normal mode frequencies and intensities (km/mol) are reported from this same level of theory.

Frequency	Intensity
70.6456	4.6157
174.7477	10.1311
384.5709	0.1339
384.6424	0.1841
454.9874	7.3328
2169.1925	516.653



Figure B.5: The optimized geometry of the quintet MnCO^+Ar calculated with the B3LYP functional using Gaussian2003. The Def 2 TZVPP basis set was used for all atoms.

Table B.7: The unscaled normal mode frequencies and intensities (km/mol) are reported from this same level of theory.

Frequency	Intensity
41.6503	5.1936
64.9502	3.7359
169.8701	7.8971
291.418	0.2668
336.164	1.4049
403.76	1.0449
2192.7254	544.971



Figure B.6: The optimized geometry of the septet MnCO⁺Ar calculated with the B3LYP functional using Gaussian2003. The Def 2 TZVPP basis set was used for all atoms.

Table B.8: The unscaled normal mode frequencies and intensities (km/mol) are reported from this same level of theory.

Frequency	Intensity
42.35002504	5.1936
66.04136336	3.7359
172.72401936	7.8971
296.3138224	0.2668
341.8115552	1.4049
410.543168	1.0449
2229.56318672	544.9711

Table B.9: The electronic states calculated for $\text{Mn}(\text{CO})^+\text{Ar}_2$ with the B3LYP functional using Gaussian03. The Def 2 TZVPP basis set was used for all atoms.

Isomer	Total Energy (Hartrees)	Relative Energy (kcal/mol)
$^3\text{Mn}(\text{CO})^+\text{Ar}_2$	-2319.18677207	+30.6
$^5\text{Mn}(\text{CO})^+\text{Ar}_2$	-2319.2354864	+1.46
$^7\text{Mn}(\text{CO})^+\text{Ar}_2$	-2319.2378266	0.0

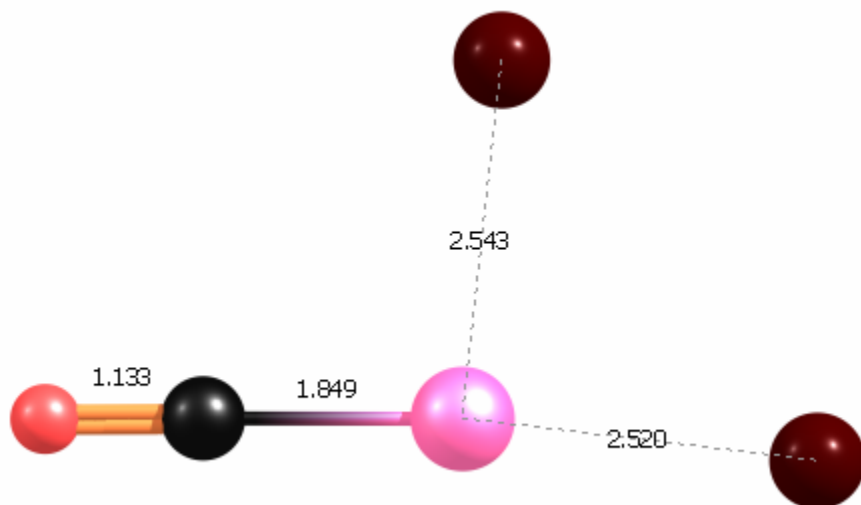


Figure B.7: The optimized geometry of the triplet MnCO^+Ar_2 calculated with the B3LYP functional using Gaussian2003. The Def 2 TZVPP basis set was used for all atoms.

Table B.10: The unscaled normal mode frequencies and intensities (km/mol) are reported from this same level of theory.

Frequency	Intensity
67.4989	0.8764
79.55	3.8183
80.4459	0.7618
154.0469	11.4492
164.7087	8.4297
396.2145	0.1092
428.5384	0.4933
461.6942	10.1385
2150.2994	556.1642

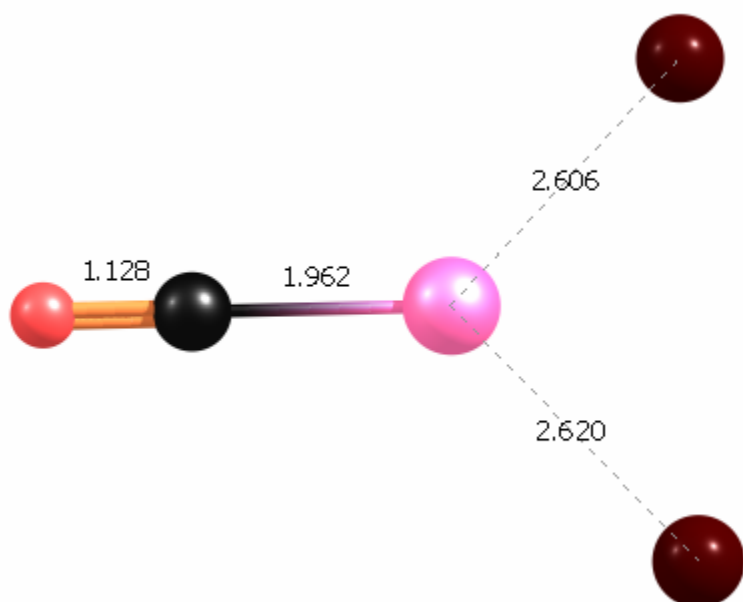


Figure B.8: The optimized geometry of the quintet MnCO^+Ar_2 calculated with the B3LYP functional using Gaussian2003. The Def 2 TZVPP basis set was used for all atoms.

Table B.11: The unscaled normal mode frequencies and intensities (km/mol) are reported from this same level of theory.

Frequency	Intensity
22.5106299	4.2078
41.7110589	0.8839
41.7977181	4.4896
132.7672103	14.1337
141.3680356	9.2037
288.9571787	0.3304
309.9603999	2.7228
404.5456068	0.8735
2182.7644071	591.0659

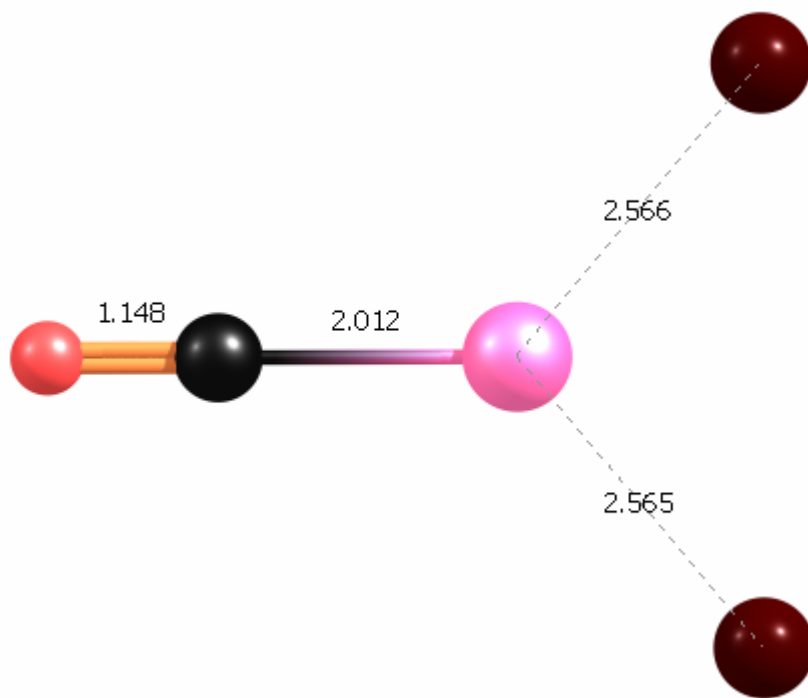


Figure B.9: The optimized geometry of the septet MnCO^+Ar_2 calculated with the B3LYP functional using Gaussian2003. The Def 2 TZVPP basis set was used for all atoms.

Table B.12: The unscaled normal mode frequencies and intensities (km/mol) are reported from this same level of theory.

Frequency	Intensity
32.5515004	6.1282
41.0905484	0.46
92.4910319	12.2476
177.5513149	6.6884
188.9356518	22.4593
319.5013597	4.0443
485.9052897	13.3593
2211.8001414	852.7135

Table B.13: The electronic states calculated for $\text{Mn}(\text{CO})_2^+$ with the B3LYP functional using Gaussian03. The Def 2 TZVPP basis set was used for all atoms.

Isomer	Total Energy (Hartrees)	Relative Energy (kcal/mol)
$^5\text{Mn}(\text{CO})_2^+$	-1377.5260269	0.0
$^3\text{Mn}(\text{CO})_2^+$	-1377.4810479	+28.2
$^1\text{Mn}(\text{CO})_2^+$	-1377.4360506	+56.4



Figure B.10: The optimized geometry of the singlet MnCO₂⁺ calculated with the B3LYP functional using Gaussian2003. The Def 2 TZVPP basis set was used for all atoms.

Table B.14: The unscaled normal mode frequencies and intensities (km/mol) are reported from this same level of theory.

Frequency	Intensity
83.8262	3.496
306.3249	0
306.3285	0.0008
346.2978	0.0001
379.9617	84.5977
511.4033	6.3032
511.4538	6.3984
2195.9135	1184.122
2248.9814	0.0293



Figure B.11: The optimized geometry of the triplet MnCO_2^+ calculated with the B3LYP functional using Gaussian2003. The Def 2 TZVPP basis set was used for all atoms.

Table B.15: The unscaled normal mode frequencies and intensities (km/mol) are reported from this same level of theory.

Frequency	Intensity
86.7587	3.5912
305.5303	0
305.5353	0.0003
351.2383	0.0001
382.5427	97.0855
519.3888	6.89
519.4352	6.9845
2181.8451	1352.4584
2241.5233	0.0302



Figure B.11: The optimized geometry of the quintet MnCO_2^+ calculated with the B3LYP functional using Gaussian2003. The Def 2 TZVPP basis set was used for all atoms.

Table B.16: The unscaled normal mode frequencies and intensities (km/mol) are reported from this same level of theory.

Frequency	Intensity
53.8068	4.7225
266.7266	0.0001
273.2929	0
302.3241	0.0088
304.2598	0.0003
346.6147	81.9415
423.1696	1.0879
2198.0229	1457.6683
2258.613	0.0288

Table B.17: The electronic states calculated for $\text{Mn}(\text{CO})_2^+\text{Ar}$ with the B3LYP functional using Gaussian03. The Def 2 TZVPP basis set was used for all atoms.

Isomer	Total Energy (Hartrees)	Relative Energy (kcal/mol)
$^5\text{Mn}(\text{CO})_2^+\text{Ar}$ (C_{2v})	-1905.0813517	0.0
$^3\text{Mn}(\text{CO})_2^+\text{Ar}$ (C_{2v})	-1905.0415629	25.0
$^1\text{Mn}(\text{CO})_2^+\text{Ar}$ (C_{2v})	-1904.9991976	51.6
$^3\text{Mn}(\text{CO})_2^+\text{Ar}$ ($\text{D}_{\infty h}$)	-1905.0310439	31.6
$^1\text{Mn}(\text{CO})_2^+\text{Ar}$ ($\text{D}_{\infty h}$)	-1377.4360506	59.8

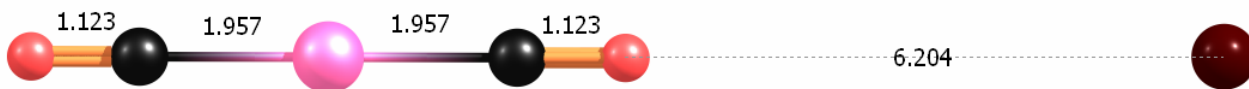


Figure B.12: The optimized geometry of the $D_{\infty h}$ singlet MnCO_2^+Ar calculated with the B3LYP functional using Gaussian2003. The Def 2 TZVPP basis set was used for all atoms.

Table B.18: The unscaled normal mode frequencies and intensities (km/mol) are reported from this same level of theory.

Frequency	Intensity
4.3255	2.1478
5.9651	0.5393
84.5669	3.3761
84.7186	3.482
307.2115	0.0001
307.6395	0
345.7954	0.0004
379.2864	85.0479
511.6249	6.3723
511.6678	6.3768
2194.9621	1190.31
2247.9914	0.0268

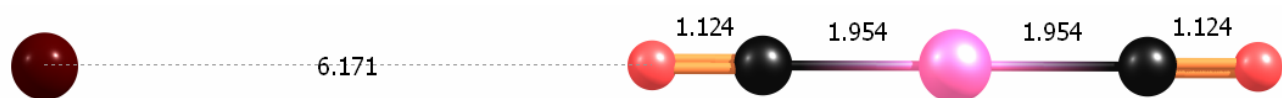


Figure B.13: The optimized geometry of the $D_{\infty h}$ triplet MnCO_2^+Ar calculated with the B3LYP functional using Gaussian2003. The Def 2 TZVPP basis set was used for all atoms.

Table B.19: The unscaled normal mode frequencies and intensities (km/mol) are reported from this same level of theory.

Frequency	Intensity
4.0252	2.3781
13.0775	0.3118
86.6695	3.4844
86.8271	3.5834
305.1532	0.0021
306.5886	0
350.8039	0.0001
382.0319	97.3958
519.2259	6.9606
519.2883	6.9514
2181.9487	1358.6181
2241.5395	0.0144

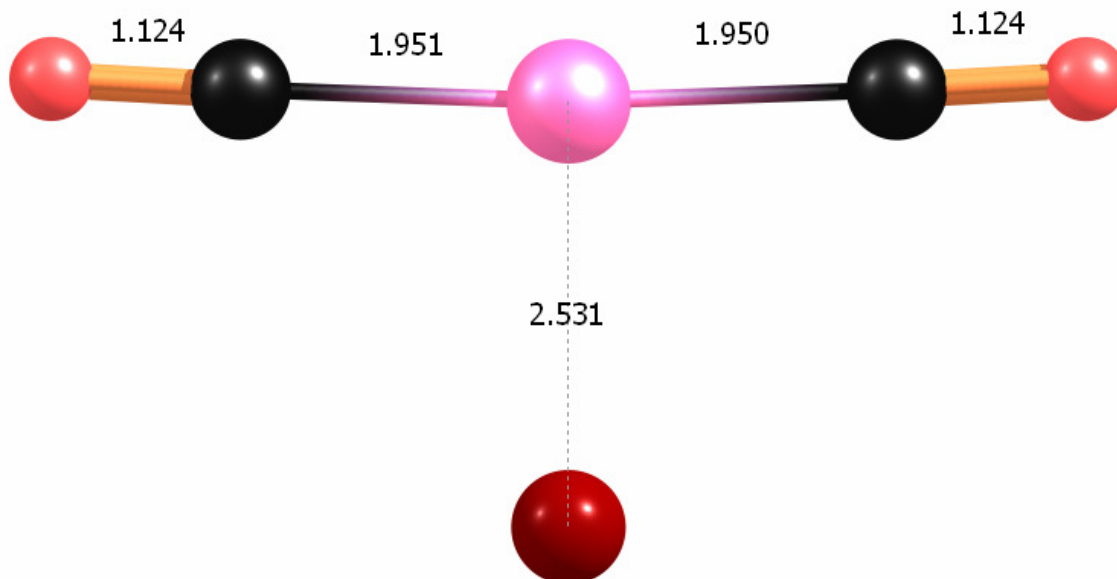


Figure B.14: The optimized geometry of the C_{2v} singlet $MnCO_2^+Ar$ calculated with the B3LYP functional using Gaussian2003. The Def 2 TZVPP basis set was used for all atoms.

Table B.20: The unscaled normal mode frequencies and intensities (km/mol) are reported from this same level of theory.

Frequency	Intensity
79.634	1.0721
86.186	3.1119
86.6014	0.4368
163.84	10.3022
307.0769	0
344.0355	3.3382
346.7092	0.2096
380.981	93.1804
518.865	6.7326
527.8785	5.3788
2180.3339	1255.9719
2235.7876	8.6381

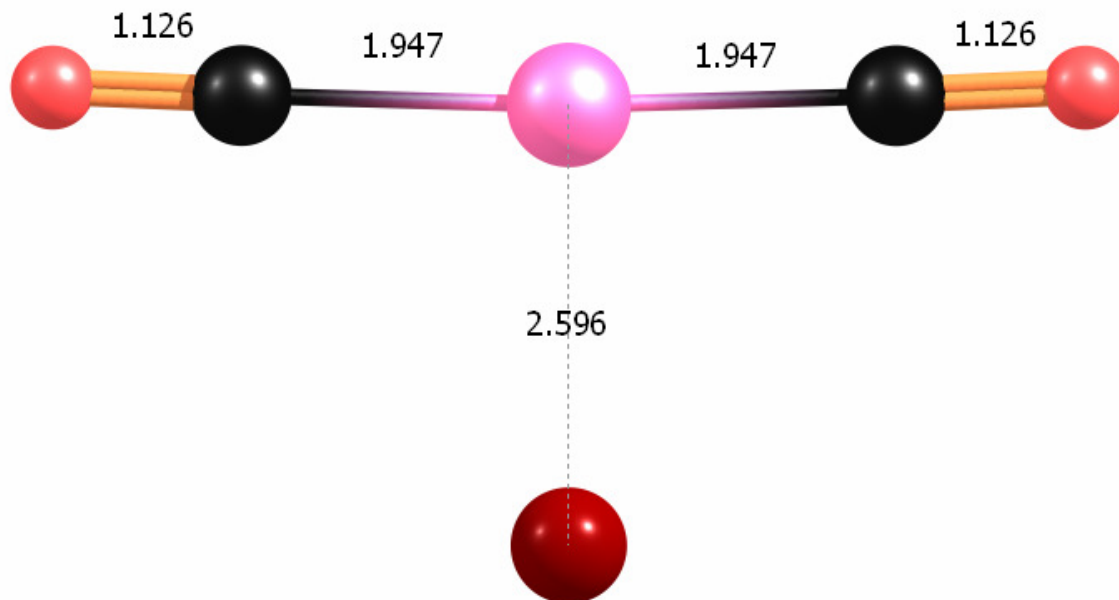


Figure B.15: The optimized geometry of the C_{2v} triplet $MnCO_2^+ Ar$ calculated with the B3LYP functional using Gaussian2003. The Def 2 TZVPP basis set was used for all atoms.

Table B.21: The unscaled normal mode frequencies and intensities (km/mol) are reported from this same level of theory.

Frequency	Intensity
80.6551	0.3834
83.2265	0.6035
88.3366	3.1612
142.538	11.7666
309.6151	0
341.8406	1.8439
352.2335	0.1804
384.0082	104.3811
526.6341	7.1748
534.8235	6.2612
2166.3757	1406.4026
2228.1798	7.2284

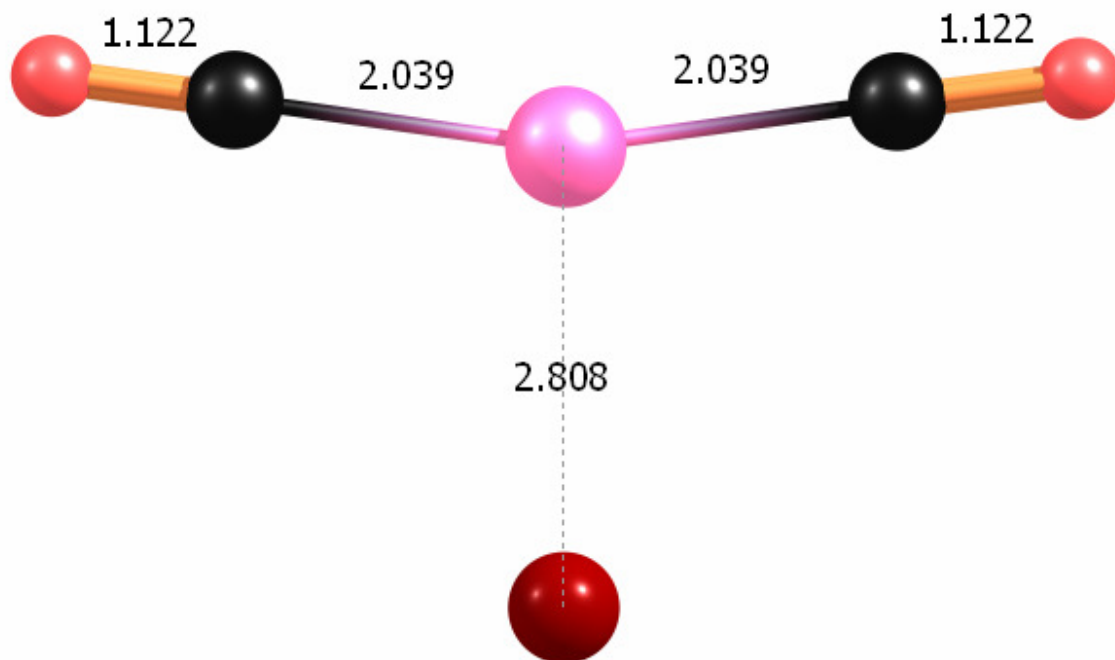


Figure B.16: The optimized geometry of the C_{2v} quintet $MnCO_2^+Ar$ calculated with the B3LYP functional using Gaussian2003. The Def 2 TZVPP basis set was used for all atoms.

Table B.22: The unscaled normal mode frequencies and intensities (km/mol) are reported from this same level of theory.

Frequency	Intensity
36.1021	0.6614
51.0578	3.7838
62.188	3.0999
93.6787	14.6777
268.7948	0
271.9758	0.1985
296.6307	0.0875
311.0474	0.098
337.7028	0.0636
339.6802	89.871
2184.955	1566.7883
2249.3428	14.4681

Table B.23: The electronic states calculated for $\text{Mn}(\text{CO})_3^+$ with the B3LYP functional using Gaussian03. The Def 2 TZVPP basis set was used for all atoms.

Isomer	Total Energy (Hartrees)	Relative Energy (kcal/mol)
$^3\text{Mn}(\text{CO})_3^+$	-1490.8678704	0.0
$^1\text{Mn}(\text{CO})_3^+$	-1490.8521369	+9.8

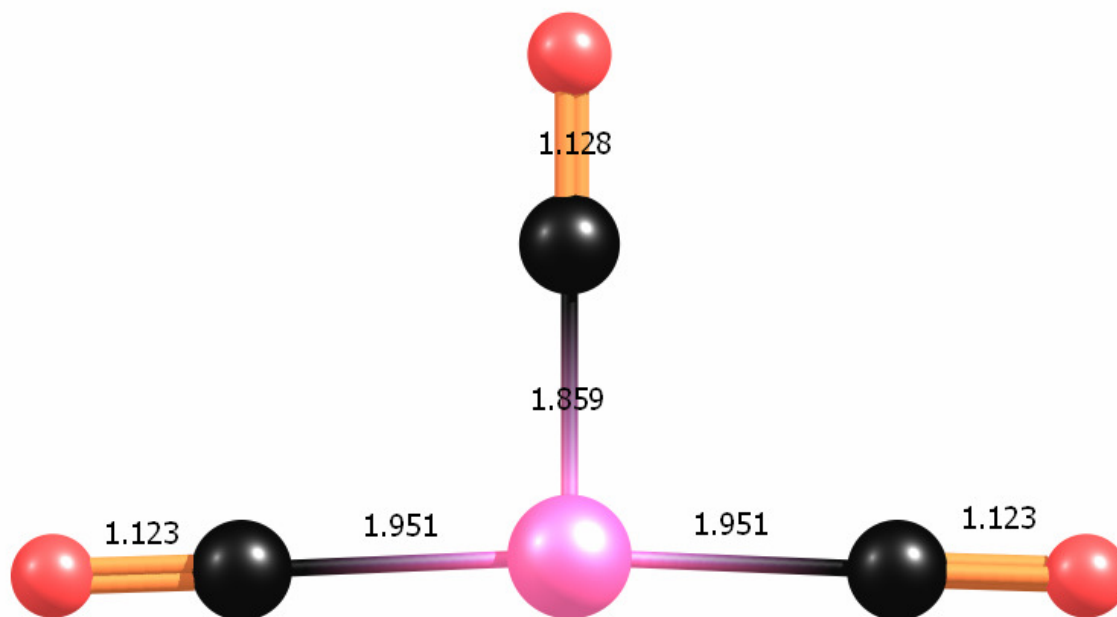


Figure B.17: The optimized geometry of the singlet MnCO_3^+ calculated with the B3LYP functional using Gaussian2003. The Def 2 TZVPP basis set was used for all atoms.

Table B.24: The unscaled normal mode frequencies and intensities (km/mol) are reported from this same level of theory.

Frequency	Intensity
86.0486	1.6426
86.1389	3.6939
91.8506	2.3144
309.002	0
332.1149	0.2724
338.6181	2.5081
348.1265	0.1619
364.2219	60.9571
414.4884	6.7098
512.042	6.7689
547.0457	29.0876
564.5003	12.9134
2171.7547	485.7967
2195.3477	1096.0341
2247.2493	0.1921

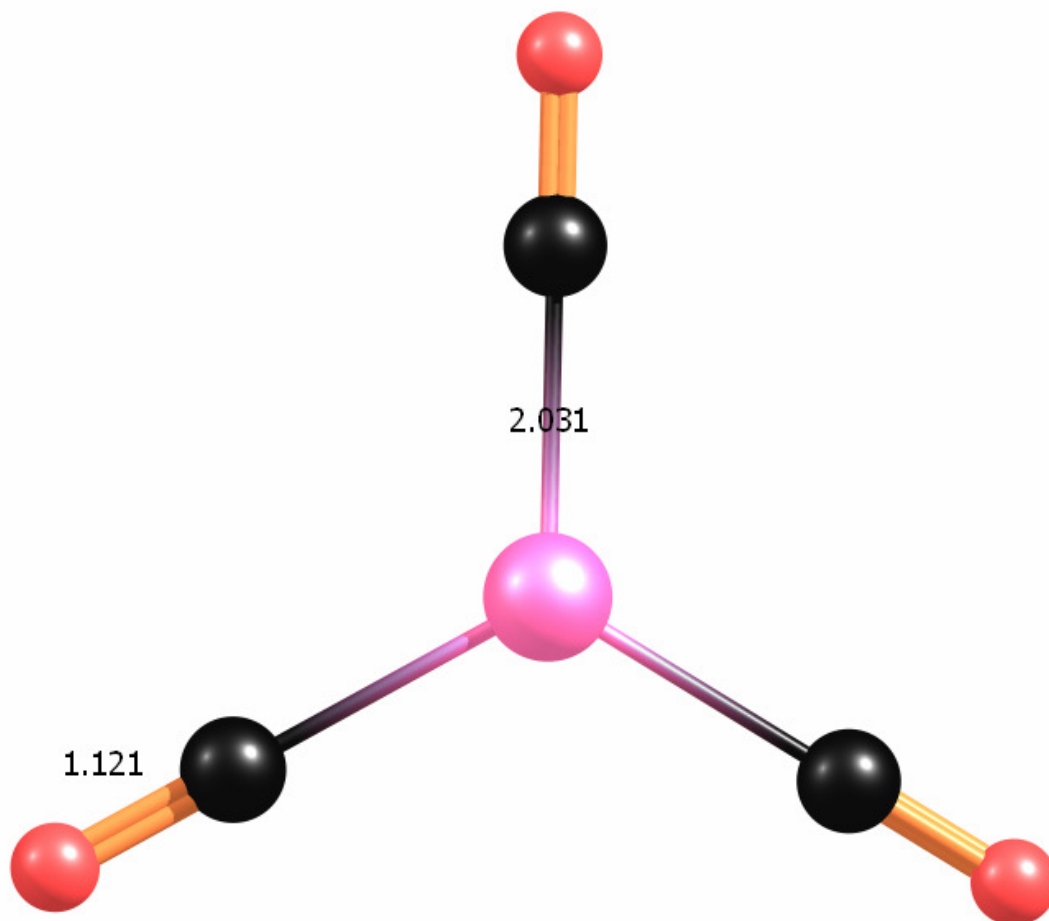


Figure B.18: The optimized geometry of the triplet MnCO_3^+ calculated with the B3LYP functional using Gaussian2003. The Def 2 TZVPP basis set was used for all atoms.

Table B.25: The unscaled normal mode frequencies and intensities (km/mol) are reported from this same level of theory.

Frequency	Intensity
52.1164	0.8045
52.3618	0.7999
151.7627	0.0616
261.7952	0
262.5215	0.0002
272.0616	0.0004
279.6747	0.0009
324.1325	13.3121
324.3711	12.7244
338.0154	9.6324
338.3345	10.1385
2217.0137	677.5297
2217.2405	677.1024
2253.5408	0.0117

Table B.26: The electronic states calculated for $\text{Mn}(\text{CO})_3^+\text{Ar}$ with the B3LYP functional using Gaussian03. The Def 2 TZVPP basis set was used for all atoms.

Isomer	Total Energy (Hartrees)	Relative Energy (kcal/mol)
$^3\text{Mn}(\text{CO})_3^+\text{Ar}$	-1490.8678704	0.0
$^1\text{Mn}(\text{CO})_3^+\text{Ar}$	-1490.8521369	+16.8

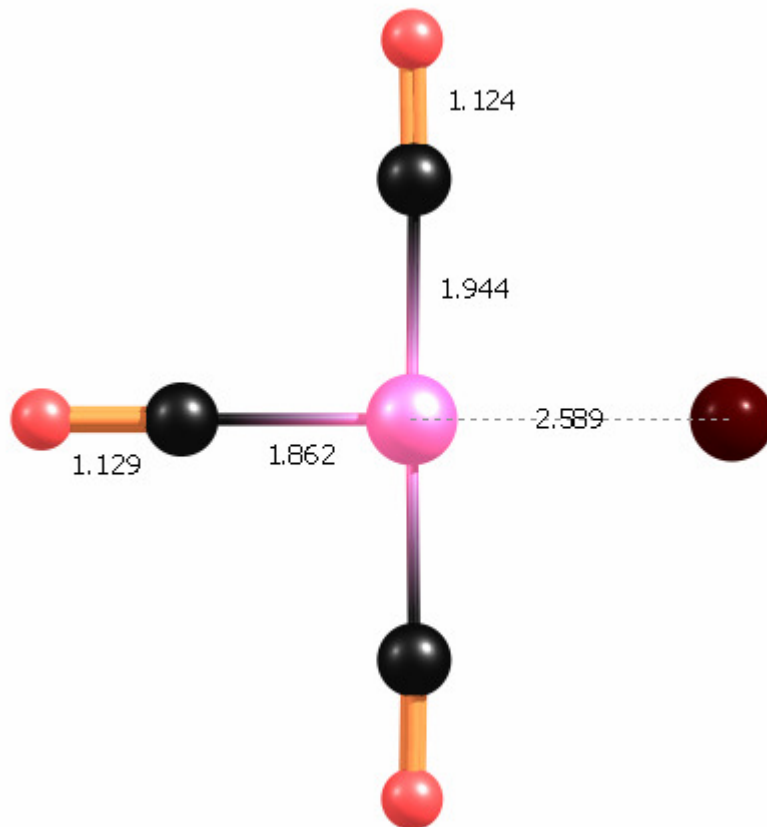


Figure B.19: The optimized geometry of the singlet MnCO_3^+Ar calculated with the B3LYP functional using Gaussian2003. The Def 2 TZVPP basis set was used for all atoms.

Table B.27: The unscaled normal mode frequencies and intensities (km/mol) are reported from this same level of theory.

Frequency	Intensity
46.2022	0.2075
84.1048	0.002
86.3021	0.5174
97.827	1.5851
100.303	3.3777
140.8163	7.8331
310.7243	0
342.2543	1.4244
363.698	5.7257
374.2155	59.8051
377.9805	0.0035
419.2191	5.1988
525.9224	9.5662
566.2441	26.5075
579.2025	20.0699
2165.9099	508.3688
2185.8155	1111.1453
2239.6236	12.8435

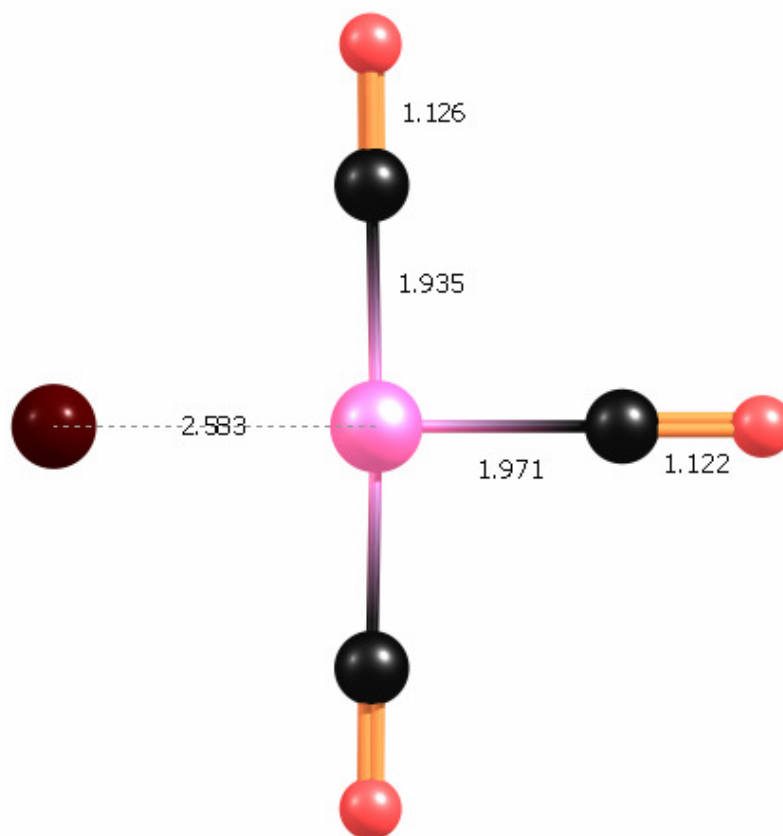


Figure B.20: The optimized geometry of the triplet MnCO_3^+Ar calculated with the B3LYP functional using Gaussian2003. The Def 2 TZVPP basis set was used for all atoms.

Table B.28: The unscaled normal mode frequencies and intensities (km/mol) are reported from this same level of theory.

Frequency	Intensity
30.3546	0.2524
71.109	1.1213
88.6854	0.4471
90.7317	0.4734
91.0797	3.0856
139.8383	8.044
307.7917	0.3379
312.1041	0
352.1408	1.229
352.2957	0.2799
358.8038	2.6568
374.9689	72.566
494.092	29.5117
526.656	7.5777
566.9224	22.607
2160.4723	1382.7244
2200.9457	220.4474
2242.0763	140.7375

Table B.29: The electronic states calculated for $\text{Mn}(\text{CO})_4^+$ with the B3LYP functional using Gaussian03. The Def 2 TZVPP basis set was used for all atoms.

Isomer	Total Energy (Hartrees)	Relative Energy (kcal/mol)
$^3\text{Mn}(\text{CO})_4^+$	-1604.2834421	+8.8
$^1\text{Mn}(\text{CO})_4^+$	-1604.2974166	0.0

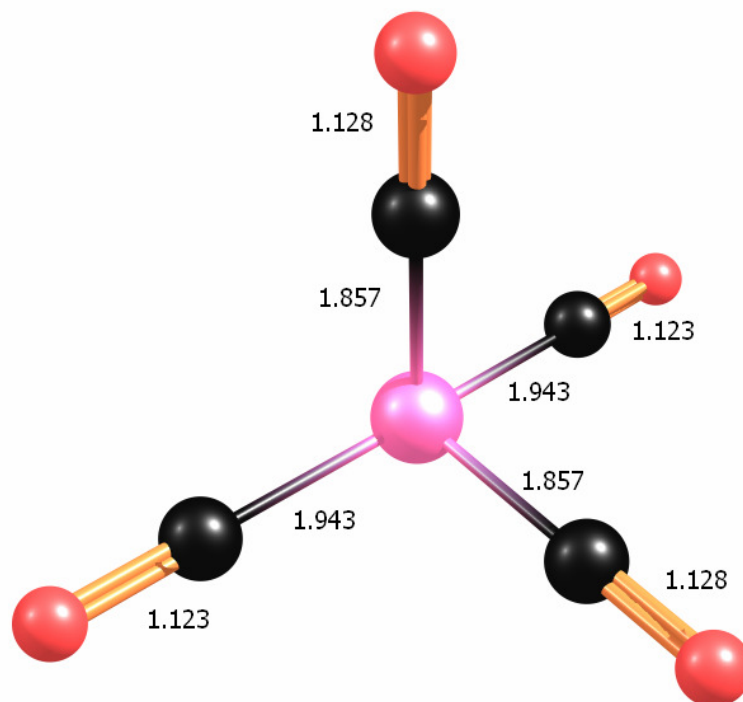


Figure B.21: The optimized geometry of the singlet MnCO_4^+ calculated with the B3LYP functional using Gaussian2003. The Def 2 TZVPP basis set was used for all atoms.

Table B.30: The unscaled normal mode frequencies and intensities (km/mol) are reported from this same level of theory.

Frequency	Intensity
75.5384	0.0163
87.0049	2.0648
89.2598	0
99.842	3.7451
107.5603	2.6482
333.0057	0.9559
334.7666	0.0275
336.9572	3.1785
358.4295	0.8053
359.3794	47.2363
402.6064	2.6794
414.6243	11.4326
506.9677	6.3267
535.8577	0
553.0921	37.5704
592.5866	22.3053
612.96	22.8879
2162.1125	648.1413
2179.3107	347.9399
2193.4853	1045.4758
2245.4511	0.5811

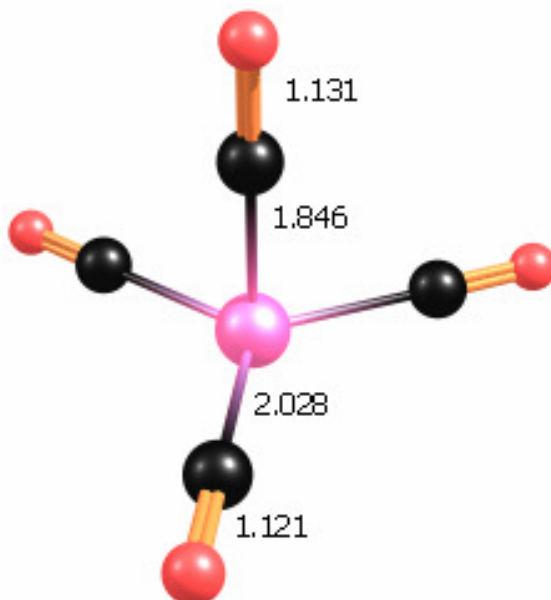


Figure B.22: The optimized geometry of the triplet MnCO_4^+ calculated with the B3LYP functional using Gaussian2003. The Def 2 TZVPP basis set was used for all atoms.

Table B.31: The unscaled normal mode frequencies and intensities (km/mol) are reported from this same level of theory.

Frequency	Intensity
46.0296	0.2309
46.1106	0.2377
69.8791	1.5531
83.6306	2.4967
83.8098	2.4855
264.0668	2.976
271.7731	0.0008
299.7473	6.6592
300.2167	6.6695
311.3003	7.7539
311.5344	7.5284
328.7057	1.9914
328.8369	2.0538
349.7981	0.0558
461.3483	19.4701
518.9504	2.2778
519.3229	2.266
2145.8524	557.8059
2221.421	612.7398
2221.6622	612.8877
2254.1757	0.9229

Table B.32: The electronic states calculated for $\text{Mn}(\text{CO})_4^+\text{Ar}$ with the B3LYP functional using Gaussian03. The Def 2 TZVPP basis set was used for all atoms.

Isomer	Total Energy (Hartrees)	Relative Energy (kcal/mol)
$^3\text{Mn}(\text{CO})_4^+\text{Ar}$	-2131.8435635	+9.5
$^1\text{Mn}(\text{CO})_4^+\text{Ar}$	-2131.8586255	0.0

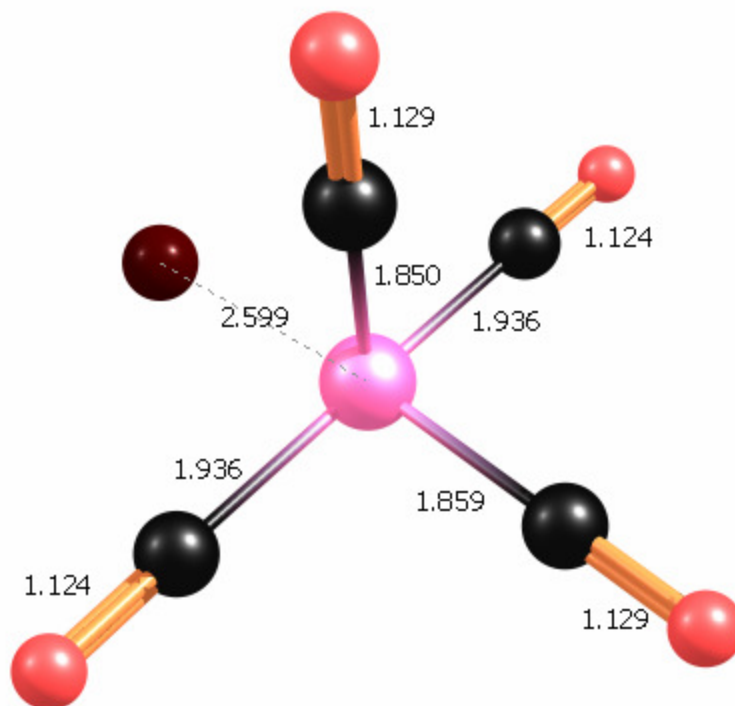


Figure B.23: The optimized geometry of the singlet MnCO_4^+Ar calculated with the B3LYP functional using Gaussian2003. The Def 2 TZVPP basis set was used for all atoms.

Table B.33: The unscaled normal mode frequencies and intensities (km/mol) are reported from this same level of theory.

Frequency	Intensity	Frequency	Intensity
49.5837	0.192	2156.0055	656.3193
78.2713	0.0027	2173.3548	357.3662
81.1211	0.0179	2173.3548	357.3662
90.704	0.0018	2239.3187	13.9388
91.0375	1.1477		
105.6489	1.1117		
106.0982	2.5914		
138.9229	8.4281		
338.2413	0.0703		
341.6113	2.006		
364.7405	13.6151		
370.5912	36.3961		
378.2163	1.0243		
409.8236	1.7265		
420.2471	11.3292		
519.9366	6.1708		
546.5625	0.0004		
566.9758	38.3117		
600.8803	31.2744		
626.7629	27.7977		

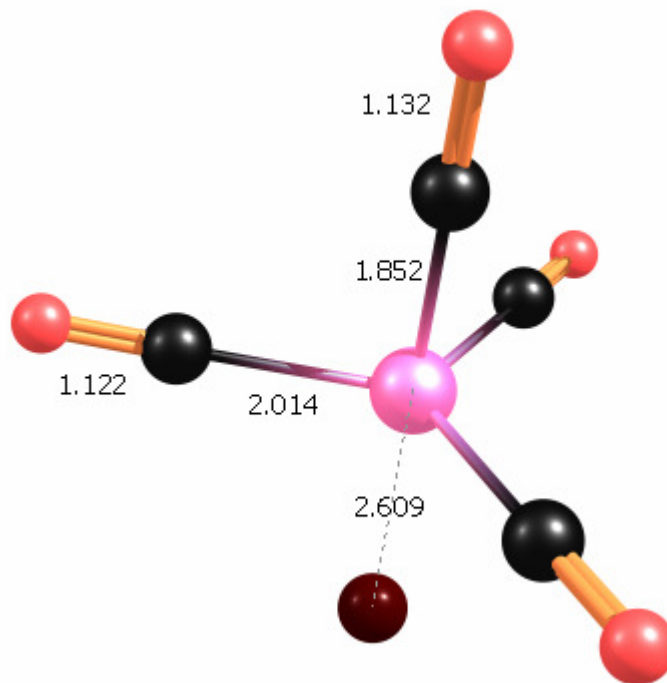


Figure B.24: The optimized geometry of the triplet MnCO_4^+Ar calculated with the B3LYP functional using Gaussian2003. The Def 2 TZVPP basis set was used for all atoms.

Table B.34: The unscaled normal mode frequencies and intensities (km/mol) are reported from this same level of theory.

Frequency	Intensity	Frequency	Intensity
44.135	0.011	2141.3687	519.773
44.2162	0.0107	2209.5024	643.6963
73.1179	0.0037	2209.6803	644.4617
73.174	0.003	2244.8676	5.7349
80.5668	0.4506		
95.3088	2.0714		
95.4125	2.0714		
131.8756	6.3388		
269.3755	2.3428		
277.4414	0.0002		
318.0464	18.8799		
318.3394	18.7691		
335.6728	1.5816		
335.8249	1.585		
341.7954	0.0137		
342.0058	0.0219		
401.8417	0.1046		
463.3341	15.4843		
548.0073	5.532		
548.1495	5.5362		

Table B.35: The electronic states calculated for $\text{Mn}(\text{CO})_5^+$ with the B3LYP functional using Gaussian03. The Def 2 TZVPP basis set was used for all atoms.

Isomer	Total Energy (Hartrees)	Relative Energy (kcal/mol)
$^3\text{Mn}(\text{CO})_5^+$	-1717.7017608	+8.7
$^1\text{Mn}(\text{CO})_5^+$	-1717.7156852	0.0

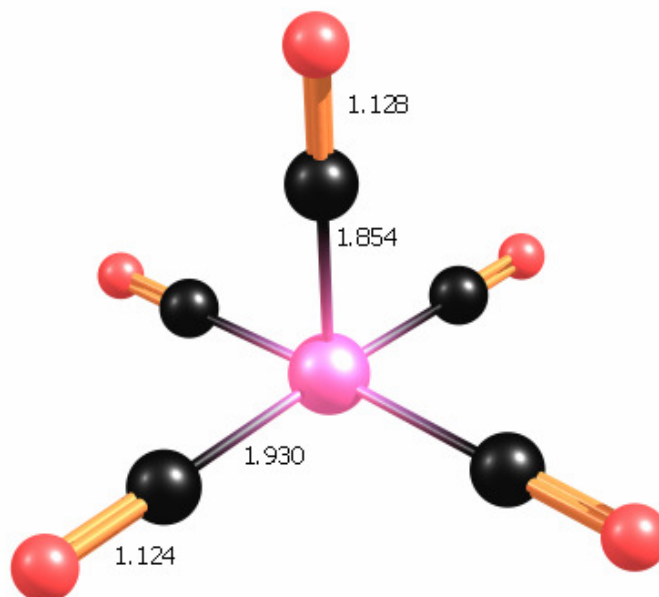


Figure B.25: The optimized geometry of the singlet MnCO_5^+ calculated with the B3LYP functional using Gaussian2003. The Def 2 TZVPP basis set was used for all atoms.

Table B.36: The unscaled normal mode frequencies and intensities (km/mol) are reported from this same level of theory.

Frequency	Intensity	Frequency	Intensity
63.3663	0	2189.655	1018.8948
83.8945	0.0336	2205.5653	0.1387
83.9143	0.0329	2253.7948	0.0128
94.0365	0.0001	2189.6371	1016.7945
103.6617	2.704		
103.6661	2.6994		
106.9966	1.9598		
339.2844	0.0044		
339.2871	0.0045		
342.2778	0		
345.9192	1.8715		
346.786	0.0004		
377.0902	36.8785		
377.2123	37.0287		
414.2325	4.7441		
481.5476	0		
532.363	0.0834		
532.854	4.3025		
532.8955	4.2922		
611.9108	68.8749		
611.9946	68.5807		
615.1775	73.1974		
2169.5288	494.379		

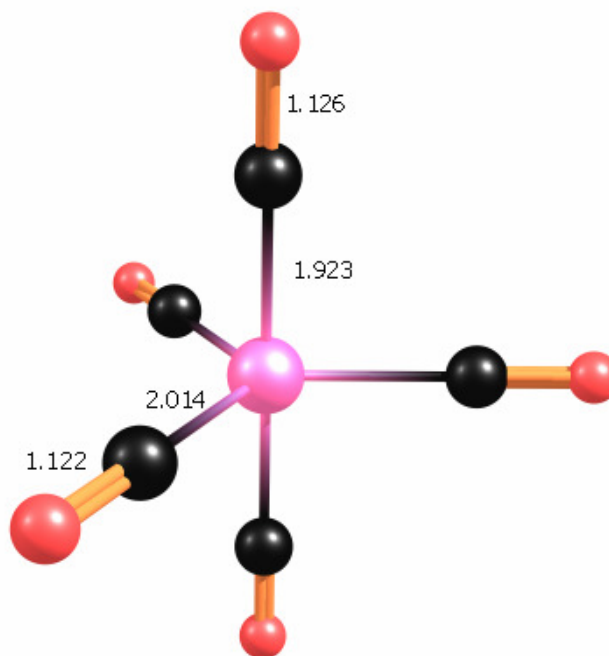


Figure B.26: The optimized geometry of the triplet MnCO_5^+ calculated with the B3LYP functional using Gaussian2003. The Def 2 TZVPP basis set was used for all atoms.

Table B.37: The unscaled normal mode frequencies and intensities (km/mol) are reported from this same level of theory.

Frequency	Intensity	Frequency	Intensity
40.4411	0.0465	2195.8748	0.1199
40.7508	0.0465	2219.7068	534.7334
78.5915	2.8535	2220.3291	534.0161
81.6188	0.0003	2254.1656	0.0574
81.8148	0.0017	574.8279	46.0856
98.6748	1.2025		
98.7436	1.1979		
271.5616	0.0002		
276.6809	0		
311.5735	7.3628		
311.7226	7.4317		
321.9469	0.0003		
321.979	0.0007		
340.5714	3.2264		
341.0239	3.3281		
350.7868	23.9505		
357.0482	0.035		
478.9678	58.9083		
497.2059	0.0033		
497.4936	0.0064		
574.5952	46.0306		

Table B.38: The electronic states calculated for $\text{Mn}(\text{CO})_5^+\text{Ar}$ with the B3LYP functional using Gaussian03. The Def 2 TZVPP basis set was used for all atoms.

Isomer	Total Energy (Hartrees)	Relative Energy (kcal/mol)
$^3\text{Mn}(\text{CO})_5^+\text{Ar}$	-2245.2526065	+13.6
$^1\text{Mn}(\text{CO})_5^+\text{Ar}$	-2245.2743638	0.0

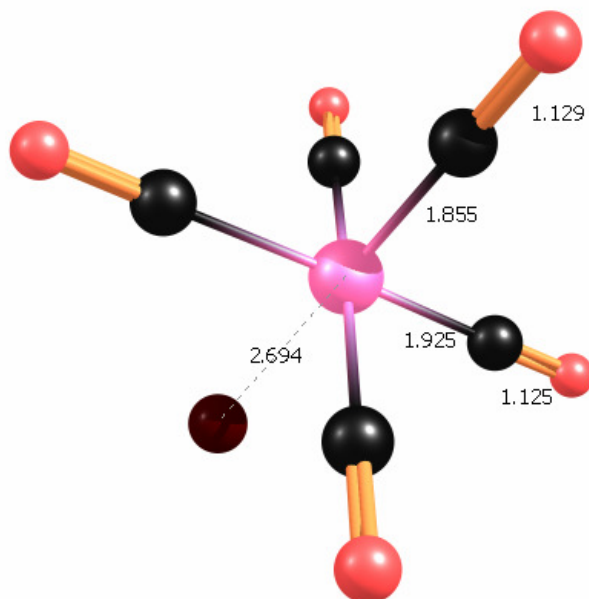


Figure B.27: The optimized geometry of the singlet MnCO_5^+Ar calculated with the B3LYP functional using Gaussian2003. The Def 2 TZVPP basis set was used for all atoms.

Table B.39: The unscaled normal mode frequencies and intensities (km/mol) are reported from this same level of theory.

Frequency	Intensity	Frequency	Intensity
67.2367	0.0006	622.2448	83.2069
67.3847	0.0005	622.4853	83.1528
67.762	0.0001	627.4512	71.7093
87.404	0.0004	2166.5892	505.0654
87.4944	0.0011	2184.1727	1006.9511
94.5657	0.0005	2184.3538	1008.8674
98.1908	0.0183	2200.378	2.3467
109.1418	1.9145	2249.5388	8.5205
109.1854	1.9234		
124.5352	6.1019		
344.6664	0.0024		
349.062	0.8586		
351.1357	0.0081		
364.8373	0.0267		
364.9271	0.0426		
384.2126	36.3811		
384.4326	36.4882		
418.6774	3.6984		
496.9047	0.0004		
534.5841	0.026		
537.8876	4.2698		
538.1876	4.427		

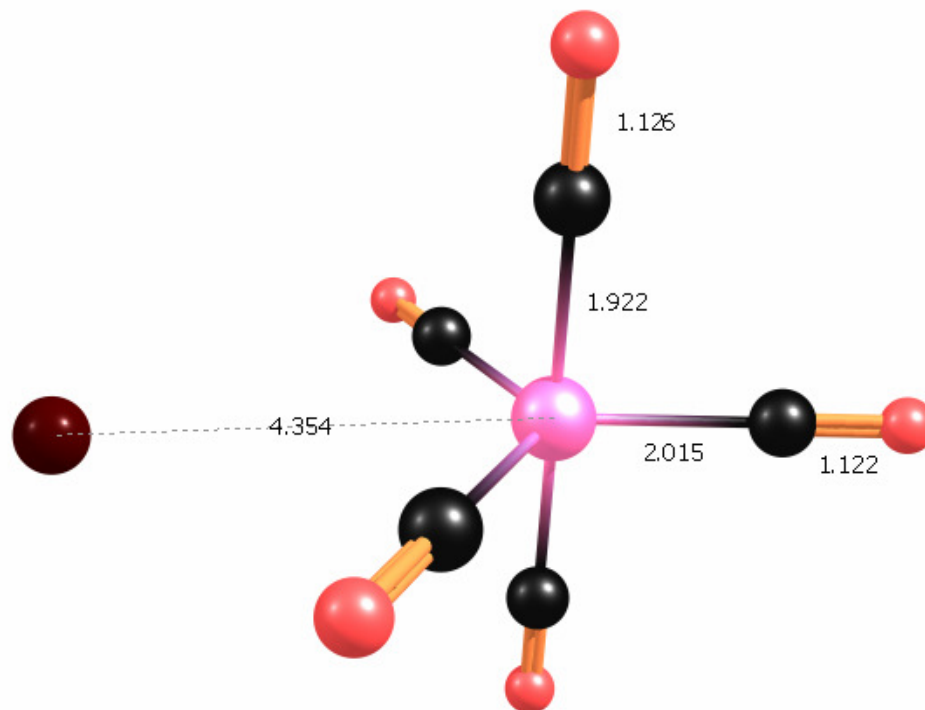


Figure B.28: The optimized geometry of the triplet MnCO_5^+Ar calculated with the B3LYP functional using Gaussian2003. The Def 2 TZVPP basis set was used for all atoms.

Table B.40: The unscaled normal mode frequencies and intensities (km/mol) are reported from this same level of theory.

Frequency	Intensity	Frequency	Intensity
12.469	0.4813	479.7077	58.3231
24.2703	1.4244	574.1871	46.6513
40.7902	0.0182	496.6241	0.2176
43.136	0.0218	498.6589	0.0422
78.9326	2.8075	576.0901	45.5963
81.397	0.0042	2165.4182	1267.3372
82.0329	0.0103	2195.3564	0.5181
98.3327	1.1643	2219.262	526.7751
98.7238	1.3554	2219.7344	532.7951
271.4351	0.0231	2253.8128	0.0884
276.3111	0.0059		
310.5703	7.7216		
311.8613	8.2577		
322.0082	0.0005		
322.4703	0.0005		
338.4069	2.4154		
343.0435	3.1813		
351.8469	23.9028		
357.5698	0.009		

Table B.41: The electronic states calculated for $\text{Mn}(\text{CO})_6^+$ with the B3LYP functional using Gaussian03. The Def 2 TZVPP basis set was used for all atoms.

Isomer	Total Energy (Hartrees)	Relative Energy (kcal/mol)
$^3\text{Mn}(\text{CO})_6^+$	-1831.0570285	+48.0
$^1\text{Mn}(\text{CO})_6^+$	-1831.1335673	0.0

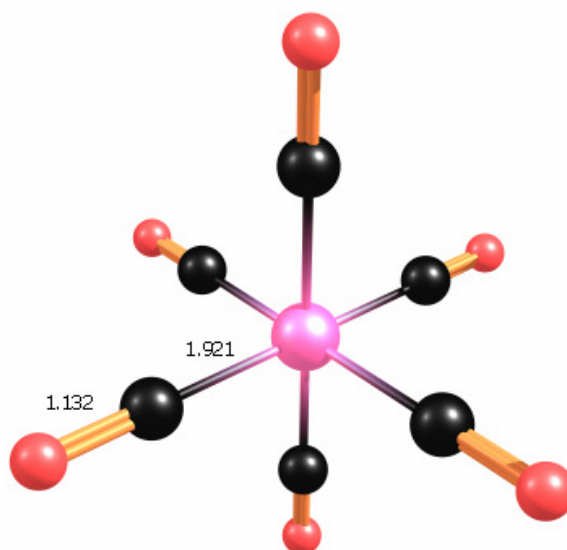


Figure B.29: The optimized geometry of the singlet MnCO_6^+ calculated with the B3LYP functional using Gaussian2003. The Def 2 TZVPP basis set was used for all atoms.

Table B.42: The unscaled normal mode frequencies and intensities (km/mol) are reported from this same level of theory.

Frequency	Intensity	Frequency	Intensity
71.8181	0	634.9132	159.1256
71.9896	0	634.9997	159.1359
72.1385	0.0001	635.3162	159.2944
97.4876	0	2188.6346	1061.8458
97.5373	0	2188.7466	1061.9249
97.6479	0	2188.795	1061.6888
111.832	1.6634	2203.2033	0.0004
111.9494	1.6462	2203.3091	0.0003
111.9885	1.6522	2263.773	0
346.3477	0		
346.7283	0		
346.9465	0		
355.6877	0		
357.001	0		
357.1499	0		
392.9206	27.065		
393.0154	27.0006		
393.1387	26.9253		
498.2843	0.0001		
498.4255	0.0002		
498.6078	0.0001		
544.3517	0		
544.4125	0		
544.6071	0		

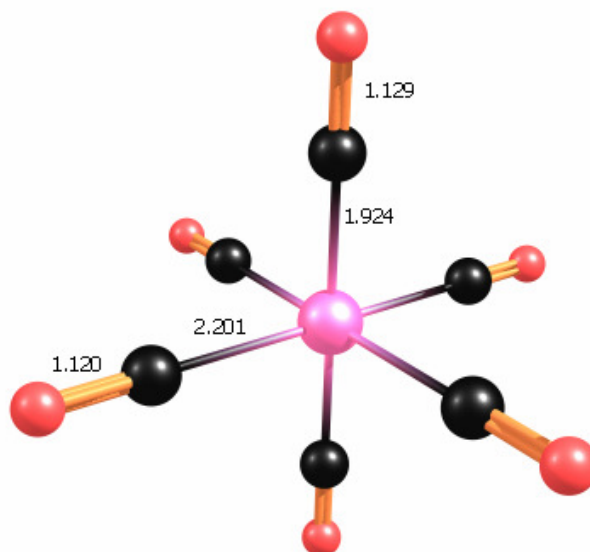


Figure B.30: The optimized geometry of the triplet MnCO_6^+ calculated with the B3LYP functional using Gaussian2003. The Def 2 TZVPP basis set was used for all atoms.

Table B.43: The unscaled normal mode frequencies and intensities (km/mol) are reported from this same level of theory.

Frequency	Intensity	Frequency	Intensity
42.9385	0.0004	572.776	33.8699
42.9757	0.0002	572.8199	33.9249
46.4868	0	2142.8706	1321.4663
53.0081	0	2183.4986	0
64.8108	0	2229.9892	0.0279
64.8501	0	2230.2735	507.6358
68.5707	1.6362	2230.3026	507.0552
88.3619	3.6484	2260.4358	0
88.4102	3.632		
115.7592	2.1064		
116.0587	2.1435		
145.9965	0		
219.1549	0		
240.7706	0		
240.9993	0		
264.6451	0.7715		
264.7818	0.7577		
298.958	0		
306.5727	0.0001		
342.9662	0.2288		
360.3145	0		
425.9476	0		
426.0182	0		
448.9003	130.8353		

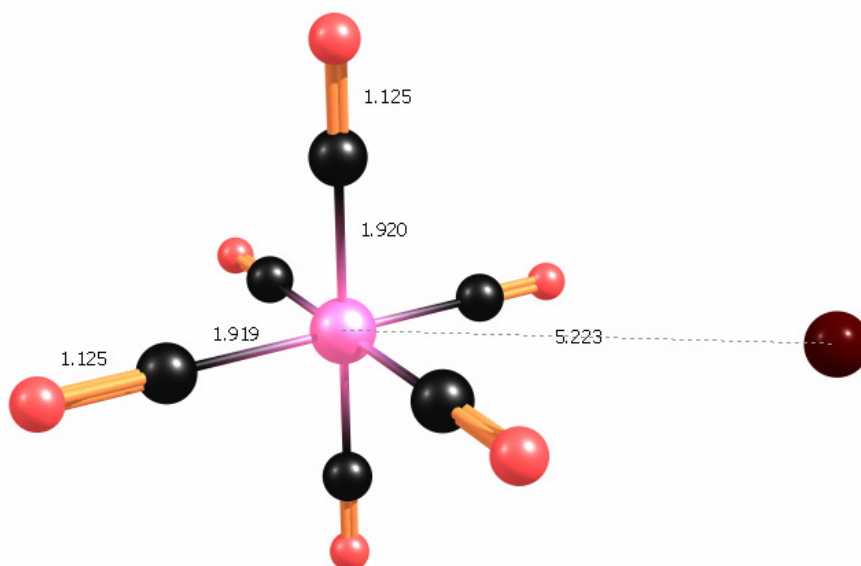


Figure B.31: The optimized geometry of the singlet MnCO_6^+Ar calculated with the B3LYP functional using Gaussian2003. The Def 2 TZVPP basis set was used for all atoms.

Table B.44: The unscaled normal mode frequencies and intensities (km/mol) are reported from this same level of theory.

Frequency	Intensity	Frequency	Intensity
-4.1823	0.2531	514.0785	0.002
16.0756	0.3309	534.2191	0.1148
16.7735	0.9537	534.4302	0.0008
72.8945	0	534.5937	0.0186
73.4723	0.0003	649.5874	150.4693
73.6612	0.0029	649.8455	147.7595
95.4178	0	649.9842	144.3484
95.4719	0.0001	2189.0322	968.0903
96.4676	0.0041	2189.6843	971.8209
111.0985	1.7845	2189.7647	978.4836
111.1214	1.7848	2203.565	1.7562
111.5575	1.8884	2204.0724	2.5768
347.8103	0.0006	2261.3687	0.0393
348.0271	0.0008		
348.0699	0.0002		
353.6074	0.0033		
356.2463	0.0045		
356.4015	0.0082		
394.7823	27.4746		
395.2475	27.3737		
395.2708	26.6161		
513.89	0.0032		
513.925	0.0439		

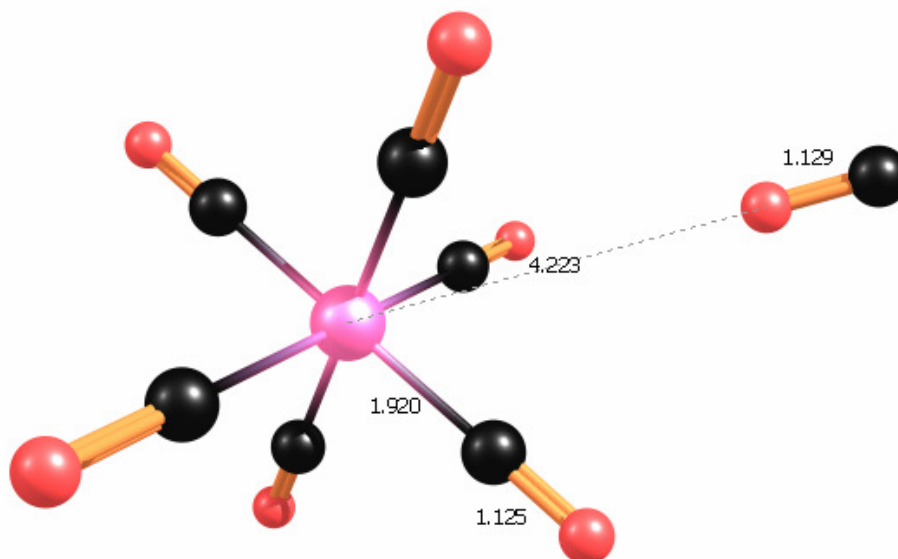


Figure B.32: The optimized geometry of the singlet MnCO_7^+ calculated with the B3LYP functional using Gaussian2003. The Def 2 TZVPP basis set was used for all atoms.

Table B.45: The unscaled normal mode frequencies and intensities (km/mol) are reported from this same level of theory.

Frequency	Intensity	Frequency	Intensity
19.066	0.1878	514.3734	0.0018
21.0114	0.1844	534.1691	0.334
38.4457	1.1192	534.4448	0.042
62.0615	0.0029	534.6721	0.0031
62.4334	0.0009	649.4655	162.074
72.8199	0.0001	650.284	143.9728
74.6479	0.0017	650.4249	143.8158
75.0712	0.0022	2182.1816	512.7895
95.7258	0.0016	2188.9655	950.4522
95.9431	0.0013	2189.0803	949.5067
97.2305	0.0566	2190.0437	655.4132
111.0333	1.7647	2203.5247	5.9538
111.2423	1.7619	2203.6548	6.468
113.1191	1.9119	2261.3329	0.1178
347.6868	0.0001		
348.33	0.0001		
354.1326	0.0015		
356.9041	0.0025		
356.9779	0.0031		
395.2791	26.8215		
395.6116	26.5364		
395.8515	26.4005		
513.7532	0.0035		
514.1664	0.0027		

APPENDIX C

INFRARED SPECTROSCOPY AND STRUCTURES OF COPPER CARBONYL CATIONS, $\text{Cu}(\text{CO})_n^+$ ($n=1-8$)

The complete citation for reference number 59 is :

Gaussian 03, Revision B.02, M. J. Frisch, G. W. Trucks, H. B. Schlegel, G. E. Scuseria, M. A. Robb, J. R. Cheeseman, J. A. Montgomery, Jr., T. Vreven, K. N. Kudin, J. C. Burant, J. M. Millam, S. S. Iyengar, J. Tomasi, V. Barone, B. Mennucci, M. Cossi, G. Scalmani, N. Rega, G. A. Petersson, H. Nakatsuji, M. Hada, M. Ehara, K. Toyota, R. Fukuda, J. Hasegawa, M. Ishida, T. Nakajima, Y. Honda, O. Kitao, H. Nakai, M. Klene, X. Li, J. E. Knox, H. P. Hratchian, J. B. Cross, C. Adamo, J. Jaramillo, R. Gomperts, R. E. Stratmann, O. Yazyev, A. J. Austin, R. Cammi, C. Pomelli, J. W. Ochterski, P. Y. Ayala, K. Morokuma, G. A. Voth, P. Salvador, J. J. Dannenberg, V. G. Zakrzewski, S. Dapprich, A. D. Daniels, M. C. Strain, O. Farkas, D. K. Malick, A. D. Rabuck, K. Raghavachari, J. B. Foresman, J. V. Ortiz, Q. Cui, A. G. Baboul, S. Clifford, J. Cioslowski, B. B. Stefanov, G. Liu, A. Liashenko, P. Piskorz, I. Komaromi, R. L. Martin, D. J. Fox, T. Keith, M. A. Al-Laham, C. Y. Peng, A. Nanayakkara, M. Challacombe, P. M. W. Gill, B. Johnson, W. Chen, M. W. Wong, C. Gonzalez, and J. A. Pople, Gaussian, Inc., Pittsburgh PA, 2003.

Table C1: The electronic states calculated for $\text{Cu}(\text{CO})_2^+$ with the B3LYP functional using Gaussian03. The Def 2 TZVPP basis set was used for all atoms.

Isomer	Total Energy (Hartrees)	Relative Energy (kcal/mol)
$^1\text{Cu}(\text{CO})_2^+$	-1867.0917464	0.0
$^3\text{Cu}(\text{CO})_2^+$	-1866.9204464	+107.5

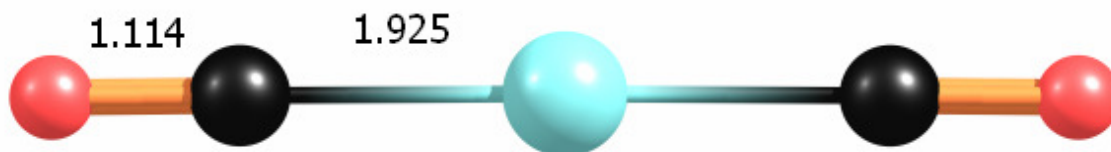


Figure C1: The optimized geometry of the singlet $\text{Cu}(\text{CO})_2^+$ calculated with the B3LYP functional using Gaussian2003. The Def 2 TZVPP basis set was used for all atoms.

Table C2: The unscaled normal mode frequencies and intensities (km/mol) are reported from this same level of theory.

Frequency	Intensity
53.5	1.0
283.2	0
283.4	0
313.9	0
334.0	1.4
334.1	1.4
372.8	18.0
2303.3	367.1
2326.4	0.1

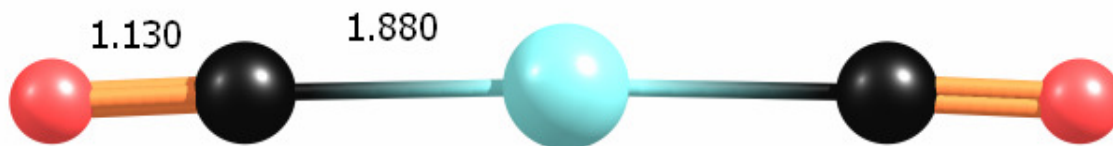


Figure C2: The optimized geometry of the triplet $\text{Cu}(\text{CO})_2^+$ calculated with the B3LYP functional using Gaussian2003. The Def 2 TZVPP basis set was used for all atoms.

Table C3: The unscaled normal mode frequencies and intensities (km/mol) are reported from this same level of theory.

Frequency	Intensity
-147.9	56.9
84.6	4.0
314.3	0
357.9	0
387.3	0
412.9	0.5
470.8	73.9
2029.3	3929.5
2220.3	0.2

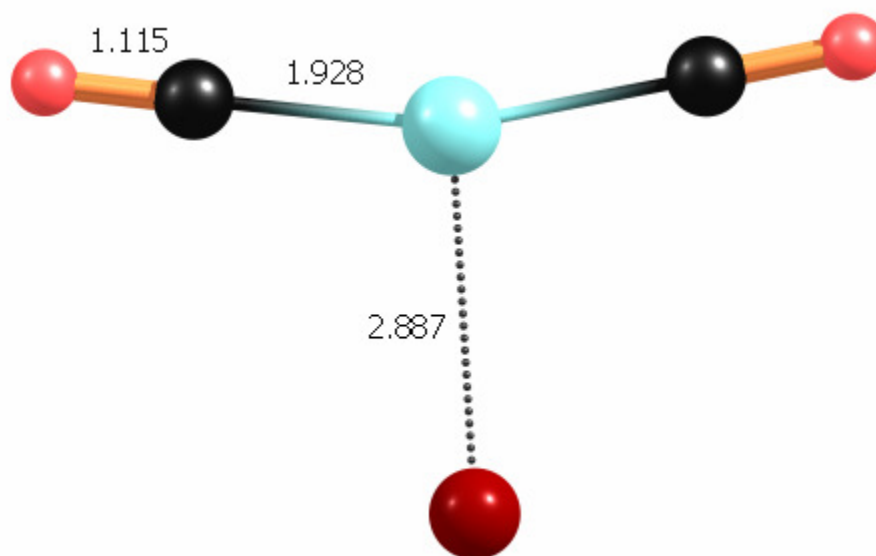


Figure C3: The optimized geometry of the singlet $\text{Cu(CO)}_2^+\text{Ar}$ calculated with the B3LYP functional using Gaussian2003. The Def 2 TZVPP basis set was used for all atoms.

Table C4: The unscaled normal mode frequencies and intensities (km/mol) are reported from this same level of theory.

Frequency	Intensity
35.4	0.8061
41.2	4.119
54.5	1.0718
71.4	6.2
278.0	0
288.2	0
310.3	0.
326.2	1.5
334.6	0.2
365.6	17.6
2295.2	383.2
2317.8	9.8

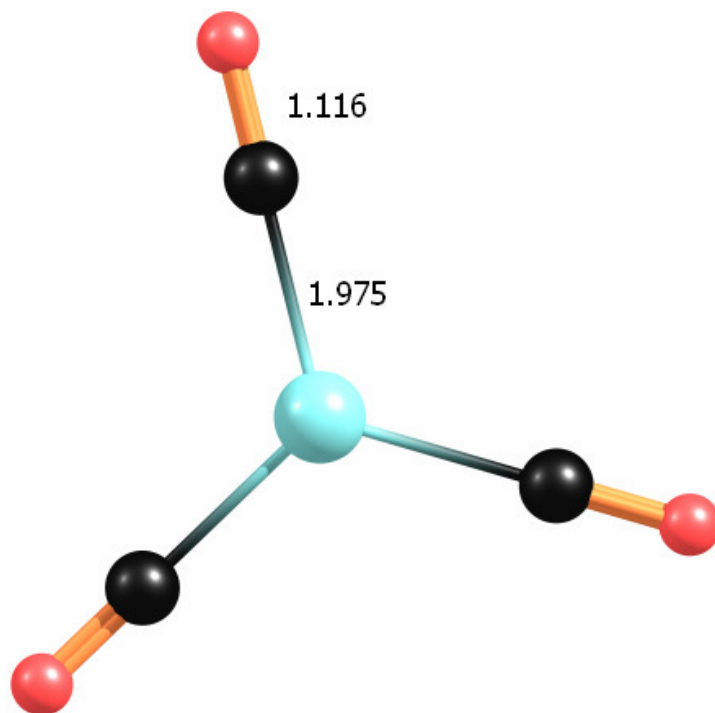


Figure C4: The optimized geometry of the singlet $\text{Cu}(\text{CO})_3^+$ calculated with the B3LYP functional using Gaussian2003. The Def 2 TZVPP basis set was used for all atoms.

Table C5: The unscaled normal mode frequencies and intensities (km/mol) are reported from this same level of theory.

Frequency	Intensity
57.5	0.1
57.5	0.1
62.9	1.1
246.6	0
246.6	0
257.2	0
275.5	0
286.8	7.9
286.9	7.9
322.7	3.6
352.7	0.3
352.7	0.3
2281.9	289.1
2281.9	289.1
2303.1	0

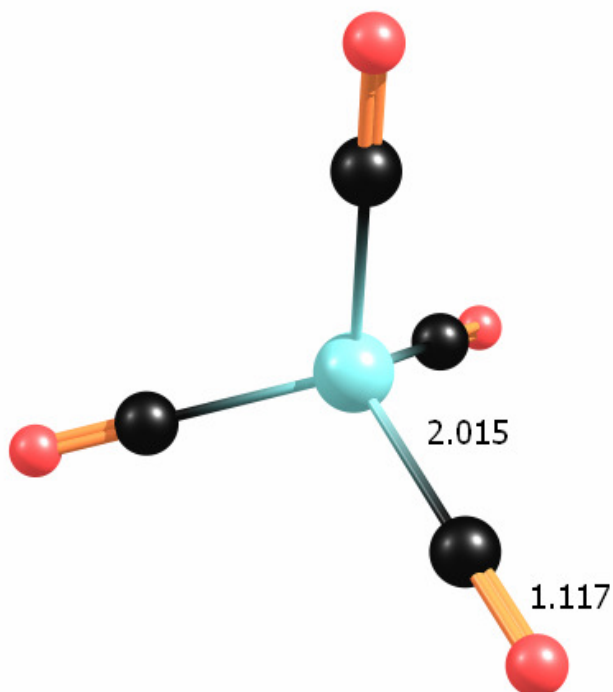


Figure C5: The optimized geometry of the singlet Cu(CO)_4^+ calculated with the B3LYP functional using Gaussian2003. The Def 2 TZVPP basis set was used for all atoms.

Table C6: The unscaled normal mode frequencies and intensities (km/mol) are reported from this same level of theory.

Frequency	Intensity
52.5	0
52.7	0
63.3	0.2
63.8	0.2
64.0	0.2
230.4	0
231.1	0
231.4	0
246.5	4.5
247.3	4.
248.0	3.2
249.6	1.6
330.5	1.4
331.6	0.4
331.8	1.0
331.9	0.8
333.1	0.9
2271.5	253.2
2272.1	251.3
2272.5	251.0
2294.1	0.1

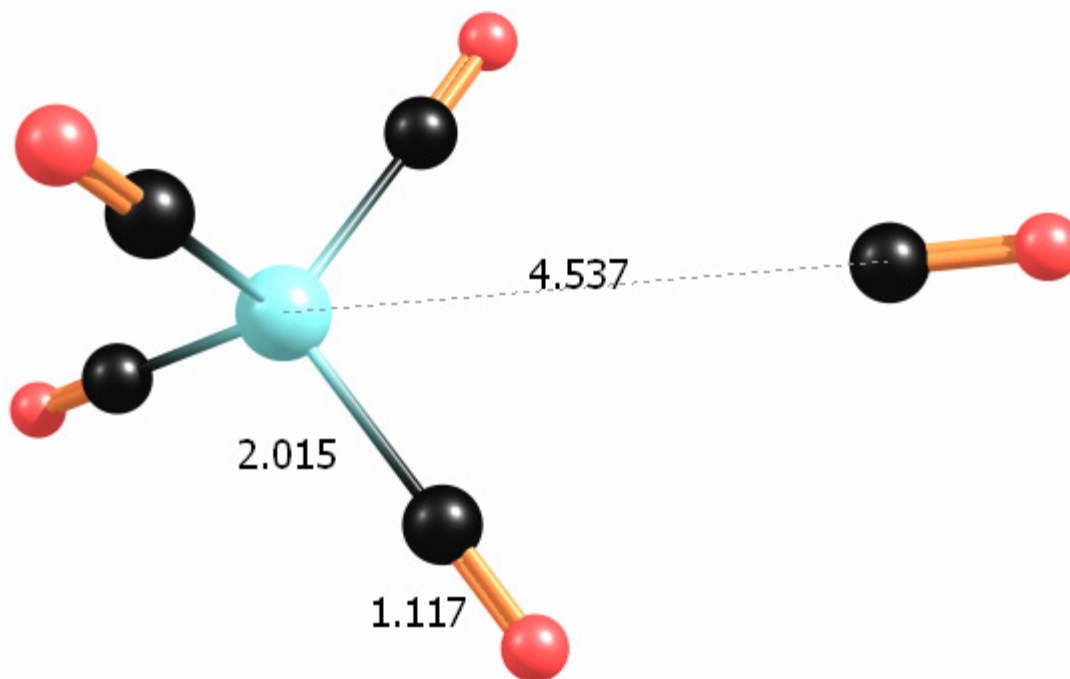


Figure C6: The optimized geometry of the singlet $\text{Cu}(\text{CO})_5^+$ calculated with the B3LYP functional using Gaussian2003. The Def 2 TZVPP basis set was used for all atoms.

Table C7: The unscaled normal mode frequencies and intensities (km/mol) are reported from this same level of theory.

Frequency	Intensity	Frequency	Intensity
-1.3	0.2	332.7	0.9
24.1	0.3	2242.6	79.0
31.6	1.2	2269.6	256.8
52.8	0	2270.7	252.4
54.9	0.1	2271.5	239.2
63.4	0.2	2271.5	239.2
64.3	0.2	2292.9	0.1
66.5	0.2		
73.8	0		
79.2	0		
230.6	0		
230.9	0		
231.8	0		
246.6	4.5		
247.3	3.9		
248.5	4.0		
249.8	1.4		
330.0	2.1		
331.7	1.0		
331.7	0.5		
332.6	1.2		

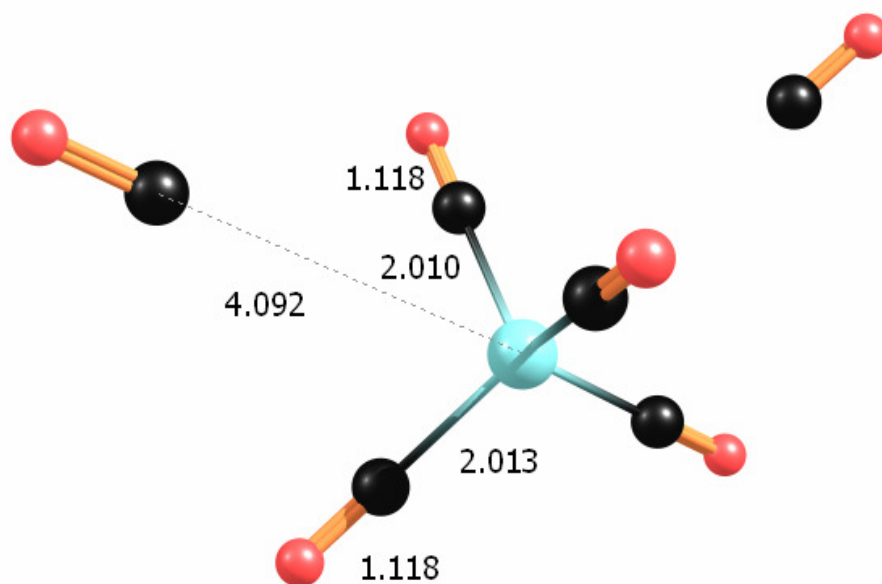


Figure C7: The optimized geometry of the singlet $\text{Cu}(\text{CO})_5^+$ calculated with the B3LYP functional using Gaussian2003. The Def 2 TZVPP basis set was used for all atoms.

Table C8: The unscaled normal mode frequencies and intensities (km/mol) are reported from this same level of theory.

Frequency	Intensity	Frequency	Intensity
4.2	0.2	331.7	1.1
7.8	0.3	331.8	1.4
9.3	0.4	332.6	1.0
15.8	0.1	333.1	2.0
36.6	1.0	334.2	1.0
38.6	1.7	2245.3	95.1
52.4	0	2246.0	53.9
53.4	0	2267.3	251.7
63.9	0.2	2267.4	251.6
64.2	0.3	2267.8	243.9
64.5	0	2290.3	0.1
70.2	0		
72.4	0		
72.9	0		
73.7	0		
231.4	0		
233.3	0		
234.8	0		
246.7	4.4		
248.1	3.9		
250.7	4.2		
251.6	1.3		

Table C9: The electronic states calculated for $\text{Cu}(\text{CO})_6^+$ with the B3LYP functional using Gaussian03. The Def 2 TZVPP basis set was used for all atoms.

Isomer	Total Energy (Hartrees)	Relative Energy (kcal/mol)
$^1\text{Cu}(\text{CO})_6^+$	-2320.5969872	0.0
$^3\text{Cu}(\text{CO})_2^+$	-2320.4671964	+81.4

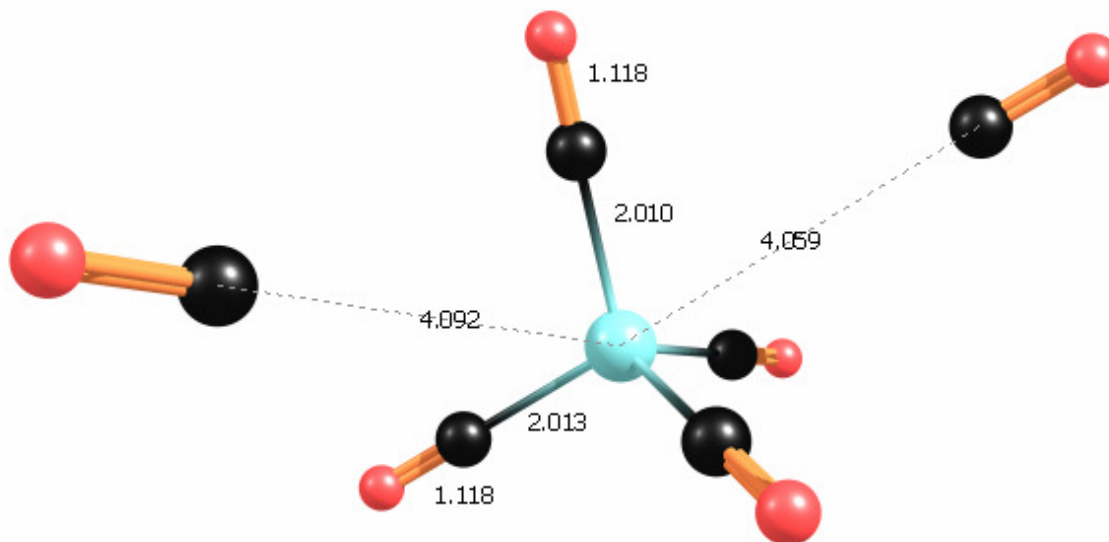


Figure C8: The optimized geometry of the singlet $\text{Cu}(\text{CO})_6^+$ calculated with the B3LYP functional using Gaussian2003. The Def 2 TZVPP basis set was used for all atoms.

Table C10: The unscaled normal mode frequencies and intensities (km/mol) are reported from this same level of theory.

Frequency	Intensity	Frequency	Intensity
4.2	0.2	331.7	1.1
7.8	0.3	331.8	1.4
9.3	0.4	332.6	1.0
15.8	0.1	333.1	2.0
36.6	1.0	334.2	1.0
38.6	1.7	2245.3	95.1
52.4	0	2246.0	53.9
53.4	0	2267.3	251.7
63.9	0.2	2267.4	251.6
64.2	0.3	2267.8	243.9
64.5	0	2290.3	0.1
70.2	0		
72.4	0		
72.9	0		
73.7	0		
231.4	0		
233.3	0		
234.8	0		
246.7	4.4		
248.1	3.9		
250.7	4.2		
251.6	1.3		

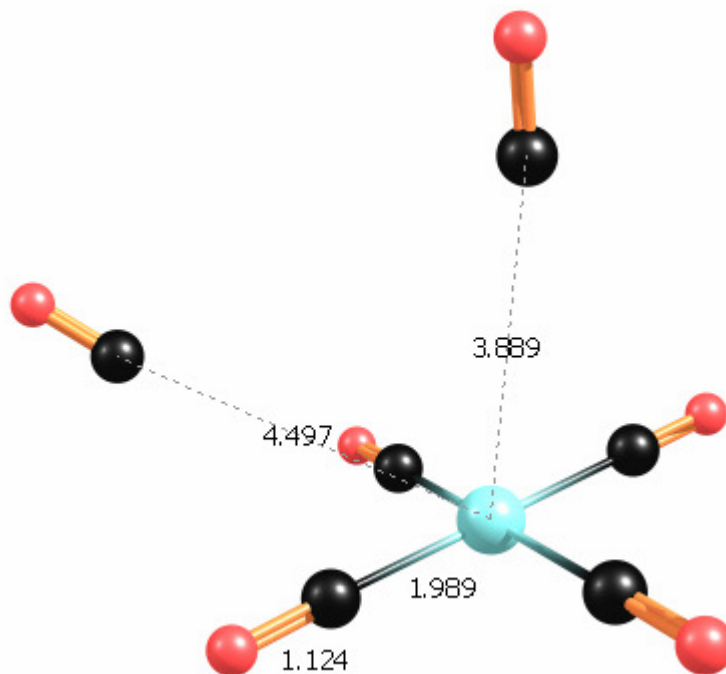


Figure C9: The optimized geometry of the triplet $\text{Cu}(\text{CO})_6^+$ calculated with the B3LYP functional using Gaussian2003. The Def 2 TZVPP basis set was used for all atoms.

Table C11: The unscaled normal mode frequencies and intensities (km/mol) are reported from this same level of theory.

Frequency	Intensity	Frequency	Intensity
-5.2	0.1	275.0	0.2
8.5	0.1	276.8	1.4
9.7	0.1	315.0	0.1
17.2	0	331.1	20.8
32.3	0.2	331.9	20.4
35.0	1.3	383.7	0.7
39.3	2.3	384.7	0.1
57.8	0.3	437.2	0.3
61.0	0.3	447.5	0
75.7	1.8	2137.5	1420.9
75.9	1.5	2143.0	1952.4
77.6	0.4	2145.6	587.4
82.0	1.4	2243.4	34.3
82.4	1.1	2244.4	96.9
85.2	0.9	2256.7	0.5
221.3	0		
244.6	0		
273.2	16.8		

Table C12: The electronic states calculated for $\text{Cu}(\text{CO})_6^+$ with the B3LYP functional using Gaussian03. The Def 2 TZVPP basis set was used for all atoms.

Isomer	Total Energy (Hartrees)	Relative Energy (kcal/mol)
$^1\text{Cu}(\text{CO})_7^+$	-2433.9622961	0.0
$^3\text{Cu}(\text{CO})_7^+$	-2433.8323164	+81.6

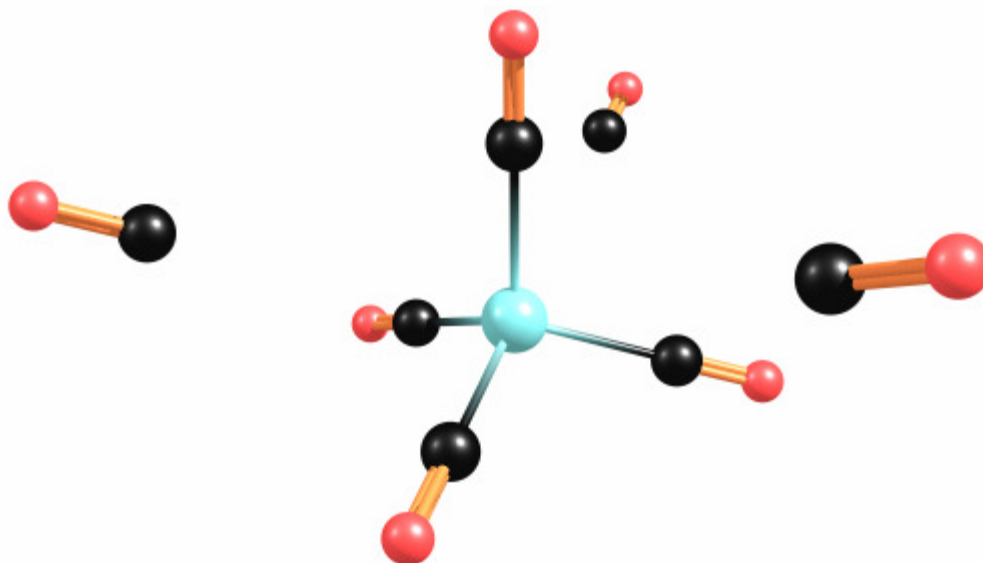


Figure C9: The optimized geometry of the singlet $\text{Cu}(\text{CO})_7^+$ calculated with the B3LYP functional using Gaussian2003. The Def 2 TZVPP basis set was used for all atoms.

Table C13: The unscaled normal mode frequencies and intensities (km/mol) are reported from this same level of theory.

Frequency	Intensity	Frequency	Intensity
5.5	0.2	235.4	0
6.6	0.6	248.4	4.7
7.4	0.4	249.1	4.6
10.9	0.2	250.0	2.5
12.8	0.1	252.5	2.0
13.7	0.1	332.0	1.3
36.7	0.5	332.5	1.9
38.2	1.7	332.6	0.8
39.2	1.7	334.0	2.0
52.4	0	334.4	1.4
53.1	0	2243.7	101.5
63.9	0.3	2244.0	86.6
64.2	0.3	2244.7	38.3
64.5	0.3	2265.5	250.9
71.5	0	2265.7	250.5
72.0	0	2266.0	241.7
72.6	0	2288.9	0.1
73.5	0.1		
73.7	0.1		
74.6	0.1		
233.5	0		
233.7	0		

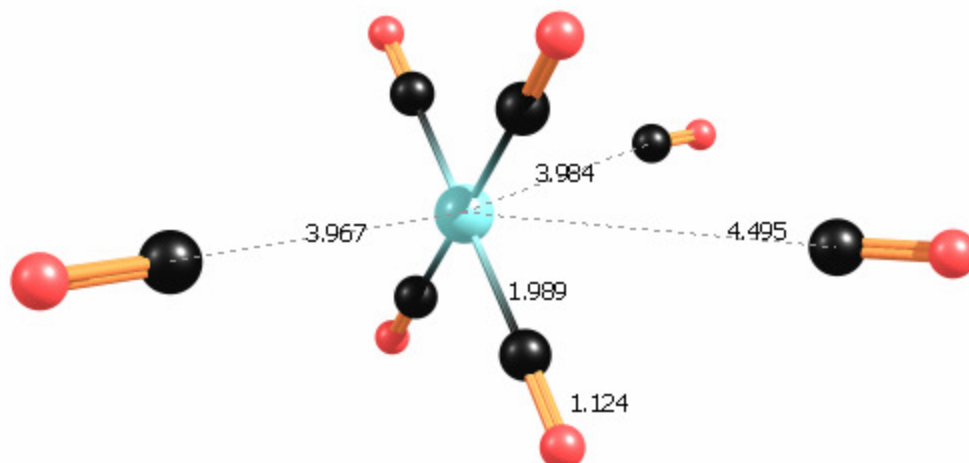


Figure C10: The optimized geometry of the triplet $\text{Cu}(\text{CO})_7^+$ calculated with the B3LYP functional using Gaussian2003. The Def 2 TZVPP basis set was used for all atoms.

Table C14: The unscaled normal mode frequencies and intensities (km/mol) are reported from this same level of theory.

Frequency	Intensity	Frequency	Intensity
-8.0	0	269.1	4.6
-7.6	0.3	270.6	3.9
-4.7	0.3	308.1	0.7
4.7	0.2	324.7	20.4
8.5	0	325.3	20.2
19.7	0	375.4	0.8
30.3	0.3	376.3	0.1
32.7	2.2	427.7	0.5
33.0	0.4	439.5	0
38.8	2.4	2082.0	1201.9
57.9	0.5	2090.6	2039.9
59.8	0.4	2099.6	766.4
60.5	0	2191.7	64.8
61.4	0.1	2192.6	84.6
73.8	2.2	2193.9	58.2
74.5	1.5	2206.1	1.9
75.7	0.7		
79.6	1.9		
82.1	0.8		
83.6	0.8		
217.4	0		
239.0	0		
265.0	10.5		

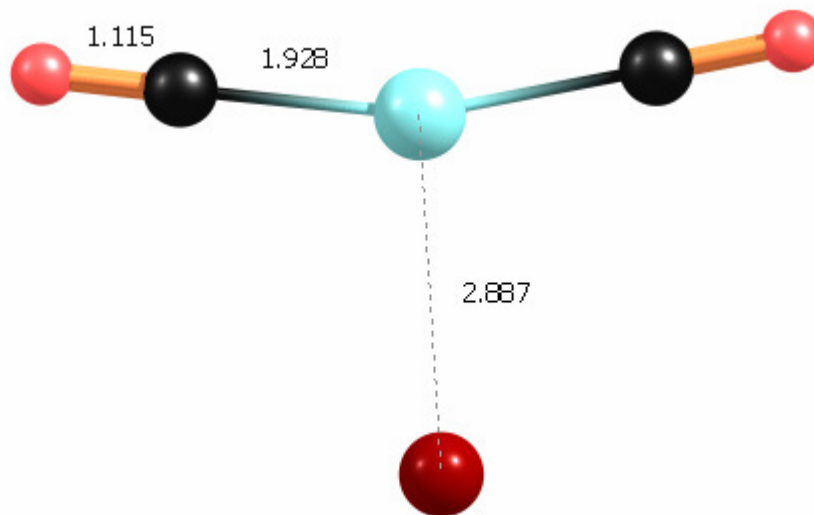


Figure C.11: The optimized geometry of the singlet $\text{Cu}(\text{CO})_2^+\text{Ar}$ calculated with the B3LYP functional using Gaussian2003. The Def 2 TZVPP basis set was used for all atoms.

Table C.15: The unscaled normal mode frequencies and intensities (km/mol) are reported from this same level of theory.

Frequency	Intensity
35.4	0.8
41.2	4.1
54.5	1.0
71.4	6.2
278.0	0
288.2	0
310.3	0
326.2	1.5
334.6	0.2
365.6	17.6
2295.2	383.2
2317.8	9.8

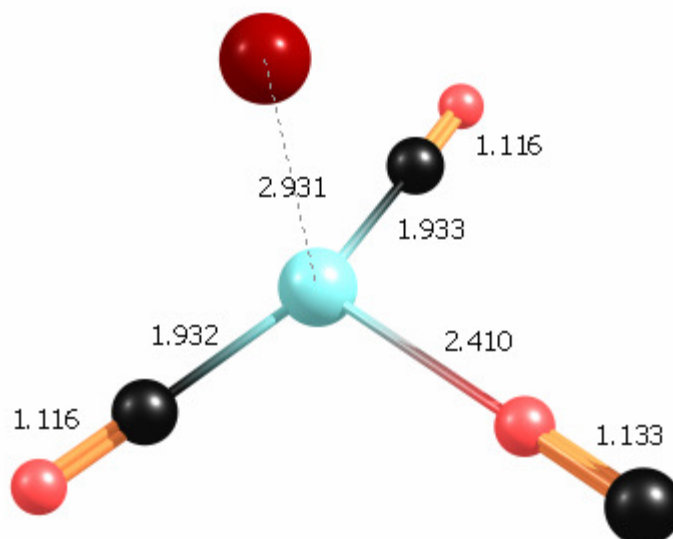


Figure C.11: The optimized geometry of the singlet $\text{Cu}(\text{CO})_3^+\text{Ar}$ calculated with the B3LYP functional using Gaussian2003. The Def 2 TZVPP basis set was used for all atoms.

Table C.15: The unscaled normal mode frequencies and intensities (km/mol) are reported from this same level of theory.

Frequency	Intensity
28.7	0.1
30.4	0.2
41.8	3.3
42.0	1.1
45.7	3.2
63.9	3.8
95.8	1.6
98.4	0.1
106.0	7.5
277.5	0
283.1	0.1
307.5	0
320.6	0.3
336.9	0.5
353.6	16.8
2148.7	220.4
2283.9	405.8
2306.2	27.4

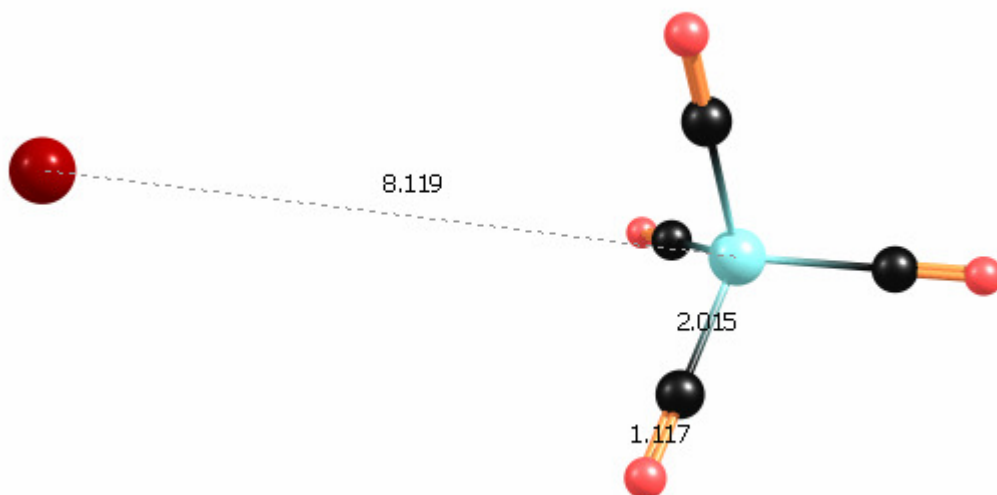


Figure C.12: The optimized geometry of the singlet $\text{Cu}(\text{CO})_4^+\text{Ar}$ calculated with the B3LYP functional using Gaussian2003. The Def 2 TZVPP basis set was used for all atoms.

Table C.15: The unscaled normal mode frequencies and intensities (km/mol) are reported from this same level of theory.

Frequency	Intensity	Frequency	Intensity
-3.2	0.5	2271.3	252.1
-2.3	0.2	2271.4	251.1
0.8	0.7	2271.4	251.1
52.3	0	2293.4	0
52.6	0		
63.3	0.2		
63.5	0.2		
63.7	0.2		
230.4	0		
230.9	0		
231.1	0		
247.0	4.5		
247.2	4.6		
247.4	4.5		
248.8	0.1		
330.8	1.4		
331.3	0.4		
331.5	1.4		
331.8	0.3		
332.0	1.0		

APPENDIX D

INFRARED PHOTODISSOCIATION SPECTROSCOPY OF BENZENE VANADIUM CARBONYL CATIONS, $\text{bz-V}^+(\text{CO})_n$ STRUCTURES, ENERGETICS, AND VIBRATIONS

The complete citation for reference number 41 is :

Gaussian 03, Revision B.02, M. J. Frisch, G. W. Trucks, H. B. Schlegel, G. E. Scuseria, M. A. Robb, J. R. Cheeseman, J. A. Montgomery, Jr., T. Vreven, K. N. Kudin, J. C. Burant, J. M. Millam, S. S. Iyengar, J. Tomasi, V. Barone, B. Mennucci, M. Cossi, G. Scalmani, N. Rega, G. A. Petersson, H. Nakatsuji, M. Hada, M. Ehara, K. Toyota, R. Fukuda, J. Hasegawa, M. Ishida, T. Nakajima, Y. Honda, O. Kitao, H. Nakai, M. Klene, X. Li, J. E. Knox, H. P. Hratchian, J. B. Cross, C. Adamo, J. Jaramillo, R. Gomperts, R. E. Stratmann, O. Yazyev, A. J. Austin, R. Cammi, C. Pomelli, J. W. Ochterski, P. Y. Ayala, K. Morokuma, G. A. Voth, P. Salvador, J. J. Dannenberg, V. G. Zakrzewski, S. Dapprich, A. D. Daniels, M. C. Strain, O. Farkas, D. K. Malick, A. D. Rabuck, K. Raghavachari, J. B. Foresman, J. V. Ortiz, Q. Cui, A. G. Baboul, S. Clifford, J. Cioslowski, B. B. Stefanov, G. Liu, A. Liashenko, P. Piskorz, I. Komaromi, R. L. Martin, D. J. Fox, T. Keith, M. A. Al-Laham, C. Y. Peng, A. Nanayakkara, M. Challacombe, P. M. W. Gill, B. Johnson, W. Chen, M. W. Wong, C. Gonzalez, and J. A. Pople, Gaussian, Inc., Pittsburgh PA, 2003.

Table D1: The electronic states calculated for $\text{bz-V}^+(\text{CO})_3$ with the B3LYP functional using Gaussian03. The 6-31+G* basis set was used for all atoms.

Isomer	Total Energy (Hartrees)	Relative Energy (kcal/mol)
$^1\text{bz-V}^+(\text{CO})_3$	-1516.0043133	+10.1
$^3\text{bz-V}^+(\text{CO})_3$	-1516.02046684	0.0
$^5\text{bz-V}^+(\text{CO})_3$	-1515.97840344	+26.4

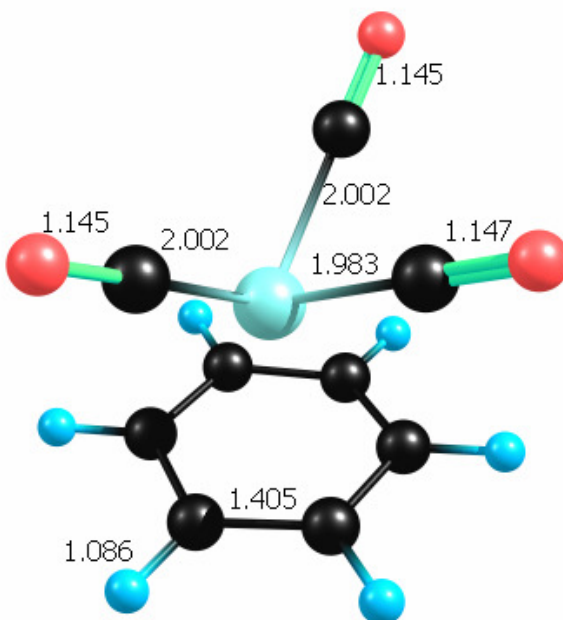


Figure D1: The optimized geometry of the singlet $\text{bz-V}^+(\text{CO})_3$ calculated with the B3LYP functional using Gaussian2003. The 6-31+G* basis set was used for all atoms.

Table D2: The unscaled normal mode frequencies and intensities (km/mol) are reported from this same level of theory.

Frequency	Intensity	Frequency	Intensity	Frequency	Intensity
13.4	0.1	616.5	0.3	2087.3	571.1
68.1	0.6	663.0	1.0	2093.3	1148.7
89.5	0.3	799.2	38.8	2146.1	665.6
93.9	2.4	928.7	1.2	3215.0	0.1
99.9	1.9	929.1	1.3	3220.2	0.8
110.6	0.4	991.0	2.9	3223.1	1.3
242.8	3.9	991.3	0.2	3229.5	4.8
252.0	1.1	1018.5	4.4	3231.6	5.6
280.0	1.4	1020.0	0.1	3237.4	1.1
312.2	0.6	1026.3	0.7		
352.4	11.6	1036.3	0		
357.6	16.6	1062.0	0		
382.3	14.6	1193.8	4.0		
417.5	3.1	1195.3	1.5		
423.1	0.4	1197.0	2.1		
438.0	0.3	1375.4	12.8		
462.4	37.3	1381.3	0		
464.7	30.7	1496.3	14.3		
552.1	21.0	1507.8	23.8		
569.2	45.3	1566.5	26.5		
604.3	0.5	1590.0	9.2		

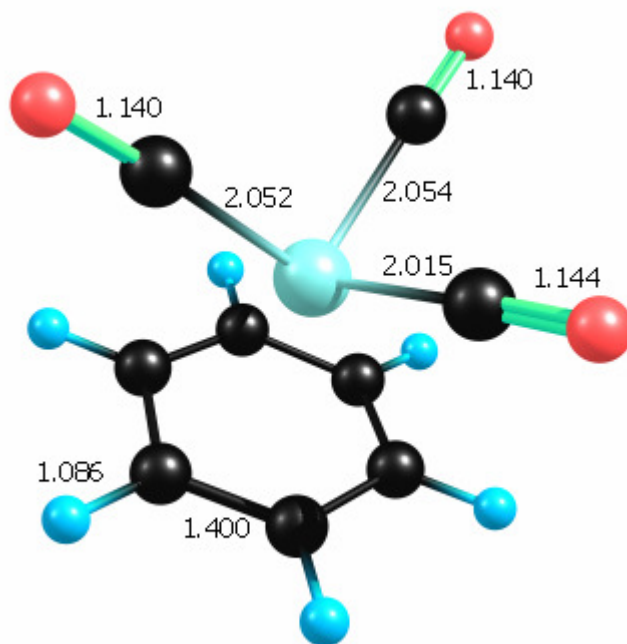


Figure D2: The optimized geometry of the triplet $\text{bz-V}^+(\text{CO})_3$ calculated with the B3LYP functional using Gaussian2003. The 6-31+G* basis set was used for all atoms.

Table D3: The unscaled normal mode frequencies and intensities (km/mol) are reported from this same level of theory.

Frequency	Intensity	Frequency	Intensity	Frequency	Intensity
10.8	0.2	904.4	0.4	3232.6	5.6
46.2	3.6	912.4	1.5	3236.2	7.2
62.9	0	964.1	12.7	3240.3	1.8
77.2	1.3	984.0	1.1		
82.0	1.5	1011.2	4.6		
98.6	0.5	1017.8	0.1		
233.6	7.0	1024.2	3.0		
241.0	1.9	1032.8	0		
258.2	3.8	1049.5	1.3		
309.8	0.9	1182.6	5.0		
312.5	1.4	189.5	3.7		
337.2	9.5	1193.7	1.3		
358.4	2.0	1376.5	0.1		
367.7	12.0	1378.9	8.3		
382.4	12.4	1489.2	9.7		
403.4	19.0	1496.6	8.9		
427.3	6.2	1551.8	30.0		
431.0	37.6	1569.9	33.6		
483.8	44.8	2113.4	688.7		
488.4	32.0	2118.3	1076.1		
605.3	0.8	2169.0	633.1		
615.2	0.1	3218.1	0.2		
658.5	0.9	3220.7	0.3		
789.2	49.8	3226.6	3.3		

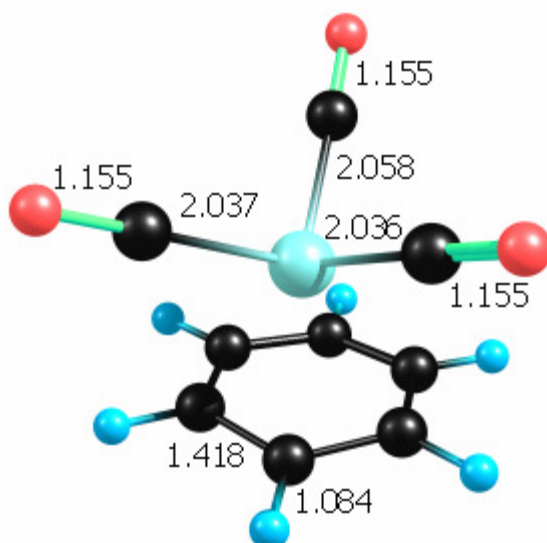


Figure D4: The optimized geometry of the quintet $\text{bz-V}^+(\text{CO})_3$ calculated with the B3LYP functional using Gaussian2003. The 6-31+G* basis set was used for all atoms.

Table D5: The unscaled normal mode frequencies and intensities (km/mol) are reported from this same level of theory.

Frequency	Intensity	Frequency	Intensity	Frequency	Intensity
17.0	0	930.9	3.9	3401.4	4.6
26.7	0	966.2	0.1	3406.3	6.1
58.1	0.6	1013.4	7.6	3415.5	1.4
63.1	0.4	1041.3	4.7		
71.9	0.7	1066.3	1.6		
80.4	0	1081.6	3.0		
131.2	0.5	1097.7	0.9		
137.3	1.2	1103.9	1.3		
248.8	1.4	1110.1	1.3		
256.2	0.2	1275.3	1.3		
302.2	1.2	1291.2	2.1		
329.0	7.2	1295.6	5.9		
338.5	0.2	1359.8	3.6		
364.4	1.2	1496.0	0.2		
386.5	4.1	1590.6	24.1		
391.0	23.1	1598.3	29.6		
397.5	9.0	1649.2	9.3		
407.7	21.1	1655.0	18.0		
440.2	6.4	2138.4	729.0		
460.1	9.3	2140.9	564.1		
654.0	0	2187.1	388.6		
661.1	2.4	3385.0	0		
695.5	11.7	3389.2	0		
789.8	111.7	3392.6	1.9		

Table D6: The electronic states calculated for $\text{bz-V}^+(\text{CO})_4$ with the B3LYP functional using Gaussian03. The 6-31+G* basis set was used for all atoms.

Isomer	Total Energy (Hartrees)	Relative Energy (kcal/mol)
$^1\text{bz-V}^+(\text{CO})_4$	-1629.3696866	0.0
$^3\text{bz-V}^+(\text{CO})_4$	-1629.3401201	+18.6
$^5\text{bz-V}^+(\text{CO})_4$	-1629.3046839	+40.8

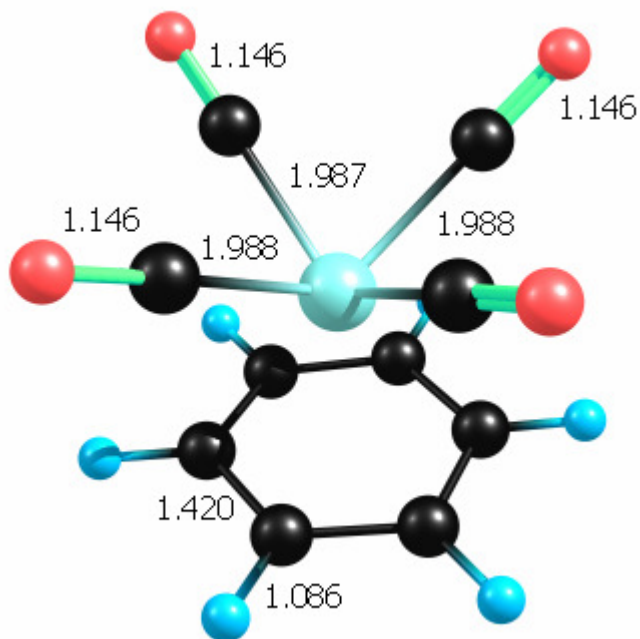


Figure D5: The optimized geometry of the singlet $\text{bz-V}^+(\text{CO})_4$ calculated with the B3LYP functional using Gaussian2003. The 6-31+G* basis set was used for all atoms.

Table D7: The unscaled normal mode frequencies and intensities (km/mol) are reported from this same level of theory.

Frequency	Intensity	Frequency	Intensity	Frequency	Intensity
10.3	0	575.1	60.2	1509.5	25.2
70.4	0	577.1	61.1	1578.8	19.9
94.0	1.1	607.7	0.4	1598.6	0.5
95.4	1.2	609.7	48.8	1598.6	0.5
103.0	3.8	614.5	8.7	2091.8	1150.8
107.3	0	671.4	0.1	2092.9	1157.9
120.6	0.5	801.4	40.7	2103.2	6.8
121.0	0.6	930.2	3.4	2148.7	600.8
243.9	0.6	938.9	3.8	3216.8	0.4
247.5	2.4	995.5	0.1	3221.3	0.2
274.2	0.1	1001.6	0.2	3224.9	0.1
321.0	0	1023.0	0	3230.8	5.8
356.5	0	1028.2	4.2	3233.8	7.6
366.1	5.7	1036.0	0.2	3237.7	0.5
406.1	10.8	1042.1	0.1		
406.7	8.1	1059.6	0		
428.6	0.3	1197.0	3.9		
430.9	0	1199.3	0.4		
439.9	0.5	1200.9	0.4		
459.6	33.2	1383.5	0		
463.2	33.9	1386.3	3.2		
561.6	0	1501.0	19.3		

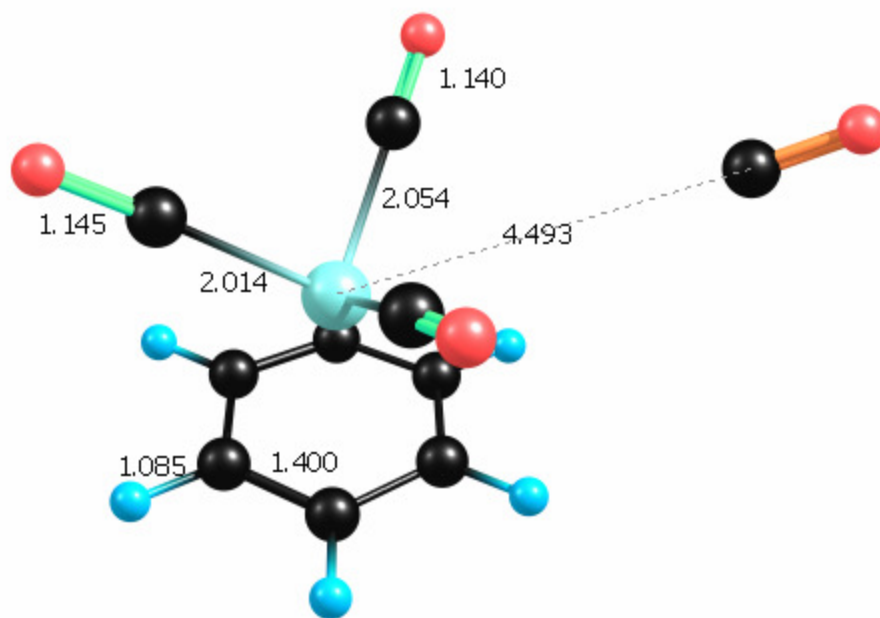


Figure D6: The optimized geometry of the triplet $\text{bz-V}^+(\text{CO})_4$ calculated with the B3LYP functional using Gaussian2003. The 6-31+G* basis set was used for all atoms.

Table D8: The unscaled normal mode frequencies and intensities (km/mol) are reported from this same level of theory.

Frequency	Intensity	Frequency	Intensity	Frequency	Intensity
-7.6	0.1	484.2	47.8	1568.4	32.8
5.4	0.7	488.7	30.4	2111.2	718.3
16.1	0.2	605.7	0.8	2117.5	1027.2
26.0	0.8	615.7	0.1	2168.2	625.7
51.5	2.7	658.8	0.8	2228.3	84.2
63.1	0	789.2	52.0	3218.4	0.4
64.7	0	903.3	0.1	3220.7	0.3
67.9	0	912.4	1.5	3227.7	2.2
78.8	1.2	961.3	10.9	3233.1	5.5
81.8	1.5	984.4	1.2	3237.2	6.8
98.4	0.6	1011.6	4.1	3240.6	1.3
236.6	5.4	1017.7	0.1		
241.7	2.3	1024.5	3.1		
257.9	3.4	1032.3	0		
311.2	0.5	1049.2	1.5		
314.2	1.5	1183.3	3.9		
337.1	9.0	1188.1	3.4		
359.3	1.8	1192.9	1.2		
368.1	12.0	1376.5	0.1		
383.1	12.2	1379.4	8.5		
403.6	17.7	1489.8	9.8		
428.2	7.8	1496.2	8.6		
431.6	38.2	1554.2	28.1		

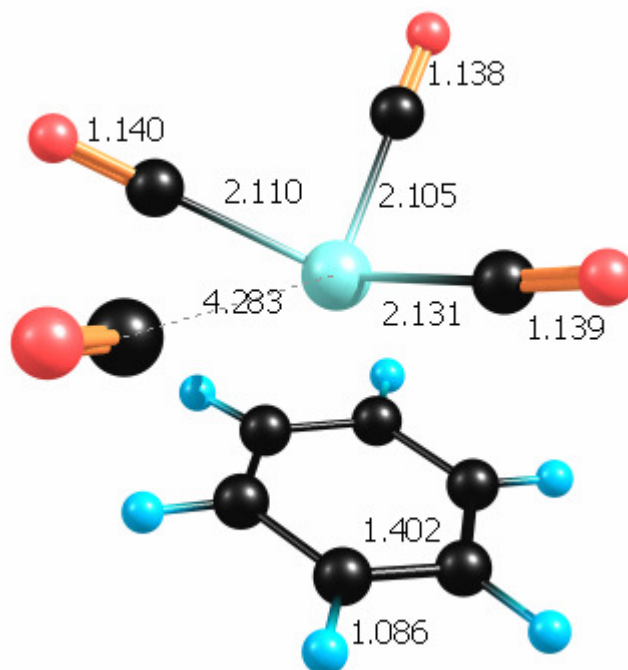


Figure D7: The optimized geometry of the quintet $\text{bz-V}^+(\text{CO})_4$ calculated with the B3LYP functional using Gaussian2003. The 6-31+G* basis set was used for all atoms.

Table D9: The unscaled normal mode frequencies and intensities (km/mol) are reported from this same level of theory.

Frequency	Intensity	Frequency	Intensity	Frequency	Intensity
8.9	0.2	389.3	9.3	1512.8	17.9
17.0	0.5	392.3	0.8	1608.0	6.9
24.4	0.3	427.7	0.1	1610.0	6.5
32.2	0.4	610.0	0	2137.8	943.9
36.6	0	611.0	0.2	2145.5	568.0
55.2	0.4	684.2	6.7	2186.3	444.5
57.7	0.9	739.7	96.0	2229.2	84.9
62.6	0	892.2	0.4	3199.8	0.3
64.7	0.5	903.5	0.2	3207.6	0.2
66.8	0.1	982.4	1.1	3209.9	0.9
70.1	0.2	999.8	4.6	3218.4	0.5
89.3	1.1	1008.7	0.8	3219.9	0
113.0	0.4	1020.8	0.3	3229.4	0
196.2	3.2	1031.0	2.3		
261.0	0.6	1051.1	1.4		
267.8	3.1	1057.4	1.3		
285.1	2.4	1190.1	0.1		
298.0	0.7	1199.4	0.3		
308.3	4.9	1206.1	2.3		
319.0	10.0	1342.0	1.8		
339.2	14.7	1386.0	0		
365.3	9.6	1507.6	18.6		

Table D10: The electronic states calculated for $\text{bz-V}^+(\text{CO})_5$ with the B3LYP functional using Gaussian03. The 6-31+G* basis set was used for all atoms.

Isomer	Total Energy (Hartrees)	Relative Energy (kcal/mol)
$^1\text{bz-V}^+(\text{CO})_5$	-1742.6903576	0.0
$^3\text{bz-V}^+(\text{CO})_5$	-1742.65946234	+19.4

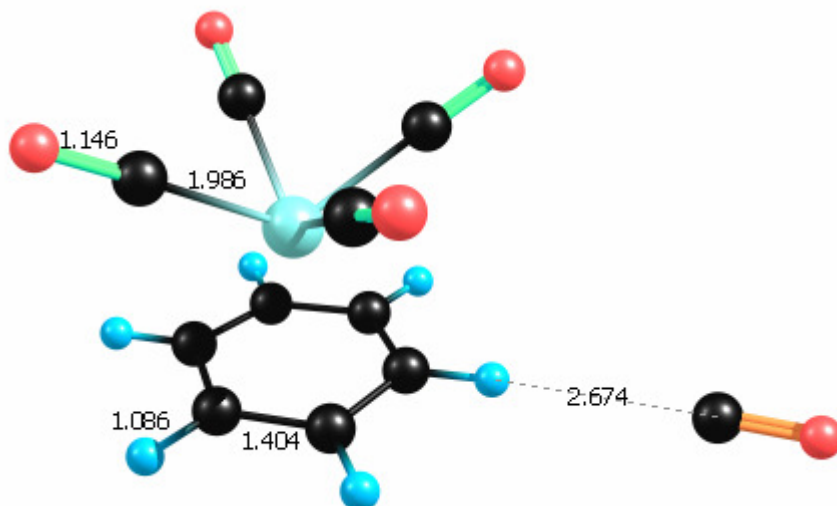


Figure D8: The optimized geometry of the singlet $\text{bz-V}^+(\text{CO})_5$ calculated with the B3LYP functional using Gaussian2003. The 6-31+G* basis set was used for all atoms.

Table D11: The unscaled normal mode frequencies and intensities (km/mol) are reported from this same level of theory.

Frequency	Intensity	Frequency	Intensity	Frequency	Intensity
-5.8	0.2	463.0	33.1	1579.2	11.7
7.7	0.7	563.0	0	1599.1	7.5
12.1	0.1	575.3	62.1	2090.6	1164.2
54.9	2.2	577.3	61.2	2091.7	1180.3
68.8	0	607.7	12.5	2101.9	0.3
85.2	0	610.3	39.8	2148.0	590.8
88.2	0.1	614.2	5.1	2233.4	82.8
93.8	1.1	671.1	0.1	3215.2	11.0
94.9	1.8	808.1	39.4	3219.4	5.6
102.2	3.6	939.4	3.2	3219.4	5.6
107.1	0	942.8	3.7	3221.1	11.2
120.9	0.3	995.3	0.5	3228.8	16.5
121.1	0.5	1011.3	0.8	3230.1	7.6
242.0	0.8	1023.1	0.4	3235.6	0.5
247.9	2.3	1030.0	3.1		
272.6	0.2	1036.9	0		
321.0	0	1047.8	0.5		
358.2	0.2	1060.9	0.1		
365.4	4.8	1197.6	1.6		
406.9	9.9	1201.3	2.0		
407.5	7.8	1205.0	1.5		
426.4	0.5	1385.1	1.9		
430.9	0	1387.8	0.7		
440.0	0.2	1501.1	22.6		
459.8	35.5	1512.3	23.8		

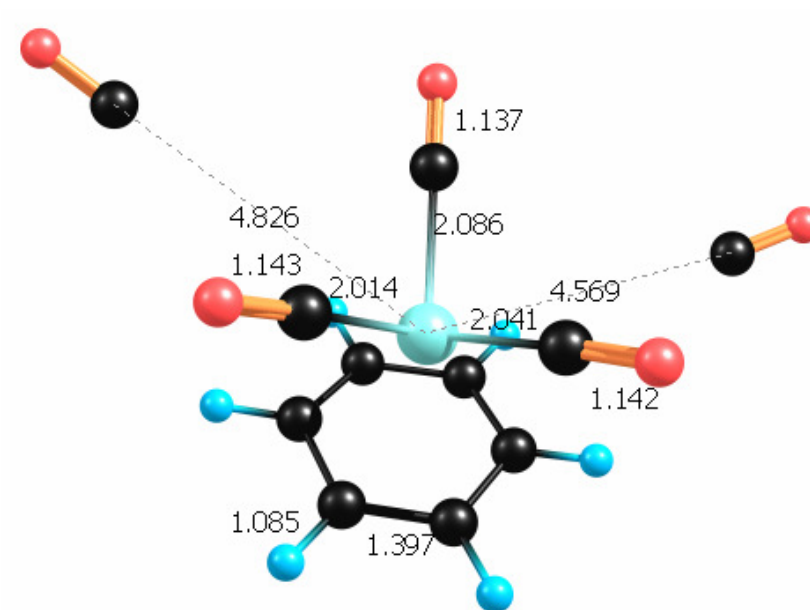


Figure D9: The optimized geometry of the triplet $\text{bz-V}^+(\text{CO})_5$ calculated with the B3LYP functional using Gaussian2003. The 6-31+G* basis set was used for all atoms.

Table D12: The unscaled normal mode frequencies and intensities (km/mol) are reported from this same level of theory.

Frequency	Intensity	Frequency	Intensity	Frequency	Intensity
-8.7	0	387.6	13.9	1485.8	7.0
4.8	0.1	419.2	2.9	1536.3	34.2
11.9	0.2	433.7	40.3	1580.3	32.0
20.2	1.9	470.3	37.3	2113.1	944.5
25.5	0	497.0	48.0	2129.0	840.4
31.5	2.6	605.7	0.3	2178.1	631.3
35.9	1.2	616.0	0.4	2223.4	87.3
58.5	0	658.4	0.8	2229.9	86.4
63.1	0	788.8	51.6	3219.6	0.6
64.5	0	901.0	0	3221.4	0.5
66.8	0.1	912.1	1.5	3229.1	0.5
74.6	0.3	964.5	7.9	3233.7	5.3
76.3	1.1	983.5	1.5	3238.6	7.8
81.4	1.6	1002.1	6.9	3241.5	0.8
96.1	0.4	1015.3	1.1		
231.5	3.7	1023.2	3.2		
240.4	2.5	1031.7	0.3		
268.3	3.5	1049.0	1.0		
298.3	1.1	1176.9	3.6		
313.5	2.7	1189.7	0.9		
324.1	12.4	1193.2	3.9		
352.3	6.3	1375.9	1.0		
361.4	4.3	1376.9	7.9		
1498.6	11.1				